Heidi Jo Newberg Jeffrey L. Carlin *Editors*

Tidal Streams in the Local Group and Beyond

Observations and Implications





Astrophysics and Space Science Library

Volume 420

Editorial Board

Chairman

W.B. Burton, National Radio Astronomy Observatory, Charlottesville, VA, USA (bburton@nrao.edu); University of Leiden, The Netherlands (burton@strw.leidenuniv.nl)

F. Bertola, University of Padua, Italy

C.J. Cesarsky, Commission for Atomic Energy, Saclay, France

P. Ehrenfreund, Leiden University, The Netherlands

O. Engvold, University of Oslo, Norway

A. Heck, Strasbourg Astronomical Observatory, France

E.P.J. Van Den Heuvel, University of Amsterdam, The Netherlands

V.M. Kaspi, McGill University, Montreal, Canada

J.M.E. Kuijpers, University of Nijmegen, The Netherlands

H. Van Der Laan, University of Utrecht, The Netherlands

P.G. Murdin, Institute of Astronomy, Cambridge, UK

B.V. Somov, Astronomical Institute, Moscow State University, Russia

R.A. Sunyaev, Space Research Institute, Moscow, Russia

More information about this series at http://www.springer.com/series/5664

Heidi Jo Newberg • Jeffrey L. Carlin Editors

Tidal Streams in the Local Group and Beyond

Observations and Implications



Editors
Heidi Jo Newberg
Department of Physics, Applied Physics and Astronomy
Rensselaer Polytechnic Institute
Troy, NY, USA

Jeffrey L. Carlin
Department of Physics, Applied Physics
and Astronomy
Rensselaer Polytechnic Institute
Troy, NY, USA

ISSN 0067-0057 ISSN 2214-7985 (electronic)
Astrophysics and Space Science Library
ISBN 978-3-319-19335-9 ISBN 978-3-319-19336-6 (eBook)
DOI 10.1007/978-3-319-19336-6

Library of Congress Control Number: 2015956760

Springer Cham Heidelberg New York Dordrecht London © Springer International Publishing Switzerland 2016

This work is subject to copyright. All rights are reserved by the Publisher, whether the whole or part of the material is concerned, specifically the rights of translation, reprinting, reuse of illustrations, recitation, broadcasting, reproduction on microfilms or in any other physical way, and transmission or information storage and retrieval, electronic adaptation, computer software, or by similar or dissimilar methodology now known or hereafter developed.

The use of general descriptive names, registered names, trademarks, service marks, etc. in this publication does not imply, even in the absence of a specific statement, that such names are exempt from the relevant protective laws and regulations and therefore free for general use.

The publisher, the authors and the editors are safe to assume that the advice and information in this book are believed to be true and accurate at the date of publication. Neither the publisher nor the authors or the editors give a warranty, express or implied, with respect to the material contained herein or for any errors or omissions that may have been made.

Cover illustration: The "Field of Streams" (after Belokurov, V., Zucker, D.B., Evans, N.W. et al., 2006, ApJL, 642, L137 as reproduced with more recent data by Matthew Newby) shows the density of main sequence turnoff stars in the north Galactic cap, color coded by distance. Blue is closer and red is farther away. The stars were selected from the Sloan Digital Sky Survey Data Release 10. This beautiful image shows that the outer stellar halo is dominated by several large "streams" of stars. These stars were ripped from their progenitor dwarf galaxies by tidal forces in the Milky Way. The image is plotted in Equatorial coordinates with declination-corrected bins of 0.25 degree × 0.25 degree each.

Printed on acid-free paper

Springer International Publishing AG Switzerland is part of Springer Science+Business Media (www.springer.com)

Preface

This book introduces the field of tidal streams, charts the major discoveries that brought us to our current understanding, and gives the reader a sense of the field as we know it. Because this field is quite young, the researchers who made major contributions are still active in the field. I am quite fortunate and grateful that many of these wonderful people agreed to contribute chapters to this book. Their expertise and willingness to share it in this way were essential to the book's success. I would particularly like to thank my co-editor Jeff Carlin for stepping in to bridge any scientific or technical gaps that arose. In addition to having made important contributions to the field of tidal streams, he has an incredible ability to spot grammar and spelling errors, which was put to great use as he copy edited every single chapter of this book. I am quite happy with the result.

There are some notable scientists in this field who were not available or were not asked to write chapters, and because of this I am sure that there is wisdom that has not been passed down in this volume. I hope that we have at least done a reasonable job of covering the major results presented in their papers. I apologize in advance to those whose work was missed or was not as fully represented as it could have been.

One of the things I have personally learned in writing and editing this book is that each of us watches the field evolve from our own vantage point. We do not know everything that has been discovered, or we learn about results in different orders, and we are not all influenced by the same results in the same way. In editing the chapters of this book, my primary intent was to improve clarity and style and to cover as much material as possible without duplication. I think it is important that in each chapter the historical viewpoint is that of the authors of that chapter at the time the chapter was written.

This book certainly will not be the definitive book on tidal streams, in the sense that definitive implies the material presented is final, settled, or inarguable. I have personally learned an enormous amount in researching my portion of this book and in editing the contributions of others. Our knowledge of tidal streams and the information they give us on the quantity and location of dark matter in the Milky Way is still evolving. Keep in mind that writing the book took about 2 years, and the chapters of more conscientious writers were finished months ahead of those

vi Preface

for whom deadlines are less important. Some important findings presented in this volume were discovered while the chapters were being written!

I consciously decided not to attempt to make all of the chapters completely consistent. We do not all agree on the identity of the tidal streams. There is stellar structure in the plane of the Milky Way that some believe was ripped from dwarf galaxies as they fell in to our galaxy, and others are just as sure is material thrown up from the disk. We don't all agree about whether all of the material in the orbital plane of the Sagittarius dwarf tidal stream was ripped from the Sagittarius dwarf galaxy, or whether it came from multiple infalling dwarf galaxies, or how many times the Sagittarius dwarf tidal stream wraps around the Milky Way. We don't all agree that all of the objects identified as tidal streams are actually tidal debris, and we certainly don't all agree on the fluffier structures of stars that we call "clouds." But the chapters in this book outline the published work of experts in the field, as interpreted by experts in the field, and will serve as a reliable guide to our current best understanding.

I hope this book will teach you as much as I have learned in editing it, and that it will inspire you to solve the many outstanding questions it describes.

Troy, NY, USA August 2015 Heidi Jo Newberg

Contents

1	Intr	oduction to Tidal Streams	1
	Heio	li Jo Newberg	
	1.1	An Overview of Tidal Streams and Halo Substructure	1
	1.2	The Discovery of Tidal Streams in the Milky Way	4
		1.2.1 Dwarf Galaxies and Moving Groups	4
		1.2.2 Halo Substructure in the Era of Large Surveys	7
	1.3	Observational Techniques for Finding Substructure	15
		1.3.1 Standard Candles and Photometric Parallax	15
		1.3.2 Matched Filter Techniques	17
		1.3.3 Statistical Photometric Parallax	19
	1.4	Co-moving Groups of Stars	21
	1.5	Chemical Tagging	22
	1.6	Constraining Dark Matter, the Formation of the Milky	
		Way, and Cosmology with Tidal Streams	23
		1.6.1 Rapid Collapse vs. Hierarchical Mergers	23
		1.6.2 Constraining Dark Matter with Tidal Streams	24
	1.7	Disk Response to Tidal Interactions	25
	1.8	Future Prospects	26
	Refe	erences	27
2	The	Sagittarius Dwarf Tidal Stream(s)	31
	Dav	id R. Law and Steven R. Majewski	
	2.1	Introduction	31
	2.2	Historical Remarks and Basic Structure of the Sagittarius System	32
	2.3	Stellar Populations Within the Sagittarius System	37
		2.3.1 Stellar Populations in the Sagittarius Core	37
		2.3.2 Stellar Populations in the Sagittarius Streams	41
		2.3.3 Chemical Evolution of the Sagittarius System	42
		2.3.4 Sagittarius Star Clusters	44

viii Contents

	2.4	Numerical Models of the Sagittarius-Milky Way System	45
		2.4.1 General Approach	45
		2.4.2 Constraints on the Shape of the Galactic Dark	
		Matter Halo	48
		2.4.3 Constraining the Mass of the Galactic Disk	51
	2.5	Mass, Luminosity and Mass-to-Light Ratio of Sagittarius	52
	2.6	Outstanding Issues Regarding the Detailed Structure	
		of the Sagittarius System	54
		2.6.1 A Bifurcated Stream Density Profile	54
		2.6.2 Multiply-Wrapped Sagittarius Streams	56
	Refe	erences	59
3	The	Monoceros Ring, and Other Substructure Near the	
		actic Plane	63
		n Yanny and Heidi Jo Newberg	
	3.1	The Monoceros Ring Is Discovered and Named	63
	3.2	Dragged In or Dredged Up? The Debate Over the Origin	
		of the Monoceros Ring	67
	3.3	Properties of the Monoceros Structure	71
	3.4	The Canis Major Dwarf Galaxy Controversy	77
	3.5	The Triangulum-Andromeda, and Other Low Latitude,	
		Stream-Like Substructures Near the Anticenter	79
	3.6	Explaining the Monoceros Ring and Other Low Latitude	
		Substructures with a Corrugated Milky Way Disk	80
	3.7	Future Prospects.	84
	Refe	erences	84
4	Ctoll	lar Streams and Clouds in the Galactic Halo	87
•		J. Grillmair and Jeffrey L. Carlin	07
	4.1	Observational Techniques	87
	4.2	Currently Known Stellar Debris Streams and Clouds	07
	4.2	in the Galactic Halo	89
		4.2.1 Streams with Known or Likely Globular Cluster	09
		Progenitors	98
		4.2.2 Streams with Presumed Dwarf Galaxy Progenitors	101
		4.2.3 Clouds and Other Diffuse Stellar Structures	101
	4.3	Future Discoveries	103
		erences	110
5		ematically Detected Halo Streams	113
		tin C. Smith	
	5.1	Introduction to Kinematic Streams	113
	5.2	Local Kinematic Streams	115
		5.2.1 The Helmi Stream	
		5.2.2 Other Early Discoveries	118

Contents ix

		5.2.3 Streams in the Geneva-Copenhagen Survey	119		
			123		
	5.3	Distant Halo Streams	130		
	5.4	Future Prospects	133		
	Refe	erences	136		
6	Orio	gins and Interpretation of Tidal Debris	141		
•		nryn V. Johnston			
	6.1	•	141		
	6.2		142		
	6.3	· · · · · · · · · · · · · · · · · · ·	143		
			143		
			149		
		6.3.3 Application: Models of Streams	151		
	6.4	Morphologies of Individual Debris Structures in			
		Observable Co-ordinates	153		
		6.4.1 Young Debris	154		
			155		
	6.5	Debris in a Cosmological Context: Modeling and			
			156		
		$oldsymbol{arepsilon}$	157		
		$oldsymbol{arepsilon}$	158		
		1 11	162		
	6.6	1	165		
	Refe	erences	166		
7	Tida	al Debris as a Dark Matter Probe	169		
	Kath	nryn V. Johnston and Raymond G. Carlberg			
	7.1		169		
	7.2	$oldsymbol{c}$	171		
			173		
			175		
		· · · · · · · · · · · · · · · · · · ·	176		
	7.3	<u> </u>	178		
			178		
			180		
			187		
	Refe	erences	188		
8	Substructure and Tidal Streams in the Andromeda Galaxy				
			191		
		ette M.N. Ferguson and A.D. Mackey			
	8.1		191		
	8.2		193		
	8.3		194		
	8.4	Major Tidal Features in the Halo of M31	196		

x Contents

	8.5	Understanding the Nature and Origin of Tidal Features in M31	200
		8.5.1 The Giant Stellar Stream	200
		8.5.2 Other Inner Halo Substructure	205
		8.5.3 Outer Halo Substructure	207
	8.6	Globular Clusters as Probes of Tidal Streams in M31	208
	8.7	Tidal Streams from M31's Satellite Galaxies	212
	8.8	Summary and Future Prospects	213
	Refe	erences	215
9	Stell	lar Tidal Streams in External Galaxies	219
	Jeffr	rey L. Carlin, Rachael L. Beaton, David Martínez-Delgado,	
	and l	R. Jay Gabany	
	9.1	Introduction	220
	9.2	Stellar Streams: Detection Methods and Examples	220
		9.2.1 Resolved Stellar Structures in the Local Group	221
		9.2.2 Detection Methods in and Beyond the Local Group	221
		9.2.3 Unresolved Features Beyond the Local Group	224
		9.2.4 Resolved Structures Beyond the Local Group	226
	9.3	•	228
	9.4	8	230
	9.5	The Role of Interactions Within Dwarf Galaxy Halos	234
		9.5.1 Observational Evidence for Substructure at Dwarf	
			235
			236
	9.6		239
	9.7	Future Prospects	241
	Refe	erences	243
T.	dev		247
	- X		/4/

Chapter 1 Introduction to Tidal Streams

Heidi Jo Newberg

Abstract Dwarf galaxies that come too close to larger galaxies suffer tidal disruption; the differential gravitational force between one side of the galaxy and the other serves to rip the stars from the dwarf galaxy so that they instead orbit the larger galaxy. This process produces "tidal streams" of stars, which can be found in the stellar halo of the Milky Way, as well as in halos of other galaxies. This chapter provides a general introduction to tidal streams, including the mechanism through which the streams are created, the history of how they were discovered, and the observational techniques by which they can be detected. In addition, their use in unraveling galaxy formation histories and the distribution of dark matter in galaxies is discussed, as is the interaction between these dwarf galaxy satellites and the disk of the larger galaxy.

1.1 An Overview of Tidal Streams and Halo Substructure

The Milky Way is a large, spiral galaxy. It is composed of stars, gas, and dark matter within its "halo," which is the region within which the matter is gravitationally bound. Like other similar galaxies in the Universe, the Milky Way is also orbited by gravitationally bound satellites that contain their own stars, gas, and/or dark matter. Globular clusters contain stars densely packed into small volumes, but are generally free of gas and dark matter. There are 157 known globular clusters in the Milky Way (Harris 2010). Dwarf galaxies contain stars, and sometimes gas, and are generally thought to contain large amounts of dark matter (though the dark matter content of dwarf galaxies is debated). There are about 30 known dwarf galaxies in the Milky Way (McConnachie 2012). We generally think of globular clusters as having one generation of star formation, and dwarf galaxies as more massive satellites with ongoing star formation, but the distinction between these two classes of objects has become more blurred as we find fainter dwarf galaxies and more

H.J. Newberg (⋈)

Department of Physics, Applied Physics and Astronomy, Rensselaer Polytechnic Institute, 110 8th St., Troy, NY 12180, USA

1

e-mail: heidi@rpi.edu

2 H.J. Newberg

complex globular clusters. Dwarf galaxies can contain globular clusters or be orbited by smaller dwarf galaxies.

When a globular cluster or a dwarf galaxy comes too close to the Milky Way, our galaxy's gravitational potential pulls harder on the part of the stellar association that is closer to the Galactic center than on the part that is farther away. This differential force is called a *tidal* force, since it is similar to the mechanism that causes the ocean tides on Earth. On Earth, it is the gravity of the Moon (and also the Sun) that pulls harder on the oceans that face it than on the oceans on the opposite side. This difference force stretches the oceans and raises the ocean levels on the sides of the Earth that are towards and away from the Moon.

Tidal forces on stars (or dark matter) in dwarf galaxies and globular clusters pull them off of their satellite of origin, and into tidal streams that can encircle the Galaxy. Stars that have been tidally stripped from a satellite of the Milky Way, and that are moving more slowly or are closer to the Galactic center than the satellite's center of mass, will be pulled into lower energy orbits, which are slightly closer to the Galactic center and have shorter orbital periods. Tidally stripped stars that are moving more quickly or are farther from the Galactic center than the center of mass of the dwarf galaxy or globular cluster will be pulled into higher energy orbits and thus orbit more slowly. The physics is analogous to that of planets orbiting the Sun; inner planets move faster than outer planets. At the point that the stars are no longer trapped by the gravity of the dwarf galaxy (or globular cluster), they orbit the Milky Way instead of the center of mass of the satellite. At that point, they are part of the tidal tail. As the orbital periods of Milky Way halo satellites are of order hundreds of thousands or a billion years, the timescale over which tidal streams evolve is also billions of years.

The content and density of dwarf galaxies is known to vary as a function of radius. A typical model for a dwarf galaxy includes ten times more dark matter than baryonic matter. The dark matter has a much larger scale radius than the baryonic matter, which is more centrally located. There is typically radial structure in the stellar populations as well; younger, more metal-rich stars are more centrally located than the older stellar populations. These radial gradients in the content of dwarf galaxies are imprinted on the structure of tidal streams.

Stars and dark matter whose populations are distributed at larger radius from a dwarf galaxy center will be preferentially stripped from the dwarf galaxy at an earlier time (though there is some mixing of material from all radii in the stripping process). Material in the tidal streams that is stripped first will generally be located farthest from the dwarf galaxy (though it is not a strict time sequence along the stream because the stripped stars have a distribution of energies at the time they became unbound). Therefore, we expect the dark matter to be stripped first, followed by the older populations, followed by the younger populations. This can lead to a trend in stellar populations (and chemical abundance) along the stream.

In addition to radial gradients, dwarf galaxies could have their own possibly complex or asymmetric shapes; they could be rotating, and often contain globular clusters within their gravitational potential. Each of these more complex attributes could contribute to the structure of the stream. At least some of the globular clusters

in the halo of the Milky Way are believed to have been accreted when dwarf galaxies fell in and then were assimilated (along with their globular clusters) into the stellar halo. Globular clusters themselves, regardless of their origin, may become tidally disrupted, though until they become unbound to the dwarf galaxy they would be shielded from the tidal forces of the Milky Way.

The length of the tidal tails depends on the mass and scale radius of the satellite (which determine how easy it will be to strip the stars), the path along which the satellite orbits the Milky Way, and the length of time the satellite has been orbiting. While early papers on tidal streams supposed that all tidal stream progenitors had been orbiting the Milky Way for the age of the Universe, more recent papers recognize that the Milky Way galaxy has likely built up over the age of the Universe through merger processes, and the smaller galaxies that are merging now are likely to have been captured at later times. Since the tidal forces on a satellite are stronger closer to the Galactic center, more material is stripped from the satellite and acquired by the tidal tails when the satellite is at perigalacticon. The variable rate of mass loss from the progenitor satellite will also lead to structure in the tidal tails. Models for generating the tidal stream from the Sagittarius dwarf galaxy, for example, often segregate the tidal stream stars by the perigalactic passage during which they were stripped.

Observed tidal streams of stars could have a known progenitor which still survives, despite the fact that some of its stars have been removed. Streams might also have no known progenitor either because the satellite from which it formed has been completely disrupted into the tidal stream, or because it has yet to be discovered (for example it might be hidden behind the Galactic disk). Stars that have been stripped by tidal forces are subsequently incorporated into the stellar halo, while still maintaining some kinematical and chemical memory of their origin.

Before the discovery of tidal streams, the stellar halo was modeled as a smooth distribution of stars, fit by a power law profile ($\rho \sim r^{-\alpha}$, where ρ is the density, r is the distance from the Galactic center, and α is a number close to 3.5; the distribution was often additionally "squashed," in the sense that the density fell off more rapidly in the direction perpendicular to the Galactic plane). This was sensible when it was expected that halo stars were formed during a rapid collapse of a monolithic gas cloud from which the Milky Way was formed (Eggen et al. 1962; ELS). It even seemed sensible when the subsequent model of Searle and Zinn (1978; SZ), which described the buildup of stars in the halo through mergers, was proposed; it was assumed that there were so many individual tidal streams that formed the halo that the overall density was relatively smooth.

We know now that tidal streams cause significant density substructure in galactic halos. Most of the earlier measurements of the parameters in the original power law models depended on which lumps of tidal debris were probed by the observations. While it is now clear that at least some of the halo built up through recent mergers, a portion of the halo stars could be part of a smooth density distribution. If there was an early period of rapid merging, the result would still be a smoothly varying spatial distribution of stars that also appears well-mixed in velocity. It is not currently known whether *all* of the stars in the halo were born in other, smaller galaxies that

4 H.J. Newberg

later merged with the Milky Way, or whether some of the stars were formed during an initial, rapid collapse of the Milky Way, as proposed by ELS in 1962. Power law models are still fit to the shape of the stellar halo, but a conscious choice must be made about whether to fit the density as a smooth component plus significant overdensities in large tidal streams, or whether to average the halo density over large volumes and thus include the large tidal streams in the fit.

In fact, the majority of the tidal debris that has so far been discovered is between 20 and 50 kpc of the Galactic center. It may be that interior to the Solar Circle the stellar halo consists of so many tidal streams that have been dispersed over so many orbits that the result is indistinguishable from a rapid collapse. Farther than 50 kpc, the satellites are subject to very weak tidal forces, very long orbital times, and may be very late to fall into the Milky Way's gravitational well. Therefore, these very distant satellites might not have formed tidal tails. Studies indicate that the fraction of halo stars in substructures is a few tens of percent within 30 kpc of the Galactic center, and the fraction increases at larger radii (see Ivezić et al. 2012, and references therein).

The Milky Way stellar halo may have a smooth, well-mixed component. But it also contains dwarf galaxies, globular clusters, tidal streams, and "clouds." The "clouds" are density enhancements in the halo that are many kiloparsecs across and could not possibly be gravitationally bound, but are also not drawn out into linear structures like tidal streams. These structures are thought to be the result of a minor mergers that come in on highly eccentric orbits, which take them near (or through) the center of the Milky Way. Simulations show that these mergers could result in a pile-up of stars at the apogalacticon of the orbit, which would look like a large cloud when viewed from inside the Milky Way.

In addition to the Milky Way, tidal streams have also been observed in other galaxies (see, e.g., Chaps. 8 and 9 of this volume). These streams are most notable in large galaxies close to the Milky Way, such as the Andromeda galaxy (M31; discussed in Chap. 8). Note that we are using the term "tidal stream" to mean the stars pulled from a satellite during a minor merger with a much larger galaxy. This is a distinct phenomenon from the ejection of stars or gas that may occur during a major merger between two galaxies of similar size. Major mergers can form structures that give a stream-like appearance. A classic example of this latter type of structure is the Antennae Galaxies (NGC 4038 and NGC 4039).

1.2 The Discovery of Tidal Streams in the Milky Way

1.2.1 Dwarf Galaxies and Moving Groups

During the last two decades of the twentieth century, following the landmark paper of Searle and Zinn (1978), the Galactic structure community began to consider the possibility that dwarf galaxy mergers could be shaping the morphology of the Galactic halo. Rodgers et al. (1981) observed metal-rich, main sequence A stars near the south Galactic pole. Because these stars were far from the star-forming

regions of the Galactic disk, and main sequence A stars have a limited lifetime (and therefore cannot be found far from their place of birth), they concluded that the A stars could have been the result of an encounter between the Milky Way and a dwarf galaxy. Although twenty years later these stars were identified as more likely blue stragglers in the thick disk (Girard et al. 2004), the paper was important in pushing astronomers to look for halo moving groups that would result from dwarf galaxy mergers. At that time, blue straggler stars were thought to exist only in globular clusters, where the high stellar density would result in stellar mergers and/or larger binary fraction.

It was quite reasonable in the 1980s to assume that all main sequence A stars must be young. In fact, a decade later, Preston et al. (1994) were still operating under the assumption that blue stragglers were preferentially found in the high stellar density environments of globular clusters; field main sequence stars were still strongly argued to be young. We now believe that some (or all) blue stragglers are the result of mergers of binary stars. This process produces a high mass main sequence star long after the initial formation of the stellar population. Blue stragglers can form at any time, in any stellar population, regardless of stellar density.

Though evidence for moving groups of halo stars continued to grow through the late 1980s and early 1990s, the first solid evidence for tidal streams in the Galactic halo was presented by Majewski et al. (1996). This paper is the third in a series that measures the proper motions and radial velocities of stars near the north Galactic pole, within 8 kpc of the Galactic plane, and finds a retrograde moving group of 20 stars with a net velocity down towards the Galactic plane. In addition to this dominant group, they find evidence for additional velocity substructure. Though this particular moving group has not yet been connected to other tidal substructure, many observations have since shown the same phenomenon; if a small volume of halo stars are studied, significant structure in the velocities of the stars is observed. At the same time, theoretical studies of the growth of galaxies in cold dark matter (CDM) cosmology concluded that galaxies grew through mergers (Frenk et al. 1988).

The discovery of the Sagittarius dwarf galaxy, which appeared to be in the process of tidal disruption (Ibata et al. 1994), added to the evidence for hierarchical merging. Here was a modern-day example of a dwarf galaxy in the process of being assimilated into our galaxy. Milky Way globular clusters were identified as possibly stripped from the Sagittarius dwarf spheroidal (Da Costa and Armandroff 1995). And Lynden-Bell and Lynden-Bell (1995) suggested that other halo globular clusters could represent "ghostly streams" from dwarf galaxy mergers with the Milky Way, though they were not able to show that any of their suggested streams were "unequivocally real."

In the last decade of the twentieth century, people were talking about kinematic discovery of tidal streams in the halo, but there was no expectation that the tidal streams would be detectable in stellar density. There were expected to be a large number of tidal streams, that came in from random directions, and each contributed a very small fraction of the density at any position in the halo. The tidal debris from dwarf galaxies would be detectable as a moving group in the Galactic halo

for more than a gigayear (Johnston et al. 1995) and would remain on great circles for more than a gigayear (Johnston et al. 1996). Because models of dwarf galaxy tidal disruption showed that the Sagittarius dwarf galaxy could not have survived on its present orbit for the age of the Milky Way, models with mass-to-light ratios of 100 were put forward to explain its survival until the present day (Ibata et al. 1997). Later, it would be suggested that dwarf galaxies could be deflected into their present orbits by other dwarf galaxies or by the large number of dark subhalos expected to be present in the Milky Way's halo, so that it was not required for the Sagittarius dwarf in particular to have survived on its current orbit for a substantial fraction of the age of the Universe.

It should be noted here that there is a vast literature on galaxy mergers in the second half of the twentieth century, and it is a bit difficult to define when the community started to recognize halo substructures in external galaxies that are similar to the Sagittarius dwarf tidal stream in our galaxy. The term "tidal stream" was used to describe the distortions induced in galaxies during major mergers, rather than the way we are using it in this book: to describe a group of stars that have been torn off of a much smaller satellite during an accretion event. Conference proceedings were published showing very faint tidal features in external galaxies in the late 1990s, but we particularly highlight a paper by Shang et al. (1998), that was published at about the same time the Sagittarius dwarf and its tidal stream were being discovered in the Milky Way. In this paper they discovered a dwarf galaxy in NGC 5907 that is of similar size to the Sagittarius dwarf galaxy. They suggested that this dwarf galaxy could be causing the previously observed warp in H I. They also identified a faint, elliptical ring that appeared to be the remains of a dwarf galaxy that had been tidally disrupted.

Helmi et al. (1999) successfully identified kinematic substructure in the stellar halo near the Sun, where accurate 3D velocities were available. They examined the 3D kinematics of 97 low metallicity giant and RR Lyrae stars within 1 kpc of the Sun, and found that about 10% of them had similar velocities. We show a re-reduction of Hipparcos catalog data used in that paper in Fig. 1.1. Helmi et al. concluded that 10% of all metal-poor halo stars outside of the solar circle were accreted from one dwarf galaxy merger with the Milky Way, under the assumption that the local halo represented the halo as a whole. While the moving group of stars was confirmed by Chiba and Beers (2000), the idea that it represented a component of the entire halo was not. Subsequent papers refer to the moving group as a tidal stream from a satellite that was accreted 6–9 billion years ago, and which comprises about 5% of the local halo (Kepley et al. 2007).

This success in kinematic detection of halo substructure helped to launch the "Spaghetti Survey" (Morrison et al. 2000) which aimed to find kinematic substructures through the Milky Way halo using high latitude pencil beam surveys; small fields were imaged in colors that allowed the photometric identification of red giant and blue horizontal branch stars, for which spectra were later obtained. The final sample (Starkenburg et al. 2009) included 101 well-observed halo giant stars, of which 20% were known to be members of tidal streams. The survey concluded that between 10 and 100% of halo stars are in (presumably accreted) substructure.

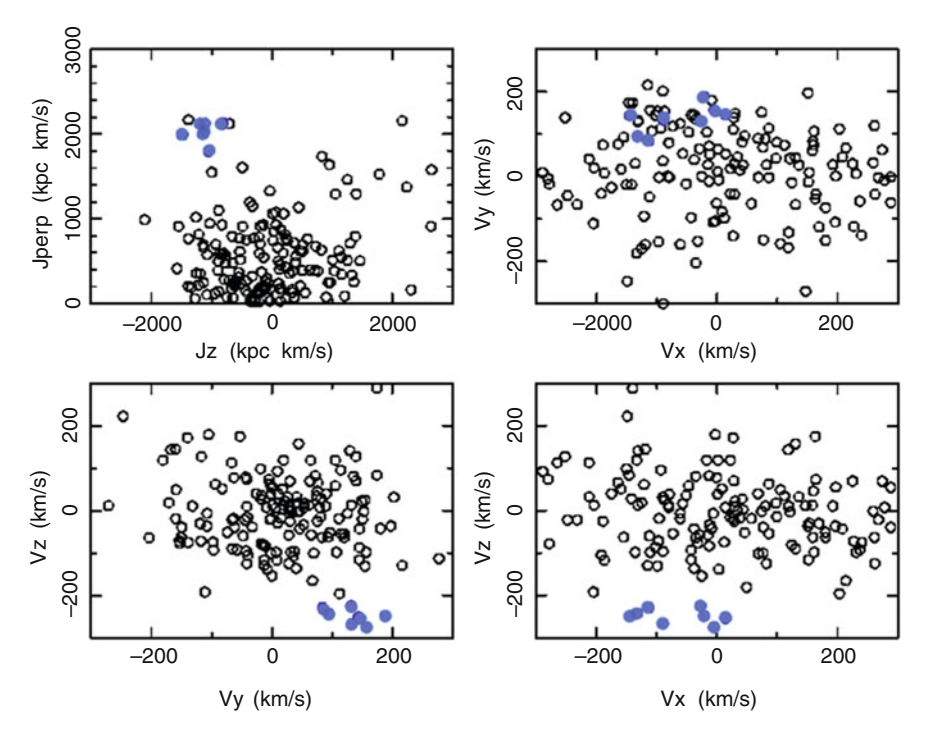


Fig. 1.1 These panels show the local velocity distribution and angular momentum $(J_Z \text{ and } J_{\text{perp}} = \sqrt{J_X^2 + J_Y^2})$, in Galactic *XYZ* coordinates, of nearby stars in the Hipparcos survey, following Helmi et al. (1999). Here, *X* points in the direction from the Sun to the Galactic center, *Y* is in the direction of solar motion, and the coordinate system is *right-handed*. The sign of the angular momentum is opposite to the original paper, which used a *left-handed* coordinate system. The *blue filled circles* identify stars in a coherent halo moving group

1.2.2 Halo Substructure in the Era of Large Surveys

The Sloan Digital Sky Survey (SDSS; York et al. 2000) was designed to map the large scale structure of the Universe by measuring the positions of galaxies. The distances to about one million of the brightest galaxies in 10,000 square degrees would be measured from spectroscopically determined redshifts. The brightest galaxies would be selected from a high accuracy imaging survey of the sky in five optical passbands: u, g, r, i, and z. Although the extragalactic program provided the primary science driver for the survey, the project provided tremendous opportunities for all other areas of astronomy, and was particularly influential in fostering the field of tidal streams.

First light for the SDSS was obtained in May of 1998, when the imaging survey began with observations of a 2.5°-wide stripe of data along the Celestial Equator (since observations on the equator did not require the telescope to track).

8 H.J. Newberg

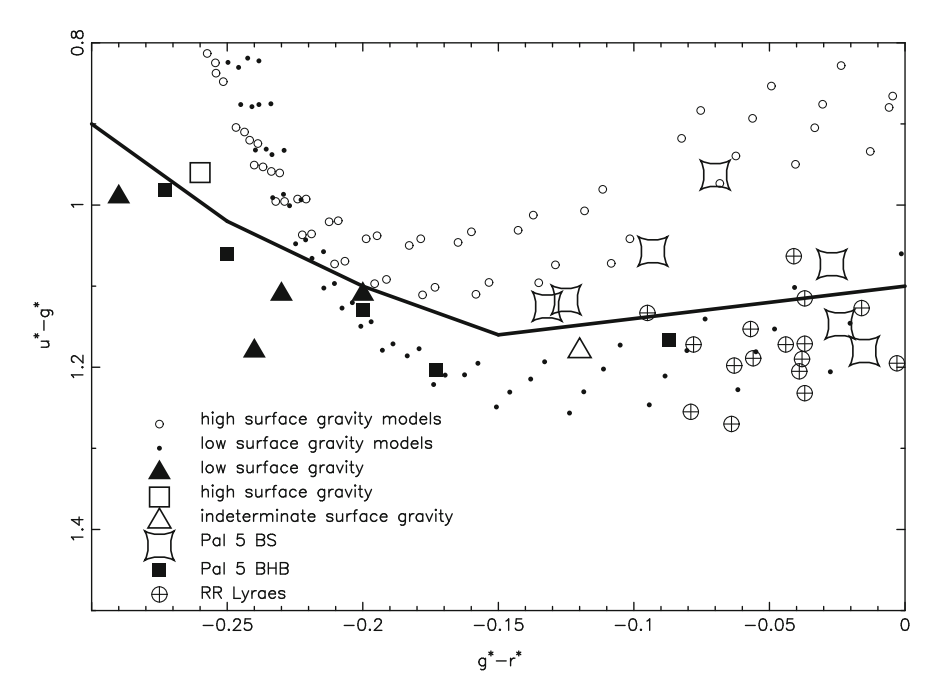


Fig. 1.2 This plot shows how low surface gravity BHB stars can be separated from high surface gravity BS stars using *ugr* colors. The colors of model stars, with varying metallicity, are from Lenz et al. (1998). Also shown are colors of BHB and BS stars in Pal 5, and several other stars with spectroscopically determined surface gravities. The *heavy black line* is the empirical curve that roughly separates BHBs and BSs by color. Adapted from Figure 10 of Yanny et al. (2000)

Unexpected density substructure in the Galactic halo was apparent from the very beginning, though because these were early data reductions it took us some time to believe that what we were seeing was not an observational artifact.

The first (gravitationally unbound) halo substructure in density was found from blue horizontal branch and blue straggler stars in the first 2.5° -wide stripe of SDSS imaging data on the Celestial Equator. Yanny et al. (2000) selected blue stars (-0.3 < g - r < 0.0), that were initially expected to consist entirely of blue horizontal branch stars; main sequence A stars and blue stragglers were generally thought to be absent in field halo populations. This paper showed that there were two large over-densities of stars—one in the north Galactic cap, and one in the south. It was also shown that the overdensities included both blue horizontal branch stars and blue stragglers. The blue stragglers were two magnitudes fainter, and could be roughly separated from the BHB population with ugr colors (Figs. 1.2 and 1.3). The structure in the north Galactic cap was also discovered in SDSS RR Lyrae stars at about the same time (Ivezić et al. 2000). Because these substructures were diffuse and unlikely to be gravitationally bound, we assumed they were two separate, tidally disrupting structures in the Galactic halo.

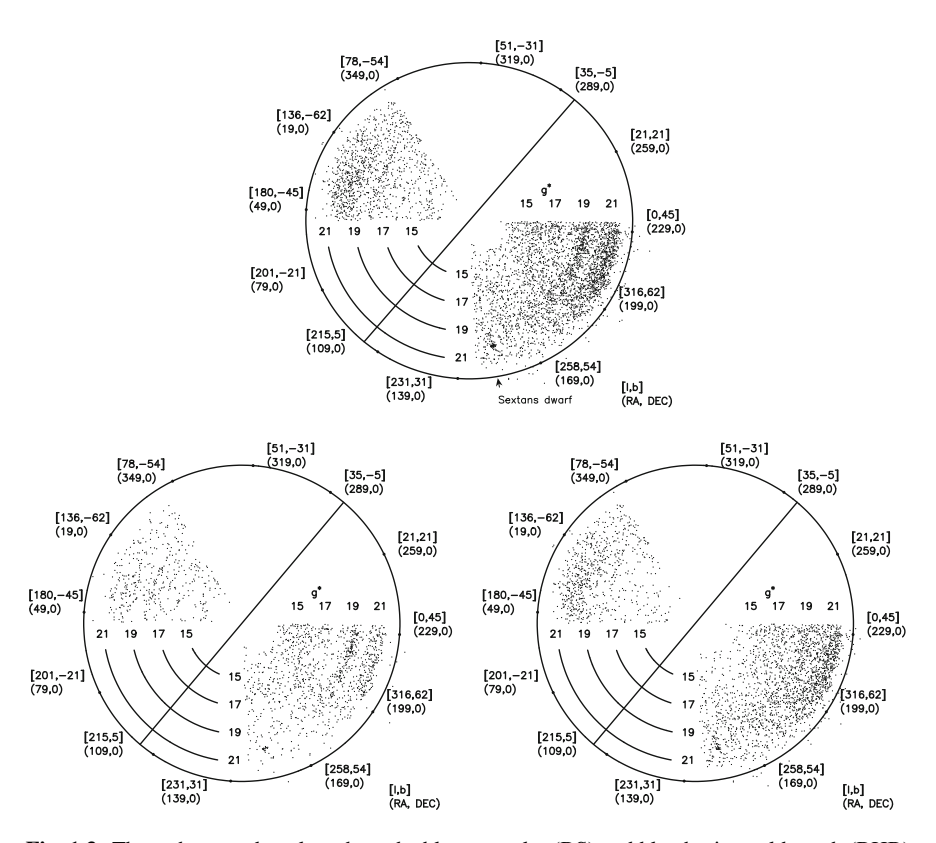


Fig. 1.3 These three wedge plots show the blue straggler (BS) and blue horizontal branch (BHB) stars along the Celestial Equator, as selected from early data from the SDSS. Galactic coordinates are in square brackets and Equatorial coordinates are in parentheses; the *solid line* shows the intersection of the Celestial Equator and the Galactic plane. The *top plot* shows all stars with dereddened colors $0.8 < u^* - g^* < 1.5$ and $-0.3 < g^* - r^* < 0.0$; the *lower plots* show BHBs (*left*) and BSs (*right*), selected by color as shown in Fig. 1.2. The denser arcs at $195^\circ < \alpha < 230^\circ$ and $20^\circ < \alpha < 40^\circ$ show the positions where the Sagittarius dwarf tidal stream crosses through the Celestial Equator. The fainter arcs (larger *g* magnitude) are the intrinsically fainter BS stars, at the same distance as the BHB stars, which are about two magnitudes brighter. Notice that the BHB stars in the southern (*upper left*) part of the Sagittarius stream appear to be offset in angle from the BS stars. It turns out that the Cetus Polar Stream (CPS Newberg et al. 2009), which is very rich in BHB stars, happens to cross through the Celestial equator at almost the same position as the Sgr dwarf tidal stream, and most of the southern BHBs that we originally thought were part of the Sgr stream are actually from the CPS. Adapted from Figures 3, 11, and 12 from Yanny et al. (2000)

It turned out, though, that these two apparently separate structures are two cross sections through the Sagittarius dwarf tidal stream, which is the most prominent tidal stream in the Milky Way. This was shown by Ibata et al. (2001b), who traced the tidal stream across the sky with carbon stars. Two years later, this tidal stream was traced across the sky in M giant stars identified photometrically in the Two

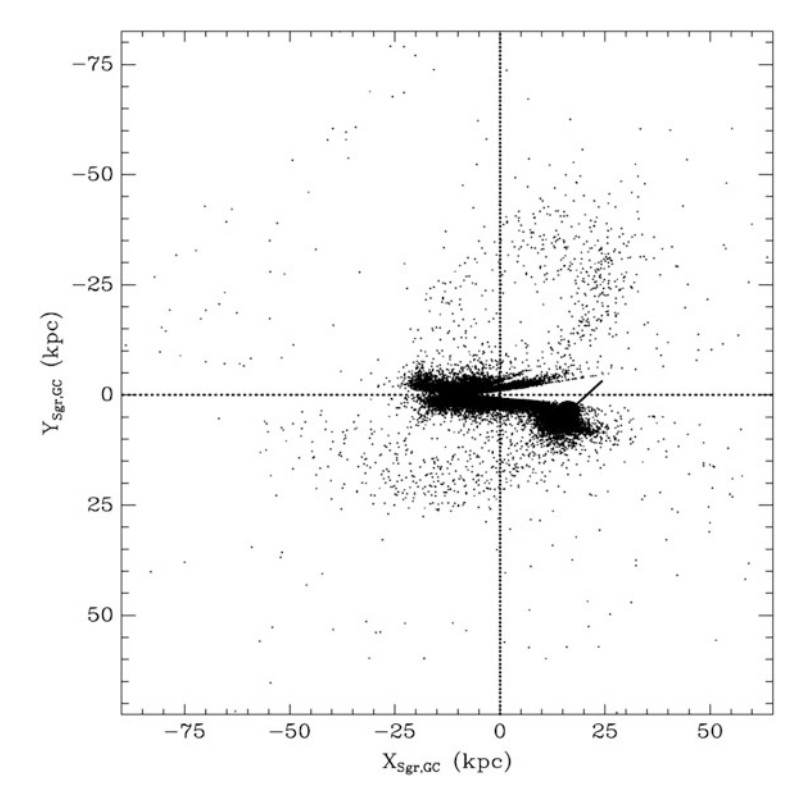


Fig. 1.4 The positions of M giant stars within 10° of the Sgr dwarf tidal stream, selected from 2MASS, are shown. The $(X_{Sgr,GC}, Y_{Sgr,GC})$ coordinates are the Sagittarius dwarf stream coordinates, where the stream is in the plane $Z_{Sgr,GC} = 0$. Because the Sgr stream is close to polar, this plot is roughly equivalent to Galactic Z vs. X, where the *center* of the Galaxy is at (0,0), the Sun is at X = -8.5, Y is the direction of solar motion, and Z points towards the north Galactic pole. The Sgr dwarf is shown by a *large filled circle* and a *line* indicating the direction of its motion. The M giants trace the path of the Sgr dwarf tidal stream all the way around the Galaxy. Adapted from Figure 11 from Majewski et al. (2003)

Micron All-Sky Survey (Fig. 1.4, Majewski et al. 2003). The discovery of a large tidal stream in the Milky Way galaxy was quickly followed up by the discovery of a large tidal stream in the Andromeda galaxy (Ibata et al. 2001a), the Milky Way's nearest neighbor.

Thus was born the field of tidal streams. Although the Sagittarius dwarf galaxy tidal stream remains the most prominent and well-studied tidal stream in the Milky Way, even fifteen years later we are still struggling to model the tidal disruption of this dwarf galaxy. At first, many researchers assumed that the tidal stream from the Sagittarius dwarf galaxy was an anomaly—that this was the only tidal stream that would be identified as a stellar overdensity rather than a co-moving group of stars. The discovery of density substructure was, after all, unexpected.

It was not long, however, before additional substructure began to be discovered. Vivas et al. (2001) found an overdensity of RR Lyrae stars in the Virgo constellation. Tidal tails were found extending tens of degrees from the Pal 5 globular cluster (Odenkirchen et al. 2001; Rockosi et al. 2002). Previous to these papers, globular cluster "tidal tails" referred to stars outside the tidal radius of the globular cluster, that were identified as "wings" in the density profiles (Grillmair et al. 1995).

In 2002, Newberg et al. made the seminal discovery that the density of main sequence turnoff stars in the Galactic halo is quite lumpy, and is a poor fit to a smooth, power law density profile. The density of turnoff stars on the Celestial Equator (Fig. 1.5) includes a wealth of halo substructure. In this slice through the Celestial Equator, one can see the Sagittarius dwarf tidal stream in both the northern and southern Galactic hemispheres; the Pal 5 globular cluster, which turns out to have long tidal tails; the overdensity in Virgo that was identified by Vivas et al. (2001); stellar concentrations towards the Galactic center that could be due to a smooth component of the stellar spheroid, but also include stars in what was later named the Hercules-Aquila Cloud (Belokurov et al. 2007); a controversial overdensity near the anticenter commonly referred to as the "Monoceros Ring;" a more distant overdensity south of the Galactic plane called the "Triangulum-Andromeda Stream" (identified in the original paper as Monoceros in the south); and two concentrations of closer stars near the anticenter (one in the north and one in the south) that appeared be due to the disk but at the time did not fit any disk model.

Also in 2002, Ferguson et al. showed that there was spatial and metallicity substructure in the halo and outer disk of M31 (Fig. 1.6), using red giant branch stars in a panoramic photometric survey of this galaxy. M31 is the closest large, spiral galaxy to the Milky Way, and has provided a complementary view of tidal structure in spiral galaxies. While the Milky Way allows us to see stream structure in three dimensions, it is much easier to see the overall halo structure in external galaxies.

The discovery of lumpy outer halos containing tidally disrupting dwarf galaxies in both the Milky Way and Andromeda (M31) bolstered the idea that galaxy formation happens through a series of mergers. The lumps in the halo are evidence that small mergers continue to happen at late times, and the Sagittarius dwarf galaxy is an example of a merger that is still happening today. Since these discoveries, many more tidal streams have been discovered in both galaxies, and also in galaxies outside of the Local Group.

An amazing map of the density of Milky Way turnoff stars, color-coded by distance (see Fig. 1.7), was published by Belokurov et al. (2006); it shows the most prominent tidal streams in the north Galactic cap, spread out across the sky. In this image one can see not only the Sagittarius dwarf tidal stream, but also a fainter tidal stream next to it that may also be associated with Sagittarius. So far no model has been able to simultaneously fit both of the "bifurcated" streams. The Virgo Overdensity is also conspicuous, as is the "Monoceros Ring," and another smaller tidal stream called the "Orphan Stream" because it has no known dwarf galaxy progenitor. The Orphan Stream progenitor either has yet to be discovered or has been completely disrupted.

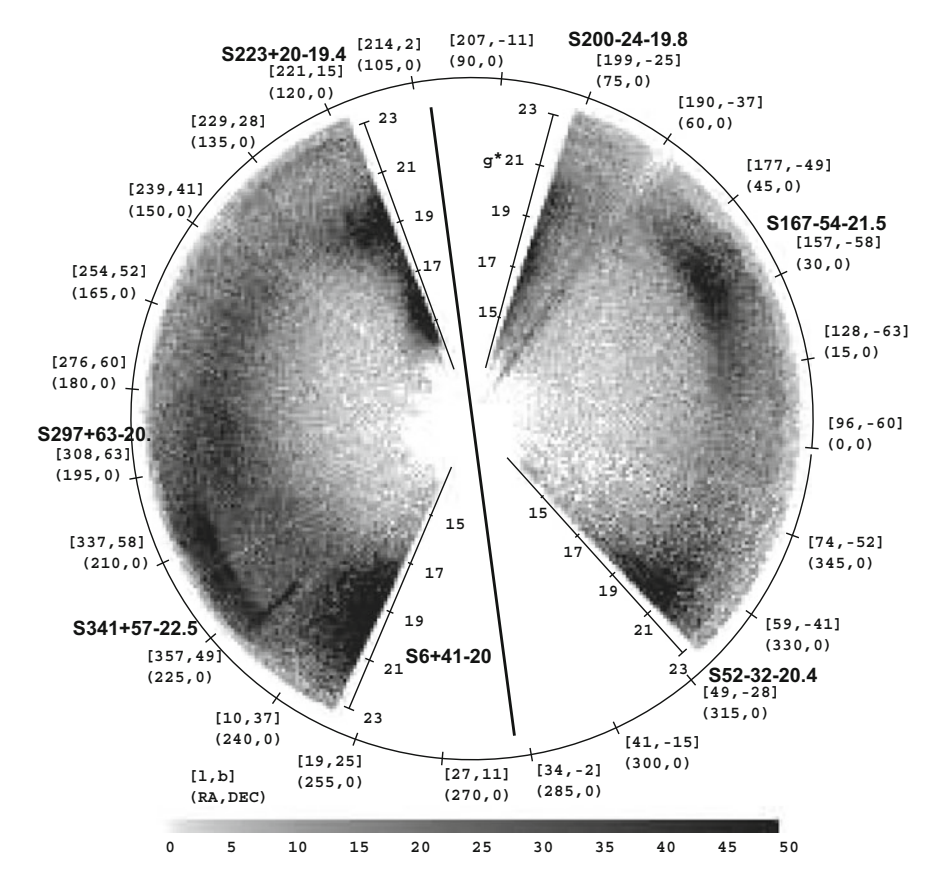


Fig. 1.5 Wedge plot (g vs. RA) showing the density of 334,066 SDSS turnoff stars (0.1 < (g-r) < 0.3) on the Celestial equator. This illustrates the discovery that the Milky Way's stellar halo contains a tremendous amount of density substructure. The extent and nature of this substructure remains an active area of research, but much of the observed substructure arises from dwarf galaxies that have fallen into the Milky Way and been tidally disrupted. The angle shows right ascension, and apparent g* magnitude increases along radius. The solid line indicates the intersection between the Celestial Equator and the Galactic plane. The Pal 5 globular cluster is evident at $(\alpha, g) = (229^{\circ}, 21)$; the radial extent in the diagram is due to the spread in the absolute magnitudes of turnoff stars. The Sagittarius stream is at $(l, b, g) = (341^{\circ}, 57^{\circ}, 22.5)$ in the north Galactic cap, and at $(l, b, g) = (167^{\circ}, -54^{\circ}, 21.5)$ in the south Galactic cap. The Virgo Overdensity is at $(l, b, g) = (297^{\circ}, 63^{\circ}, 20.0)$. The Hercules-Aquila Cloud juts out from the overdensity at $(l, b, g) = (52^{\circ}, -32^{\circ}, 20.4)$. There is a region of high extinction near $\alpha = 60^{\circ}$ that affects the identification of turnoff stars; the radial feature there is not an actual density substructure. Near the Galactic anticenter, $70^{\circ} < \alpha < 135^{\circ}$, overdensities can be seen north of the plane at g = 15 (attributed to the disk in the original paper), south of the plane at g = 17 (identified as the Monoceros ring in the south by Ibata et al. 2003), north of the plane at g = 19.4 (the Monoceros Ring), and south of the plane at g = 20 (the Triangulum-Andromeda stream, identified as the Monoceros ring in the south in the original paper). The feature labeled $(l, b, g) = (6^{\circ}, 41^{\circ}, 20)$ is the only overdensity that could plausibly represent the smooth distribution of spheroid stars that had been previously expected. Adapted from Figure 1 from Newberg et al. (2002)

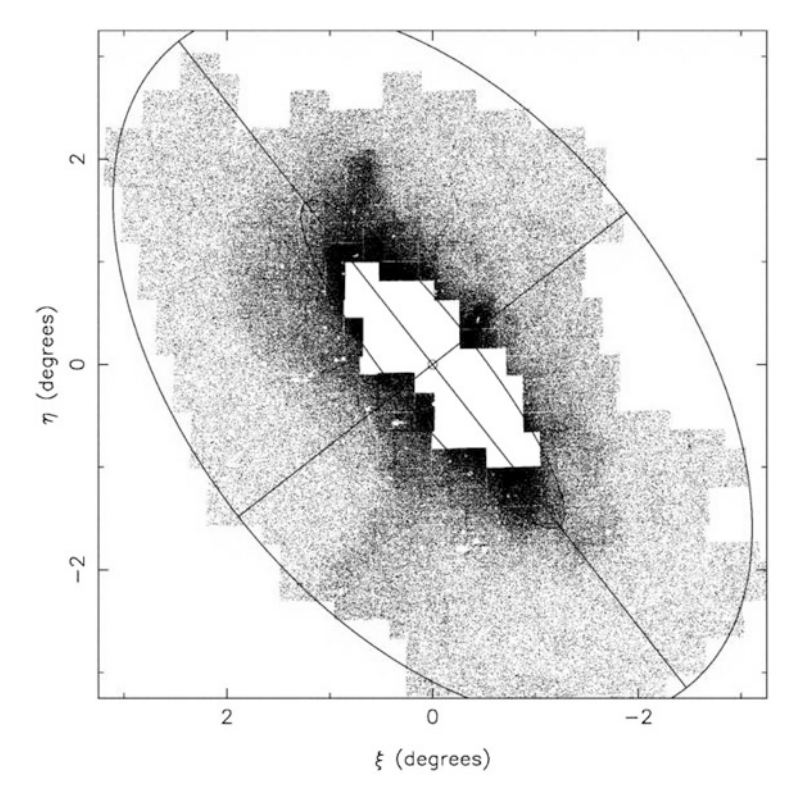


Fig. 1.6 We show the surface density of redder red giant branch (RGB) stars in Andromeda (M31). The *outer ellipse* has a semimajor axis length of 55 kpc; the *inner ellipse* has a semimajor axis of 27 kpc and is well outside of the region containing the optical disk of M31. Halo substructure, including the giant stellar stream at $(\xi, \eta) = (0.5, -1.5)$ and lumpy structure surrounding the disk, is apparent. This image showed that the halo of Andromeda contained significant density substructure, just as is seen in the Milky Way. Adapted from Figure 2 from Ferguson et al. (2002)

Also apparent, nearer to the Galactic center, is the Hercules-Aquila "cloud." Overdensities that are not long and thin like tidal streams, but instead look like large, amorphous clumps are referred to as "clouds." These could be produced by tidal debris from a dwarf galaxy on an orbit that takes it near the center of the Milky Way galaxy (Hernquist and Quinn 1988). The tidal disruption is severe as the dwarf galaxy goes through the center of the Milky Way, where the tidal forces are strong. The stars that have been tidally stripped then orbit back and forth through the Galactic center, spending a larger fraction of their time at apogalacticon, where they are observed as amorphous "clouds" of stars. Note, however, that it has been suggested that at least one of these clouds (the Virgo Overdensity) could be the disrupted remains of a dwarf galaxy that is on a highly eccentric orbit, but just recently passed perigalacticon and thus does not consist of debris piled up at the apocenter of its orbit (Carlin et al. 2012).

14

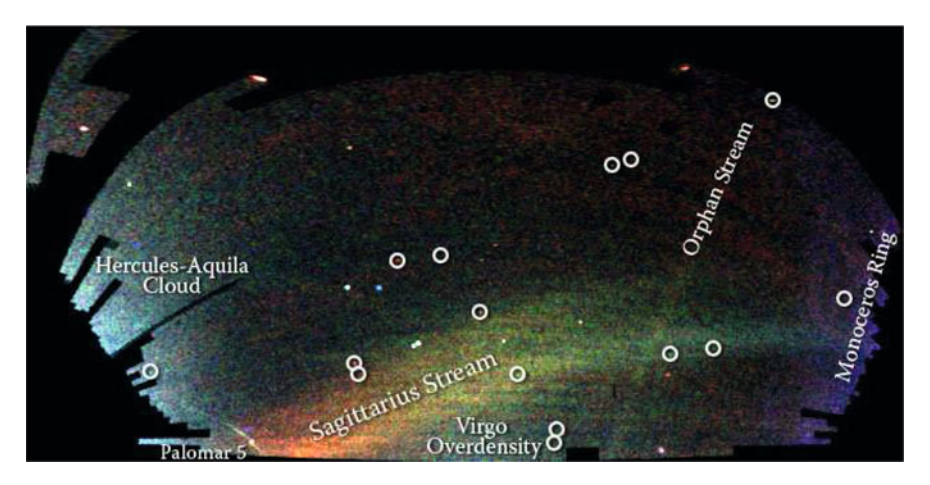


Fig. 1.7 This spectacular image of density substructure in the Milky Way's stellar halo is known as the "Field of Streams." Declination vs. right ascension (increasing towards the *left*) is shown for SDSS turnoff stars in the north Galactic cap. This is an RGB composite where *blue* represents the brighter (closer than about 15 kpc) stars, and *red* represents the faintest (more distant than about 25 kpc) stars. Note that there appear to be two branches to the Sagittarius Stream, and a multitude of halo substructures. The *circles* indicate the positions of new Milky Way satellites discovered in SDSS data; two are faint globular clusters and the others are faint dwarf galaxies. Image credit: V. Belokurov and the Sloan Digital Sky Survey

While this section gives an historical account of the major observational milestones in the beginning of the field of tidal streams, the succeeding chapters of this book describe in detail the discoveries that have since been made. When spatial substructure in the halo was first discovered, Don York, from the University of Chicago, said we had discovered "Eggen's spaghetti sky." The same Olin Eggen that is famous for a paper suggesting the Milky Way formed from the rapid gravitational collapse of a cloud of gas (Eggen et al. 1962) is also famous for seeing clumps of stars in imaging data, and in particular introducing the concept of "moving groups" of stars (Eggen 1958a,b,c; Eggen and Sandage 1959)—stars that are in a similar volume of space and moving in the same direction. Although his moving groups are likely from tidal disruption of open clusters in the disk rather than dwarf galaxies and globular clusters in the halo, the image of a sky filled with stars from tidally disrupted clusters mixed together like a bowl of spaghetti is a common analogy. Majewski et al. (1996) make a similar analogy to a "can of worms." However, the width of these stellar streams is astonishing. The tidal stream from the Sagittarius dwarf galaxy, for example, has a width of about 6 kpc. For reference, the distance from the Sun to the Galactic center is about 8 kpc, and the radius of the disk is about 15 kpc. The width of 6 kpc is a substantial fraction of the width of the Milky Way. Although tidal streams from globular clusters might create "spaghetti" in the sky, dwarf galaxies like Sagittarius are made of much thicker pasta! Perhaps we should call it the "rigatoni sky!" This is of course written in jest, but one should not forget the enormous spatial extent of some of these streams and clouds.

1.3 Observational Techniques for Finding Substructure

Tidal streams can either be identified as an overdensity of stars in the halo, or by finding stars with similar locations and velocities (using angular momentum alleviates the need for co-location). The latter technique will allow the identification of tidal streams with lower surface density, a longer time since disruption of the satellite, or which are closer to the Galactic center where the stellar density is higher.

1.3.1 Standard Candles and Photometric Parallax

The most straightforward way to identify tidal streams by stellar density is to determine the three dimensional positions of halo stars and then look for localized regions that have densities higher than their surroundings. Measuring positions in 3D requires that one know the distance to each star, so particular stars with known absolute magnitude (standard candles) must be selected. Often, these standard candles are selected photometrically based on their colors, but they might also be selected from spectroscopy or as variable stars.

Figure 1.8 shows a color-magnitude diagram (CMD) of stars from the Palomar 5 globular cluster, showing typical features for an old, metal-poor stellar population. The brighter stars (which allow us to probe the distant halo) include blue horizontal branch stars, RR Lyrae variables, red giant branch stars, M giants, blue stragglers, K giant stars, and turnoff stars (note that not all of these types are present in Pal 5!). There are advantages and disadvantages to using each type of star.

Horizontal branch stars are good standard candles because they occupy a very narrow range of absolute magnitude. Blue horizontal branch stars (BHBs) can be preferentially selected by blue color, though with some contamination from blue straggler stars, which have the surface gravities of main sequence stars. However, BHBs are only present in very old, metal-poor stellar populations, and there are relatively few stars of this type. Red horizontal branch stars are more difficult to identify due to confusion with giant branch stars and much fainter main sequence stars

RR Lyrae stars are even better standard candles, but are harder to identify (usually through multi-epoch variability studies), and also appear only in intermediate-age, fairly metal-poor populations. RR Lyrae stars are even sparser tracers of the stellar density than horizontal branch stars. Additional observations (spectra and/or time-series photometry) are required to determine the distance to each RR Lyrae star.

M giant stars are extremely bright, but only found in metal-rich stellar populations, which are rare in the halo of the Milky Way. In fact the only verified tidal stream that has been traced with M giant stars is the largest and most apparent overdensity: the Sagittarius dwarf tidal stream (see Chap. 2). The Monoceros Ring, Triangulum-Andromeda cloud (see Chap. 3), and Pisces Overdensity (Sharma et al. 2010) have also been studied in M giants.

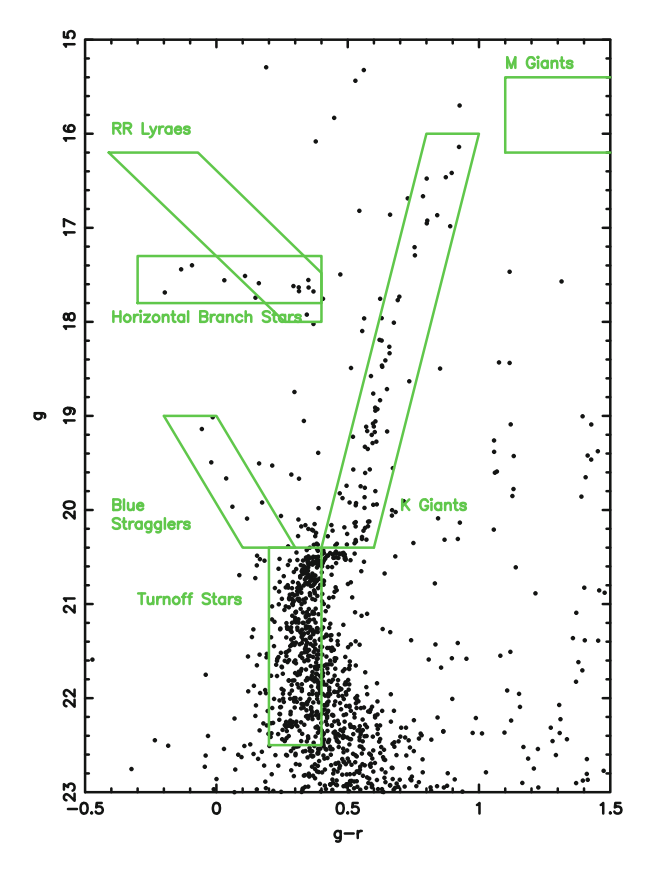


Fig. 1.8 The color-magnitude diagram shows stars that can be used to trace Galactic structure. The *black points* are SDSS stars within four arcminutes of the Pal 5 globular cluster, and represent the distribution of stars in the halo population. In a magnitude-limited survey, brighter stars sample the galaxy to larger distances, but they are not very numerous. Turnoff stars have been popular for tracing halo structure because they are easily identified by *color*, and are the brightest of the more numerous main sequence stars. The drawback to turnoff stars is that they have a large spread in absolute magnitude, so individually they are not good standard candles. This difficulty is somewhat mitigated by the fact that, for halo stars in the Milky Way, the absolute magnitude distribution is not a strong function of population. Therefore, statistical photometric parallax can be used to recover the underlying density distribution from the positions and apparent magnitudes of turnoff stars. Adapted from Figure 1 of Newberg (2013)

K giant stars are a natural choice for tracing stellar densities because they are more numerous than other stars of similar intrinsic brightness, and present in all old stellar populations. The main drawback to using K giant stars is that spectra (or specialized filters that are particularly sensitive to the gravity of K stars; see, e.g., Majewski et al. 2000) are required to separate K giants from the much more numerous K dwarf stars in the disk, which have similar apparent magnitudes as K giant stars in the halo. Additionally, the absolute magnitude depends on the age and

metallicity, and is a strong function of color (red giant branches are nearly vertical in the CMD); the measured distances will depend heavily on the model used to calibrate them.

Blue stragglers are best separated from blue horizontal branch stars using spectra, but they can be roughly separated if there is data in the u, g, and r filters. These stars are not usually used to trace stellar populations because they are not good standard candles (absolute magnitude is a strong function of color), they are fairly rare, and they are not as bright as giant stars so they do not probe as far in distance. However, they are often observed in tidal streams, two magnitudes fainter than the blue horizontal branch stars, and must be considered particularly when using BHB stars to trace stellar density.

Turnoff stars are much more numerous than any of the other types of stars considered above, but they are by far the worst standard candles—spanning at least two magnitudes at about constant color. When using this type of star to measure density along the line-of-sight, it is advantageous to use *statistical photometric parallax*, which is described in Sect. 1.3.3.

1.3.2 Matched Filter Techniques

Matched filter techniques are used in many applications to optimally extract signal from noise. In general, one convolves the observed, noisy signal (as a function of either space or time) with a template (filter) that looks like the expected signal. This will enhance signal and suppress noise.

In this case, we would like to find the angular density of stars in a tidal stream population (that have a known distribution in color and apparent magnitude), while filtering out stars that are from other disk or halo populations (for which it is also possible to construct an expected distribution in color and apparent magnitude).

Matched filtering was first used to detect tidal streams by Rockosi et al. (2002), who discovered the tidal tails of the Pal 5 globular cluster in SDSS data. The matched filter technique described here follows the description in that paper. In this version of the matched filter, the cluster stars that are in regions of the color-magnitude diagram where few background stars are expected are weighted more heavily; a *minimum variance estimate* (defined below) for the number of cluster stars is derived, rather than a maximum signal-to-noise estimate. By more heavily weighting the stream detections in regions of low background, systematics from poor knowledge of the background are reduced.

One defines a normalized probability in color-magnitude space that describes where one expects to find stars in the stellar population of the stream (including primarily turnoff, giant, and blue horizontal branch) as N_{str} . In the case of Pal 5, the CMD of the cluster itself, normalized so the total probability integrated over the whole color-magnitude diagram is one, is used for N_{str} . In addition, one defines a probability (per element of solid angle) in color-magnitude space for the background, N_{bg} . In general, this background depends on Galactic latitude and

18 H.J. Newberg

longitude. Then, an estimate for the number of stream stars, α , in a given solid angle can be found by minimizing the following expression for χ^2 :

$$\chi^2 = \sum_{color,mag} \frac{\{N(color,mag) - [\alpha N_{str}(color,mag) + N_{bg}(color,mag)]\}^2}{N_{bg}(color,mag)},$$

where N(color, mag) is the number of stars in a particular color, magnitude bin, per element of solid angle. The sums are over all of the bins that have a non-zero number of stars expected in the stream. The background must be constructed so that the expected number of stars is also non-zero in all of these bins. This equation can be solved for the α that corresponds to the minimum χ^2 by setting the first derivative with respect to α equal to zero:

$$\alpha = \frac{\sum\limits_{color,mag}(\frac{N(color,mag)N_{str}(color,mag)}{N_{bg}(color,mag)} - N_{str}(color,mag))}{\sum\limits_{color,mag}\frac{N_{str}^2(color,mag)}{N_{bg}(color,mag)}}.$$

In the limit of infinitely small bins, the first term in the numerator can be replaced by a sum of $N_{str}(color, mag)/N_{bg}(color, mag)$ for each of the observed stars in a particular solid angle. The second term in the numerator and the denominator can be replaced by an integral over color-magnitude space rather than a sum over the individual bins.

In the case of Pal 5 tidal tails, N_{str} was derived from stars with high membership probability in the globular cluster. The background distribution, N_{bg} , was derived from stars in several square degree patches of actual SDSS data near the globular cluster. Because the background distribution was derived from the actual survey data, it includes features due to both the survey itself (including increased color errors and decreased completeness near the limiting magnitude of the survey), and the density distribution of stellar populations in the Milky Way. The tidal tails of Pal 5 were expected to be at about the same distance from the Sun as the cluster itself across the region surveyed, so no shift in apparent magnitudes of stream stars was considered. Because the parts of the background color-magnitude diagram that varied across the part of the sky surveyed were at colors and magnitudes where there were few stream stars, a varying background distribution was not considered in this paper. Rockosi et al. constructed a smoothed density plot of the tidal tails of Pal 5 with a resolution of 0.09° by finding the optimal value of α as a function of sky position.

Grillmair and Johnson (2006) modified this matched filter technique so that it could be applied to the discovery of tidal streams when the distance to the streams and the stellar population is not known a priori. The description here follows Grillmair (2009).

The probability distribution for the stream stars is generated from globular cluster stars observed in SDSS data. The mean g-r and r-i colors are determined for a fixed set of g magnitudes in each of the clusters; colors at other magnitudes are interpolated. The distribution can be shifted brighter or fainter to account for different distances to the tidal debris. The relative number of stars expected in the stream as a function of apparent magnitude (the luminosity function) is determined from example globular clusters with very deep photometry available, and modified by the expected completeness as a function of apparent magnitude for the SDSS survey. It is broadened in color by the amount of the expected photometric error as a function of apparent magnitude. An additional broadening with $\sigma=0.02$ magnitudes is also applied to account for the intrinsic dispersion in the colors of giant branch stars.

This new technique makes it possible to create a set of 2D pictures of the sky that show the matched-filter density maps of different stellar populations at different distances. These can then be searched for linear structures that indicate the presence of a tidal stream. One creates "filters" that consist of the expected color-magnitude distribution of stream stars in the SDSS, at different distances and using different globular cluster distributions as the template. A variety of background distributions, distances, and stellar populations, are used to create the 2D pictures. One can scan through a distance series of these pictures, for a fixed stellar population, to pick out linear structures that might vary in distance as a function of position in the sky.

1.3.3 Statistical Photometric Parallax

If one observes objects whose stellar type can be identified from photometry, and which therefore have a known absolute magnitude, then distances to these objects can be determined by *photometric parallax* (see Sect. 3.1). An example where photometric parallax for a large number of stars was used to measure the density of stars in the Milky Way is Jurić et al. (2008). They estimated the distances to 48 million SDSS stars of type G and later, under the assumption that they were main sequence stars (which most of them undoubtedly are), and using a photometric calibration from Ivezić et al. (2008). From the estimates of the individual distances, the positions of each star were derived, and from the resulting stellar densities the structure of the Milky Way (including tidal substructures) was derived.

In contrast, *statistical photometric parallax* (Newberg 2013) uses a statistical approach to determine the underlying spatial density of stars from the distribution of observed apparent magnitudes. It differs from *photometric parallax* because distances are not determined individually for each star. This technique has been used to determine the spatial distribution of stars in the Sagittarius dwarf tidal stream, using turnoff stars from the SDSS (Newby et al. 2013). Although turnoff stars have a wide variety of absolute magnitudes, and are thus not very good standard candles,

they are quite useful for density mapping because they are much more numerous than giant stars, and can be seen at larger distances than fainter, lower mass main sequence stars. Statistical photometric parallax is most successful for measuring structures with comparable (or higher) stellar density than the background at their location.

The basic concept of statistical photometric parallax is demonstrated in Fig. 1.5. There is a narrow, radial feature at RA = 229° at an apparent magnitude of $g \sim 21$. This feature is the globular cluster Pal 5, whose stars are all essentially the same distance from the Sun, but the apparent magnitudes of the turnoff stars in the figure span an apparent magnitude range from $g \sim 20$ to $g \sim 22.5$. The large range of apparent magnitude is a result of the large range of absolute magnitudes of turnoff stars. In fact, one could make a histogram of the apparent magnitudes of the Pal 5 turnoff stars, shift it by the distance modulus to Pal 5, and obtain the distribution of absolute magnitudes of color-selected Pal 5 turnoff stars.

Newby et al. (2011) showed that the distribution of absolute magnitudes of color-selected turnoff stars were similar for all halo globular clusters observed in the SDSS. This surprising observation is apparently a result of the age-metallicity relation for the Milky Way galaxy. Older stellar populations should have fainter, redder turnoffs because a larger number of the more massive stars have had time to evolve away from the main sequence. On the other hand, the older stellar populations are typically more metal-poor, and metal-poor main sequence stars are brighter and bluer than metal-rich stars of the same mass. It is surprising, but apparently true, that in the halo of the Milky Way these two effects nearly cancel so that the distribution of absolute magnitudes of blue turnoff stars is essentially the same for all halo stellar populations. Although the color of the turnoff will be slightly different for different ages and metallicities, the absolute magnitude distributions are surprisingly similar.

This age-metallicity conspiracy provides a great opportunity to apply statistical photometric parallax to measure the spatial density of halo stars, including the substructure from tidal streams. The observed halo substructure, for example as depicted in Fig. 1.5, represents the actual density structure, convolved with the absolute magnitude distribution of halo turnoff stars, and then modified by the observational constraints.

To determine the spatial density, we first construct a parameterized spatial density model. Given a particular set of parameters, one constructs the expected density distribution over a particular volume, derives from this the expected apparent magnitude distribution as a function of angular position in the sky (taking into account the known absolute magnitude distribution of turnoff stars), and then applies observational biases such as completeness. This expected distribution of stars can then be compared with the observed distribution of stars. The parameters can be optimized to most closely match the observed data. For example, Cole et al. (2008) used a maximum likelihood technique that was optimized with conjugate gradient descent to measure the density of tidal streams, and in particular the Sagittarius dwarf tidal stream, in the halo.

As with matched filtering, proper application of this technique includes many subtleties. For example, if turnoff stars are selected in a narrow color range, then the distribution of stars selected will depend on the color errors. Typically color errors increase considerably near the observation limits, so that stars with a wider range of colors are sampled at the faint end of the survey. Because there are few stars bluer than the turnoff, and many intrinsically fainter main sequence stars redder than the turnoff, the distribution of absolute magnitudes of apparently faint stars in a magnitude-limited survey includes a larger number of intrinsically faint stars.

A benefit of the statistical photometric parallax technique is that once the spatial density of a halo substructure is determined, it is possible to *statistically* remove stars with the spatial distribution of one halo structure or substructure from the sample, so that the remainder of the sample can be studied. Note, however, that it is not possible to determine which stars are actually a part of that structure or substructure.

1.4 Co-moving Groups of Stars

Several halo substructures have been initially identified as a group of stars of similar type (RR Lyrae, BHB, etc.), in a small volume, that have similar velocities. In some cases, these co-moving stars have been associated with a stellar overdensity that is clearly the result of tidal stripping. In other cases the spatial extent of the related stars is unknown. In this case the association may be referred to as an Element of Cold Halo Substructure (ECHOS, Schlaufman et al. 2009). The disadvantage to this technique is that it requires that the stars have known radial velocities as measured from stellar spectra, or measured proper motions, or both. The advantage is that as an increasing amount of astrometric and spectroscopic data become available, this technique will allow us to detect and characterize halo substructure with much lower density contrast that results from small mergers, old mergers, mergers where the satellite has been widely spatially dispersed (for example by passing through the center of the Milky Way), or tidal streams in high density regions of the Milky Way. Kinematically identified halo moving groups are covered in more detail in Chap. 5.

Halo tidal streams have not been identified inside the Solar Circle (within 8 kpc of the center of the Milky Way). This could be because these more central halo stars formed in situ or because they are due to a large number of well-mixed mergers. If the central regions formed from mergers, it might be possible to separate the stars into groups with similar angular momentum. The angular momentum coherence will persist for much longer than spatial coherence, and all of the stars that fall in with a particular satellite have similar angular momentum (see Chap. 6).

22 H.J. Newberg

1.5 Chemical Tagging

A star's chemical composition is determined by the chemical composition of the gas cloud from which it formed. Stars in the same open cluster or globular cluster are thought to be coeval and therefore have similar chemical composition (though at least some globular clusters contain more than one stellar population). If one assumes that most stars are born in star clusters, and that stars maintain a memory of the gas cloud in which they were formed because their outer layers contain the same chemical ratios as those gas clouds, then one could attempt to group stars by the cluster in which they were born (Freeman and Bland-Hawthorn 2002). This requires that one make very accurate measurements of a few tens of elemental abundances with high resolution spectroscopy. The hope is that the chemical abundances of primordial clusters are different enough that they are distinguishable in the observable abundance space. Chemical tagging, particularly of the Galactic disk, is the primary science driver of the GALAH survey (De Silva et al. 2015).

In contrast to star clusters, dwarf galaxies generally contain more than one episode of star formation. While studies of the angular momentum of halo stars will elucidate the history of satellite mergers that built up the halo, studies of stellar chemistry can tell us about the individual star clusters from which the stellar populations are composed. In particular, the lowest metallicity stars tell us about the conditions in the early Universe, when these stars formed, and about the earliest chemical enrichment processes. Intermediate metallicity stars require more than one episode of star formation (which is not guaranteed if gas is ejected from low mass dwarf galaxies in the first epoch of star formation), and teach us about the environments in which the stars were formed throughout the evolution of the Universe. It would be incredible if, at some time in the future, we could build up a record of both the accretion event in which each halo star became a part of the Milky Way, and the star formation event in which that star was born, within the accreted satellite.

Currently, only the simplest chemical tagging techniques have been applied to the detection of tidal streams (for example, the detection of debris from the globular cluster Omega Cen via its unique abundance signatures by Majewski et al. 2012), though streams are often characterized by their chemical composition.

Of particular interest is the variation of chemical composition as a function of the distance from the progenitor. Because the outer (higher velocity dispersion) layers of a satellite are tidally stripped first, the tidal streams can tell us about the density structure of the progenitor dwarf galaxy. We expect that higher metallicity stars are more centrally located in the dwarf galaxy, and therefore will be stripped at later times and be preferentially located nearer to the progenitor dwarf galaxy in the tidal stream. In fact, metallicity gradients have been reported in the Sagittarius dwarf tidal stream (see Chap. 2).

1.6 Constraining Dark Matter, the Formation of the Milky Way, and Cosmology with Tidal Streams

1.6.1 Rapid Collapse vs. Hierarchical Mergers

In the late twentieth century, there was rapid evolution in our understanding of galaxy formation. Eggen, Lynden-Bell and Sandage are credited with putting forward the monolithic "rapid collapse" picture of the formation of the Milky Way, in which halo stars were formed during the collapse of a proto-Galactic gas cloud. This picture was well summarized in a review by Eggen et al. (1973): "The oldest Population II objects (subdwarfs, globular clusters, metal-poor RR Lyrae stars) formed when the galaxy was extended and far from equilibrium, before much metal enrichment occurred. The remainder of the galaxy continued contraction to a disc-like configuration, approximately in centrifugal equilibrium, and dissipated the necessary energy before forming stars; rapid metal enrichment took place. This is the disc population. The residual gas settled to a very flat disc in which the star formation is still going on; this is the Population I."

Searle and Zinn (1978) painted a competing picture of galaxy formation, in which they proposed "that the gas from which the clusters and stars of the outer halo formed continued to fall into the Galaxy for some time after the collapse of its central regions had been completed; that the interactions of the infalling gas dissipated much of its kinetic energy and gave rise to transient high-density regions in which the halo stars and clusters formed; that these regions dispersed even while they underwent chemical evolution; that the stars and clusters that had formed within them eventually fell into dynamical equilibrium with the Galaxy and constitute its present outer halo, while the gas lost from these protogalactic starforming regions was eventually swept into the galactic disk." In other words, the halo stars are stars formed in other, smaller galaxies and clusters, which later merged with a galaxy that had already formed. This grew into the "hierarchical merger" scenario, in which the Milky Way grew to its current size through mergers of smaller galaxies and stellar associations.

The hierarchical merger picture has been borne out both by simulations (e.g., Kauffmann et al. 1993; Springel et al. 2005) and by the fact that we are observing recent and present-day accretion of small galaxies into the Milky Way halo. Note, however, that the majority of the merging may have happened at early times, and thus the rapid collapse model is not completely incorrect. Also, hydrodynamical simulations suggest that galactic disks may have formed through steady flow of cold gas into massive dark matter halos (Dekel et al. 2009).

Because many stars currently in the Milky Way (particularly halo stars) could have been formed in smaller galaxies and later accreted, the star formation history in our galaxy may be different from the history of structure formation. For example, the composition of stars that were formed outside the Milky Way does not tell us anything about the composition or density of the gas in the Milky Way at the time that star was formed. There could be an epoch of star formation that is followed by an epoch of merging.

1.6.2 Constraining Dark Matter with Tidal Streams

In the standard Λ CDM model (Spergel et al. 2015) of the Universe, most of the mass in galaxies like the Milky Way is made of dark matter, which interacts with itself and the rest of the mass in the Universe only through gravity. Around Milky Way-sized dark matter halos, there could be thousands of dark matter subhalos that are the size of typical dwarf galaxies. Because this matter does not interact with light, we cannot see it directly. Instead we infer its existence from the motions of objects (such as stars and galaxies) that we can see, and from gravitational lensing of objects such as galaxies and QSOs.

Although the stars in the Milky Way halo (often called spheroid stars) represent only 1% of the stars in the halo, they provide an archaeological record of our galaxy's merger history. A significant fraction (or maybe all) spheroid stars were formed in other, smaller, galaxies that fell into and were ripped apart by the Milky Way. Any dark matter associated with those galaxies is incorporated into the dark matter halo of the Milky Way. At least some of the Milky Way globular clusters are believed to have come into the Milky Way with dwarf galaxies that are now disrupted.

The disruption of dwarf galaxies into particular Milky Way tidal streams is typically modeled using *N*-body simulations. In these simulations, the Milky Way is often assumed to be a fixed potential, and the progenitor satellite is modeled as a symmetric distribution of *N* (say 10,000 or 100,000) particles of equal mass, whose positions and velocities then evolve through time due to gravitational forces from each other and from the fixed Milky Way potential. Since satellites at 20–50 kpc from the Galactic center take of order a billion years to orbit once, these simulations are typically run for billions of years. However, they cannot be trusted further back in time than about 3 billion years, since the gravitational field of the Milky Way galaxy should evolve with time—particularly at early times in the Universe. These *N*-body simulations can be used to constrain the properties of the progenitor, the orbit of the satellite from which it was derived, and the gravitational potential of the Milky Way itself.

Alternatively, tidal streams and halo substructure can be modeled in the cosmological context using *N*-body or hydrodynamic simulations of galaxy formation in general. In this case, galaxy(ies) and tidal streams will be produced, but will not match the observed galaxies and tidal streams we observe in the Universe today. However, they can be used to ask whether the types of structures we see are consistent with the models. Examples of large simulations of galaxy formation include: the Aquarius Project (Springel et al. 2008), Via Lactea (Diemand et al. 2008) and Illustris (Vogelsberger et al. 2014).

Because the stars in the tidal streams were ripped from their progenitor satellites by the Milky Way's gravity, and their subsequent orbits are determined by the Milky Way's gravity, tidal streams hold great promise for teaching us about the gravitational potential of the Milky Way. Because the majority of the mass in the Milky Way is believed to be made of dark matter particles, tidal streams could tell us the density distribution of dark matter.

Although in principle one could determine the three dimensional position and velocity of any star in the Milky Way, stars in tidal streams are the only ones that we know where they were in the past. We know that tidal stream stars were all once co-located on the same progenitor satellite. This is the property of tidal stream stars that makes them potentially very valuable tracers of the Galactic potential.

Dark matter in the Milky Way galaxy can be described by its overall shape. In addition to this overall (smoothly varying) density distribution, the radial velocities of the stars in dwarf galaxies suggest that these satellites contain a large fraction of dark matter (Simon and Geha 2007). Moreover, cosmological models of structure formation produce galaxies with many more "subhalos" than there are observed dwarf galaxy satellites; there could be many dwarf galaxy sized lumps of dark matter, that do not contain stars, in orbit around the Milky Way.

Tidal streams have been used to constrain dark matter in all of these contexts (see Chap. 7). The Sagittarius tidal stream in particular (see Chap. 2) has been used to infer a triaxial shape for the Milky Way's dark matter halo. Dark matter subhalos can weakly interact with stream stars creating a wider stellar stream, or strongly interact with stream stars, throwing them out of the stream and creating gaps. The width (or alternatively velocity dispersion) of tidal streams gives some indication of the mass of the progenitor, which can in principle be compared with the number of stars observed to determine the amount of dark matter in a progenitor dwarf galaxy.

1.7 Disk Response to Tidal Interactions

When large dwarf galaxies (or dark matter subhalos) pass close to the Milky Way, the disk can also respond to the gravity of the dwarf galaxy (Hunter and Toomre 1969; Weinberg and Blitz 2006). Historically, this mechanism was studied as the origin of the observed warp in the Galactic disk, and in particular the warp was thought to be the result of an interaction with the Large Magellanic Cloud (LMC). After the discovery of the Monoceros Ring (See Chap. 3), disk response to passing satellites was proposed as a mechanism to explain the presence of this highly controversial structure in the plane of the Milky Way (Kazantzidis et al. 2008; Younger et al. 2008). Later work focused on the Sagittarius dwarf galaxy, which is known to be close to passing through the disk, as the most likely perturber (Purcell et al. 2011).

Surveys of stars have corroborated this picture of disk oscillations. Coherent disk velocity substructure was observed in the SDSS (Widrow et al. 2012), the RAdial Velocity Experiment (RAVE; Williams et al. 2013), and the Large Area Multi-Object fiber Spectroscopic Telescope (LAMOST; Carlin et al. 2013). Oscillations in the disk density have also been observed as a function of height above the plane (Yanny and Gardner 2013), and distance from the Galactic center (Xu et al. 2015).

The observed density waves are in reasonable agreement with the simulations of Gómez et al. (2013), who calculated the effects of the Sagittarius dwarf galaxy on the disk.

Evidence for wavelike disk oscillations has also been found in the Andromeda galaxy. Andromeda's NE clump (see Chap. 8), 40 kpc from the galaxy center, is thought to be composed of disk stars, possibly tossed away from the disk plane by an encounter with the dwarf galaxy progenitor of Andromeda's Giant Stellar Stream (Richardson et al. 2008; Bernard et al. 2015). It is unclear how the corrugations in Galactic gas and star forming regions observed in our galaxy (Quiroga 1974), and in others (Florido et al. 1991; Alfaro et al. 2001; Matthews and Uson 2008), are related to the disk oscillations that are being observed in Milky Way disk stars, but the subhalos have also been proposed to explain the ripples in the gas (Chakrabarti and Blitz 2009). One wonders whether, if disk oscillations could be caused by galactic subhalos, whether they also induce spiral structure.

1.8 Future Prospects

A very dynamic picture of present-day galaxies is emerging. The stellar halos of large galaxies appear to be composed (in part or in total) of stars that have been tidally stripped from smaller galaxies that have fallen into the larger galaxy's gravitational field. Massive subhalos (including dark matter-only subhalos, if they exist) could be exciting waves in galactic disks. We expect that subhalos could produce a time-varying gravitational field in the Milky Way, that could among other things produce gaps in tidal streams. There is even a possibility that very massive infalling dwarf galaxies could be significantly moving the center of mass of the larger galaxy, affecting not only the disk but also the paths of the dwarf galaxies and associated tidal streams (Gómez et al. 2015).

As ongoing and future surveys provide us with large numbers of radial velocities and proper motions of Galactic stars (the largest of these surveys will come from the ESO Gaia satellite), it will be possible to map a larger fraction of halo substructure kinematically (see Chap. 5), and to better constrain the properties of the streams we have already identified. This better data will allow us to trace tidal stream substructure with higher fidelity, and thus help clarify which stars in tidal streams originated on the same Milky Way satellite. We will be able to map the spatial extent of kinematically identified streams (which have density contrast too low to follow by density alone), and the kinematic substructure of tidal streams that have been identified by density contrast.

The Sagittarius dwarf tidal stream (see Chap. 2) presents an illuminating example of how far we have come in understanding tidal streams, and how far we still have to go. This stream is the largest and best studied of the Milky Way tidal streams, but continues to defy a clear explanation of how its structure evolved to match these observations. We have traced the tidal stream more than 360° around the Milky Way in K/M giant, BHB, and turnoff stars. We have measured the velocities of stream

stars and their velocity dispersion, mapped the stream width and the density profile along the stream, measured the chemical compositions and chemical gradients along the stream, compared the properties of the stars in the stream with those in the progenitor galaxy, and identified apparent bifurcations of the stream into two pieces in both the north and south Galactic caps. However, we are still wondering what combination of Galactic potential and dwarf galaxy progenitor would give rise to these observations. On the observational side, it is not a certainty that all of the identified parts of the stream are associated with a single dwarf galaxy progenitor. On the theoretical side, we struggle with how spatially and temporally complex the model for the Galactic potential should be. We also note that the properties of the progenitor dwarf, including rotation, substructure, satellites, and the radial profiles of the stellar and dark matter constituents, can give rise to observable complexity in the resulting tidal stream. On the one hand, tidal streams have the potential to provide us with a wealth of information about our galaxy and the satellites that have fallen into it. On the other hand, they require us to understand a large number of complexities to reach definite conclusions.

Better understanding of tidal streams will lead to better understanding of galaxy evolution, and to better constraints on the distribution of dark matter, both in the progenitor dwarf galaxies that are thought to have very high mass-to-light ratios, and in the Milky Way galaxy itself. Techniques for constraining the spatial structure of dark matter are currently in development (see Chaps. 6 and 7). We still face challenges in understanding the dynamical systems that we are modeling, and in parameterizing the dark matter distribution, that could be quite complex both spatially and in time. However, the wealth of streams also provides a large number of constraints that one day might unravel the dark matter puzzle.

Acknowledgements HJN gratefully acknowledges Brian Yanny's help in generating Fig. 1.1 of this chapter. Lee Newberg was very helpful in taking over domestic duties so she could write and edit. HJN was partially supported by grants NSF AST 14-09421 and NSF AST 09-37523, by the MilkyWay@home volunteers and supporters, and in particular by Manit Limlamai, Babette Josephs, Lee Newberg, the Marvin Clan, and the 2015 Breakthrough Prize in Fundamental Physics.

References

```
Alfaro, E. J., Pérez, E., González Delgado, R. M., Martos, M. A., & Franco, J. 2001, ApJ, 550, 253 Belokurov, V., Zucker, D. B., Evans, N. W., et al. 2006, ApJ Lett, 642, L137 Belokurov, V., Evans, N. W., Bell, E. F., et al. 2007, ApJ Lett, 657, L89 Bernard, E. J., Ferguson, A. M. N., Richardson, J. C., et al. 2015, MNRAS, 446, 2789 Carlin, J. L., Yam, W., Casetti-Dinescu, D. I., et al. 2012, ApJ, 753, 145 Carlin, J. L., DeLaunay, J., Newberg, H. J., et al. 2013, ApJ Lett, 777, L5 Chakrabarti, S., & Blitz, L. 2009, MNRAS, 399, L118 Chiba, M., & Beers, T. C. 2000, AJ, 119, 2843 Cole, N., Newberg, H. J., Magdon-Ismail, M., et al. 2008, ApJ, 683, 750 Da Costa, G. S., & Armandroff, T. E. 1995, AJ, 109, 2533 De Silva, G. M., Freeman, K. C., Bland-Hawthorn, J., et al. 2015, MNRAS, 449, 2604
```

28 H.J. Newberg

Dekel, A., Birnboim, Y., Engel, G., et al. 2009, Nature, 457, 451

Diemand, J., Kuhlen, M., Madau, P., et al. 2008, Nature, 454, 735

Eggen, O. J. 1958a, MNRAS, 118, 65

Eggen, O. J. 1958b, MNRAS, 118, 154

Eggen, O. J. 1958c, MNRAS, 118, 560

Eggen, O. J., & Sandage, A. R. 1959, MNRAS, 119, 255

Eggen, O. J., Lynden-Bell, D., & Sandage, A. R. 1962, ApJ, 136, 748

Eggen, O. J., Freeman, K. C., & Rodgers, A. W. 1973, Reports on Progress in Physics, 36, 625

Ferguson, A. M. N., Irwin, M. J., Ibata, R. A., Lewis, G. F., & Tanvir, N. R. 2002, AJ, 124, 1452

Florido, E., Battaner, E., Sanchez-Saavedra, M. L., Prieto, M., & Mediavilla, E. 1991, MNRAS, **251**, 193

Freeman, K., & Bland-Hawthorn, J. 2002, ARA&A, 40, 487

Frenk, C. S., White, S. D. M., Davis, M., & Efstathiou, G. 1988, ApJ, 327, 507

Girard, T. M., Dinescu, D. I., van Altena, W. F., et al. 2004, AJ, 127, 3060

Gómez, F. A., Minchev, I., O'Shea, B. W., et al. 2013, MNRAS, 429, 159

Gómez, F. A., Besla, G., Carpintero, D. D., et al. 2015, ApJ, 802, 128

Grillmair, C. J. 2009, ApJ, 693, 1118

Grillmair, C. J., Freeman, K. C., Irwin, M., & Quinn, P. J. 1995, AJ, 109, 2553

Grillmair, C. J., & Johnson, R. 2006, ApJ, 639, L17

Harris, W. E. 2010, arXiv:1012.3224

Helmi, A., White, S. D. M., de Zeeuw, P. T., & Zhao, H. 1999, Nature, 402, 53

Hernquist, L., & Quinn, P. J. 1988, ApJ, 331, 682

Hunter, C., & Toomre, A. 1969, ApJ, 155, 747

Ibata, R. A., Gilmore, G., & Irwin, M. J. 1994, Nature, 370, 194

Ibata, R. A., Wyse, R. F. G., Gilmore, G., Irwin, M. J., & Suntzeff, N. B. 1997, AJ, 113, 634

Ibata, R., Irwin, M., Lewis, G., Ferguson, A. M. N., & Tanvir, N. 2001a, Nature, 412, 49

Ibata, R., Irwin, M., Lewis, G. F., & Stolte, A. 2001b, ApJ Lett, 547, L133

Ibata, R. A., Irwin, M. J., Lewis, G. F., Ferguson, A. M. N., & Tanvir, N. 2003, MNRAS, 340, L21

Ivezić, Ž., Goldston, J., Finlator, K., et al. 2000, AJ, 120, 963

Ivezić, Ž., Sesar, B., Jurić, M., et al. 2008, ApJ, 684, 287

Ivezić, Ž., Beers, T. C., & Jurić, M. 2012, ARA&A, 50, 251

Johnston, K. V., Spergel, D. N., & Hernquist, L. 1995, ApJ, 451, 598

Johnston, K. V., Hernquist, L., & Bolte, M. 1996, ApJ, 465, 278

Jurić, M., Ivezić, Ž., Brooks, A., et al. 2008, ApJ, 673, 864

Kauffmann, G., White, S. D. M., & Guiderdoni, B. 1993, MNRAS, 264, 201

Kazantzidis, S., Bullock, J. S., Zentner, A. R., Kravtsov, A. V., & Moustakas, L. A. 2008, ApJ, 688, 254

Kepley, A. A., Morrison, H. L., Helmi, A., et al. 2007, AJ, 134, 1579

Lenz, D. D., Newberg, J., Rosner, R., Richards, G. T., & Stoughton, C. 1998, ApJ Suppl, 119, 121

Lynden-Bell, D., & Lynden-Bell, R. M. 1995, MNRAS, 275, 429

Majewski, S. R., Munn, J. A., & Hawley, S. L. 1996, ApJ Lett 459, L73

Majewski, S. R., Ostheimer, J. C., Kunkel, W. E., & Patterson, R. J. 2000, AJ, 120, 2550

Majewski, S. R., Skrutskie, M. F., Weinberg, M. D., & Ostheimer, J. C. 2003, ApJ, 599, 1082

Majewski, S. R., Nidever, D. L., Smith, V. V., et al. 2012, ApJ Lett, 747, L37

Matthews, L. D., & Uson, J. M. 2008, AJ, 135, 291

McConnachie, A. W. 2012, AJ, 144, 4

Morrison, H. L., Mateo, M., Olszewski, E. W., et al. 2000, AJ, 119, 2254

Newberg, H. J., Yanny, B., Rockosi, C., et al. 2002, ApJ, 569, 245

Newberg, H. J., Yanny, B., & Willett, B. A. 2009, ApJL, 700, L61

Newberg, H. J. 2013, IAU Symposium, 289, 74

Newby, M., Newberg, H. J., Simones, J., Cole, N., & Monaco, M. 2011, ApJ, 743, 187

Newby, M., Cole, N., Newberg, H. J., et al. 2013, AJ, 145, 163

Odenkirchen, M., Grebel, E. K., Rockosi, C. M., et al. 2001, ApJ Lett, 548, L165

Preston, G. W., Beers, T. C., & Shectman, S. A. 1994, AJ, 108, 538

Purcell, C. W., Bullock, J. S., Tollerud, E. J., Rocha, M., & Chakrabarti, S. 2011, Nature, 477, 301 Quiroga, R. J. 1974, Ap&SS, 27, 323

Richardson, J. C., Ferguson, A. M. N., Johnson, R. A., et al. 2008, AJ, 135, 1998

Rockosi, C. M., Odenkirchen, M., Grebel, E. K., et al. 2002, AJ, 124, 349

Rodgers, A. W., Harding, P., & Sadler, E. 1981, ApJ, 244, 912

Searle, L., & Zinn, R. 1978, ApJ, 225, 357

Schlaufman, K. C., Rockosi, C. M., Allende Prieto, C., et al. 2009, ApJ, 703, 2177

Shang, Z., Zheng, Z., Brinks, E., et al. 1998, ApJ Lett, 504, L23

Sharma, S., Johnston, K. V., Majewski, S. R., et al. 2010, ApJ, 722, 750

Simon, J. D., & Geha, M. 2007, ApJ, 670, 313

Spergel, D. N. 2015, Science, 347, 1100

Springel, V., White, S. D. M., Jenkins, A., et al. 2005, Nature, 435, 629

Springel, V., Wang, J., Vogelsberger, M., et al. 2008, MNRAS, 391, 1685

Starkenburg, E., Helmi, A., Morrison, H. L., et al. 2009, ApJ, 698, 567

Vivas, A. K., Zinn, R., Andrews, P., et al. 2001, ApJ Lett, 554, L33

Vogelsberger, M., Genel, S., Springel, V., et al. 2014, MNRAS, 444, 1518

Weinberg, M. D., & Blitz, L. 2006, ApJ Lett, 641, L33

Widrow, L. M., Gardner, S., Yanny, B., Dodelson, S., & Chen, H.-Y. 2012, ApJ Lett, 750, L41

Williams, M. E. K., Steinmetz, M., Binney, J., et al. 2013, MNRAS, 436, 101

Xu, Y., Newberg, H. J., Carlin, J. L., et al. 2015, ApJ, 801, 105

Yanny, B., Newberg, H. J., Kent, S., et al. 2000, ApJ, 540, 825

Yanny, B., & Gardner, S. 2013, ApJ, 777, 91

York, D. G., Adelman, J., Anderson, J. E., Jr., et al. 2000, AJ, 120, 1579

Younger, J. D., Besla, G., Cox, T. J., et al. 2008, ApJ Lett, 676, L21

Chapter 2 The Sagittarius Dwarf Tidal Stream(s)

David R. Law and Steven R. Majewski

Abstract The Milky Way's prominent and widely studied Sagittarius (Sgr) dSph tidal stream has proven a valuable tool for exploring a number of problems in galactic astronomy. In this review of the Sgr system, we present a descriptive portrait of the most salient and unambiguous observational properties (e.g., location, radial velocity, proper motion, and chemical composition) of the Sgr core and tidal streams as they are presently known. We discuss how the history of these observations has shaped the development of numerical models of the system over time, and some of the major conclusions that have been drawn from such modeling efforts with regard to the size and shape of the Milky Way's gravitational potential and the patterns of enrichment throughout its stellar halo. Finally, we summarize some of the known failings of the present models, which we lay out as a challenge for future progress on understanding this remarkable and fortuitous example of hierarchical galaxy growth via merging in action.

2.1 Introduction

As the most prominent and extensive coherent stellar feature in the Milky Way halo, the Sagittarius (Sgr) dSph tidal stream is the most widely studied halo substructure to date, and it has become an important tool for exploring a number of problems in galactic astronomy. The Sgr system stands out among tidal debris systems identified in the Milky Way, and even in other galaxies, in that the progenitor of the stream is still visible and can be studied and compared to an approximately comparable mass of material that has been pulled out of that progenitor. As far as can be ascertained, the core of the satellite is representative of the types of dark matter dominated systems containing baryonic components that are predicted as the seeds

D.R. Law (⊠)

Space Telescope Science Institute, 3700 San Martin Drive, Baltimore, MD 21218, USA e-mail: dlaw@stsci.edu

S.R. Majewski

Department of Astronomy, University of Virginia, P.O. Box 400325, Charlottesville, VA 22904-4325, USA

e-mail: srm4n@virginia.edu

of hierarchical galaxy formation in Λ CDM models of large scale structure formation in the Universe. Thus, in the Sgr system we witness a vivid example of Milky Way satellite cannibalization in action—one whose structure, dynamics and chemistry can be studied in great detail throughout both a bound progenitor core and out into extended, unbound tidal tails.

It is rare in astronomy to have the ability to explore a single example of a physical process where we can glimpse the before, during and after states—in this case represented by the bound core of the satellite, the "halo" of the satellite where the tidal stripping is ongoing, and the extended tidal tails, respectively. As a whole, the Sgr system is an exemplary textbook on the formation of stellar (and dark matter) halos, and grants insights into the origin of the diversity and chemodynamical histories of stars and star clusters in our halo.

It is also rare to have very specific, extended mapping of a Galactic orbit, a goldmine for measuring the shape and strength of the underlying, driving gravitational potential. The stars and star clusters of the Sgr stream provide a "trail of breadcrumbs" that delineates the full phase space path of the Sgr core through the Milky Way. Because the satellite orbits between Galactocentric radii of about 20–60 kpc, the breadcrumb trail provides some of the strongest constraints to date on the mass distribution and shape of the Galactic dark matter halo on these vast scales. And, because of the ability of other large orbiting masses to perturb and scatter stars out of tidal streams, the coherence of the Sgr stream can constrain the likelihood of its previous encounters with other large orbiting bodies (e.g., the Magellanic Clouds) and even the degree of lumpiness of the halo dark matter distribution.

In this review of the Sgr system, we first focus on a descriptive portrait of its most salient and unambiguous observational properties as they are presently known. We then discuss the best fitting numerical models to these properties, leading to a straw man model that can explain these properties. These models lend important insights into both the history of this tidal encounter as well as the gravitational structure of the Milky Way. Despite the many successes of the numerical simulations, there are also several known failings revealed by the very latest observations, which we lay out as a challenge for future progress on understanding this remarkable merger system.

2.2 Historical Remarks and Basic Structure of the Sagittarius System

The Sgr core was discovered in the course of Rodrigo Ibata's dissertation work on the Galactic bulge (Ibata et al. 1994). The very distended structure of this dwarf galaxy, combined with its relative proximity to the Galactic center ($[l, b] = [5.6^{\circ}, -14.2^{\circ}]$)—both unusual properties compared to those of the previously known dwarf spheroidal-like Milky Way satellites—were immediately recognized as providing a compelling case of a satellite enduring tidal distress, distortion and

even disruption (Ibata et al. 1994, 1995). Adding to the interest was the finding that four globular clusters (M 54, Arp 2, Terzan 7, Terzan 8) lie close to or within Sgr's large core. In hindsight, it's somewhat remarkable that, despite the number of analyses of the distribution of globular clusters in the Milky Way in the decades prior to the Sgr discovery, this unusual constellation of clustered clusters was not previously noted as peculiar.

The discovery of this unusual satellite galaxy immediately spurred observational efforts to find evidence for extended tidal tails, and *N*-body simulations to model the apparent interaction of Sgr and the Milky Way. Totten and Irwin (1998), using a survey of ~100 high-latitude carbon stars—a common stellar type in the Sgr core (Whitelock et al. 1996) indicative of the presence of a significant intermediate aged population—were the first to show that the tails of Sgr likely extended around the sky. Early photometric and spectroscopic pencil-beam surveys sought and detected many pieces of the expected stellar stream (Mateo et al. 1998; Majewski et al. 1999; Ivezić et al. 2000; Dohm-Palmer et al. 2001; Martínez-Delgado et al. 2001, 2002; Vivas et al. 2001; Dinescu et al. 2002; Kundu et al. 2002). A detailed summary of these early detections is shown in Fig. 2.1. Meanwhile, a number of early *N*-body simulations attempted to assemble the available piecemeal data into a coherent model of the system (e.g., Velazquez and White 1995; Johnston et al.

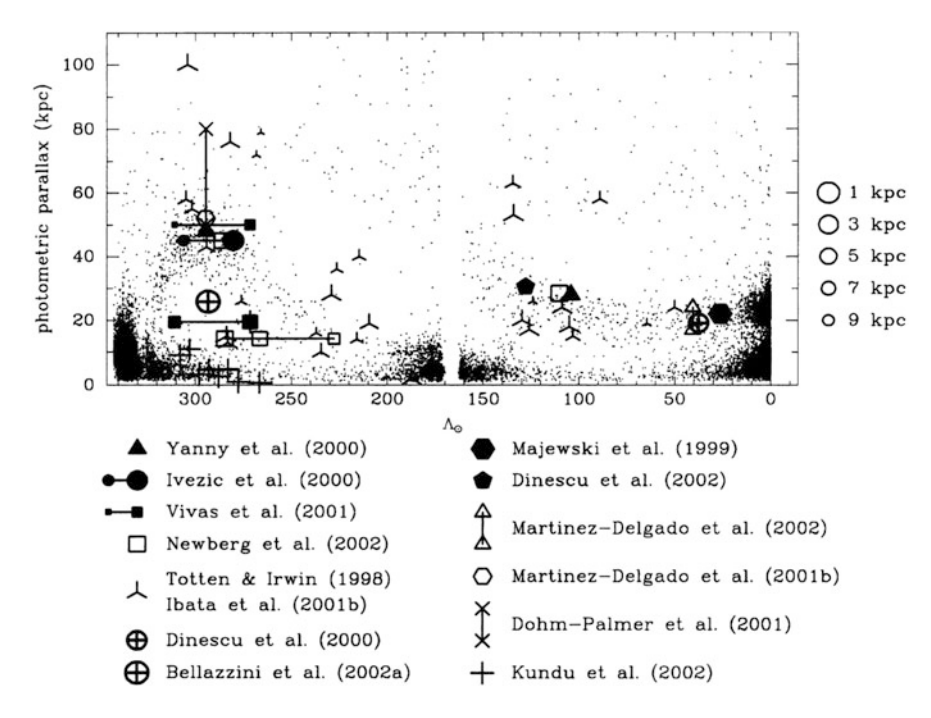


Fig. 2.1 Summary plot of early detections of the Sgr stream (reprinted from Majewski et al. 2003). The *individual dots* represent 2MASS color-selected, candidate M giant stars. Λ_{\odot} is the angular distance along the Sgr tidal stream from the Sgr dSph galaxy

1995; Johnston et al. 1999; Edelsohn and Elmegreen 1997; Ibata et al. 1997, 2001a; Helmi and White 2001). Despite the vagaries of the often disparate constraints available at the time, the early simulations nevertheless arrived at a generally coherent picture of the interaction, including relatively accurate assessments of the near-polar orientation (e.g., Velazquez and White 1995), direction of motion (e.g., Edelsohn and Elmegreen 1997), and size of the Sgr orbit as traced by the debris (e.g., Johnston et al. 1999). Less certain and more difficult to establish were the mass and mass-to-light (M/L) ratio of the parent satellite (with estimates ranging from \sim 2 to \sim 100—e.g., Ibata et al. 1997; Helmi and White 2001; see Sect. 2.5), the net length of the stellar streams (and therefore the duration of its disruption; see Sect. 2.6.2), and the number and type of globular clusters Sgr contributed to the halo (e.g., Lynden-Bell and Lynden-Bell 1995; Bellazzini et al. 2002; Palma et al. 2002; see Sect. 2.3.4).

The advent of large-scale and all-sky photometric surveys radically improved the observational situation. Newberg and Yanny, using early data releases from the Sloan Digital Sky Survey (SDSS; which provided wide area views of stellar densities with great statistical significance), established more firmly the sky positions of various parts of the Sgr stream (Yanny et al. 2000; Newberg et al. 2002, 2003); additional explorations of early SDSS data (e.g., Ivezić et al. 2000; Ibata et al. 2001b; Helmi 2004; Sirko et al. 2004) substantiated the likely prevalence of Sgr tidal debris throughout the halo. The fortunate circumstance that the Sgr dwarf contains a substantial population of metal-rich stars also means that both the core and tails contain a number of M giant stars bright enough to be in the Point Source Catalog (PSC) of the Two Micron All-Sky Survey (2MASS; Skrutskie et al. 2006). Ibata et al. (2002) exploited this fact to establish more firmly the orientation of the stream based on fragmentary sky coverage from early release 2MASS data, but the full expanse of the stream came into vividly sharp focus when Skrutskie and Majewski plotted the positions of M giants in the full-sky 2MASS PSC. An "unwrapped" all-sky view of those 2MASS M giants is shown in Fig. 2.2, and, with estimated distances, in Fig. 2.1.²

With a precise, full-sky mapping of the stream finally in hand, Majewski et al. (2003) showed that the Sgr stellar tidal streams stretch in looping rosettes \sim 360° around the Milky Way (e.g., as illustrated in Fig. 2.3). Starting from the Sgr core at a distance of \sim 28 kpc from the Sun (Siegel et al. 2007),³ the trailing Sgr stream arcs through the Southern Galactic Hemisphere at a roughly constant heliocentric

¹This all-sky "discovery" image, virtually unaltered from its first plotting, is shown as Fig. 3 in Majewski et al. (2003).

²Note that the Sgr debris plane, as defined by these M giants, has a pole in Galactic coordinates of $(l, b) \sim (272^{\circ}, -12^{\circ})$; by coincidence, this pole has a Galactic longitude very similar to the pole of the ecliptic plane, although the latter is inclined with respect to the Sgr debris plane by about 18° (the ecliptic has a pole of $[l, b] = [276^{\circ}, -30^{\circ}]$).

 $^{^3}$ Estimates of the distance of the Sgr core range from \sim 24 to 30 kpc (see review by Kunder and Chaboyer 2009). The Siegel et al. (2007) value of 28 kpc derives from isochrone fitting to precision Hubble Space Telescope photometry of the Sgr core.

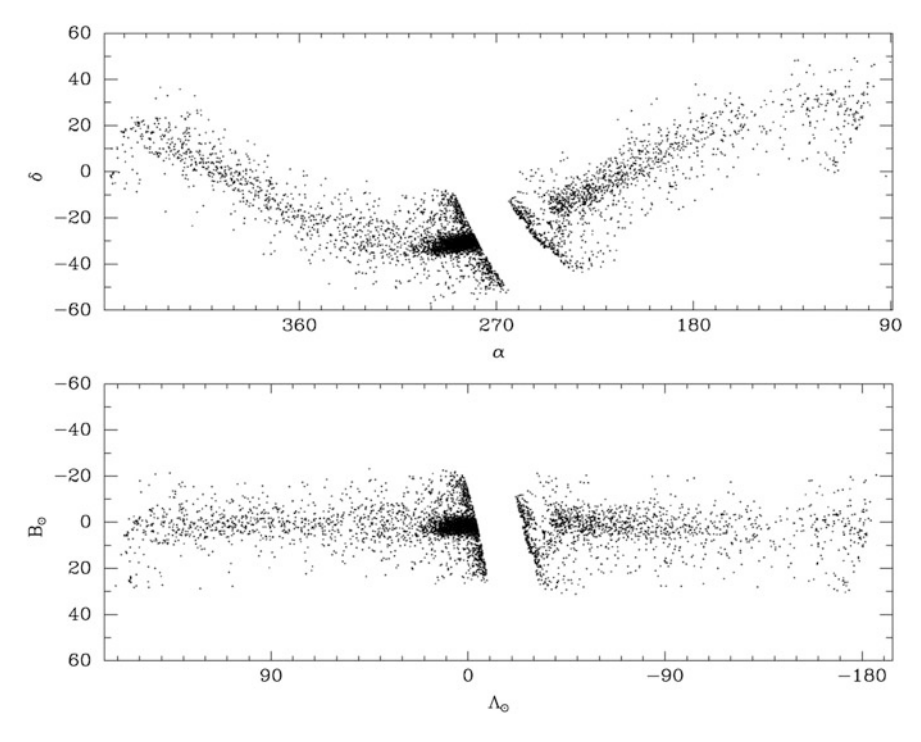


Fig. 2.2 All-sky plot of the path of the Sgr stream as traced by 2MASS-selected M giants in celestial and Sgr-stream coordinate reference frames. (Reprinted from Majewski et al. 2003)

distance of \sim 20–25 kpc before receding to larger distance as it approaches the previous apogalacticon of the Sgr orbit in the direction of the Galactic anticenter (see further discussion in Sect. 2.6.2). In contrast, the leading stream reaches apogalacticon at a distance of \sim 50 kpc, thereafter passing through the North Galactic Cap before diving back down towards the Galactic disk (see Fig. 2.3 for an illustrative diagram).

With the addition of radial velocity data from follow-up spectroscopic observations of M giants across a wide expanse of the trailing (Majewski et al. 2004) and leading (Law et al. 2004) streams it was possible to refine greatly numerical simulations of the Sgr debris (e.g., Law et al. 2005, see details in Sect. 2.4) and begin to explore subtle details such as the lumpiness of the Galactic dark matter halo (Majewski et al. 2004) and precessional variation in the orbital plane induced by a non-spherical Milky Way potential (Helmi 2004; Johnston et al. 2005). Because the all-sky 2MASS data confirmed the earlier observation of Ibata et al. (2001a) that the orbital plane of the Sgr stream does not precess substantially over the observed length of the tidal streams (see discussion by Johnston et al. 2005, but also cf. more recent treatments taking advantage of detailed analysis of SDSS data by Newby et al. 2013 and Belokurov et al. 2014), Majewski et al. (2003) introduced a spherical polar coordinate system for which the primary ("equatorial") great circle is defined

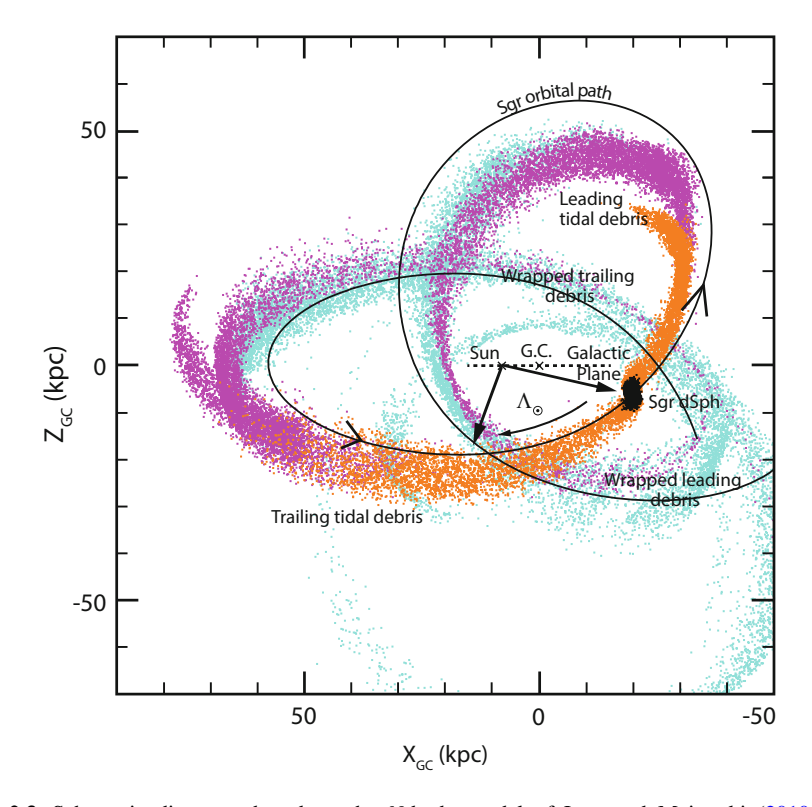


Fig. 2.3 Schematic diagram—based on the *N*-body model of Law and Majewski (2010a)—showing the salient features of the Sgr stream system and illustrating the Λ_{\odot} coordinate system. Colored points represent tidal debris color-coded by the pericentric passage on which it became unbound from Sgr (with orange the most recent and cyan the most ancient); the solid black line indicates the orbit of the Sgr core (arrows indicate direction of motion), and highlights the degree to which the tidal debris is offset from the actual orbital path of the satellite. $X_{\rm GC}$ and $Z_{\rm GC}$ represent standard left-handed Galactocentric Cartesian coordinates

by the Sgr tidal debris and for which the prime meridian of longitude (Λ_{\odot}) is centered on the Sgr core. In this heliocentric coordinate system, Λ_{\odot} increases in the opposite direction to the orbital motion of the dwarf, with the principal wraps of the trailing/leading arm lying at positive/negative longitudes respectively (see Figs. 2.1, 2.2, and 2.3).⁴

While the 2MASS M giants nicely trace the trailing stream throughout the entirety of the Southern Galactic Hemisphere, the path of the 2MASS M giant tracers within the leading stream as it traverses the North Galactic Cap (e.g., $\Lambda_{\odot} \sim 255^{\circ}$, or Fig. 2.1 and $\alpha < 180^{\circ}$ in Fig. 2.2) is somewhat difficult to

⁴Note that because this Λ_{\odot} , B_{\odot} coordinate system is defined by the *tidal debris* path (which does experience some precession, albeit small), the actual center of the Sgr dSph itself does not lie perfectly at the origin, but at (Λ_{\odot} , B_{\odot}) = (0.00°, +1.48°); see Majewski et al. (2003).

follow, and was misinterpreted as to imply a substantially foreshortened leading stream by Majewski et al. (2003). However, in a remarkably detailed Northern Hemisphere view provided by the SDSS-DR5 photometric catalog (see Fig. 1.7 in Chap. 1), Belokurov et al. (2006) showed that the Sgr leading arm arcs over the solar neighborhood and re-enters the Galactic disk in the direction of the Galactic anticenter at $\alpha \sim 120^\circ$ and a distance of $\sim 10-15\,\mathrm{kpc}$ from the Sun (see also Newberg et al. 2007). Additional radial velocity data and distance measures calibrated against RR Lyrae stars presented by Yanny et al. (2009) confirmed this picture.

Taken together, the 2MASS and SDSS data present a comprehensive portrait of the Sgr stream that has been broadly confirmed by more recent observations using RR Lyrae from the Southern Edgeworth-Kuiper Belt Object survey (Prior et al. 2009); SDSS-selected M giants (Keller et al. 2010), blue horizontal branch stars (Clewley and Jarvis 2006; Ruhland et al. 2011) and F-turnoff stars (Newby et al. 2013); red clump stars (Correnti et al. 2010; Carrell et al. 2012); PanSTARRS observations (Slater et al. 2013); and CFHT MegaCam photometry (Pila-Díez et al. 2014). As discussed in Sect. 2.4, these data form a solid empirical foundation for more recent numerical models that are largely successful in reproducing the brightest and (dynamically) youngest sections of the Sgr stream.

2.3 Stellar Populations Within the Sagittarius System

2.3.1 Stellar Populations in the Sagittarius Core

Although the Sgr core is often described as a dwarf spheroidal (dSph) galaxy on the basis of its morphology, estimates of its total luminosity (Sect. 2.5) would make it the brightest of the Milky Way dSphs, between the luminosities of the brighter Small Magellanic Cloud (SMC) dwarf irregular (dIrr) and fainter Fornax dSph galaxies. Another way that Sgr resembles the SMC and Fornax galaxies is in having a protracted star formation history ranging from ancient stellar populations to relatively recent ones. This characteristic is typical of not only the dIrr galaxies of the Local Group, but also the Local Group dwarf elliptical (dE) galaxies (which are all satellites of M31) and Leo I, another of the very largest Milky Way dSphs (see review by Dolphin et al. 2005). The dSph morphology may be the end state of the dynamical evolution of dwarf disk systems after "tidal stirring" (e.g., Łokas et al. 2012), a mechanism that may explain the morphological diversity of these otherwise similar (in stellar populations and luminosity) systems.

That Sgr has a complex star formation history was recognized almost immediately; for example, Ibata et al. (1995) showed that it contained a strong intermediate-aged population and some metallicity spread, reminiscent of Fornax, and, like Fornax (and the Magellanic Clouds of course), Sgr has its own globular cluster system. The stars of intermediate age (\sim 4–8 Gyr) and metallicity ([Fe/H] \sim -0.2

to -0.6) dominate the dwarf (more than 80% of its stars) over its great extent (Bellazzini et al. 1999a,b, 2006a; Layden and Sarajedini 2000; Monaco et al. 2002; Giuffrida et al. 2010) and include the prominent population of M giants and carbon stars found in the core (Whitelock et al. 1996; Cole 2001; Majewski et al. 2003) and that have been stripped off into the tidal tails (Totten and Irwin 1998; Ibata et al. 2001a; Majewski et al. 2003, see Fig. 2.2).

However, early photometric work in the center of Sgr also confirmed it to have a pair of distinct metal-poor red giant branches as well as both strong blue and red horizontal branches corresponding, respectively, to those of M 54 and a more broadly distributed metal-poor field star population apparently a few Gyr younger than M54 (Sarajedini and Layden 1995; Layden and Sarajedini 1997, 2000; Monaco et al. 2003). The widespread distribution of a metal-poor Sgr population was, of course, evident by the numerous RR Lyrae stars that aided early mappings of the dSph core (Alard 1996; Cseresnjes et al. 2000). That this metal-poor Sgr population constitutes only $\sim 12\,\%$ of the core (Monaco et al. 2003; Bellazzini et al. 2006a) is no doubt a reflection not of the true star formation history of the progenitor, but rather the preferential net loss of metal-poor stars over the course of Sgr's tidal stripping history (Majewski et al. 2002; Bellazzini et al. 2006a; Chou et al. 2007; Monaco et al. 2007; Law and Majewski 2010a).

A most intriguing discovery, hinted at in early studies of the Sgr color-magnitude diagram (Sarajedini and Layden 1995; Bellazzini et al. 1999a,b; Layden and Sarajedini 1997, 2000) is the apparent presence of what look to be young, blue main sequence turnoff stars in a "blue plume," as well as corresponding red giants spectroscopically shown to have metallicities reaching to solar abundance (Bonifacio et al. 2000; Smecker-Hane and McWilliam 2002; Monaco et al. 2005; Chou et al. 2007; Sbordone et al. 2007); these early studies suggested ages for this population ranging from 0.5 to 2.5 Gyr.

Eventually a detailed portrait of the stellar populations in the Sgr core was possible via analysis of deep Hubble Space Telescope (HST) Advanced Camera for Surveys (ACS) data taken centered on the M54 globular cluster, which apparently lies at the very center of Sgr (although cf. Siegel et al. 2011). Population synthesis of these ACS data by Siegel et al. (2007) shows the diversity and relative proportions of stellar populations in the Sgr core described above (Fig. 2.4), as leads to the derivation of a broad, though fairly monotonically varying age-metallicity distribution suggestive of numerous star forming episodes leading to a steady chemical enrichment with time (Fig. 2.5). A similar age-metallicity relation (AMR) derived earlier from ground-based photometry by Layden and Sarajedini (2000) showed that the central Sgr star clusters track the same AMR (prefacing the discovery that the cluster chemistry also tracks that of the Sgr field—Sect. 2.3.3). The youngest identified stellar population in the Sgr core is confirmed to be a mere 0.7 Gyr old; this implies that the Sgr system had been forming stars even as it was being tidally disrupted over the past several billion years. This also suggests that apart from seeing Sgr at an interesting time in its dynamical evolution, we are also seeing it at a relatively unique time in its star formation history given the fact that despite this relatively recent star formation there is no longer any gas present in the dwarf

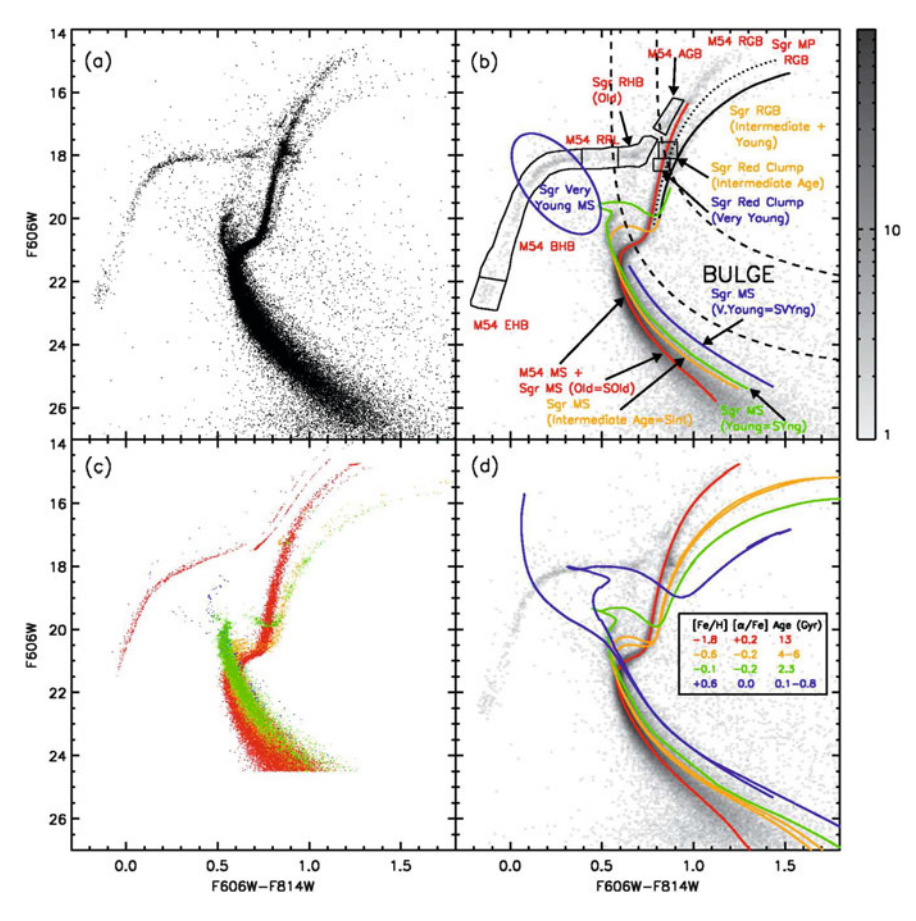


Fig. 2.4 Color-magnitude diagrams (CMDs) of the Sgr core, from HST/ACS photometry of a field centered on the cluster M 54, reproduced from Siegel et al. (2007). (a) The raw HST CMD. (b) A Hess diagram of the field with various features identified with specific populations, either M 54 or Sgr. (c) A simulation of the complex observational CMD using population synthesis. (d) The observed Hess diagram overlaid with theoretical isochrones derived from the population synthesis

(Koribalski et al. 1994; Burton and Lockman 1999). The last of the Sgr dSph's gas was either consumed in this last, relatively recent star formation episode, or perhaps stripped off fairly recently, within the last 0.2–0.3 Gyr (Putman et al. 2004).

Of course, these ACS data are specifically focused on a tiny patch of the center of the Sgr core, whereas the various populations have different spatial distributions outside of the center. This is evident by the metallicity gradients observed across the Sgr core (Bellazzini et al. 1999a; Alard 2001; McDonald et al. 2013)—now definitively mapped (see Fig. 2.6) using both medium and high resolution spectroscopy (Majewski et al. 2013; Hasselquist et al. 2015)—and a result of different relative densities of the constituent stellar populations as a function of radius. In this regard, the Sgr core is once again similar to the Fornax dSph (e.g.,

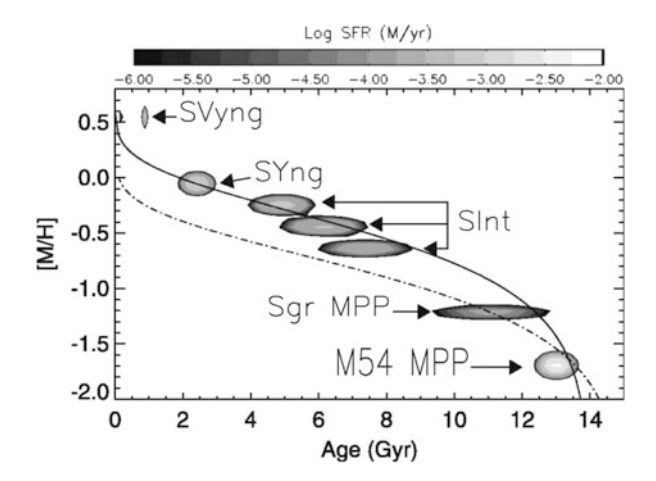


Fig. 2.5 The age-metallicity relation (AMR) for the Sgr core as determined by population synthesis of HST/ACS imaging of its very center, from Siegel et al. (2007). Distinct contributions are from the metal-poor M54 population (M54 MPP), Sgr's metal-poor population (Sgr MPP), intermediate age population (SInt), young population (SYng), and very young population (SVyng). The *dot-dash line* represents a closed-box evolutionary model, while the *solid line* is a model with faster enrichment

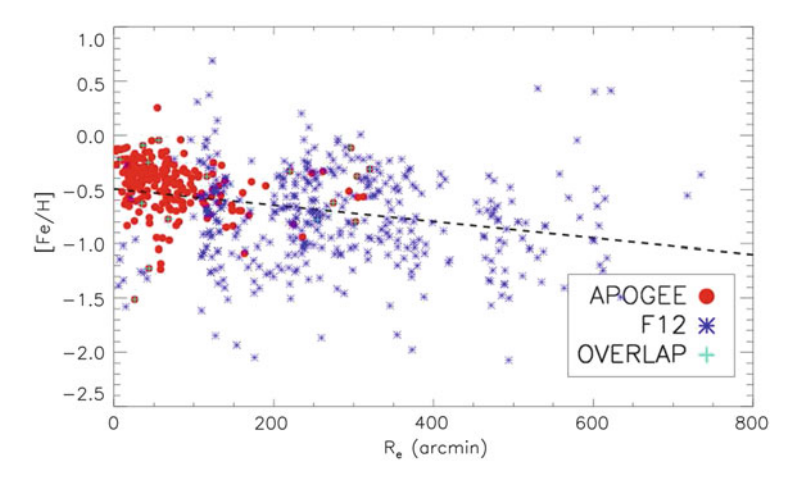


Fig. 2.6 Metallicities for Sgr stars as a function of elliptical radius (i.e., the radius normalized to the equivalent isopleth distance along the major axis for the best fitting ellipse to the surface density of M giants—for example the radius in the direction of the minor axis, b, would be multiplied by a/b, where a is the major axis) in the dSph. Blue asterisks are abundances measured from infrared Ca triplet lines in $R \sim 15,000$ spectra from the Frinchaboy et al. (2012) sample. The red filled circles show measurements of iron lines in $R \sim 22,500$ spectra from Data Release 10 (DR10) of the APOGEE project. Stars sampled by both surveys are shown with plus signs and with the APOGEE [Fe/H]. The dashed line is a fit using a robust iterative outlier rejection method. (Figure courtesy of Sten Hasselquist)

Battaglia et al. 2006), as well as other Milky Way dSphs (e.g., Sculptor, Sextans, Leo I, Leo II, Draco— Tolstoy et al. 2004; Battaglia et al. 2011; Kirby et al. 2011). As in these other systems the different spatial extents for the constituent populations reflects different dynamics for these populations, which also give rise to radial gradients in velocity dispersion across the dwarf (for the case of Sgr, see Majewski et al. 2013 and Hasselquist et al. 2015).

2.3.2 Stellar Populations in the Sagittarius Streams

One expects overlap between the stellar populations seen in the Sgr core with those represented in the Sagittarius streams. However, because the most loosely bound stars in a dwarf galaxy or star cluster tend to have the largest mean internal (to the dwarf galaxy) orbital radii, tidal stripping generally eats away a satellite star system from the outside. When the orbit of that satellite in the parent potential lends itself to the formation of long, coherent tidal streams—as in the case of Sgr—one can, to first order, read the variation in radial properties (e.g., the chemistry and ages of stars) of the original satellite as the variation of those properties along the tidal streams. Of course, the situation is complicated by any star formation proceeding on timescales similar to the stripping timescale, as well as the fact that there is a "smearing out" of information by orbital phase overlap of stars stripped at different times (see, e.g., the overlap along the tidal streams of particles color-coded for different perigalacticon release in Fig. 2.3). Indeed, global variations in mean metallicity along the Sgr stream have clearly been identified (Bellazzini et al. 2006a; Chou et al. 2007; Monaco et al. 2007; Keller et al. 2010; Shi et al. 2012; Carlin et al. 2012), stretching from a $\langle \text{Fe/H} \rangle \sim -0.4$ near the Sgr core to $\langle \text{Fe/H} \rangle \sim -1.1$ at the greatest angular extents sampled thus far. These variations along the stream have been interpreted as indicating the likelihood of a strong metallicity gradient in the progenitor satellite (Bellazzini et al. 2006a; Chou et al. 2007; Keller et al. 2010).

A key lesson illustrated by these assessments of metallicity variations within the Sgr core (Sect. 2.3.1) and along the stream is that because of the time dependence of the specific populations contributed to the Milky Way halo, the *current* content of a dSph is *not* representative of what it contributed to the halo; differences in metallicity distribution functions between the satellite and the tails are clear (Chou et al. 2007; Monaco et al. 2007). This process is easily demonstrated by N-body simulations with even simple assumptions of the progenitor metallicity distributions (Law and Majewski 2010a, hereafter cited as "LM10"). Thus, it is risky to draw conclusions regarding the role or magnitude of accretion in galactic halos by comparing their stellar content to those in their currently bound satellites. The problem is exacerbated by the dominant contribution to stellar halos from satellites accreted early on, whereas current satellites have typically been accreted more recently (Font et al. 2006). In the same context, if one wants an accurate portrait of the *true* star formation and chemical history of any particular satellite galaxy, one may have to *reconstruct it* by carefully accounting for the (likely different, or

different proportions of) stellar populations that have been previously stripped away (Chou et al. 2007; Majewski et al. 2002).

2.3.3 Chemical Evolution of the Sagittarius System

Overall metallicity trends across the Sgr core and tidal tails are reinforced by more detailed exploration of their chemical abundance patterns. Chou et al. (2010) show strong differences in s-process abundances (e.g., the heavy to light s-process element ratio [La/Y]) between Sgr tail and core stars. Only by putting together data from both the core and tails is the complete chemical history of Sgr revealed: the Ti, Y and La abundances across all metallicities reveals Sgr to have abundance patterns—and therefore an enrichment history—that closely resemble those of other dSphs and the Large Magellanic Cloud for these elements, only with different timescales for that enrichment, as reflected in *shifts* in the global abundance patterns with metallicity (Δ [Fe/H]). But these patterns are seen to be distinct from those seen in Milky Way stars in the solar neighborhood—e.g., with Sgr showing a heavy s-process enhancement (La) and light s-process deficit (Y) with respect to Milky Way field stars (Bonifacio et al. 2000; Smecker-Hane and McWilliam 2002; Sbordone et al. 2007; Chou et al. 2010; McWilliam et al. 2013).

Other significant differences with Milky Way stars are seen by deficiencies in $[\alpha/\text{Fe}]$ elements (especially O and Mg, but also for Si, Ca and Ti), as well as for [Na/Fe], [Al/Fe] and [Cu/Fe] (see references in previous paragraph, as well as Bonifacio et al. 2004; Carretta et al. 2010; Hasselquist et al. 2015). These deficiencies could imply that Sgr's initial mass function (IMF) was deficient in the most massive Type II supernovae ("SNe"; McWilliam et al. 2013), or that the galaxy was not able to hold onto the yields from its Type II SNe. That Sgr is enhanced in heavy s-process elements like La and Nd (and that these increase with [Fe/H]), but not in the light s-process elements may be because of the dominance of leaky-box chemical enrichment of Sgr from low mass, metal-poor AGB stars that continued over multiple generations (McWilliam et al. 2013). When seen together with the contrasting evidence of "normal"—i.e., Milky Way-like—r-process enrichment (e.g., [Eu/Fe] versus [Fe/H]; Bonifacio et al. 2000; McWilliam et al. 2013), the collective chemical properties of Sgr core stars have been interpreted as indicating a chemical evolution whereby the low $[\alpha/Fe]$ in Sgr are not from the traditional mechanism of (time-delayed) introduction of substantial iron from Type Ia SNe at low metallicity, but rather from a steep IMF, reflecting strong deficiencies in the number of high mass (> \sim 30 M $_{\odot}$) stars (McWilliam et al. 2013). However it occurred, the overall chemical evolution of the Sgr field stars is shared with stars in its globular clusters (Fig. 2.7), as well as between stars in the core and tidal tails (Chou et al. 2007; Monaco et al. 2007; Keller et al. 2010).

Regardless of the origin of these unusual Sgr chemical patterns, they are shared with other dwarf galaxies like the Large Magellanic Cloud and the Fornax dSph (Chou et al. 2010; McWilliam et al. 2013). The general distinctness of this chemistry

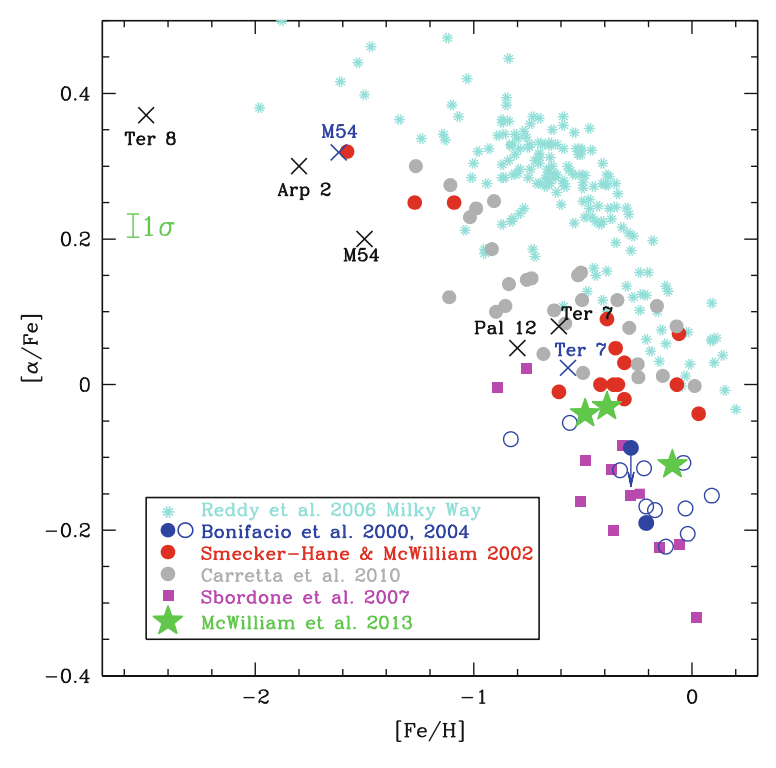


Fig. 2.7 The overall decline in $[\alpha/\text{Fe}]$ with [Fe/H], which occurs at lower metallicities than for Milky Way stars (*cyan points*), is seen to be shared by the old Sgr clusters M 54, Arp 2 and Ter 8, as well as by the younger Sgr clusters Pal 12 and Ter 7. The figure, adapted from McWilliam et al. (2013), includes cluster data (*crosses*) from Brown et al. (1999), Cohen (2004), Sbordone et al. (2007), Mottini et al. (2008), and Carretta et al. (2010), as well as Sgr field stars from Bonifacio et al. (2000), Bonifacio et al. (2004), Smecker-Hane and McWilliam (2002), Sbordone et al. (2007), and Carretta et al. (2010). The data on Milky Way stars are from Reddy et al. (2006). (Figure courtesy of Andrew McWilliam and Sten Hasselquist)

from that observed in local Milky Way stars—and yet that there also remain some chemical properties thought unique to Sgr (e.g., the lowest [Rb/Zr] ratio known; McWilliam et al. 2013)—means that there are ample signatures useful for identifying Sgr stars now in the Milky Way field star population through "chemical fingerprinting". Large-scale, high resolution spectroscopic surveys of the Milky Way, such as the GALAH (Zucker et al. 2012) and Gaia/ESO (Gilmore et al. 2012) surveys in the Southern Hemisphere as well as the dual hemisphere APOGEE-2 project (Majewski et al. 2015) have the capability to take advantage of these signatures to more completely map the current phase space distribution of Sgr stars throughout our Galaxy. No doubt, many more surprises are in store for us when this more complete mapping of the Sgr system and the numerous dimensions offered by exploiting the information contained in the chemical content of its stars are in hand.

2.3.4 Sagittarius Star Clusters

The census of stars and clusters observed to be in tidal streams gives extremely useful insights into the types of stars and clusters that are contributed to large, Milky Way-like galaxies through hierarchical merging, and on what timescales these accumulated debris are accreted. The properties of globular clusters have long played a central role in ascertaining how the Milky Way formed, with intense focus on the question of how those clusters that formed in situ differ from those contributed through accretion (e.g., Searle and Zinn 1978). The prevailing lore descended from Searle and Zinn is that clusters with properties conventionally interpreted as indicating that they are "younger"—e.g., clusters with horizontal branches too red for their metallicity (the second parameter effect) or with brighter main sequence turnoff magnitudes—would most likely be associated with accretion (e.g., Rodgers and Paltoglou 1984; Zinn 1993, 1996).

Thus, it is of great interest to determine what part of cluster parameter space is occupied by clusters we can see in the very process of being accreted. A census of likely Sgr stream clusters was compiled by Law and Majewski (2010b), which identified nine moderate (Ter 7, Pal 12, NGC 5053) to high (M 54, Arp 2, Ter 8, NGC 5634, Whiting 1, Berkeley 29) confidence candidates, based on matches to the present day configuration of Sgr debris as given by numerical simulations (LM10). This group of clusters closely follows the age-metallicity relation of stars in the Sgr core by Siegel et al. (2007, Fig. 2.5), but, surprisingly, yields few candidate clusters with a second parameter effect. This is in contrast to the cluster populations currently bound to the Magellanic Clouds and Fornax dSphs (e.g., Buonanno et al. 1999), which will likely, someday, also be contributed to the Milky Way halo. This contrast would seem to suggest that Sgr provides a striking counterexample to the traditional interpretation of the origins of "old" versus "young" clusters by suggesting that the strength of second parameter expression is less a division between accreted vs. in situ-formed clusters and perhaps more simply a property exhibiting diversity among different cluster-contributing parent satellites.

However, the latter census of Sgr-contributed clusters must be updated, in light of the newly identified failure of the LM10 model to match the extreme ends of the Sgr trailing arm (Sect. 2.6.2) and the fact that several of the Law and Majewski (2010b) Sgr cluster candidates are identified with older parts of that arm. The possible need to now include NGC 2419 among the Sgr candidates (Sect. 2.6.2) will not change the above interpretation regarding the diversity of cluster types that can be contributed to the halo, given that the extremely low metallicity and large age of this cluster matches the properties of other Sgr candidates, but it does raise interesting new questions given that now the *two*

largest Milky Way halo globular clusters (M 54, NGC 2419)⁵ may be associated with Sgr.⁶ An exciting parallel development that promises even more vital insights into these questions is the ability to now study the properties of globular clusters in tidal streams in *other* spiral galaxies (Mackey et al. 2014).

2.4 Numerical Models of the Sagittarius-Milky Way System

Using the Sgr stream to put constraints on the shape and strength of the Milky Way's gravitational potential is an industry that extends back to the first, rudimentary assessments of the stream orientation and extent on the sky (e.g., Mateo et al. 1998; Majewski et al. 1999; Martínez-Delgado et al. 2001; Ibata et al. 2001a) and the first *N*-body models of its interaction with the Milky Way (Velazquez and White 1995; Johnston et al. 1995; Johnston et al. 1999; Edelsohn and Elmegreen 1997). Now that the Sgr system has been extraordinarily well mapped over the entire sky, the breadth of these data have allowed construction of remarkably detailed models of the Sgr dwarf and the Galactic gravitational potential in which it orbits.

Chapters 6 and 7 detail the theoretical processes of tidal stream formation and the determination of the shape/substructure of the Galactic gravitational potential (and thus the dark matter halo) from these tidal streams. In the present section, we describe the specific strategies that have been applied to constrain the properties of the Milky Way gravitational potential using the Sgr system, along with their successes and failings in reproducing the observational data.

2.4.1 General Approach

Although the detailed strategies for simulating the Sgr—Milky Way interaction can vary, a common approach follows that originally described by Johnston et al. (1995), in which the Milky Way is represented by a smooth, rigid potential and Sgr is represented by a collection of self-gravitating particles whose interaction is calculated using a self-consistent field code (e.g., Hernquist and Ostriker 1992).⁷

⁵We exclude ω Cen as *the* largest Milky Way halo cluster on the grounds that it appears that this object is, itself, the residual core of an accreted dwarf galaxy—e.g., Lee et al. (1999), Majewski et al. (2000), and Bekki and Freeman (2003).

⁶Whether M 54 lies exactly at the nucleus of the Sgr dSph (e.g., Bellazzini et al. 2008) or \sim 2 kpc in front (Siegel et al. 2011) of the dSph center is itself an open question.

⁷An alternative, and substantially faster method to this form of *N*-body modeling the Sgr stream is that used by Ibata et al. (2013) and Gibbons et al. (2014), who approximate streams via swarms of test-particles emanating from the L1 (for the leading arm) and L2 (for the trailing arm) Lagrange points around the satellite.

A three-component model is often adopted for the Galactic gravitational potential, consisting of a Miyamoto and Nagai (1975) disk, Hernquist spheroid, and logarithmic dark matter halo of the general forms, respectively:

$$\Phi_{\text{disk}} = -\frac{GM_{\text{disk}}}{\sqrt{R^2 + (a + \sqrt{z^2 + b^2})^2}},$$
(2.1)

$$\Phi_{\text{sphere}} = -\frac{GM_{\text{sphere}}}{r+c},\tag{2.2}$$

$$\Phi_{\text{halo}} = v_{\text{halo}}^2 \ln(R^2 + (z^2/q^2) + d^2),$$
(2.3)

where $M_{\rm disk}$ and $M_{\rm sphere}$ represent the mass of the Galactic stellar disk and spheroid respectively, $v_{\rm halo}$ sets the mass scale of the Galactic dark matter halo, the parameters (a,b,c,d) represent physical length scales of the various components, R and z are cylindrical polar coordinates, r is the spherical polar coordinate, and q is a scale factor determining the polar flattening of the Galactic dark matter halo. Typically in simulations of minor mergers like the Sgr system, the particles within the satellite itself are distributed according to a Plummer (1911) model:

$$\Phi_{\text{Sgr}} = -\frac{GM_{\text{Sgr}}}{\sqrt{r^2 + r_0^2}},$$
(2.4)

where M_{Sgr} and r_0 are the mass and radial scalelength of Sgr respectively. While many studies do not distinguish between dark and luminous matter components in the original Sgr progenitor, others (e.g., Łokas et al. 2010; Peñarrubia et al. 2011) adopt more physical models having a two-component disk embedded within an NFW (Navarro et al. 1997) dark matter halo. Nevertheless, the simple Plummer model core is consistent with observations that suggest no significant rotation within the Sgr core (Peñarrubia et al. 2011; Frinchaboy et al. 2012), whereas mass-follows-light models have had reasonably good success in modeling satellites stripped to radii where both dark and baryonic matter are being lost (Sohn et al. 2007; Muñoz et al. 2008).

Although the details vary from study to study, some combination of the above parameters are held fixed (e.g., the local circular speed $V_{\rm LSR}$, although see Carlin et al. 2012), while others are varied along with the orbital velocity of the Sgr core until the resulting model best matches observational measurements of the Sgr stream. While the radial velocity of Sgr is well-known ($v_{\rm GSR}=171\,{\rm km\,s^{-1}}$, Ibata et al. 1997) and can hence be held fixed, the proper motion of the dwarf (Dinescu

⁸It has been shown (Mayer et al. 2001; Bullock and Johnston 2005; Klimentowski et al. 2007) that when satellites are undergoing significant tidal stripping they actually evolve into systems resembling and behaving like mass-follows-light models.

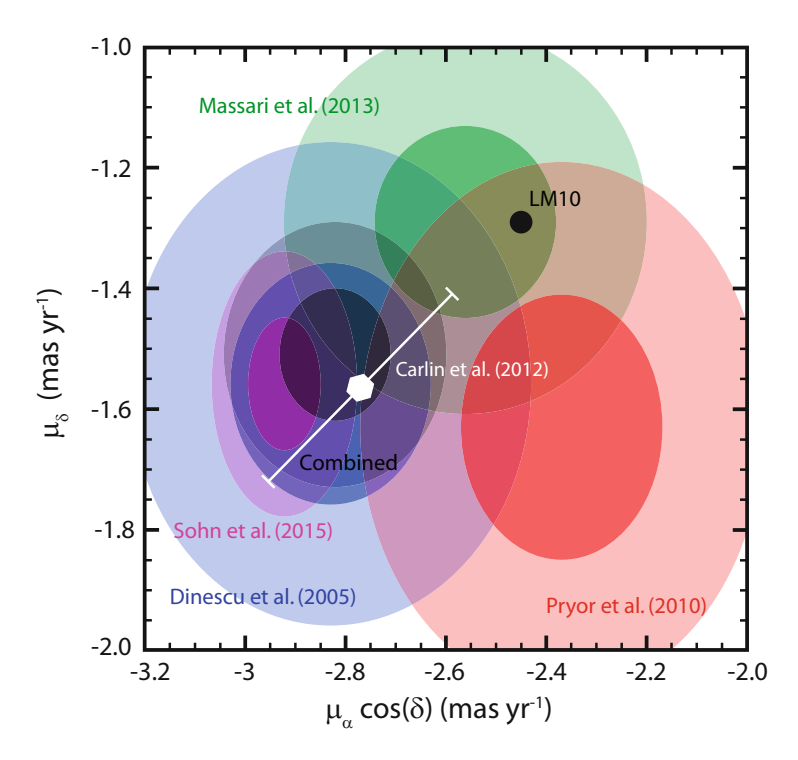


Fig. 2.8 Estimates of the proper motion of the Sgr core from Dinescu et al. (2005, *blue shaded region*), Pryor et al. (2010, *red shaded region*), Massari et al. (2013, *green shaded region*), Sohn et al. (2015, *purple shaded region*), and all four estimates combined (*black shaded region*). Note that all estimates have been corrected to the Sgr center of mass as described by Sohn et al. (2015). The *black filled circle* indicates the Sgr core proper motion derived by LM10 using *N*-body models of the stellar tidal streams, while the *white hexagon* is the proper motion derived by Carlin et al. (2012) using the LM10 model adapted to a local circular speed of $264 \pm 23 \,\mathrm{km \, s^{-1}}$

et al. 2005; Pryor et al. 2010; Massari et al. 2013; Sohn et al. 2015), is sufficiently uncertain (see Fig. 2.8) that the strongest constraints on the proper motion can actually be obtained by the requirement that Sgr tidal debris lie within the observed orbital plane. In the study of LM10, the instantaneous orbital pole of Sgr was fixed by the observed plane of the tidal debris and the radial velocity by the observed value of Ibata et al. (1997), whereas the tangential velocity of Sgr was allowed to vary freely until the simulated radial velocities along the trailing arm best matched observations. This was repeated for a variety of Galactic potential models to seek one that best matched the observed angular path and radial velocity of observed Sgr stream stars (see Fig. 2.9).

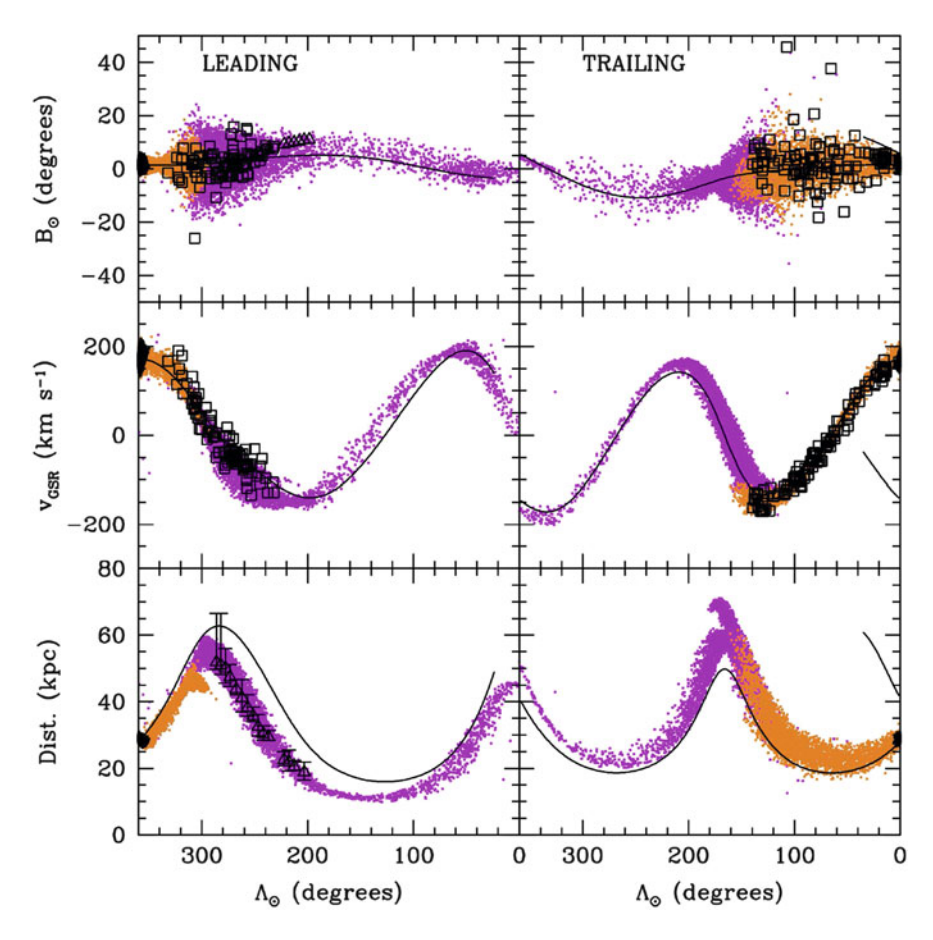


Fig. 2.9 Best-fit Sgr disruption model from LM10. *Black points* represent the bound core of Sgr, while *orange* and *magenta points* are simulated tidal debris torn off the dwarf on successive perigalactica (see Fig. 2.3). *Open symbols* represent a combination of 2MASS and SDSS observational data. (Reproduced from LM10)

2.4.2 Constraints on the Shape of the Galactic Dark Matter Halo

Because Sgr orbits at distances of about 20–60 kpc from the Galactic center, its orbit is most sensitive to the amount and distribution of non-baryonic (i.e., dark) matter within and across those Galactic radii, and initial estimates from the apparently strong planarity of Sgr debris on the sky suggested that the Galactic dark halo is approximately spherical in this range of Galactocentric distances (Ibata et al. 2001a). Improved observational coverage and increasingly detailed modeling of the stream soon led, however, to conflicting conclusions regarding the shape of the

Galactic halo, depending on whether the position of the stream on the sky or the radial velocities of stars within the stream were given more weight in constraining the models. The precise angular position of stellar debris across the sky is, of course, a function of the orbital trajectory of the parent satellite on the sky, but that trajectory is a function of time due to imposed orbital plane precession if the dominant potential is non-spherical, with the direction of that precession having opposite signs for prolate versus oblate halos. Thus, any variation in the orbital plane of Sgr debris on the sky is a reflection of the orbital plane precession of the Sgr core and will have been strongly influenced by the shape of the gravitational potential. Meanwhile, radial variations of the Sgr debris are a function of both the radial form of the potential as well as its three-dimensional shape, and these radial variations are most easily reflected in the observed line-of-sight velocities (which are *much* easier to measure accurately than are the distances of the stream stars).

Early investigations of the combined Sgr velocity-position data showed the contradictory results that only models with an oblate to spherical dark halo can reproduce the angular path of the leading stream on the sky well (Johnston et al. 2005; Law et al. 2005; Fellhauer et al. 2006; Martínez-Delgado et al. 2007), but these same models cannot at the same time match the observed radial velocities of those stars (these models predict infalling velocities of the northern leading arm debris that are far too extreme). On the other hand, models with a prolate dark halo can match the leading arm velocities well, but not their positions on the sky (Helmi 2004; Law et al. 2005). The heart of the leading arm velocity/position conundrum can be seen in Fig. 2.10: While prolate models force the leading arm to arc well over the solar neighborhood (left panel) and thereby reduce the observed line-ofsight velocities of the constituent stream stars as needed to match the observations, the angular precession experienced by the leading arm in such a prolate potential is in strong conflict with the observed positions of the leading stream on the sky (right panel). Ironically, in contrast to the great discriminating power of the Sgr leading arm, the observed runs of position and velocity of the southern (dynamically young) parts of trailing stream seem to have little sensitivity to the shape of the adopted halo potential.

In hindsight, it is perhaps not too surprising that a solution to this quandary is offered by modeling the dark halo as having a *triaxial* configuration instead of the axisymmetric form described by Eq. (2.3). As demonstrated by Law et al. (2009) and LM10, such a gravitational potential makes possible *N*-body simulations that can simultaneously match the positions, velocities, and distances of both trailing and leading arm stars (see Figs. 2.9 and 2.11). Similar results were found by Peñarrubia et al. (2010) using more physically-motivated, "NFW" (Navarro et al. 1997) models for the Galactic dark matter distribution, and Deg and Widrow (2013) using a Bayesian probability analysis.

Despite the success of this triaxial halo model, it is, however, a quite unsatisfying one because of the seemingly unlikely shape and orientation of the inferred dark matter distribution—i.e., strongly oblate (yielding a potential with triaxial 3-D axis ratios of [minor/major] = $[c/a]_{\phi}$ = 0.72 and [intermediate/major] = $[b/a]_{\phi}$ = 0.99), but with the minor axis within 7° of the Galactic X-axis (i.e., axis along

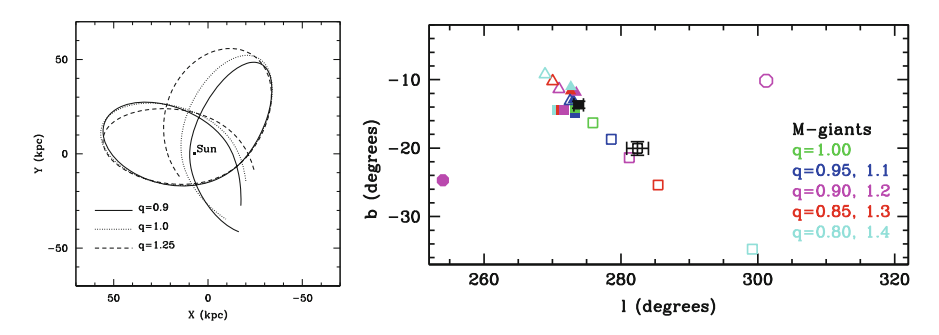


Fig. 2.10 Left panel: side view of Sgr orbital paths in oblate, spherical, and prolate Galactic potentials; note the proximity of the leading arm to the Sun in oblate and spherical models, resulting in maximal projection of the orbital velocity of stream stars onto the line of sight. Right panel: positions of apparent orbital poles for observed 2MASS M giants (black squares) and simulated tidal debris (colored symbols). Open (filled) symbols represent the planar poles of leading (trailing) debris; colored squares (triangles) represent simulations in oblate (prolate) potentials color-coded according to the oblateness (prolateness) of the simulation. Note that almost any model halo matches the position of the trailing debris (solid symbols), whereas only an oblate model (in this case, best matched by a q=0.90 oblateness) can match the orbital poles of the leading arm debris (open symbols). To demonstrate the potential influence of orbital plane precession on the Sgr core over greater spans of time, the figure includes circles that represent the orbital poles expected for even older tidal debris as calculated in a q=0.90 simulation. Figures reproduced from Law et al. (2005) and Johnston et al. (2005)

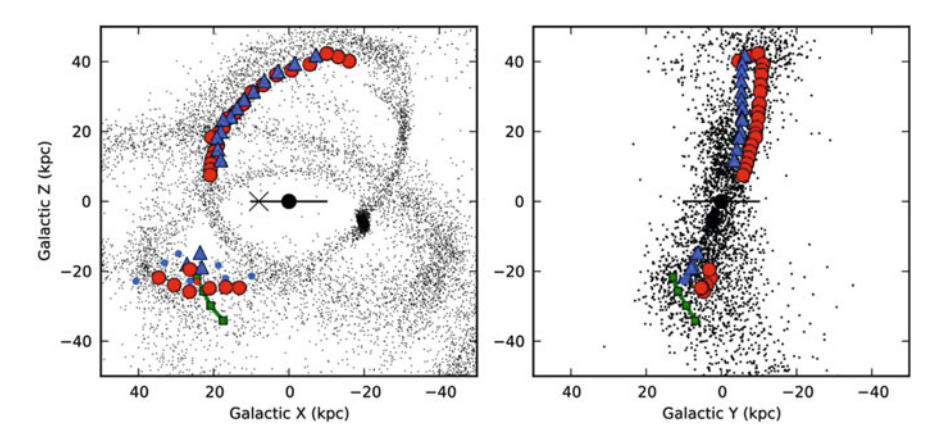


Fig. 2.11 Pan-STARRS observations of stars in the trailing Sgr debris stream (*colored points* with Z < 0) and SDSS observations of stars in the leading Sgr debris stream (*colored points* with Z > 0; note imperfect distance calibration as plotted here) overplotted against the LM10 model. Figure adapted from Slater et al. (2013)

the Sun-Galactic Center line). Such an unexpected orientation, being so strongly non-axisymmetric in the Galactic disk plane, is difficult to reconcile with stable disk star orbits and Cold Dark Matter models generally, which typically produce galaxies having aligned disk and halo minor axes (e.g., Debattista et al. 2008, 2013). Thus, such a well-functioning, utilitarian *numerical* model may not correspond to an identically matching *physical shape* for the intrinsic Galactic potential.

To escape such awkwardness, several, more prosaic, physical scenarios have been proffered that might yield a similar numerical solution. One alternative explanation explored by LM10 focused on the contributing gravitational influence of the Magellanic Clouds, which are orbiting in a plane whose axis is within 1° of that found for the minor axis of the numerically-derived triaxial halo. Although LM10 found that an LMC-mass in an LMC-orbital plane may perturb the Sgr orbit significantly, this issue is somewhat complicated by the issue of whether the LMC is on its first passage around the Milky Way (Besla et al. 2007; Kallivayalil et al. 2013), so that there may not have been sufficient time for the Clouds to exert the net required influence. More recently, Vera-Ciro and Helmi (2013) have had success matching observations by adopting an even more complex Galactic potential than that of LM10—i.e., one that includes a variable shape with radius, from a "ACDMnormal", oblate potential flattened to the disk plane at small radius and only evolving into the triaxial LM10 shape at large radius. Moreover, the unusual outer shape of the dark halo, the authors claim, can be accounted for by including perturbations from the LMC, thereby leading to an entirely "ACDM-palatable" composite gravitational potential. Similarly, Ibata et al. (2013) find that numerical models with a spherical halo can fit the Sgr debris streams if a rising Galactic rotation curve outside the solar circle is adopted—although this solution does result in an extremely large virial mass of $2.6-3.1 \times 10^{12} M_{\odot}$ for the Milky Way, which is inconsistent with other recent results using constraints from Sgr debris (e.g., Gibbons et al. 2014; see Sect. 2.6.2).

2.4.3 Constraining the Mass of the Galactic Disk

The Sgr stream is nearly polar and aligned closely to the Galactic X-Z plane. This particular orientation means that the proper motions of Sgr stream stars enable a measurement of the Local Standard of Rest (LSR) velocity, that, unlike most other methods, is independent of knowledge of the solar Galactocentric distance (Majewski et al. 2006). Because of the fortuitous orientation of the Sgr debris plane, the measured V motion (equivalently, the $\mu_I \cos b$) of Sgr trailing arm stars

⁹Note that the parameters a, b, and c cited here are the commonly used names for the longest to shortest dimensions of a triaxial potential, respectively, and should not be confused with the variables of the same name commonly used as length scale parameters in the defined gravitational potentials given in Eqs. (2.1)–(2.3) above.

is almost completely due to solar reflex motion, and the trailing arm arcs across the Southern Galactic Hemisphere at close enough distances that measuring accurate proper motions is tractable.

As part of a proper motion program in the Kapteyn Selected Areas (SAs; Kapteyn 1906), relatively recent, new epoch photographic observations have been matched to Mt. Wilson 60-in. plates taken from 1909–1912 (for J. Kapteyn) to derive $\sim 1-2$ mas yr⁻¹ per star proper motions in numerous SAs, including SAs intersecting the Sgr trailing arm (e.g., Casetti-Dinescu et al. 2006). With extensive spectroscopic observations to enable the identification of numerous Sgr stream stars in each of a half dozen SAs, the mean proper motions of the Sgr trailing arm have been measured to 0.2–0.7 mas yr⁻¹ per field by Carlin et al. (2012). Using LM10-based models, but rerun with self-consistent gravitational potentials, the simulated Sgr debris yields a best match to the observations when the LSR velocity is Θ_{LSR} = $264 \pm 23 \,\mathrm{km}\,\mathrm{s}^{-1}$ (Carlin et al. 2012), which is higher than has been traditionally assumed, but consistent with other more recent determinations of Θ_{LSR} based on radio-interferometric proper motions of star forming regions in the outer disk (Reid et al. 2009) and Sgr A* (Reid and Brunthaler 2004), as well as the kinematics of disk stars from the SDSS APOGEE (Bovy et al. 2012) and SEGUE surveys (Schönrich 2012).

Carlin et al. (2012) found that these LM10-variant model fits that simultaneously reproduce known position, distance, and velocity trends of the Sgr tidal streams, but with a significantly increased Θ_{LSR} , can only be achieved by increasing the Galactic bulge and disk mass while leaving the dark matter halo fixed to LM10-like values. However, an apparent bonus of these self-consistent Milky Way models is that they imply a proper motion for the Sgr core that is much more consistent with the mean of astrometric observations available at the time (Dinescu et al. 2005; Pryor et al. 2010) than that from an LM10 model with the traditional $\Theta_{LSR} = 220 \,\mathrm{km \, s^{-1}}$ (Fig. 2.8). This satisfying self-consistency has thus far been upheld by more recent measurements of the Sgr core proper motion by Massari et al. (2013) and Sohn et al. (2015), though the latter authors also find that a somewhat smaller LSR velocity than found by Carlin et al. (though still larger than the traditional 220 km s⁻¹, and closer to the Reid et al. values cited above) might also provide a good match to the Sgr core proper motion if the distance of the core were assumed to be closer to 24 kpc than the (Siegel et al. 2007) value of 28 kpc assumed by LM10.

2.5 Mass, Luminosity and Mass-to-Light Ratio of Sagittarius

To place the Sgr system within the context not only of the Milky Way satellite system, but also within the expected distributions of the masses of accreted bodies for Milky Way-like systems predicted by hierarchical galaxy formation models more generally, it is of interest to ascertain the properties of the Sgr progenitor. We have previously discussed the likely stellar population and chemical properties of the progenitor and its potential similarities to the SMC (Sect. 2.3); here we focus on

the mass and luminosity of the present and former Sgr satellite, which demonstrate further similarities to the SMC.

Initial estimates of the luminosity of the present day Sgr core by Ibata et al. (1995) varied from $M_V = -13$ to -14 depending on the assumed metallicity of the component stellar populations, while estimates by Mateo et al. (1998) found a similar range $M_V = -13.4$ to -14.6 for various models of the internal structure of Sgr and a distance modulus of $(m - M)_0 = 17.0$. With full knowledge of the distribution of stellar types in the Sgr core and tails, however (see Sect. 2.3), it is possible to estimate the total luminosity of the system more accurately. For example, Majewski et al. (2003) derived a total luminosity by integrating the King profile fit to the two-dimensional shape of Sgr based on 2MASS M giants coupled with a measurement of the satellite's central surface brightness. This method yields a total core absolute magnitude of $M_V = -13.64$ if the Siegel et al. (2007) distance modulus of $[m-M]_0 = 17.27$ is assumed; this corresponds to a core luminosity of $L_{\rm Sgr} = 2.4 \times 10^7 L_{\odot}$. Niederste-Ostholt et al. (2010) took a slightly different approach, summing available 2MASS and SDSS observations of stars in the Sgr core within the strong fall off ("break") in its radial density profile and assuming symmetry between the leading and trailing sides of the dSph to derive $M_V = -14.2 \pm 0.1 \ (L_{\rm Sgr} \sim 3 - 4 \times 10^7 L_{\odot}$, depending on the adopted luminosity function).

Given the substantial tidal disruption that Sgr has suffered, however, the luminosity of the present-day remnant dSph is only a fraction of the total luminosity of the Sgr system as a whole. Indeed, using composite luminosity profiles based on a combination of 2MASS and SDSS observations, Niederste-Ostholt et al. (2010) estimate that the present-day streams represent the *majority* of the total luminosity of the system at $\sim 7-9 \times 10^7 L_{\odot}$! Combining estimates of the luminosity in the core plus tidal streams, the total luminosity of the Sgr progenitor appears to have been $\sim 10-14 \times 10^7 L_{\odot}$ (Niederste-Ostholt et al. 2010, 2012), slightly less luminous than the present-day Small Magellanic Cloud.

Estimates of the mass of Sgr typically range from approximately a few $10^8 M_{\odot}$ to $10^9 M_{\odot}$. Early numerical models by Ibata et al. (1997) suggested that a present-day mass $\sim 10^9 M_{\odot}$ was required to explain the survival of Sgr within the Galactic gravitational potential. More recent models revise this estimate downwards somewhat, finding (LM10) that a present-day bound mass (within $\sim 4^{\circ}$ of the center) of $2.5^{+1.3}_{-1.0} \times 10^8 M_{\odot}$ best reproduces tidal streams with the observed velocity dispersion (e.g., Majewski et al. 2004; Law et al. 2004; Monaco et al. 2007). Although LM10 did not attempt to model the Sgr core in detail, simulations by Łokas et al. (2010) that more accurately treat the dark/light matter separation and account for anisotropy in fitting the observed velocity dispersion profile of the Sgr core (see, e.g., Majewski et al. 2013) obtain similar estimates of $5.2 \times 10^8 M_{\odot}$ ($2.1 \times 10^8 M_{\odot}$) within 12° (4°) of the center of the dSph (similar to the $5.8 \pm 0.5 \times 10^8 M_{\odot}$ estimate of Majewski et al. 2003).

In the cosmologically-motivated NFW dark matter halo model of Łokas et al. (2010), the initial virial mass of the Sgr progenitor would have been $\sim 1.6 \times 10^{10} M_{\odot}$, which suggests that Sgr has shed a large percentage of its initial mass over the course

of its interaction with the Milky Way. This implies that the mass-to-light ratio, Υ_{\odot} , has likely significantly evolved over the lifetime of the dwarf, from an initial value of $\Upsilon_{\odot} \sim 100$ to a present-day value of $\Upsilon_{\odot} \sim 5$ –25.

2.6 Outstanding Issues Regarding the Detailed Structure of the Sagittarius System

Lest we be complacent in believing that we have arrived at a reasonably accurate description of the Sgr-Milky Way system that adequately explains the dynamics of the merger and that successfully models the phase space distribution of Sgr debris, some recent observations reveal unexpected features belying significantly greater complexity in the system than hitherto assumed. Among the most fascinating, and at the same time vexing, discoveries is that the Sgr stream is either "bifurcated" or composed of two separate but largely parallel streams; this bifurcation cannot readily be reproduced by present numerical simulations. Additionally, several claimed detections of older sections of the stream wrapped more than 180° around the Galaxy from the Sgr core also do not comport to the most successful models, but also do not necessarily agree with one another. We end by discussing these new challenges to our understanding of the Sgr system—challenges that, as of this writing, have yet to be adequately explained by any existing model of the Sgr system.

2.6.1 A Bifurcated Stream Density Profile

Making use of the expansive and detailed view of the Sgr stream provided by SDSS imaging data, Belokurov et al. (2006) demonstrated that the Sgr leading arm bifurcates into brighter and fainter components separated by up to ~15° on the sky (see Fig. 1.7 in Chap. 1). This secondary stream appears not only to closely parallel the brighter, "primary" branch of the leading stream in position on the sky, but also in distance (within ~5 kpc; Belokurov et al. 2006; Yanny et al. 2009; Correnti et al. 2010; Ruhland et al. 2011; Slater et al. 2013), radial velocity and metallicity (Yanny et al. 2009). This fainter branch was originally thought to be an older secondary wrap of the Sgr tidal stream (Fellhauer et al. 2006), and the close adherence of the primary and secondary streams to nearly the same orbital plane was interpreted as evidence in favor of a spherical halo in which streams would experience minimal precession of the orbital poles. However, in addition to requiring halo sphericity, to have debris in so closely overlapping orbital "rosettes" also requires a very specific radial form of the Milky Way potential as well as a much longer timescale of disruption than is evident from any other observation (LM10).

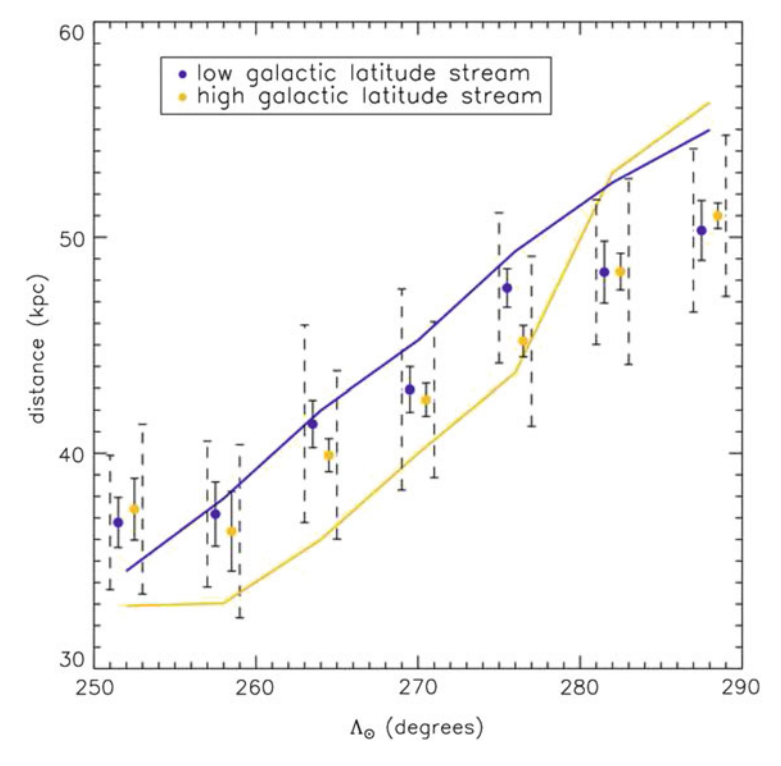


Fig. 2.12 Distances to the bright/faint branches of the Sgr leading stellar tidal stream in the Northern Galactic Hemisphere by Ruhland et al. (2011) based on blue horizontal branch (BHB) stars from SDSS DR7 (figure reproduced from that reference)

On the other hand, the similarity in distances, kinematics, and composition of the bright and faint streams (e.g., Fig. 2.12) suggests, instead, that they represent stream debris at the *same* orbital phase. LM10, for instance, noted that the angular width of simulated streams naturally vary with position along the orbit, and attempted to describe the leading-arm bifurcation as a 'spray' of stars extending from the main stream up to higher declinations. However, the resulting density profile was not a good match for the two clearly separate tracks of debris described by the observational data. In turn, Peñarrubia et al. (2010) noted that the density structure of simulated streams depends on the internal kinematics of the progenitor object, and found that a rotating Sgr progenitor can give rise to bifurcated tracks of tidal debris similar to those observed. Nevertheless, as discussed by Peñarrubia et al. (2010; see also Frinchaboy et al. 2012), this explanation seems unlikely because there is no observed rotation within the present-day remnant Sgr core (although cf. Łokas et al. 2010, who find that a morphological transformation of a rotating progenitor via tidal stirring may result in a non-rotating remnant).

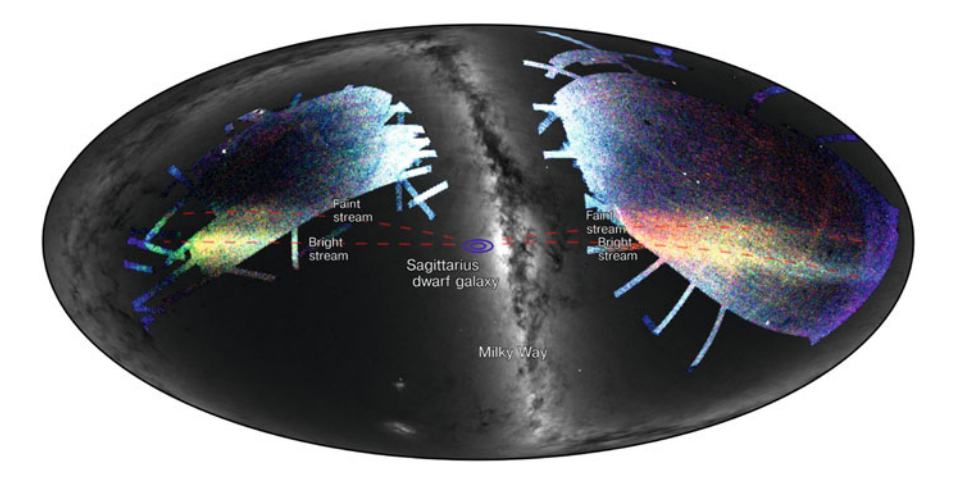


Fig. 2.13 Sgr bright and faint streams in the Northern (*right*) and Southern (*left*) Hemispheres on an Aitoff projection in the Sgr orbital plane. Image credit: S. Koposov

As if the bifurcated leading arm weren't mysterious enough, Koposov et al. (2012) have shown (Fig. 2.13) that a bifurcation also appears in the trailing arm in the Southern Galactic Hemisphere. Together, the northern and southern bifurcations evoke an impression that over a vast span of the sky the fainter, secondary Sgr stream parallels the high-surface brightness primary branch of the Sgr stream, offset by $\sim 10^{\circ}$ to lower Sgr latitude coordinates, B_{\odot} (i.e., higher declination for a given right ascension) as illustrated in Fig. 2.13.

One suggestion posited to explain these parallel tracks is that they are dual debris streams from independent bodies participating in a group infall, e.g., perhaps the present-day Sgr core was gravitationally bound to a smaller companion dwarf when it fell into the Milky Way (e.g., D'Onghia and Lake 2009; Newby et al. 2013), similar to the Large/Small Magellanic Cloud system. However, while this is an attractive paradigm, it is difficult to understand why the faint stream is always on the same side of the brighter stream and parallels it at a nearly constant angular separation throughout nearly 360° of orbital longitude when one might expect the debris streams to cross, or at least change separations, if the progenitors were orbiting semi-independently about the Milky Way center. Perhaps the combined three-body interaction might conspire to produce parallel debris streams as observed over almost a complete 360° span of sky, but presently no numerical simulation exists to demonstrate such a hypothesis.

2.6.2 Multiply-Wrapped Sagittarius Streams

While 2MASS and SDSS observations trace the Sgr tidal streams roughly 360° around the sky, numerical models based on these observations suggest that the

streams may be considerably longer and make specific predictions for where such large-phase tidal debris might be found. The model of LM10 for instance (see Fig. 2.3) predicts that the trailing tidal tail passes through apogalacticon at $\Lambda_{\odot}\sim 180^{\circ}$ and wraps back around the Galaxy in the Northern Galactic Hemisphere, tracking inside the arc of leading tidal debris at a heliocentric distance of about 20 kpc. Similarly, the leading arm of tidal debris is expected to pass through the Galactic disk plane in the direction of the Galactic anticenter and arc through the Southern Galactic Hemisphere before passing through the trailing debris stream and behind the Sgr dwarf core.

Subsequent observations by Correnti et al. (2010) appeared to confirm these predictions with the identification of a faint stream of red clump stars aligned with the Sgr orbital plane that these authors identify as belonging to the Sgr trailing arm wrapped into the Northern Galactic Hemisphere at a distance of \sim 25 kpc (see their Figs. 27 and 28). Similarly, CFHT MegaCam pencil-beam observations by Pila-Díez et al. (2014) detect both the trailing arm wrapped into the North *and* the leading arm wrapped into the south, both at distances that agree well with the LM10 model (see Fig. 2.14).

The Sgr trailing arm therefore seems to match the LM10 model at orbital longitudes $\Lambda_{\odot} = 140^{\circ}$ (in the Southern Galactic Hemisphere) and $\Lambda_{\odot} = 260^{\circ}$ (in the Northern Galactic Hemisphere), and in between is expected to reach apogalacticon at a heliocentric distance of ~60 kpc. However, through further analyses of faint stars in the SDSS, 2MASS, and WISE databases, M giant stars attributed to the trailing arm in this intervening longitude range, $\Lambda_{\odot} \sim 180^{\circ}$, have more recently been observed (Belokurov et al. 2014; Koposov et al. 2015) to reach apogalacticon at a distance not of $60 \,\mathrm{kpc}$, but $\sim 100 \,\mathrm{kpc}$ instead! Moreover, these stars, if Sgr debris, suggest an apogalactic position ($\Lambda_{\odot} = 180^{\circ}$) for the trailing arm debris more widely separated from the Sgr core than predicted by other models (e.g., LM10; see lower right panel of Fig. 2.9). While it might be possible that these stars are not actual Sgr debris, or at least not Sgr debris corresponding to the youngest parts of the trailing arm located at orbital phases of the most recent apogalacticon (i.e., the magenta-colored regions of the trailing arm as shown in the schematic model in Fig. 2.3), the detected stars appear to have radial velocities near $0\,\mathrm{km\,s^{-1}}$ (as expected for a stream near apogalacticon), and are consistent with distances measured for tentatively identified Sgr blue horizontal branch stars (Ruhland et al. 2011) and RR Lyrae (Drake et al. 2013), as well as the globular cluster NGC 2419, which was noted to align with the Sgr orbital plane a decade earlier by Newberg et al. (2003, see Fig. 2.15).

Based on initial analyses, it appears to be difficult to accommodate such a large apogalacticon distance for the Sgr trailing tidal tail while maintaining all previously-determined distances for the leading arm. Belokurov et al. (2014) hypothesize that the newly suggested angular separation of Sgr leading and trailing tail apogalactica on the sky implies that the dark matter density of the Milky Way falls off faster than the isothermal haloes typically invoked by numerical models (e.g., that of the LM10 model used as a baseline reference throughout this overview of the Sgr system). This adjustment to the adopted Galactic potential may also account for

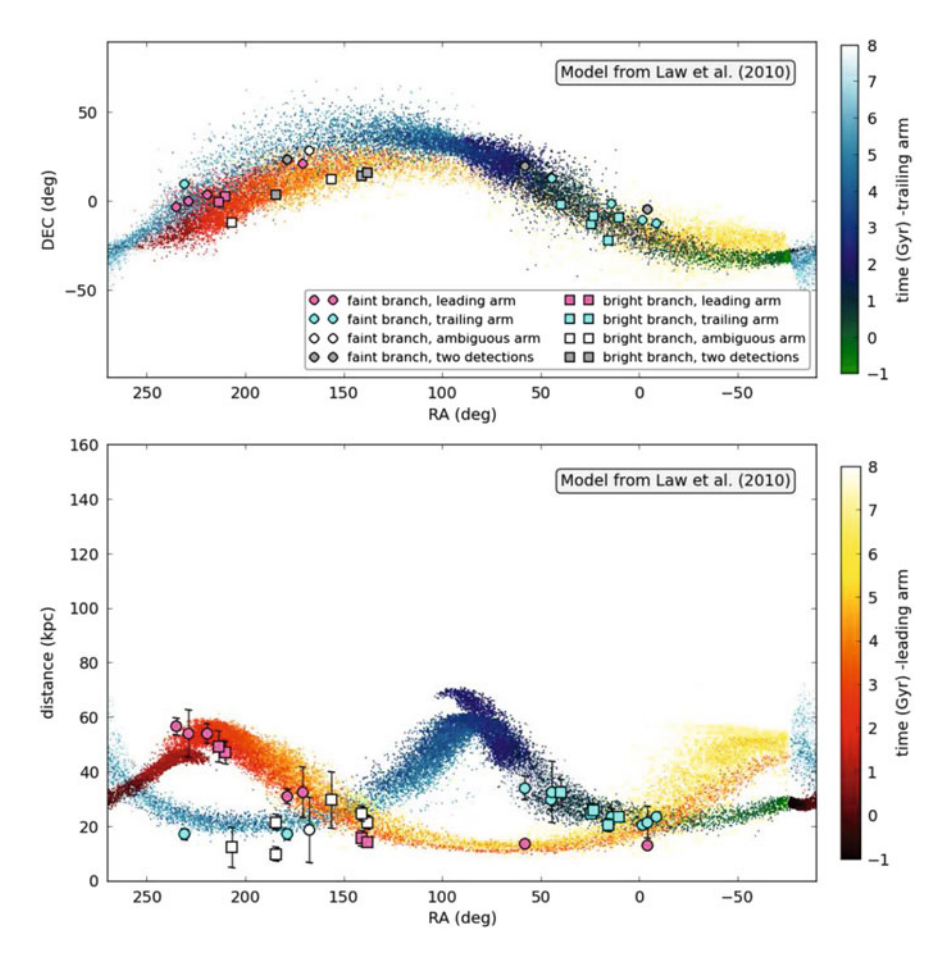


Fig. 2.14 CFHT MegaCam observations of Sgr tidal debris (*solid points*) compared to the LM10 tidal disruption model. Figure taken from Pila-Díez et al. (2014)

the vastly different *distances* predicted for this section of the trailing arm (Gibbons et al. 2014), however, it remains to be seen whether such models can account for all other extant observations of the Sgr stream. Alternatively it is possible that satisfactory solutions may be obtained by recourse to more complicated models—e.g., models that incorporate dynamical friction producing a drag on Sgr as it orbits in the Galactic potential (e.g., Zhao 2004) or that even more accurately include the perturbative effects of the Magellanic Clouds (e.g., following on the work of Vera-Ciro and Helmi 2013)—yet it is still the case that no model of the Sgr system currently exists that can now reproduce all of the presently available observational constraints. Such recurring discoveries of unexpected features of the Sgr stream humble the earnest work of the modelers, and ensure that the Sgr system will hold the attention of both observers and theorists for some time to come.

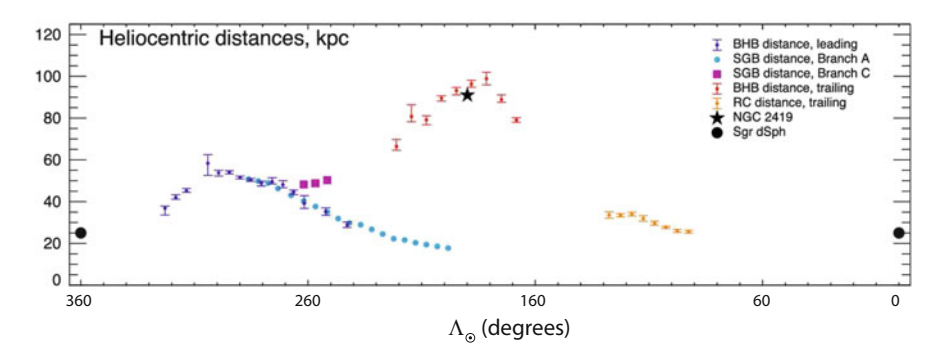


Fig. 2.15 Distances to sections of the Sgr leading and trailing streams based on recent observations by Belokurov et al. (2014). Note the *red points* around $\Lambda_{\odot} \sim 180^{\circ}$ at the unexpected distances of ~ 100 kpc. Compare to the relatively consistent apogalacticon distances predicted by the model shown in Figs. 2.9 and 2.14. Figure adapted from Belokurov et al. (2014) and converted to the Λ_{\odot} reference frame of Majewski et al. (2003)

References

Alard, C. 1996, ApJ Lett, 458, L17

Alard, C. 2001, A&A, 377, 389

Battaglia, G., Tolstoy, E., Helmi, A., et al. 2006, A&A, 459, 423

Battaglia, G., Tolstoy, E., Helmi, A., et al. 2011, MNRAS, 411, 1013

Bekki, K., & Freeman, K. C. 2003, MNRAS, 346, L11

Bellazzini, M., Ferraro, F. R., & Buonanno, R. 1999a, MNRAS, 304, 633

Bellazzini, M., Ferraro, F. R., & Buonanno, R. 1999b, MNRAS, 307, 619

Bellazzini, M., Ferraro, F. R., & Ibata, R. 2002, AJ, 124, 915

Bellazzini, M., Newberg, H. J., Correnti, M., Ferraro, F. R., & Monaco, L. 2006a, A&A, 457, L21

Bellazzini, M., Ibata, R. A., Chapman, S. C., et al. 2008, AJ, 136, 1147

Belokurov, V., Zucker, D. B., Evans, N. W., et al. 2006, ApJ Lett, 642, L137

Belokurov, V., Koposov, S. E., Evans, N. W., et al. 2014, MNRAS, 437, 116

Besla, G., Kallivayalil, N., Hernquist, L., et al. 2007, ApJ, 668, 949

Bonifacio, P., Hill, V., Molaro, P., et al. 2000, A&A, 359, 663

Bonifacio, P., Sbordone, L., Marconi, G., Pasquini, L., & Hill, V. 2004, A&A, 414, 503

Bovy, J., Allende Prieto, C., Beers, T. C., et al. 2012, ApJ, 759, 131

Brown, J. A., Wallerstein, G., & Gonzalez, G. 1999, AJ, 118, 1245

Bullock, J. S., & Johnston, K. V. 2005, ApJ, 635, 931

Buonanno, R., Corsi, C. E., Castellani, M., et al. 1999, AJ, 118, 1671

Burton, W. B., & Lockman, F. J. 1999, A&A, **349**, 7

Carlin, J. L., Majewski, S. R., Casetti-Dinescu, D. I., et al. 2012, ApJ, 744, 25

Carrell, K., Wilhelm, R., & Chen, Y. 2012, AJ, 144, 18

Carretta, E., Bragaglia, A., Gratton, R. G., et al. 2010, A&A, 520, A95

Casetti-Dinescu, D. I., Majewski, S. R., Girard, T. M., et al. 2006, AJ, 132, 2082

Chou, M.-Y., Majewski, S. R., Cunha, K., et al. 2007, ApJ, 670, 346

Chou, M.-Y., Cunha, K., Majewski, S. R., et al. 2010, ApJ, **708**, 1290

Clewley, L., & Jarvis, M. J. 2006, MNRAS, 368, 310

Cohen, J. G. 2004, AJ, 127, 1545

Cole, A. A. 2001, ApJ Lett, 559, L17

Correnti, M., Bellazzini, M., Ibata, R. A., Ferraro, F. R., & Varghese, A. 2010, ApJ, 721, 329

Cseresnjes, P., Alard, C., & Guibert, J. 2000, A&A, 357, 871

Debattista, V. P., Moore, B., Quinn, T., et al. 2008, ApJ, 681, 1076

Debattista, V. P., Roškar, R., Valluri, M., et al. 2013, MNRAS, 434, 2971

Deg, N., & Widrow, L. 2013, MNRAS, 428, 912

Dinescu, D. I., Majewski, S. R., Girard, T. M., et al. 2002, ApJ Lett, 575, L67

Dinescu, D. I., Girard, T. M., van Altena, W. F., & López, C. E. 2005, ApJ Lett, 618, L25

Dohm-Palmer, R. C., Helmi, A., Morrison, H., et al. 2001, ApJ Lett, 555, L37

Dolphin, A. E., Weisz, D. R., Skillman, E. D., & Holtzman, J. A. 2005, arXiv:astro-ph/0506430

D'Onghia, E., & Lake, G. 2009, IAU Symposium, **256**, 473

Drake, A. J., Catelan, M., Djorgovski, S. G., et al. 2013, ApJ, 765, 154

Edelsohn, D. J., & Elmegreen, B. G. 1997, MNRAS, **290**, 7

Fellhauer, M., Belokurov, V., Evans, N. W., et al. 2006, ApJ, 651, 167

Font, A. S., Johnston, K. V., Bullock, J. S., & Robertson, B. E. 2006, ApJ, 638, 585

Frinchaboy, P. M., Majewski, S. R., Muñoz, R. R., et al. 2012, ApJ, 756, 74

Gibbons, S. L. J., Belokurov, V., & Evans, N. W. 2014, MNRAS, 445, 3788

Gilmore, G., Randich, S., Asplund, M. et al. 2012, The Messenger, 147, 25

Giuffrida, G., Sbordone, L., Zaggia, S., et al. 2010, A&A, 513, A62

Hasselquist, S. et al. 2015, in preparation

Helmi, A. 2004, ApJ Lett, 610, L97

Helmi, A., & White, S. D. M. 2001, MNRAS, 323, 529

Hernquist, L., & Ostriker, J. P. 1992, ApJ, 386, 375

Ibata, R. A., Gilmore, G., & Irwin, M. J. 1994, Nature, 370, 194

Ibata, R. A., Gilmore, G., & Irwin, M. J. 1995, MNRAS, 277, 781

Ibata, R. A., Wyse, R. F. G., Gilmore, G., Irwin, M. J., & Suntzeff, N. B. 1997, AJ, 113, 634

Ibata, R., Lewis, G. F., Irwin, M., Totten, E., & Quinn, T. 2001a, ApJ, 551, 294

Ibata, R., Irwin, M., Lewis, G. F., & Stolte, A. 2001b, ApJ Lett, 547, L133

Ibata, R. A., Lewis, G. F., Irwin, M. J., & Cambrésy, L. 2002, MNRAS, 332, 921

Ibata, R., Lewis, G. F., Martin, N. F., Bellazzini, M., & Correnti, M. 2013, ApJ Lett, 765, L15

Ivezić, Ž., Goldston, J., Finlator, K., et al. 2000, AJ, 120, 963

Johnston, K. V., Spergel, D. N., & Hernquist, L. 1995, ApJ, 451, 598

Johnston, K. V., Majewski, S. R., Siegel, M. H., Reid, I. N., & Kunkel, W. E. 1999, AJ, 118, 1719

Johnston, K. V., Law, D. R., & Majewski, S. R. 2005, ApJ, 619, 800

Kallivayalil, N., van der Marel, R. P., Besla, G., Anderson, J., & Alcock, C. 2013, ApJ, 764, 161

Kapteyn, J. C. 1906, Plan of Selected Areas (Groningen: Hoitsema brothers)

Keller, S. C., Yong, D., & Da Costa, G. S. 2010, ApJ, 720, 940

Kirby, E. N., Lanfranchi, G. A., Simon, J. D., Cohen, J. G., & Guhathakurta, P. 2011, ApJ, 727, 78

Klimentowski, J., Łokas, E. L., Kazantzidis, S., et al. 2007, MNRAS, 378, 353

Koposov, S., Irwin, M., Belokurov, V., et al. 2012, ApJ, 750, 80

Koposov, S. E., Belokurov, V., Zucker, D. B., et al. 2015, MNRAS, 446, 3110

Koribalski, B., Johnston, S., & Otrupcek, R. 1994, MNRAS, 270, L43

Kunder, A., & Chaboyer, B. 2009, AJ, 137, 4478

Kundu, A., Majewski, S. R., Rhee, J., et al. 2002, ApJ Lett, 576, L125

Law, D. R., Majewski, S. R., Skrutskie, M. F., & Johnston, K. V. 2004, Satellites and Tidal Streams, 327, 239

Law, D. R., Johnston, K. V., & Majewski, S. R. 2005, ApJ, 619, 807

Law, D. R., Majewski, S. R., & Johnston, K. V. 2009, ApJ Lett, 703, L67

Law, D. R., & Majewski, S. R. 2010a, ApJ, 714, 229 (LM10)

Law, D. R., & Majewski, S. R. 2010b, ApJ, 718, 1128

Layden, A. C., & Sarajedini, A. 1997, ApJ Lett, 486, L107

Layden, A. C., & Sarajedini, A. 2000, AJ, 119, 1760

Lee, Y.-W., Joo, J.-M., Sohn, Y.-J., et al. 1999, Nature, 402, 55

Łokas, E. L., Kazantzidis, S., Majewski, S. R., et al. 2010, ApJ, 725, 1516

Łokas, E. L., Majewski, S. R., Kazantzidis, S., et al. 2012, ApJ, 751, 61

Lynden-Bell, D., & Lynden-Bell, R. M. 1995, MNRAS, 275, 429

Mackey, A. D., Lewis, G. F., Collins, M. L. M., et al. 2014, MNRAS, 445, L89

Majewski, S. R., Siegel, M. H., Kunkel, W. E., et al. 1999, AJ, 118, 1709

Majewski, S. R., Patterson, R. J., Dinescu, D. I., et al. 2000, Liege International Astrophysical Colloquia, 35, 619

Majewski, S. R., Patterson, R. J., Palma, C., et al. 2002, Modes of Star Formation and the Origin of Field Populations, 285, 199

Majewski, S. R., Skrutskie, M. F., Weinberg, M. D., & Ostheimer, J. C. 2003, ApJ, 599, 1082

Majewski, S. R., Kunkel, W. E., Law, D. R., et al. 2004, AJ, 128, 245

Majewski, S. R., Law, D. R., Polak, A. A., & Patterson, R. J. 2006, ApJ Lett, 637, L25

Majewski, S. R., Hasselquist, S., Łokas, E. L., et al. 2013, ApJ Lett, 777, L13

Majewski, S. R., Schiavon, R. P., Frinchaboy, P. M., et al. 2015, AJ, submitted (arXiv: 1509.05420)

Martínez-Delgado, D., Aparicio, A., Gómez-Flechoso, M. Á., & Carrera, R. 2001, ApJ Lett, 549, L199

Martínez-Delgado, D., Zinn, R., Carrera, R., & Gallart, C. 2002, ApJ Lett, 573, L19

Martínez-Delgado, D., Peñarrubia, J., Jurić, M., Alfaro, E. J., & Ivezić, Z. 2007, ApJ, 660, 1264

Massari, D., Bellini, A., Ferraro, F. R., et al. 2013, ApJ, 779, 81

Mateo, M., Olszewski, E. W., & Morrison, H. L. 1998, ApJ Lett, 508, L55

Mayer, L., Governato, F., Colpi, M., et al. 2001, ApJ, 559, 754

McDonald, I., Zijlstra, A. A., Sloan, G. C., et al. 2013, MNRAS, 436, 413

McWilliam, A., Wallerstein, G., & Mottini, M. 2013, ApJ, 778, 149

Monaco, L., Ferraro, F. R., Bellazzini, M., & Pancino, E. 2002, ApJ Lett, 578, L47

Monaco, L., Bellazzini, M., Ferraro, F. R., & Pancino, E. 2003, ApJ Lett, 597, L25

Monaco, L., Bellazzini, M., Bonifacio, P., et al. 2005, A&A, 441, 141

Monaco, L., Bellazzini, M., Bonifacio, P., et al. 2007, A&A, 464, 201

Miyamoto, M., & Nagai, R. 1975, PASJ, 27, 533

Mottini, M., Wallerstein, G., & McWilliam, A. 2008, AJ, 136, 614

Muñoz, R. R., Majewski, S. R., & Johnston, K. V. 2008, ApJ, 679, 346

Navarro, J. F., Frenk, C. S., & White, S. D. M. 1997, ApJ, 490, 493

Newberg, H. J., Yanny, B., Rockosi, C., et al. 2002, ApJ, 569, 245

Newberg, H. J., Yanny, B., Grebel, E. K., et al. 2003, ApJ Lett, 596, L191

Newberg, H. J., Yanny, B., Cole, N., et al. 2007, ApJ, 668, 221

Newby, M., Cole, N., Newberg, H. J., et al. 2013, AJ, 145, 163

Niederste-Ostholt, M., Belokurov, V., Evans, N. W., & Peñarrubia, J. 2010, ApJ, 712, 516

Niederste-Ostholt, M., Belokurov, V., & Evans, N. W. 2012, MNRAS, 422, 207

Palma, C., Majewski, S. R., & Johnston, K. V. 2002, ApJ, 564, 736

Peñarrubia, J., Belokurov, V., Evans, N. W., et al. 2010, MNRAS, 408, L26

Peñarrubia, J., Zucker, D. B., Irwin, M. J., et al. 2011, ApJ Lett, 727, L2

Pila-Díez, B., Kuijken, K., de Jong, J. T. A., Hoekstra, H., & van der Burg, R. F. J. 2014, A&A, 564, A18

Plummer, H. C. 1911, MNRAS, 71, 460

Prior, S. L., Da Costa, G. S., & Keller, S. C. 2009, ApJ, 704, 1327

Pryor, C., Piatek, S., & Olszewski, E. W. 2010, AJ, 139, 839

Putman, M. E., Thom, C., Gibson, B. K., & Staveley-Smith, L. 2004, ApJ Lett, 603, L77

Reddy, B. E., Lambert, D. L., & Allende Prieto, C. 2006, MNRAS, 367, 1329

Reid, M. J., & Brunthaler, A. 2004, ApJ, 616, 872

Reid, M. J., Menten, K. M., Zheng, X. W., et al. 2009, ApJ, 700, 137

Rodgers, A. W., & Paltoglou, G. 1984, ApJ Lett, 283, L5

Ruhland, C., Bell, E. F., Rix, H.-W., & Xue, X.-X. 2011, ApJ, 731, 119

Sarajedini, A., & Layden, A. C. 1995, AJ, 109, 1086

Sbordone, L., Bonifacio, P., Buonanno, R., et al. 2007, A&A, 465, 815

Schönrich, R. 2012, MNRAS, 427, 274

Searle, L., & Zinn, R. 1978, ApJ, **225**, 357

Shi, W. B., Chen, Y. Q., Carrell, K., & Zhao, G. 2012, ApJ, 751, 130

Siegel, M. H., Dotter, A., Majewski, S. R., et al. 2007, ApJ Lett, 667, L57

Siegel, M. H., Majewski, S. R., Law, D. R., et al. 2011, ApJ, 743, 20

Sirko, E., Goodman, J., Knapp, G. R., et al. 2004, AJ, 127, 899

Skrutskie, M. F., Cutri, R. M., Stiening, R., et al. 2006, AJ, 131, 1163

Slater, C. T., Bell, E. F., Schlafly, E. F., et al. 2013, ApJ, 762, 6

Smecker-Hane, T. A., & McWilliam, A. 2002, arXiv:astro-ph/0205411

Sohn, S. T., Majewski, S. R., Muñoz, R. R., et al. 2007, ApJ, 663, 960

Sohn, T. S., van der Marel, R. P., Carlin, J. L., et al. 2015, ApJ, 803, 56

Tolstoy, E., Irwin, M. J., Helmi, A., et al. 2004, ApJ Lett, 617, L119

Totten, E. J., & Irwin, M. J. 1998, MNRAS, 294, 1

Velazquez, H., & White, S. D. M. 1995, MNRAS, 275, L23

Vera-Ciro, C., & Helmi, A. 2013, ApJ Lett, 773, L4

Vivas, A. K., Zinn, R., Andrews, P., et al. 2001, ApJ Lett, 554, L33

Whitelock, P. A., Irwin, M., & Catchpole, R. M. 1996, New Astronomy, 1, 57

Yanny, B., Newberg, H. J., Kent, S., et al. 2000, ApJ, 540, 825

Yanny, B., Newberg, H. J., Johnson, J. A., et al. 2009, ApJ, 700, 1282

Zhao, H. 2004, MNRAS, 351, 891

Zinn, R. 1993, in Smith, G. H., Brodie, J. P., eds, ASP Conf. Ser. 48, The Globular Cluster-Galaxy Connection. Astron. Soc. Pac., San Francisco, p. 38

Zinn, R. 1996, Formation of the Galactic Halo...Inside and Out, 92, 211

Zucker, D. B., de Silva, G., Freeman, K. et al. 2012, in ASP Conf. Ser. 458, Galactic Archaeology:
 Near-Field Cosmology and the Formation of the Milky Way, ed. W. Aoki, M. Ishigaki, T. Suda,
 T. Tsujimoto, & N. Arimoto (San Francisco, CA: ASP), 421

Chapter 3 The Monoceros Ring and Ot

The Monoceros Ring, and Other Substructure Near the Galactic Plane

Brian Yanny and Heidi Jo Newberg

Abstract The outer Milky Way stellar structure known as "The Monoceros Ring" was discovered in imaging data in 2002. Since then, numerous photometric and spectroscopic explorations of this structure, some 18 kpc from the Galactic center and at low Galactic latitudes, have led to a rich discussion in the field on its composition, possible origins, and relevance for theories of galaxy formation and studies of dark matter. This substructure was initially thought to be either a tidal stream from a disrupted dwarf galaxy or the result of a warping and flaring of the Milky Way disk. A newer conjecture is that the structure is due to disk oscillations, possibly caused by a massive Milky Way satellite passing through the disk.

3.1 The Monoceros Ring Is Discovered and Named

One of the large overdensities discovered by Newberg et al. (2002), was a previously unknown and unexpected feature at low Galactic latitude. Although this structure looked similar to the halo structures that were being discovered at that time, a structure at latitudes $|b| < 30^{\circ}$ could as easily be associated with the Galactic disk as with the halo. Thus, a controversy over the nature of the structure ensued.

Two pieces of this low latitude feature, labeled S223+20-19.4 and S200-24-19.8, are visible in Fig. 1.5 of Chap. 1. Other pieces of this overdensity

B. Yanny (⊠)

Fermilab, 500 Pine Street, Batavia, IL 60510, USA

e-mail: yanny@fnal.gov

H.J. Newberg

Department of Physics, Applied Physics and Astronomy, Rensselaer Polytechnic Institute,

110 8th St., Troy, NY 12180, USA

e-mail: heidi@rpi.edu

¹These labels can be dissected as: "S" for stream, followed by the Galactic longitude at which the overdensity is identified, followed by the (signed) Galactic latitude of the overdensity, and then finally with the apparent magnitude of the overdensity in turnoff stars (which have an absolute magnitude of $M_g \sim 4.2$, and so a rough distance modulus can be determined). The

were identified as S218+22-19.5 and S183+22-19.4. Three of these overdensities were in the north Galactic cap; the fourth, below the plane at S200-24-19.8, was considered to be associated with the others at lower significance. All of these detections are within 40° of the Galactic anticenter at $(l,b)=(180^{\circ},0^{\circ})$. Note that the apparent magnitude of the southern overdensity is about 0.4 magnitudes fainter than those in the north (see below where relative distances of overdensities are discussed in more detail).

A sample color-magnitude Hess diagram of the stars in S223+20-19.4 is shown in Fig. 3.1. The stars with a blue turnoff at $g_0 = 19.4$ are part of a clear main sequence, indicative of a stellar population concentrated in a narrow distance range. The brighter stars (with a turnoff at $g_0 \sim 16.5$) are somewhat more spread out in apparent magnitude, and although the authors were not able to fit the magnitude distribution of the brighter stars with standard double-exponential disk profiles, these stars plausibly belonged to the disk as it was understood at the time. Examining the plot in Fig. 3.1, one could interpret the brighter $(g_0 \sim 16.5 \text{ turnoff})$ stars as disk stars, followed by a gap at greater distance from the Sun (fainter magnitude), and then an unexpected overdensity of stars 11 kpc from the Sun at a Galactic latitude of $b = 20^{\circ}$. The red stars $((g - r)_0 > 1)$ are almost entirely M-type main sequence stars in the disk. The falloff in disk stars with apparent magnitude was consistent with other measurements of the Milky Way disk, which noted a sudden drop in the density of disk stars at 14–15 kpc from the Galactic center (for example Robin et al. 1992). The low latitude structure was estimated to be about 18 kpc from the Galactic center, placing it well beyond the known stellar disk, and has a line-of-sight full width half maximum (FWHM) depth (in the third dimension of distance from the Sun) of less than 6 kpc.

Also of note in Fig. 3.1 is that the turnoff of the faint main sequence is at $(g-r)_0 \sim 0.3$, which is significantly bluer than the turnoff of the thick disk stars at $(g-r)_0 \sim 0.4$. Newberg et al. (2002) interpreted the bluer turnoff as evidence for a more metal-poor population, as had been identified in the Sagittarius dwarf tidal stream, though the effect could also be due to a population with a younger stellar age.

Figure 3.2 shows the positions of the SDSS stripes in which the Monoceros-Canis Major structure (as it was named in the original 2002 paper, based on limited SDSS sky coverage), was identified. It was assumed that the structure filled the whole space in between detections above and below the plane, including lower latitude areas where no SDSS data were available. At the time, it was expected that this structure was the result of tidal disruption of a dwarf galaxy, since the density maps looked similar to those of the Sagittarius dwarf tidal stream. However, because this structure was at low latitude, one could not rule out a disk origin for these stars.

three-dimensional naming scheme allowed the marking of star overdensities that could later be connected together to trace streams across the sky. The apparent magnitude was used instead of distance because it could be measured directly, while the distance was likely to change each time the distance scale was recalibrated. Ultimately, this naming scheme fell into disuse, as the labels of these overdensities were difficult to say and remember.

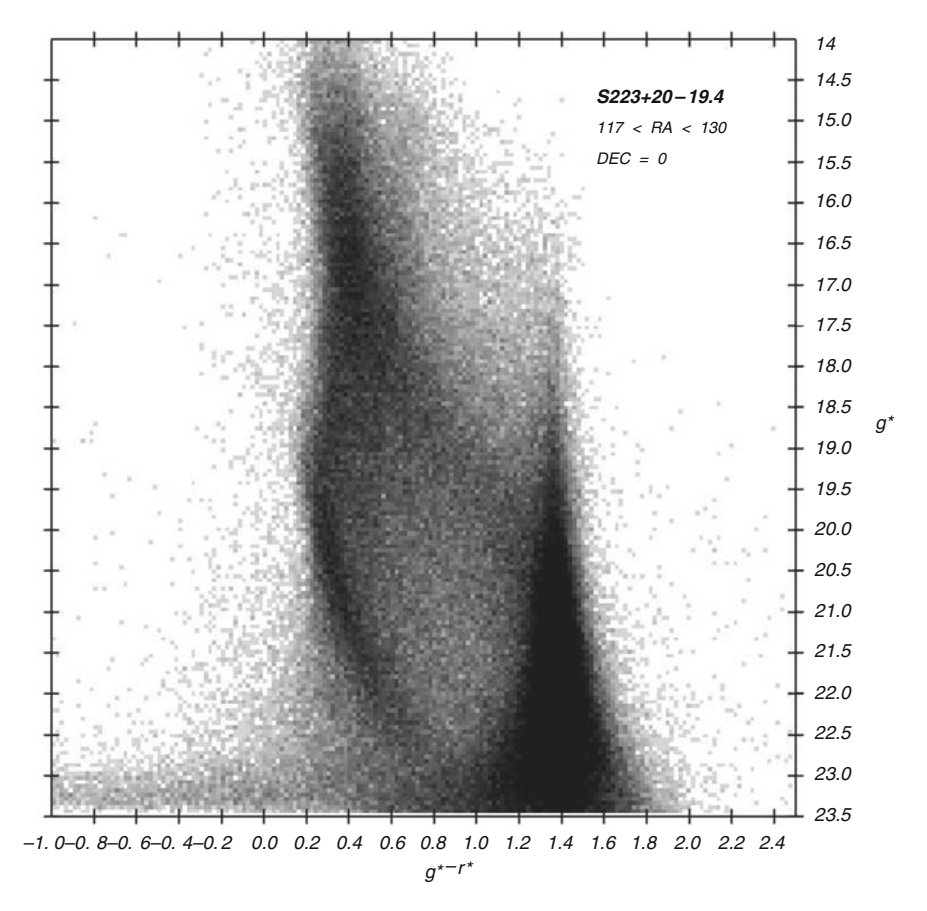


Fig. 3.1 Figure 12 from Newberg et al. (2002). The lower main sequence beginning about $[(g - r)_0, g_0] = [0.3, 19.4]$, with a turnoff distinctly bluer and fainter than that of the thick disk $[(g - r)_0, g_0] = [0.4, 16.5]$, is due to the Monoceros Ring structure. The width of the main sequence in the structure indicates that the structure cannot have a radial extent of more than a few kpc. The position of the turnoff at $g_0 = 19$ indicates that the structure is at a distance of 11 kpc beyond the Sun, or about 18 kpc from the Galactic center, since this data is in the direction $(l, b) = (223^{\circ}, 20^{\circ})$

Within a year of the original publication, two papers were published that concluded the low latitude structure was ring-like, and could potentially encircle the entire galaxy. A stellar mass of about 5×10^8 solar masses, if one extends the ring completely around the Galaxy, is consistent with both papers.

The first of these papers (Yanny et al. 2003), entitled "A low-latitude halo stream around the Milky Way," traced the structure from $180^{\circ} < l < 227^{\circ}$, and noted that it extended 5 kpc above and below the Galactic plane, though the southern portion was 2 kpc further away. The maximum line-of-sight depth of the structure was reduced to <4 kpc FWHM. Spectra of stars in the overdensity showed that the velocity dispersion (\sim 25 km/s) was similar to that measured for the Sagittarius dwarf tidal

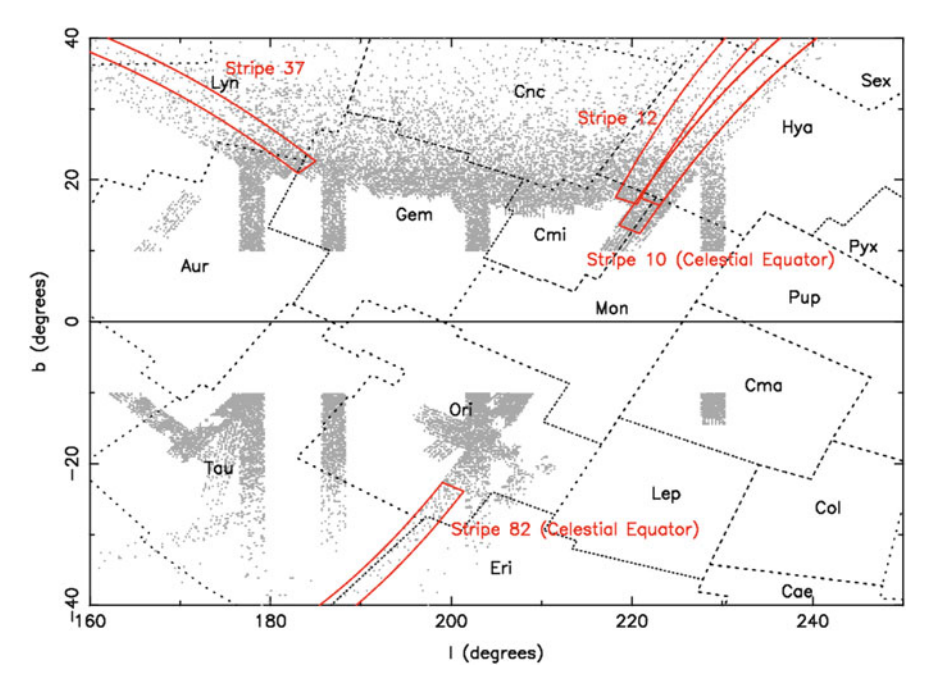


Fig. 3.2 Adapted from Fig. 26 of Newberg et al. (2002). A Galactic longitude-latitude map of the density of SDSS turnoff stars with $19 < g_0 < 19.5$ is shown. This picks out stars some 10–12 kpc from the Sun toward the anti-center. *Heavier grey* indicates larger star density. The original plot only showed data in the *red outlined* SDSS stripes, stripes 10, 12, 37, and 82. The strongest signal was seen near the end of stripe 10, near the constellation Monoceros, which led to the structure's name. The IAU constellation boundaries are delimited by *dotted lines*. *White regions* indicate a lack of SDSS data. All SDSS data from low latitude $|b| < 10^{\circ}$ regions are also excluded

stream. At the time, the authors thought that because this velocity dispersion was lower than that of the thick disk (typically 40–50 km/s) and the scale height was larger than the thick disk, they had definitive evidence that the structure was a tidal stream, even though its stars appeared to rotate in the same direction and with similar bulk velocity to the disk. It was later pointed out, however, that one could have a large scale height with a small velocity dispersion if the mass density of the disk was considerably lower. So the question of the nature of the ring remained undecided.

A second paper, simultaneously written by Ibata et al. (2003), was entitled "One ring to encompass them all: a giant stellar structure that surrounds the Galaxy." In this paper the ring is not actually traced around the entire galaxy, but is detected in the range $120^{\circ} < l < 200^{\circ}$. This paper suggests the ring could be an artifact in the disk caused by either repeated warpings (the favored explanation), a tidal stream from an accreted satellite, or part of an outer spiral arm. In this paper, the stars to the south of the plane that are associated with the ring in the north are actually *closer* to us than the ones in the north. This is in contrast to the identification made by Newberg et al. (2002); this early discrepancy in the identification of the south part

of the ring precedes a decade of literature that is inconsistent about the identification of "ring" stars south of the Galactic plane.

Soon after the two "ring" papers were published, Rocha-Pinto et al. (2003) showed that the ring was visible in M giant stars (which are by their nature fairly metal-rich), establishing that there is a range of metallicities present in this structure. They showed that the structure spanned at least 100°. Because they note that the unexpected distribution of stars covers more than one constellation, and because they believed it was the result of a tidally disrupting dwarf galaxy, due to the apparent variation in density along the structure, they renamed the structure the Galactic Anticenter Stellar Stream (GASS).

These early papers, which each used different names for the low latitude structure, and which ascribed the structure to different origins, led to a wide variety of names used to refer to it. The names include: Monoceros-Canis Major structure, One Ring, low latitude stream, Monoceros Stream, Galactic Anticenter Stellar Structure (GASS), Monoceros Overdensity, Canis Major Stream, Argo Navis Stream, stream in the Galactic plane, etc. Of all of the names, the "Monoceros Ring" label gained the most popularity. This was consistent with the practice of naming tidal streams by the constellation in which the first piece of the stream was detected, which is one of several commonly used naming schemes. The awkward Slll+bb-mm names for each detected piece of the structure all but disappeared from the literature.

3.2 Dragged In or Dredged Up? The Debate Over the Origin of the Monoceros Ring

These early papers describe an unexpected overdensity of stars at a distance of 11 kpc from the Sun, that spans at least 100° in length, is 40° from North to South (though supposed stream pieces were not directly seen to connect observationally as they crossed the high extinction region near the Galactic plane), and has coherent velocities with a velocity dispersion of 25 km/s. If this structure had been discovered at high Galactic latitude, there would have been no question that it was a tidal stream from a disrupted dwarf galaxy. But because it was discovered at low Galactic latitude, and particularly because the supposed tidal stream appeared to be on a fairly circular prograde orbit, just like the disk, one had to consider the possibility that the structure belonged to the disk. About half of the experts in the field thought it was tidal debris and the other half preferred the disk explanation.

It turns out to be quite difficult to tell which explanation is correct. Either way, the stars are moving in the same potential, so the kinematics should be similar. The Monoceros Ring stars have a lower metallicity than known disk stars, but since the metallicity of disk stars falls off with distance from the Galactic center that does not rule out a disk origin. The velocity dispersion also was not a definitive discriminator. The non-zero radial velocity at $l=180^{\circ}$ argued in favor of a tidal stream, but alternatively this could be the result of a small axial asymmetry in the



Fig. 3.3 SDSS *gri* Image of NGC 2859 constructed by Blanton and Hogg via the method described in Lupton et al. (2004). This small galaxy, while not a full sized spiral like the Milky Way, is surrounded by a planar stellar ring. There is a significant drop in star density between the end of the central 'disk' and the beginning of the stellar ring. Whether or not the Monoceros structure is separated by a similar drop in stellar density beyond the edge of the Milky Way's stellar disk, is not known

disk. Hans-Walter Rix nicely framed the debate as a question of whether the stars in the Monoceros Ring were born in smaller galaxies and "dragged in" by the Milky Way's gravity, or "dredged up" from the Milky Way's disk to higher latitudes.

If the disk disappears at 15 kpc from the Galactic center and then the Monoceros Ring appears at 18 kpc from the Galactic center, then as seen from a vantage point outside the Milky Way, our galaxy would resemble that shown in Fig. 3.3. In this image of an actual galaxy, one sees a clear ring, with a gap of lower stellar density separating the ring from a smaller stellar disk. Of course, one cannot have such a vantage point on the Milky Way.

Several authors raised the possibility that a flare of the Galactic thick disk with a scale length of $h_l = 3.5 \,\mathrm{kpc}$ (with the flaring starting at about $R_{GC} = 16 \,\mathrm{kpc}$) and accompanied by a slight warp to explain north-south differences (similar to that seen in HI gas at lower latitudes), could entirely explain the Monoceros Ring structure (Momany et al. 2006; Moitinho et al. 2006; Carraro and Costa

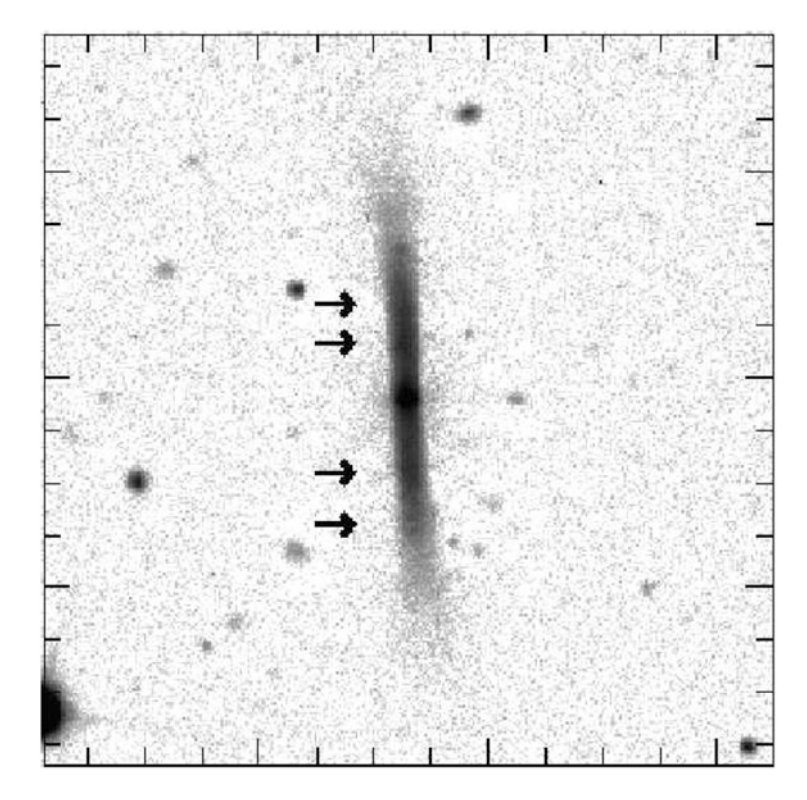


Fig. 3.4 Image from De Rijcke et al. (2003) of F288, a Fornax cluster dwarf elliptical with embedded disk. Note the significant flaring of the disk in the outer parts. Some have argued that the Monoceros structure in our own Galaxy could be produced by a similar flaring of our stellar disk

2009; Hammersley and López-Corredoira 2011; Lopez-Corredoira et al. 2012). To visualize this, see, for example, Fig. 3.4 which shows a extragalactic disk with a flare of stars embedded in a larger elliptical potential. The Monoceros Ring structure could be a manifestation of a similar flare in the outskirts of our Milky Way (López-Corredoira et al. 2002; Feast et al. 2014).

This flare-and-warp-of-the-outer-disk explanation for Monoceros, however, has difficulty explaining the narrow radial velocity dispersion of Monoceros stars in any given line of sight, relative to closer thick-disk star populations (Meisner et al. 2012).

Recent infall of gas from the outer regions of the halo can result in stars with lower metallicity than that of the local thick disk, yet still perhaps be considered disk stars (rather than a distinct stream-like structure). Yong et al. (2006) showed that some of the Cepheid variables in the disk have low metallicity and high alpha abundances, as if they had come from an accretion event, and suggested that the Monoceros Ring could be the result of a merger that contributes to the growth of the outer disk; there is marginal evidence that the "knee" in the $\lceil \alpha/\text{Fe} \rceil$ vs. $\lceil \text{Fe}/\text{H} \rceil$

distribution is at lower [Fe/H] in Monoceros stars vs. the Galactic disk, as also seen in some dSphs (Chou et al. 2010; Meisner et al. 2012). The extent of a thick disk at these large Galactic radii, however, is not clear. In fact, as Yong et al. (2006) and Schlesinger et al. (2014) show, the distinction between thin and thick disks may be an artificial one, especially at large radii and significant vertical distance where late infalling gas can lead to a metallicity gradient.

Additional measurements of the stellar thick disk geometry suggest that Monoceros and the thick disk are distinct; work by Cheng et al. (2012) suggests that the Milky Way's thick disk may actually have a short scale length, $h_l \sim 1.8$ kpc, compared with earlier estimates of exponential scale lengths of 3–3.5 kpc, and this makes it more difficult to place large numbers of thick disk stars 17–21 kpc from the Galactic center at heights up to ~ 5 kpc from the plane (as seen in Monoceros) with a flared + warped thick disk model. Also see Bovy et al. (2012) for an analysis supporting the shorter thick disk scale length.

One of the important objections to the stream explanation for the Monoceros Ring that has emerged is the difficulty in circularizing the orbit of a dwarf galaxy so that it forms a nearly circular ring in the Galactic plane. Dwarf galaxies entering the gravitational influence of the Milky Way arrive on highly elliptical or even unbound orbits and a strong interaction is needed to reduce the angular momentum of the dwarf's initial orbit and circularize it. Helmi et al. (2003) suggested that the ring could be stars at apogalacticon from a dwarf galaxy that recently passed through perigalacticon, or a shell from a minor merger. Michel-Dansac et al. (2011) pointed out that a collision between Sagittarius and a Monoceros progenitor could have circularized the orbit of a putative Monoceros progenitor, and explain the present observations.

Another explanation for the origin of a ring at a radius of $\sim 20\,\mathrm{kpc}$ from the Galactic center is given in Natarajan and Sikivie (2007). This paper points out that Sikivie (1998) predicted a caustic ring of dark matter particles 20 kpc from the Galactic center, significantly before the Monoceros Ring was discovered. This caustic ring of dark matter would result from axion dark matter that is falling into the Milky Way as in a self-similar collapse model (reminiscent of elliptical galaxy shells), but is also rotating in the same sense as the Milky Way disk. These axion particles gather in ring-like cusps at a set of harmonic Galactocentric radii (40 kpc/n, for $n=1,2,3,\ldots$). The n=2 ring is at 20 kpc from the Galactic center, and there therefore coincident with the Monoceros Ring.

However, even if the caustic ring dark matter theory turns out to be correct, it is not clear why there would be stars associated with the dark matter ring that would resemble the Monoceros Ring. Natarajan and Sikivie (2007) suggest that gas could migrate to the caustic and preferentially form stars at that distance, or alternatively that the caustic could deform the orbits of stars that have already formed so that they are preferentially found on the caustic. However, neither of these scenarios is likely to create a ring of stars that extends to heights 5 kpc above the Galactic plane, as is observed. Because a halo of axion dark matter organized into caustic rings is considered unlikely in the astronomy community, this possible origin of the Monoceros Ring has received little serious study.

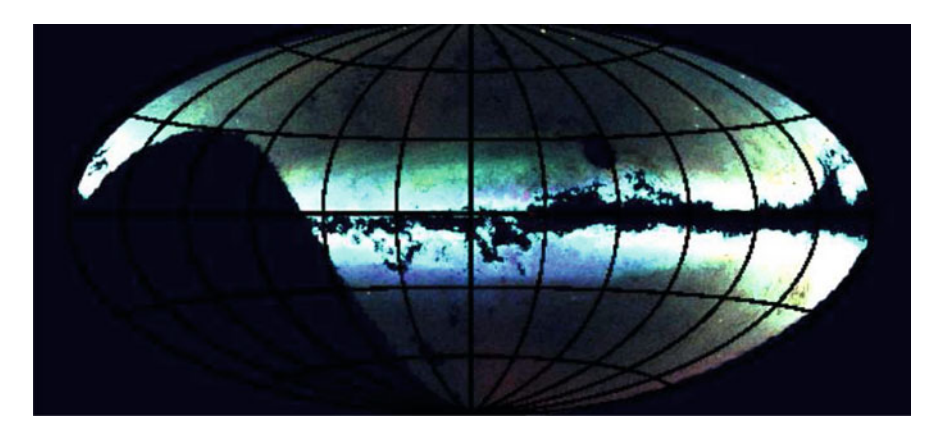


Fig. 3.5 Figure 2 of Slater et al. (2014). Star density plot of turnoff stars in three separate magnitude ranges (*blue* closest 4.8–6.3 kpc, *green* 7.6–11 kpc, *red* furthest at 14.4–17.4 kpc). The Galactic anti-center is in the middle of the figure, with the Galactic center to the far right (and wrapping to the far left). This is a Pan-STARRS view of the Monoceros Ring toward the Galactic anticenter. There are Monoceros features above (*green arcs*) and below the plane (*blue edge*), however one cannot be absolutely sure that they are the same stellar populations. In fact, one cannot continuously trace the Monoceros structure from sightlines above the plane to sightlines below the plane: The foreground dust and crowding in the plane itself at $|b| < 15^{\circ}$ block our view. Note the orientation of the horizontal (Galactic longitude) axis is reversed with respect to Fig. 3.2: the grid lines are spaced at 30° intervals, with *l* centered on the anti-center ($l = 180^{\circ}$) and increasing to the left, and Galactic latitude increasing upward

3.3 Properties of the Monoceros Structure

Observations by many subsequent authors continued to fill in the area above and below the plane of the Galaxy toward the anti-center (Rocha-Pinto et al. 2003; Vivas and Zinn 2006; Casetti-Dinescu et al. 2006, 2008, 2010; Conn et al. 2007, 2008; Sollima et al. 2011; Conn et al. 2012).

In particular, the Pan-STARRS1 survey presented the most panoramic picture of the anti-center in stellar density above and below the Milky Way plane. Figure 3.5 clearly shows the 'band-like' structure stretching from $l=100^\circ$ to 230°, and covering a large Galactic latitude range of $-30^\circ < b < 35^\circ$ in some regions (Bell et al. 2013; Slater et al. 2014). Crowding, dust, and confusion from thin disk stars at very low latitudes ($|b| < 10^\circ$) make it difficult to know if the Monoceros structure extends uniformly through the plane at $|b| \sim 0^\circ$. The large distances to faint turnoff stars on the far side of the Galaxy additionally hinder our knowledge of whether it circles completely around the Milky Way for 360° in azimuth (Carraro and Costa 2009).

Yanny et al. (2003) analyzed early SDSS spectra that were available for a number of stars in the overdensity. Radial velocities from the spectroscopic data showed that the stars were moving with the general rotation of the Galaxy (i.e. the structure was prograde). Later, an extensive photometric and spectroscopic

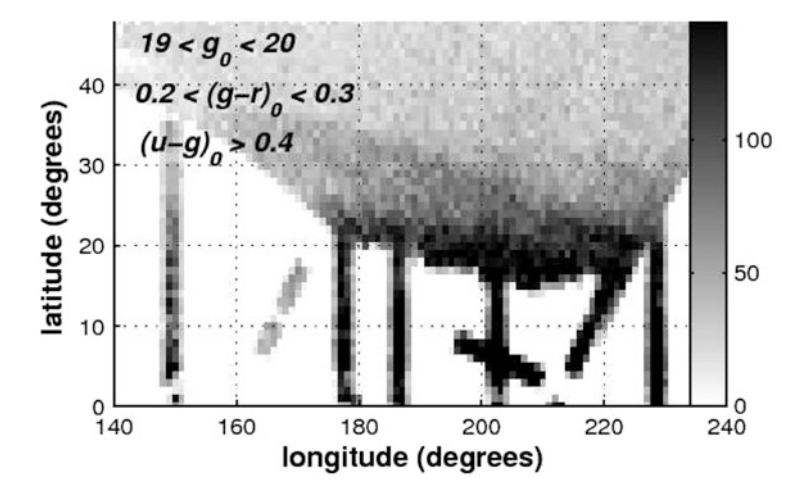


Fig. 3.6 Lower left hand panel of Fig. 1 from Li et al. (2012). Note that Galactic longitude increases *left to right*. This shows the relative density of F-type turnoff stars in SDSS toward the Galactic anti-center, highlighting stars typically \sim 11 kpc from the Sun—the distance to the ring. Note the sharp diagonal cutoff on the north side of the ring

study using SDSS, including SEGUE and SEGUE-2 spectroscopy in the anti-center region, was completed by Li et al. (2012). They conclude that the Monoceros structure has a metallicity of [Fe/H] $\sim -0.80 \pm 0.1$, and the possibly related Anti-Center Stream (ACS) has a metallicity of [Fe/H] $\sim -0.96 \pm 0.03$; the ring has a higher metallicity than the halo but slightly lower metallicity and a narrower velocity dispersion than the thick disk. Figure 3.6 shows another view of the density of turnoff stars approximately 11 kpc from the Sun toward the anti-center, taken from that paper. Data taken from a variety of literature sources are gathered into a summary plot in Fig. 3.7 (taken from Li et al. 2012), showing velocity, distance, and positions of purported Monoceros detections. In some cases velocities of individual stars are shown (i.e., M giants from Crane et al. 2003), whereas in other cases, the mean velocity of an overdensity is presented. The upper panel of Fig. 3.7 shows a significant number of Monoceros detections at $l = 180^{\circ}$ whose Galactocentric line of sight velocity differs significantly from zero, indicating that these stars are not co-rotating in lock step with the Milky Way's disk. All kinematics of Monoceros stars, however, show prograde motion, rotating with the disk, and not far in velocity from the circular motions of stars in a flat rotation curve. The stars, in particular, do not show large excursions from circular orbits, with energies similar to disk stars at the same radii from the Galactic center. That said, the work of Yanny et al. (2003), and Li et al. (2012) also showed that the relative widths of the velocity distributions of Monoceros stars are narrower than predicted from a thick disk population at the same height above the plane (Fig. 3.8).

Detailed studies of chemical abundances have been carried out by Chou et al. (2010) and Meisner et al. (2012). Meisner et al. (2012) obtained low resolution

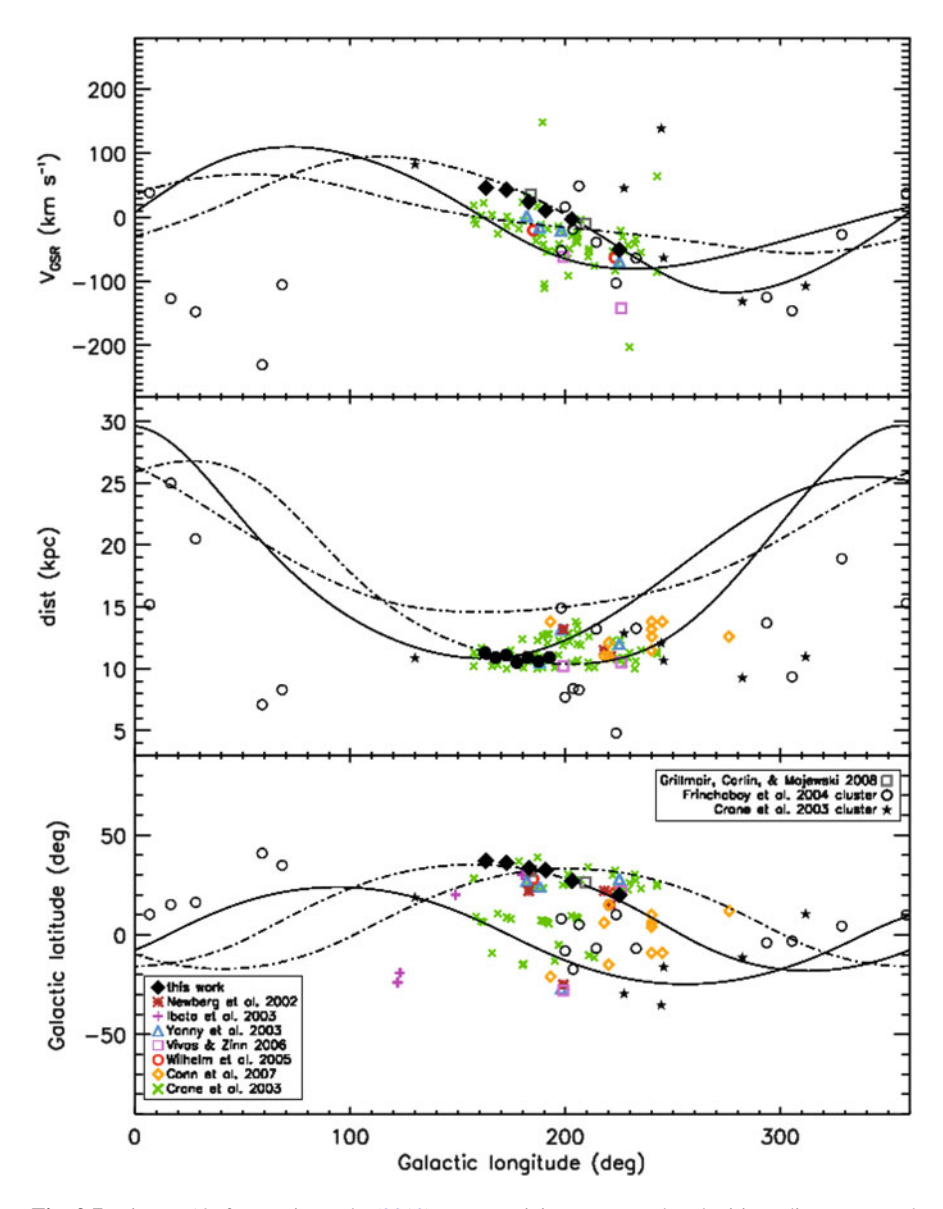


Fig. 3.7 Figure 19 from Li et al. (2012), summarizing measured velocities, distances, and positions of numerous purported detections of the Monoceros Ring from the literature. Note that some of these detections are the mean value along a line of sight, while some of these are individual stars (or *star clusters*). The *lines* are the orbit from the models of a disrupting dwarf galaxy by Peñarrubia et al. (2005). While the data generally match the model, the data tend to fill in the space between the subsequent passages of the model orbit, at the same Galactic longitude

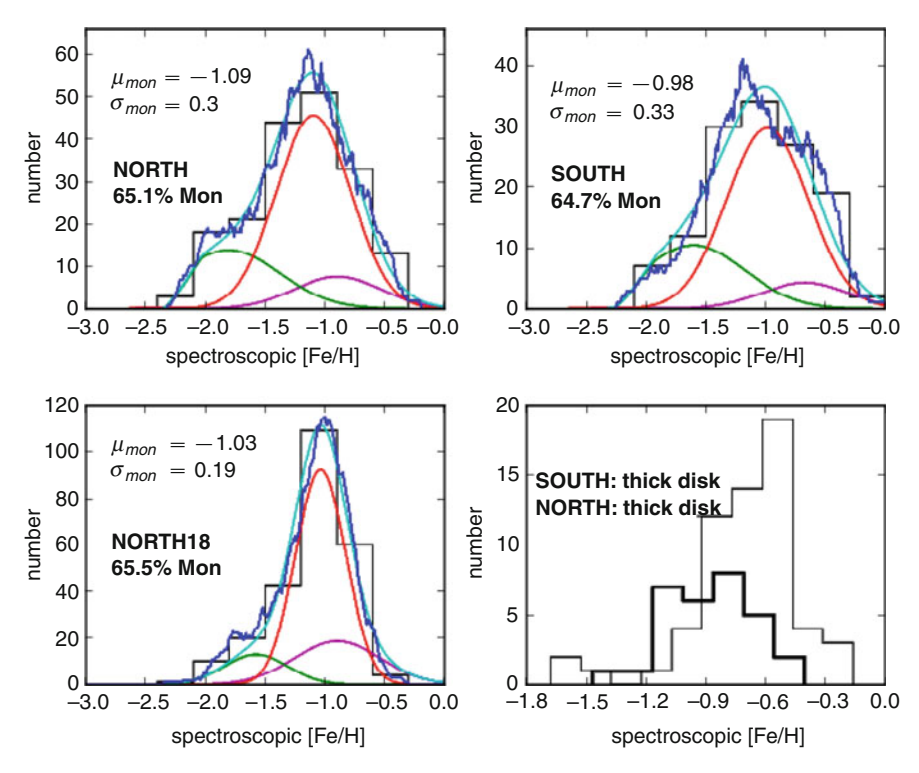


Fig. 3.8 Figure 3 from Meisner et al. (2012). The first three panels show the metallicity distributions of Monoceros candidates in three observed fields, which are decomposed into a halo (*green curve*), thick disk (*magenta*), and Monoceros (*red*) component. The sum of the three components is represented by a *solid blue curve*. Monoceros Ring candidate stars have mean metallicity [Fe/H] = -1.0 in all three fields, distinctly less than that of the thick disk ([Fe/H] = -0.9 to -0.6; *lower-right panel*)

 $(R\sim 1000)$ data for several hundred F/G stars in the anti-center at distances (magnitudes) dominated (65%) by objects in Monoceros, while obtaining valuable comparison information at the same time on halo and thick disk populations. Like Li et al. (2012), Meisner et al. (2012) find [Fe/H] ~ -1 , which is intermediate between the halo and the local thick disk; it could be consistent with a lower metallicity, accreting outer disk. It is interesting to note that Meisner et al. (2012) found significantly different metallicities for stars at the same Galactocentric radii above and below the plane ([Fe/H] = -0.65 vs. -0.87 dex respectively). One must consider if these are actually drawn from the same population of "thick disk" objects. The authors also show, with somewhat lower significance, that the Monoceros stars appear to have lower [α /Fe] values than thick disk stars (Fig. 3.9).

The references cited above have led to these basic properties of the Monoceros Ring: co-rotating with the disk (prograde), with velocities close to, but not identical to stars rotating with a flat rotation curve. Many stars are seen at significant heights

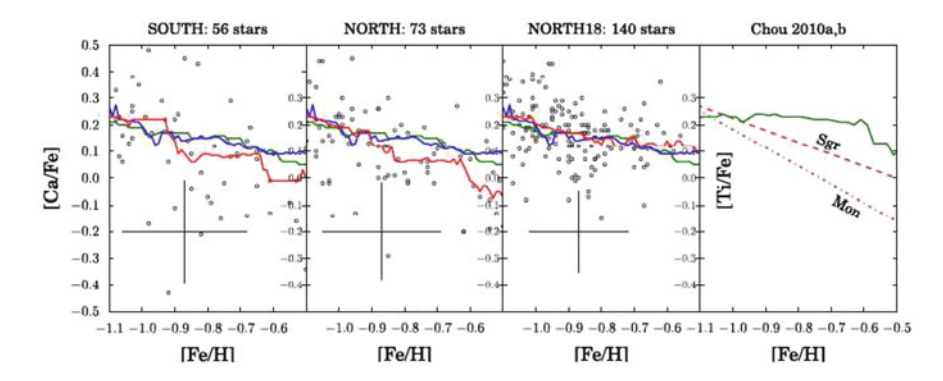


Fig. 3.9 Figure 4 of Meisner et al. (2012) showing evidence for [Ca/Fe] and [Ti/Fe] trends which are distinct from those of thick disk as well as thin disk stars. The *blue* and *green lines* in the *left three panels* represent typical [Ca/Fe] trends for thick disk and overall Galactic trends whereas the *red line* indicates the trend for Monoceros candidates. The error bars on individual stars (*open circles*) are large, as indicated by the *large cross*, but the trend appears to show a slight [Ca/Fe] difference between Monoceros and the Galactic populations in the two *leftmost panels*. In the *right panel*, trends for [Ti/Fe] from measurements of Monoceros, Sagittarius and Milky Way stars are all shown to be possibly drawn from distinct populations. See Meisner et al. for details

above and below the Galactic plane, up to |Z| > 5 kpc in many cases. A definitive connection between Monoceros stars above and below the plane has not been made, and, in fact, the stars at the same latitude appear at different Galactocentric distances above and below the plane.

The main Monoceros structure above the plane resembles a thick, filled arc encircling at least 130° of the Galaxy from $l=100^\circ$ to $l=230^\circ$ at a latitude of $-30 < b < 35^\circ$ (see Fig. 3.6 and Table 1 of Ibata et al. 2003). The initial crude estimate of Monoceros stellar metallicity by Yanny et al. (2003) of [M/H] = -1.6 ± 0.3 , based on the strength of the Ca II K line in turnoff stars and the turnoff color, has been shown to be incorrect. Several more recent estimates clearly show the bulk of the stars to have [Fe/H] near -0.95 ± 0.15 .

The presence or absence of specific stellar populations within Monoceros can help distinguish it or identify it with a disk population. For example, a significant excess (above average for our disk) of old, low metallicity RR Lyraes would point to an external (dwarf or halo) origin for Monoceros. Are RR Lyraes present in Monoceros? The answer appears to be "yes," based on work of Mateu et al. (2012) and following Vivas and Zinn (2006). Their Table 6 lists several hundred RR Lyraes found at low Galactic latitudes $|b| < 45^{\circ}$ toward the anticenter; a plot of (l, b) vs. distance (which are accurate to better than 10%) for these RR Lyrae stars is shown in Fig. 3.10. The numbers of RR Lyraes found appear to be significantly more clumped than simple extrapolations of a smooth thin or thick disk out to $R \sim 18$ kpc from the Galactic Center would predict, though the overall density of RR Lyrae in the disk is not well constrained. The objects appear roughly localized within a few kpc of R = 19 kpc. Finally, the objects in the South (with $b < 0^{\circ}$) are somewhat closer than

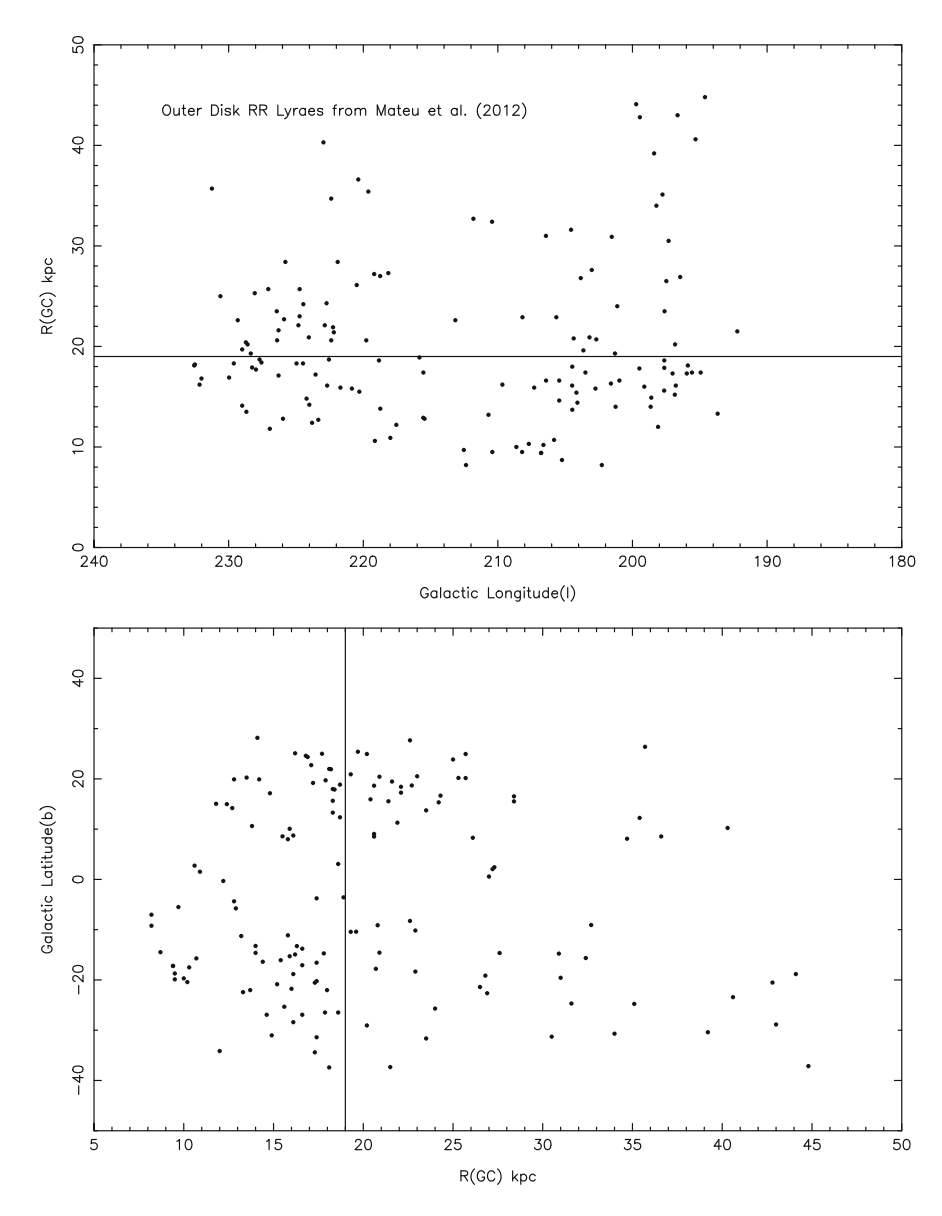


Fig. 3.10 Low-latitude anti-center RR Lyraes from Mateu et al. (2012) (see their Table 6). The upper panel shows the Galactocentric distance of each RR Lyrae vs. its Galactic longitude (1). The lower panel indicates Galactic latitude (b) vs. Galactocentric distance. Note the concentration of higher longitude objects which are slightly more distant ($R > 20\,\mathrm{kpc}$) compared with the concentration of lower longitude objects ($R < 20\,\mathrm{kpc}$). These RR Lyraes are at the correct distance and position to be Monoceros Ring members, and the overall density of old population RR Lyraes here may be more than is expected from a smoothly decreasing-with-radius Milky Way thick disk population

those in the North by a few kpc. These distances are in good agreement with those found by the Pan-STARRS survey (Slater et al. 2014), and correspond to the blue and green stellar density areas of Fig. 3.5 below and above the plane, respectively. The finding of RR Lyraes embedded within the Monoceros Ring structure indicates the presence of an old population, more typical of a halo or dwarf galaxy, rather than that of a young, more-recently formed, outer disk population. Careful follow-up is needed to understand the true significance of the apparent RR Lyrae excess, and the expected number of RR Lyraes in the thin and thick disks at $R > 10 \,\mathrm{kpc}$ from the Galactic center. Radial velocities and proper motions are also needed to determine if these RR Lyrae have the same kinematics as Monoceros Ring members. Kinman et al. (2004) has measured several radial velocities of RR Lyrae toward the anti-center, but not yet enough to definitively associate them with Monoceros Ring kinematics.

While RR Lyrae stars appear to be present in the Monoceros Ring, it has no significant blue horizontal branch star population, in contrast to the Sagittarius tidal stream. This is evidence that Monoceros and Sagittarius have distinct stellar populations and origins. There do appear to be M giants in Monoceros (Crane et al. 2003; Sharma et al. 2011), which is evidence of a more metal-rich population.

Several authors have noted that the orbits of some globular clusters appear to roughly match that of Monoceros Ring stars (Frinchaboy 2006; Frinchaboy et al. 2009; Warren and Cole 2009; Hankey and Cole 2011). While these clusters are not definitely associated with Monoceros, it is unlikely for several globular clusters, which have a spherical distribution centered on the bulge of the Galaxy, to lie in an approximately plane-like orbit at Galactocentric distances of 15–25 kpc.

The total number of stars or total mass estimate for ${\sim}60^{\circ}$ arc of Monoceros is in the range 10^7 to $10^8 M_{\odot}$ (Yanny et al. 2003; Meisner et al. 2012). Meisner quotes $3 \times 10^7 M_{\odot}$ in stars in the arc of the ring that can be seen from our location in the Galaxy looking toward the anti-center. Of course, there may be a considerable dark matter component to Monoceros.

3.4 The Canis Major Dwarf Galaxy Controversy

Interest peaked in a possible progenitor (a clump of stars which could be a tidally stripped dwarf galaxy nucleus) for Monoceros with the identification of an apparent overdensity of stars near $(l,b)=(240^\circ,-8^\circ)$, compared with the star counts at a symmetric position above the Galactic plane (Martin et al. 2004). However, Momany et al. (2004) argued that a shift of the plane due to the Galactic warp could explain the observed asymmetry. The dwarf galaxy vs. warp argument continued in a series of contentious papers in the literature.

The first model of the Monoceros Ring, under the assumption that the ring was the result of the tidal disruption of a dwarf galaxy, was developed by Peñarrubia et al. (2005) using imaging and kinematic information and assuming a progenitor

near the Canis Major location. This map reproduced within 10–20 km/s most radial velocities known for stream members and reached the correct limits in |b| above and below the plane. This model supported the existence of the Canis Major dwarf galaxy, which fit nicely into the model. Many years later, however, it was found that the model (which has a 'braid or lattice-like' structure) has trouble reproducing the more continuous 'filled-in' band-like density of stars spreading from $-30^{\circ} < b < 35^{\circ}$ such as that seen in the observations of Li et al. (2012), Bell et al. (2013), and Slater et al. (2014).

The dwarf galaxy interpretation got a boost when Dinescu et al. (2005) found that although the Canis Major stars have a rotation speed similar to thick disk stars, there is a significant proper motion perpendicular to the plane, which would not be expected for a disk population, and was in fact in the opposite direction as the motion expected from a warp.

The position of the purported dwarf in the plane made the extent of the overdensity difficult to determine. In that direction, there is unfortunately heavy, variable dust and considerable disk star crowding that makes definitive determination of the stellar properties, positions and distances quite difficult. In fact, Rocha-Pinto et al. (2006) suggested that the core of the Canis Major overdensity was an artifact of a dust extinction window, and that the asymmetry was actually part of a larger "Argo Star System." However, when Bellazzini et al. (2006) used He burning red clump stars to trace Canis Major, they found a concentrated core, but determined the Argo structure is distributed along our line of sight, and is likely to be a consequence of a warp or other asymmetry in the Milky Way.

The dwarf galaxy interpretation was again boosted due to the detection of a "Blue Plume" (Bellazzini et al. 2004) of younger stars, in addition to the main sequence of older stars, that was thought to be associated with a recent burst of star formation. However, Carraro et al. (2005) and Moitinho et al. (2006) believe this blue plume could be associated with the Norma-Cygnus spiral arm of the Milky Way. In contrast, Bellazzini et al. (2006) find that the Blue Plume follows the same distance—Galactic longitude trend as their red clump stars from Canis Major. de Jong et al. (2007) find both a young (<2 Gyr) and an old (3–6 Gyr) main sequence in the direction of the Canis Major overdensity, and therefore favor the interpretation as a dwarf galaxy.

Butler et al. (2007) show that the angular distribution of main sequence stars in the Canis Major region is highly elongated (axial ratio of at least 5:1) along the Galactic plane. Moreover, there is a younger and less extended population of stars that could be associated with the structure. They suggest that the structure could not be gravitationally bound at this time, but could be the tidal remains of a dwarf galaxy. Piatti and Clariá (2008) do not find a population of open clusters that share the properties of the purported Canis Major dwarf, and therefore do not favor the dwarf galaxy interpretation. Also, Mateu et al. (2009) do not find any excess of RR Lyraes toward the Canis Major structure.

The discussion over the nature of the Canis Major overdensity mirrors the controversy over the Monoceros Ring itself. There are two competing hypotheses:

- 1. There is a dwarf galaxy here, that could be the progenitor for the Monoceros Ring, under the assumption that the ring is formed from a tidally disrupting dwarf galaxy (Martin et al. 2004; Martínez-Delgado et al. 2005).
- 2. The asymmetry is due to a Galactic warp, and the younger stars are part of an outer spiral arm and not a dwarf galaxy remnant (Hammersley and López-Corredoira 2011; Lopez-Corredoira et al. 2012).

It has proven quite difficult to definitively decide whether these planar structures that are more than 15 kpc from the Galactic center are part of the disk or substructure in the stellar halo.

3.5 The Triangulum-Andromeda, and Other Low Latitude, Stream-Like Substructures Near the Anticenter

Majewski et al. (2004) noted an overdensity of stars at low latitude ($b \sim -23^{\circ}$) in the direction of the constellations of Triangulum and Andromeda (the TriAnd stream) at an even greater distance than the Monoceros Ring (turnoff magnitude \sim 20.5), at about 22 kpc from the Sun (Deason et al. 2014). A second structure, dubbed TriAnd2, was discovered in the same vicinity but behind it $(d_{\Omega} \sim 28 \text{ kpc})$ by Martin et al. (2007) in the foreground of imaging around M31. Velocity information of stars in TriAnd and TriAnd2 (spanning longitudes 100° < l < 160°) was obtained by Rocha-Pinto et al. (2004) and Sheffield et al. (2014). These velocities generally showed stars co-rotating with the general disk (in a prograde sense), with speeds close to but not exactly matching those of a flat rotation curve at their respective distances. Sheffield et al. (2014) finds that the velocity of TriAnd M giants matches well those of the TriAnd2 stars, and the metallicities of the more distant TriAnd2 stars, at [Fe/H] = -0.64, are slightly lower than those of TriAnd ([Fe/H] = -0.57), with both structures much more metal rich than typical Galactic halo stars at [Fe/H] = -1.6. Below we will note a recent result which interprets these stars as elements ejected from a disturbed disk.

An extensive investigation of this region using the Pan-Andromeda Archaeological Survey (PAndAS; McConnachie et al. 2009) was completed by Martin et al. (2014), in which five presumed tidal debris structures were identified. Along with TriAnd and TriAnd2, they identified the Pisces globular cluster stream (Bonaca et al. 2012; Martin et al. 2013), and two previously unknown overdensities, named the PAndAS NE blob and PAndAS MW stream. These structures are characterized by their faint, blue turnoffs that are confined to a narrow distance range at lower Galactic latitudes. While the Pisces globular cluster stream has the appearance of a well-defined stream from a cold (globular cluster) Milky Way satellite, the other structures are spatially diffuse and questionably stream-like. It has been suggested

that since these appear to be separate tidal debris structures with similar positions and velocities, they could be an example of group infall—several satellites falling into the Milky Way together (Deason et al. 2014).

Matched-filter analysis of SDSS color-magnitude data for stars, following the methods of Rockosi et al. (2002), resulted in the identification of further narrow structures (Grillmair 2006; Grillmair et al. 2008) in the anticenter region of the Galaxy, at the approximate distances where Monoceros was located. At least three, roughly parallel substructures in the Monoceros Ring were dubbed the "three stream complex," which was suggested to arise from the disruption of distinct components (such as globular clusters) of a dwarf galaxy progenitor, embedded in a broader profile that was called the Anticenter Stream (ACS). If one fits an orbit to the profile of the stream, it appears to be distinct from the Monoceros Ring, which suggests they could be separate structures. However, Carlin et al. (2010) found an unexpected proper motion for the ACS stars that deviates by 30° from the apparent direction of the stream, and in fact is nearly parallel to the Galactic plane. The Eastern Banded Structure (EBS) is another low latitude structure that was thought to be possibly associated with the ACS, but Grillmair (2011) claim that it is a separate tidal stream possibly with Hydra I (a narrow structure within the EBS) as its progenitor.

3.6 Explaining the Monoceros Ring and Other Low Latitude Substructures with a Corrugated Milky Way Disk

Kazantzidis et al. (2008) and Younger et al. (2008) raised a new possibility for the origin of the Monoceros structure. They suggested that massive dark matter subhalos passing through the disk or flyby encounters with a satellite galaxy would excite waves that produce ringlike features in the outskirts of the galaxy. They could even make filamentary structures above the disk. Purcell et al. (2011) suggested that in particular the passage of the Sagittarius dwarf galaxy through the disk might be linked to the Monoceros Ring.

The evidence for wave motion in the Milky Way disk has been growing. Widrow et al. (2012) discovered an asymmetry in disk star counts above and below the Galactic plane, that varied with distance from the disk midplane (see also Yanny and Gardner 2013). Widrow et al. (2014) suggested that these vertical oscillations could be due to breathing modes of the disk. These could be produced by a satellite galaxy (such as the Sagittarius dwarf galaxy) with large vertical motion (>50 km/s) and a surface density comparable to that of the disk. The observed perturbation of the outer HI disk of the Milky Way has also been modeled (Chakrabarti and Blitz 2009, 2011) as a disk response to the tidal action of a massive dark matter subhalo.

Local (within a few kpc) substructure in the bulk velocities of disk stars has been discovered in three major spectroscopic surveys of Milky Way stars. Williams et al. (2013) found vertical (perpendicular to the Galactic plane) velocity substructure in the RAdial Velocity Experiment (Steinmetz et al. 2006, RAVE). Widrow et al.

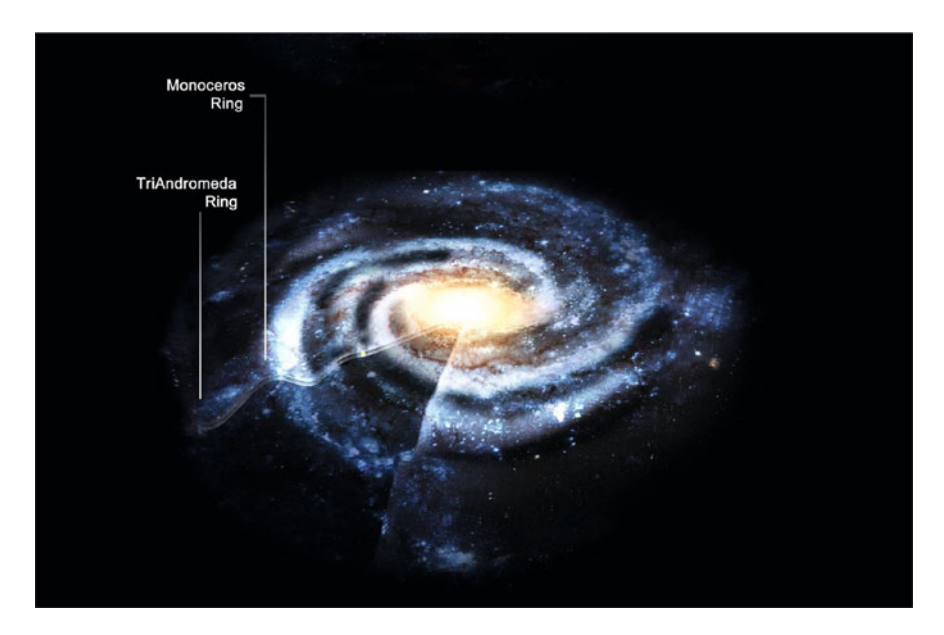


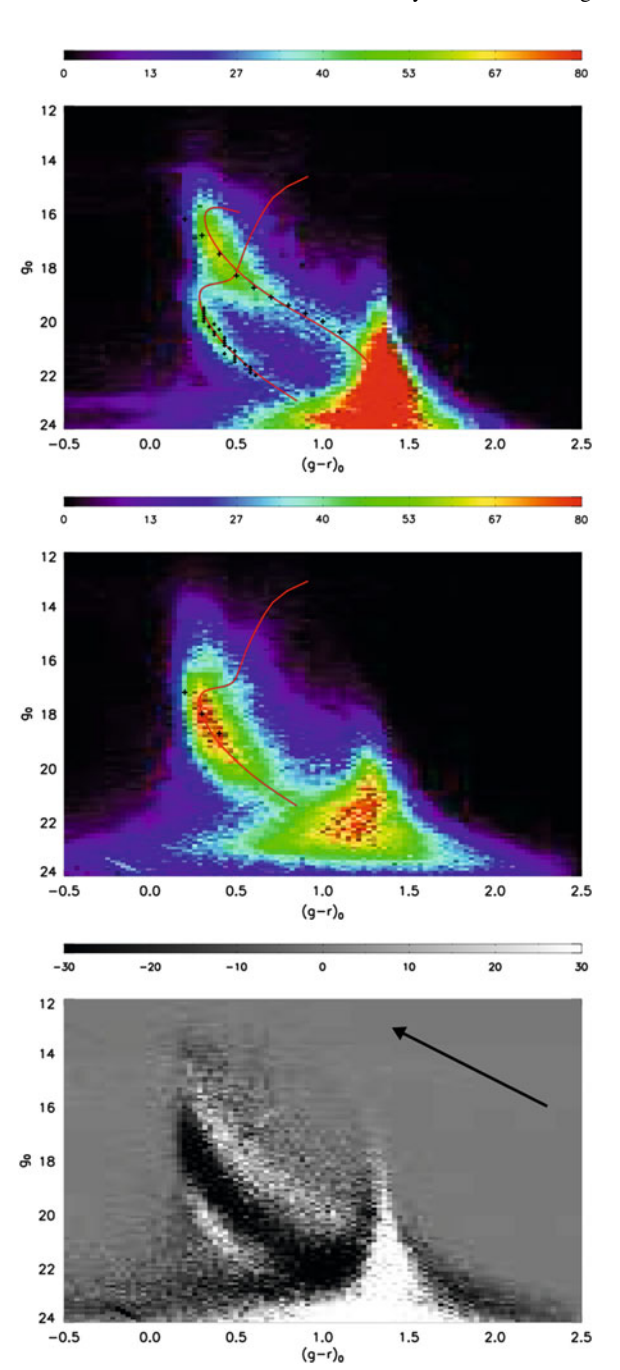
Fig. 3.11 An artist's depiction of the oscillations of the disk midplane, as discovered by Xu et al. (2015). The "wiggles" in the disk are not drawn to scale. The *yellow dot* identifies the position of the Sun. Although the disk oscillations were only observed outside the solar circle towards the anticenter, one imagines there are oscillations around the entire disk. Image credit: Rensselaer Polytechnic Institute/Dana Berry

(2012) found vertical velocity substructure in the SDSS (York et al. 2000), in addition to the vertical asymmetry previously discussed. And Carlin et al. (2013) used the Large Area Multi-Object Spectroscopic Telescope (LAMOST; Cui et al. 2012; Deng et al. 2012; Zhao et al. 2012) survey to find that stars within 2 kpc of the Sun, in the general direction of the Galactic anticenter, have both radial and vertical bulk motions.

Xu et al. (2015) showed that there is a vertical asymmetry in the disk that is a function of distance from the Galactic center, as measured in the direction of the anticenter (see Fig. 3.11). There are more stars at positive Galactic latitude 2 kpc from the Sun, more stars at negative Galactic latitude 4–6 kpc from the Sun, more stars at positive Galactic latitude 8–10 kpc from the Sun, and more stars at negative Galactic latitude 12–16 kpc from the Sun. This asymmetry is apparent in every observed direction in the Galactic longitude range $110^{\circ} < l < 229^{\circ}$, as determined by subtracting Hess diagrams of stars in $2.5^{\circ} \times 2.5^{\circ}$ patches of sky above and below the Galactic plane. A sample Hess diagram subtraction is shown in Fig. 3.12. The third oscillation lines up with the position and density of the Monoceros Ring, and the fourth lines up with the position of the TriAnd structure.

The Monoceros Ring, in this study, is shown *not* to appear both above and below the Galactic disk; it is only apparent in the north. There are excess star counts in

Fig. 3.12 The top panel shows a Hess diagram of stars selected from SDSS DR8 (Aihara et al. 2011) in the sky area $176.75^{\circ} < l < 179.25^{\circ}$ and $15^{\circ} < b < 17.5^{\circ}$. The second panel shows the stars at identical Galactic longitude, but at a symmetric position below the plane $(-17.5^{\circ} < b < -15^{\circ})$. The third panel shows a subtraction of the two Hess diagrams. White stripes indicate more stars in the north, and black stripes indicate more stars in the south. Brighter main sequences are closer to the Sun than fainter ones. This diagram shows that there is a north-south asymmetry in the number of Milky Way disk stars, that oscillates with distance from the Galactic center, as one looks toward the Galactic anticenter. The most distant southern overdensity (the TriAnd Ring) is not seen clearly in SDSS data at this low latitude due to extinction in the plane; it can be faintly seen in SDSS data with $-30^{\circ} < b < -20^{\circ}$



both the north and the south, but they are at different Galactocentric distances. It is argued that the nearer stars chosen by Ibata et al. (2003) as the Monoceros Ring in the south, and the more distant stars chosen by Newberg et al. (2002) are each in separate "rings." The more distant ring is associated with the Triangulum-Andromeda "stream."

The vertical oscillations were surprising because Galactic stellar disks are not expected to have strong localized vertical over- or under-densities; the self-gravity of the disk and dark halo quickly smooths them out on a timescale of $\sim 300\,\mathrm{Myr}$ (Sánchez-Salcedo et al. 2011). However, vertical displacement of the disk by about the amount observed by Xu et al. (2015) was predicted from simulations of the interaction of satellites with the disk (Widrow et al. 2014; Gómez et al. 2013).

In addition, Xu et al. (2015) show that the ringlike structures are roughly aligned with the spiral structure of the Milky Way. It is possible that spiral structure and disk oscillations could both be excited by the same processes. The simulations of Gómez et al. (2013) for the Sagittarius dwarf interacting with the Milky Way and of Dierickx et al. (2014) for M32 interacting with the Andromeda galaxy both produce spiral disk structure.

If the Monoceros Ring and the TriAnd Ring are part of the disk, then the stellar disk extends $\sim\!25\,\mathrm{kpc}$ from the Galactic center—significantly farther than 15 kpc as was often assumed. The explanation for previously low measurements of the disk scale length and extent is that these measurements did not take into account that the disk midplane oscillates up and down. Instead of the disk density falling off sharply 15 kpc from the Galactic center, the stars instead shift out of our line of sight. There might also be a warp and/or flare of the stellar disk, but measurements of these features would also have to be re-examined in light of the presence of disk oscillations (see Carraro 2015 for a static picture of such a warp/flare).

In this scenario, the Monoceros Ring is "dredged up" from the disk by Milky Way satellites and possibly dark matter subhalos that are "dragged in." Furthermore, the substructure of the Milky Way halo could potentially be probed by analysis of velocity and density substructure in the disk. It is possible that the disk-subhalo interactions drive the spiral structure of our Galaxy. In this picture it is unclear whether the filamentary structures including the ACS, EBS, TriAnd2, the PAndAS MW stream, and the PAndAS NE blob are tidal debris that has been "dragged in," or are due to disk oscillations and therefore "dredged up."

A feature of the Xu et al. (2015) model is that it can be used to explain not only the Monoceros Ring structure, but also the TriAnd and TriAnd2 structures. This picture is supported by Price-Whelan et al. (2015), who show that the ratio of RR Lyrae to M giant stars in the TriAnd "clouds" is similar to the disk population, and unlike any known Milky Way satellites. They suggest that in the outskirts of our Galaxy, ordinary outer disk stars are being kicked to relatively large vertical heights ($|Z| = 5-10\,\mathrm{kpc}$) as the outer disk is disturbed by interactions with large dwarfs such as Sagittarius.

3.7 Future Prospects

Although recent work indicates that the major low latitude features (the Monoceros and TriAnd Rings) could result from the response of the disk to Milky Way satellites that pass through it, this is obviously a complex problem that has not yet been fully reviewed by the community. There are many outstanding questions to be addressed. For example, the oscillating disk might favor a spiral arm explanation for the purported Canis Major dwarf galaxy, but this has not been tested against the observations. Data on the filamentary structures that appear to be related to the Monoceros and TriAnd Rings need to be re-examined in light of the new model, and future simulations that show the dynamical evolution of an outer disk buffeted by dwarf galaxies and/or dark matter subhalos will attempt to fit the data in detail. Additional data (radial velocities, proper motions, and accurate distances) need to be obtained to map the velocity and density substructure of the disk, and that substructure must be fit to disk response models to make sure one understands in detail the processes that are shaping our Milky Way. Results from the ESO Gaia satellite in particular will be of tremendous utility for tracing disk substructure. In light of Price-Whelan et al. (2015), one can learn much by comparing the detailed metallicities of Monoceros and TriAnd stars to stars at lower heights (and possibly different radii), which may have been kicked up by an interaction. The LAMOST spectroscopic survey will obtain large numbers of radial velocities of giants toward the anti-center (Yuan et al. 2015). The APOGEE program, with its high resolution IR spectrograph, has the required sensitivity and resolution (Hayden et al. 2015) to probe chemical abundance signatures of Monoceros and TriAnd stars. Full kinematics, including proper motions, connected to simulations of specific interaction events, can tell us about the relative masses of the outer disk vs. dwarfs and their associated dark matter, of which we currently have little concrete information.

Acknowledgements Brian Yanny acknowledges support from the DOE Office of Science. Heidi Jo Newberg was partially supported by grants NSF AST 14-09421 and NSF AST 09-37523, by the MilkyWay@home volunteers and supporters, and in particular by Manit Limlamai, Babette Josephs, Lee Newberg, the Marvin Clan, and the 2015 Breakthrough Prize in Fundamental Physics.

References

Aihara, H., Allende Prieto, C., An, D., et al. 2011, ApJS, 193, 29
Bell, E. F., Slater, C. T., Morganson, E., et al. 2013, American Astronomical Society Meeting Abstracts, 222, #313.02
Bellazzini, M., Ibata, R., Monaco, L., et al. 2004, MNRAS, 354, 1263
Bellazzini, M., Ibata, R., Martin, N., et al. 2006, MNRAS, 366, 865

Bonaca, A., Geha, M., & Kallivayalil, N. 2012, ApJ Lett, 760, LL6

Bovy, J., Rix, H.-W., Liu, C., et al. 2012, ApJ, 753, 148

Butler, D. J., Martínez-Delgado, D., Rix, H.-W., Peñarrubia, J., & de Jong, J. T. A. 2007, AJ, 133, 2274

Carlin, J. L., Casetti-Dinescu, D. I., Grillmair, C. J., Majewski, S. R., & Girard, T. M. 2010, ApJ, 725, 2290

Carlin, J. L., DeLaunay, J., Newberg, H. J., et al. 2013, ApJ Lett, 777, LL5

Carraro, G. 2015, arXiv:1502.03151

Carraro, G., Vázquez, R. A., Moitinho, A., & Baume, G. 2005, ApJ Lett, 630, L153

Carraro, G. & Costa, E. 2009, A&A, 493, 71

Casetti-Dinescu, D. I., Majewski, S. R., Girard, T. M., et al. 2006, AJ, 132, 2082

Casetti-Dinescu, D. I., Carlin, J. L., Girard, T. M., et al. 2008, AJ, 135, 2013

Casetti-Dinescu, D. I., Girard, T. M., Platais, I., & van Altena, W. F. 2010, AJ, 139, 1889

Chakrabarti, S., & Blitz, L. 2009, MNRAS, 399, L118

Chakrabarti, S., & Blitz, L. 2011, ApJ, 731, 40

Cheng, J. Y., Rockosi, C. M., Morrison, H. L., et al. 2012, ApJ, 752, 51

Chou, M.-Y., Majewski, S. R., Cunha, K., et al. 2010, ApJ, 720, L5

Conn, B. C., Lane, R. R., Lewis, G. F., et al. 2007, MNRAS, 376, 939

Conn, B. C., Lane, R. R., Lewis, G. F., et al. 2008, MNRAS, 390,1388

Conn, B. C., Noel, N. E. D., Rix, H.-W., et al. 2012, ApJ, 754, 101

Crane, J. D., Majewski, S. R., Rocha-Pinto, H. J., et al. 2003, ApJ, 594, L119

Cui, X.-Q., Zhao, Y.-H., Chu, Y.-Q., et al. 2012, Research in Astronomy and Astrophysics, 12, 1197

de Jong, J. T. A., Butler, D. J., Rix, H. W., Dolphin, A. E., & Martínez-Delgado, D. 2007, ApJ, 662, 259

Deason, A. J., Belokurov, V., Hamren, K. M., et al. 2014, MNRAS, 444, 3975

Deng, L.-C., Newberg, H. J., Liu, C., et al. 2012, Research in Astronomy and Astrophysics, 12, 735

De Rijcke, S., Dejonghe, H., Zeilinger, W. W., & Hau, G. K. T. 2003, A&A, 400, 119

Dierickx, M., Blecha, L., & Loeb, A. 2014, ApJ Lett, 788, LL38

Dinescu, D. I., Martínez-Delgado, D., Girard, T. M., et al. 2005, ApJ Lett, 631, L49

Feast, M. W., Menzies, J. W., Matsunaga, N., & Whitelock, P. A. 2014, Nature, 509, 342

Frinchaboy, P. M. 2006, arXiv:astro-ph/0604133

Frinchaboy, P. M., Marino, A. F., Villanova, S., et al. 2009, MNRAS, 391, 39

Gómez, F. A., Helmi, A., Cooper, A. P., et al. 2013, MNRAS, 436, 3602

Grillmair, C. J. 2006, ApJ, 651, L29

Grillmair, C. J. 2011, ApJ, **738**, 98

Grillmair, C. J., Carlin, J. L., & Majewski, S. R. 2008, ApJ, 689, L117

Hammersley, P. L., & López-Corredoira, M. 2011, A&A, 527, A6

Hankey, W. J., & Cole, A. A. 2011, MNRAS, 411, 1536

Hayden, M. R., Bovy, J., Holtzman, J. A., et al. 2015, arXiv:1503.02110

Helmi, A., Navarro, J. F., Meza, A., Steinmetz, M., & Eke, V. R. 2003, ApJ Lett, 592, L25

Ibata, R. A., Irwin, M. J., Lewis, G. F., Ferguson, A. M. N., & Tanvir, N. 2003, MNRAS, 340, L21

Kazantzidis, S., Bullock, J. S., Zentner, A. R., Kravtsov, A. V., & Moustakas, L. A. 2008, ApJ, 688, 254

Kinman, T. D., Saha, A., & Pier, J. R. 2004, ApJL, 605, L25

Li, J., Newberg, H. J, Carlin, J. L, et al. 2012, ApJ, 757, 151

López-Corredoira, M., Cabrera-Lavers, A., Garzón, F., & Hammersley, P. L. 2002, A&A, 394, 883

Lopez-Corredoira, M., Moitinho, A., Zaggia, S., et al. 2012, arXiv:1207.2749

Lupton, R., Blanton, M. R., Fekete, G., et al. 2004, PASP, 116, 133

Majewski, S. R., Ostheimer, J. C., Rocha-Pinto, H. J., et al. 2004, ApJ, 615, 738

Martin, C., Carlin, J. L., Newberg, H. J., & Grillmair, C. 2013, ApJ Lett, 765, LL39

Martin, N. F., Ibata, R. A., Bellazzini, M., et al. 2004, MNRAS, 348, 12

Martin, N. F., Ibata, R. A., & Irwin, M. 2007, ApJ Lett, 668, L123

Martin, N. F., Ibata, R. A., Rich, R. M., et al. 2014, ApJ, 787, 19

Martínez-Delgado, D., Butler, D. J., Rix, H.-W., et al. 2005, ApJ, 633, 205

Mateu, C., Vivas, A. K., Zinn, R., Miller, L., & Abad, C. 2009, AJ, 137, 4412

Mateu, C., Vivas, A. K., Downes, J. J., et al. 2012, MNRAS, 427, 3374

McConnachie, A. W., Irwin, M. J., Ibata, R. A., et al. 2009, Nature, 461, 66

Michel-Dansac, L., Abadi, M. G., Navarro, J. F., & Steinmetz, M. 2011, MNRAS, 414, L1

Meisner, A. M., Frebel, A., Juric, M., & Finkbeiner, D. P. 2012, ApJ, 753, 116

Moitinho, A., Vazquez, R. A., Carraro, G., et al. 2006, MNRAS, 368, L77

Momany, Y., Zaggia, S. R., Bonifacio, P., et al. 2004, A&A, 421, L29

Momany, Y., Zaggia, S., Gilmore, G., et al. 2006, A&A, 451, 515

Natarajan, A. & Sikivie, P. 2007, Phys Rev D, **76**, 023505

Newberg, H. J., Yanny, B., Rockosi, C., et al. 2002, ApJ, 569, 245

Peñarrubia, J., Martínez-Delgado, D., Rix, H. W., et al. 2005, ApJ, 626, 128

Piatti, A. E., & Clariá, J. J. 2008, MNRAS, 390, L54

Price-Whelan, A. M., Johnston, K. V., Sheffield, A. A., Laporte, C. F. P., & Sesar, B. 2015, MNRAS, submitted; arXiv:1503.08780

Purcell, C. W., Bullock, J. S., Tollerud, E. J., Rocha, M., & Chakrabarti, S. 2011, Nature, 477, 301 Robin, A. C., Creze, M., & Mohan, V. 1992, ApJ Lett, 400, L25

Rocha-Pinto, H. J., Majewski, S. R., Skrutskie, M. F., & Crane, J. D. 2003, ApJ, 594, L115

Rocha-Pinto, H. J., Majewski, S. R., Skrutskie, M. F., Crane, J. D., & Patterson, R. J. 2004 ApJ, 615, 732.

Rocha-Pinto, H. J., Majewski, S. R., Skrutskie, M. F., et al. 2006, ApJ Lett, 640, L147

Rockosi, C. M., Odenkirchen, M., Grebel, E. K., et al. 2002, AJ, 124, 349

Sánchez-Salcedo, F. J., Flynn, C., & Hidalgo-Gámez, A. M. 2011, ApJ Lett, 731, LL35

Schlesinger, K. J., Johnson, J. A., Rockosi, C. M., et al. 2014, ApJ, 791, 112

Sharma, S., Johnston, K. V., Majewski, S. R., Bullock, J., & Muñoz, R. R. 2011, ApJ, 728, 106

Sheffield, A., Johnston, K., Majewski, S., et al. 2014, ApJ, 793, 62

Sikivie, P. 1998, Physics Letters B, 432, 139

Slater, C. T., Bell, E. F., Schlafly, E. F., et al. 2014, ApJ, 791, 9

Sollima, A., Valls-Gabaud, D., Martinez-Delgado, D., et al. 2011, ApJ Lett, 730, L6

Steinmetz, M., Zwitter, T., Siebert, A., et al. 2006, AJ, 132, 1645

Vivas, A. K., & Zinn, R. 2006, AJ, 132, 714

Warren, S. R. & Cole, A. A. 2009, MNRAS, 393, 272

Widrow, L. M., Gardner, S., Yanny, B., Dodelson, S., & Chen, H.-Y. 2012, ApJ Lett, 750, LL41

Widrow, L. M., Barber, J., Chequers, M. H., & Cheng, E. 2014, MNRAS, 440, 1971

Williams, M. E. K., Steinmetz, M., Binney, J., et al. 2013, MNRAS, 436, 101

Xu, Y., Newberg, H. J., Carlin, J. L., et al. 2015, ApJ, 801, 105

Yanny, B., Newberg, H. J., Grebel, E. K., et al. 2003, ApJ Lett, 588, 824

Yanny, B., & Gardner, S. 2013, ApJ, 777, 91

Yong, D., Carney, B. W., de Almeida, L., & Pohl, B. L. 2006, AJ, 131, 2256

York, D. G., Adelman, J., Anderson, J. E., Jr., et al. 2000, AJ, 120, 1579

Younger, J. D., Besla, G., Cox, T. J., et al. 2008, ApJ Lett, 676, L21

Yuan, H.-B., Liu, X.-W., Huo, Z.-Y., et al. 2015, MNRAS, 448, 855

Zhao, G., Zhao, Y.-H., Chu, Y.-Q., Jing, Y.-P., & Deng, L.-C. 2012, Research in Astronomy and Astrophysics, 12, 723

Chapter 4 Stellar Streams and Clouds in the Galactic Halo

Carl J. Grillmair and Jeffrey L. Carlin

Abstract Recent years have seen the discovery of an ever growing number of stellar debris streams and clouds. These structures are typically detected as extended and often curvilinear overdensities of metal-poor stars that stand out from the foreground disk population. The streams typically stretch tens of degrees or more across the sky, even encircling the Galaxy, and range in heliocentric distance from 3 to 100 kpc. This chapter summarizes the techniques used for finding such streams and provides tables giving positions, distances, velocities, and metallicities, where available, for all major streams and clouds that have been detected as of January 2015. Sky maps of the streams are also provided. Properties of individual tidal debris structures are discussed.

4.1 Observational Techniques

With the advent of wide-area, digital sky surveys (primarily the Sloan Digital Sky Survey, SDSS, as well as the 2MASS and WISE surveys), we have seen a remarkable period of discovery in the search for Galactic substructures. From the initial detection of short tidal tails emanating from the globular cluster Palomar 5 in the SDSS commissioning data (Odenkirchen et al. 2001), to the mapping of M-giants in the Sagittarius stream completely around the sky using 2MASS (Majewski et al. 2003), our knowledge of coherent structures in the halo of our Galaxy has advanced spectacularly. While there have been many previous attempts to map large regions of sky in search of tidal streams and substructures, it appears in hindsight that these efforts were largely defeated by insufficient or non-contiguous sky coverage, variable depth or completeness, or insufficiently uniform calibration.

C.J. Grillmair (⋈)

Spitzer Science Center, Mail Stop 314-6, 1200 E. California Blvd., Pasadena, CA 91125, USA e-mail: carl@ipac.caltech.edu

J.L. Carlin

Department of Physics, Applied Physics and Astronomy, Rensselaer Polytechnic Institute, 110 8th Street, Troy, NY 12180, USA

Earlham College, Richmond, IN, USA e-mail: jeffreylcarlin@gmail.com

The streams and clouds described here were all initially detected using photometric techniques. These techniques rely on the separation in color-magnitude space of relatively low-metallicity halo stars from the far larger population of nearby foreground stars. Early efforts to detect tidal debris streams applied these techniques to photographic surveys of regions surrounding globular clusters and dwarf galaxies (Grillmair et al. 1995; Irwin and Hatzidimitriou 1995; Leon et al. 2000). The same techniques are now being applied to deeper, wider, and better calibrated large-scale digital surveys (e.g., SDSS, 2MASS, WISE, PAndAS, and Pan-STARRS). Other halo substructures have been detected in radial velocity surveys as cold (low velocity dispersion), coherent subsets of local halo stars; these are described in Chap. 5.

Early efforts at separating halo populations from foreground stars relied on fairly simple color and magnitude cuts designed to select blue main sequence turn-off stars. This technique was used with some success to find tidal streams emanating from globular clusters (Grillmair et al. 1995; Leon et al. 2000; Odenkirchen et al. 2001). Rockosi et al. (2002) subsequently demonstrated the utility of a matched filter in making better use of the available information and pushing detection limits to considerably lower surface densities. By assigning weights or likelihoods to individual stars based on their photometric uncertainties and the color-magnitude distribution of nearby field stars, the matched filter yields the optimal contrast between different stellar populations. Grillmair and Dionatos (2006a,b) adopted this technique to extend the Pal 5 tidal stream and to discover the tenuous and very cold stream GD-1. More sophisticated techniques are combining photometric selection with radial velocity surveys (e.g., Newberg et al. 2009) to push detection limits to still lower surface densities.

Several stream candidates have been detected purely photometrically as long overdensities in the SDSS and WISE surveys and await confirmation via velocity surveys. Given the low surface densities of known streams, and the fact that stars can only be assigned probabilities of being associated with either the field or the stream, it can be a fairly expensive proposition to obtain velocity information. Telescope time allocation committees are loath to grant large blocks of time when the anticipated yield might be as little as 10 % of the targets surveyed. Confirmation of some of the most tenuous streams may consequently have to wait for results of massively multiplexed spectroscopic surveys such as LAMOST (Cui et al. 2012; Deng et al. 2012; Luo et al. 2012; Zhao et al. 2012) and DESI (Dark Energy Spectroscopic Instrument; formerly known as BigBOSS).

Even while we wait for spectroscopic confirmation, more stream candidates are actively being sought. While tightly constraining the shape and extent of the Galactic potential with tidal streams will ultimately require full, six-dimensional phase space information (e.g. Willett et al. 2009; Koposov et al. 2010; Law and Majewski 2010), simply finding more streams will enable us to better understand the accretion history of the Galaxy. The distances and orientations of the streams give us some idea of their orbits and the likely distribution of their progenitors. And if we can properly quantify the current detection biases, we will also be in a better position to infer the total population of such streams and their progenitors.

4.2 Currently Known Stellar Debris Streams and Clouds in the Galactic Halo

Here we present tables that give some basic information for all of the currently known streams and clouds. We define streams as overdensities of stars that are significantly longer than they are wide. Where radial velocities have been measured, they have a narrow line-of-sight velocity dispersion that can vary with position along the stream. Narrower, lower velocity dispersion streams are thought to result from the tidal disruption of globular clusters, while wider, hotter streams are thought to result from the disruption of dwarf galaxies. Clouds, on the other hand, are spatially very large overdensities of halo stars whose origins are currently not understood. These clouds may be the tidal debris from dwarf galaxies that has piled up near the apogalactica of highly eccentric orbits. There is also evidence that at least one cloud is the disrupted remains of the core of the dwarf galaxy.

Tables 4.1 and 4.2 are primarily intended to (1) aid non-specialists in identifying unexpected features in their data, and (2) provide interested researchers with some basic parameters and references to more detailed works. The tables are neither intended nor usable for comparative studies.

Table 4.1 summarizes the basic properties of all currently known halo debris streams in order of discovery. We do not include globular or open clusters with power-law profiles extending beyond their nominal King tidal radii. Grillmair et al. (1995) and Leon et al. (2000) found such extensions around most of the globular clusters in their respective surveys. Given both these results and theoretical expectations, it is probably fair to say that it would be surprising to find a globular cluster that, if examined sufficiently deeply, did *not* show evidence of tidal stripping. We therefore list only streams and structures with a projected extent of at least a few degrees on the sky. We report all tidal streams discovered in the literature, including some that remain controversial. For example, the Monoceros Ring could actually be a feature of the Milky Way's stellar disk (see Chap. 3). The Virgo Stellar Stream (VSS) and the Virgo Overdensity (VOD) could be the same structure, or several structures that overlap in configuration space. As several deep, wide-area surveys are in progress in both hemispheres, and as the search for stellar substructures remains quite active, we expect this table to become incomplete fairly quickly.

Column descriptions for Tables 4.1 and 4.2 are as follows:

Designation: This column gives the common name by which the particular feature is known in the literature. There exists as yet no convention on how streams should be named and a delightful anarchy has ensued. In cases where the progenitor is known, the feature is quite naturally named after the progenitor (e.g., Sagittarius stream, Pal 5, NGC 5466). Some researchers have named streams after the constellations or regions of the sky in which they were first found, or in which they currently appear strongest (e.g., Monoceros, Cetus Polar Stream, Anticenter Stream, Triangulum/Pisces, Ophiuchus). Still others are named for the surveys in which they were first detected (e.g., ATLAS stream, PAndAS MW stream), after some discovery characteristic (Orphan, EBS), or

Table 4.1 Currently known halo streams

			Distance V _{hel}	Vhel		
Designation	Progenitor	Known extent	kpc	km s ⁻¹	[Fe/H]	Selected references
Sagittarius	Sagittarius	Circum-sky	7–100	(-200, +200)	(-1.15, -0.4)	(-200, +200) (-1.15, -0.4) Ibata et al. (1994), Mateo et al. (1998),
Stream	dSbh					Alard (1996), Totten and Irwin (1998),
						Ibata et al. (2001a,b), Majewski et al. (2003),
						Martínez-Delgado et al. (2004),
						Vivas et al. (2005), Belokurov et al. (2006b),
						Fellhauer et al. (2006), Bellazzini et al. (2006b),
						Chou et al. (2007), Law et al. (2009),
						Law and Majewski (2010), Keller et al. (2010)
						Carlin et al. (2012a), Koposov et al. (2012)
Virgo Stellar	NGC 2419?	NGC 2419 ? $180^{\circ} < R.A. < 195^{\circ}$ 19.6	19.6	128	-1.78	Vivas et al. (2001), Duffau et al. (2006),
Stream		$-4^{\circ} < \delta < 0^{\circ}$				Newberg et al. (2007), Duffau et al. (2014)
Palomar 5	Palomar 5	225° < R.A. < 250°	23	-55	-1.43	Odenkirchen et al. (2001, 2003, 2009),
		$-3^{\circ} < \delta < 8.5^{\circ}$				Rockosi et al. (2002),
						Grillmair and Dionatos (2006a),
						Carlberg et al. (2012)
Monoceros Ring	dG?	$108^{\circ} < R.A. < 125^{\circ}$	≈ 10.5	≈ 100	-0.8	Newberg et al. (2002), Yanny et al. (2003),
		$-3^{\circ} < \delta < -41^{\circ}$				Ibata et al. (2003), Rocha-Pinto et al. (2003),
						Peñarrubia et al. (2005), Li et al. (2012)
						Slater et al. (2014)
NGC 5466	NGC 5466	$182^{\circ} < R.A. < 224^{\circ}$ 17	17	108	-2.2	Belokurov et al. (2006a),
		$21^{\circ} < \delta < 42^{\circ}$				Grillmair and Johnson (2006),
						Fellhauer et al. (2007b), Lux et al. (2012)

Orphan Stream	dG?	$143^{\circ} < R.A. < 165^{\circ}$	20–55	(95,240)	-2.1	Grillmair (2006a), Belokurov et al. (2007a)
		$-17^{\circ} < \delta < +48^{\circ}$				Fellhauer et al. (2007a), Sales et al. (2008),
						Newberg et al. (2010), Sesar et al. (2013)
						Casey et al. (2013)
GD-1	GC?	$134^{\circ} < R.A. < 218^{\circ}$	7–10	(-200, +100)	-2.1	Grillmair and Dionatos (2006b),
		$14^{\circ} < \delta < 58^{\circ}$				Willett et al. (2009),
						Koposov et al. (2010),
						Carlberg and Grillmair (2013)
AntiCenter Stream	dG?	$121^{\circ} < R.A. < 130^{\circ}$	∞ ≈	(50, 90)	96.0—	Grillmair (2006b),
		$-3^{\circ} < +63^{\circ}$				Grillmair et al. (2008),
						Li et al. (2012)
EBS	GC?	$132^{\circ} < R.A. < 137^{\circ}$	10	(71, 85)	-1.8	Grillmair (2006b), Grillmair (2011),
		$-3^{\circ} < \delta < 16^{\circ}$				Li et al. (2012)
Acheron	GC?	232° < R.A. < 258°	3.5-3.8		-1.7?	Grillmair (2009)
		$3^{\circ} < \delta < 20^{\circ}$				
Cocytos	GC?	$197^{\circ} < R.A. < 257^{\circ}$	11		-1.7?	Grillmair (2009)
		$8^{\circ} < \delta < 30^{\circ}$				
Lethe	GC?	$176^{\circ} < R.A. < 252^{\circ}$	13		-1.7?	Grillmair (2009)
		$22^{\circ} < \delta < 37^{\circ}$				
Styx	Bootes III?	$201^{\circ} < R.A. < 250^{\circ}$,	45		-2.2?	Grillmair (2009)
		$21^{\circ} < \delta < 31^{\circ}$				
Cetus Polar	NGC 5824?	$NGC 5824$? $19^{\circ} < R.A. < 37^{\circ}$	24–36	(-200, -160) -2.1	-2.1	Newberg et al. (2009),
Stream		$-11^{\circ} < \delta < +39^{\circ}$				Yam et al. (2013)

(continued)

Table 4.1 (continued)

			Distance	Vhel		
Designation	Progenitor	Known extent	kpc	km s ⁻¹	[Fe/H]	Selected references
Pisces/	GC?	$21^{\circ} < R.A. < 24^{\circ}$	35	120	-2.2	Bonaca et al. (2012b), Martin et al. (2013),
Triangulum		$23^{\circ} < \delta < 40^{\circ}$				Martin et al. (2014)
Alpheus	NGC 288?	22° < R.A. < 28°	1.6-2.0		-1.0?	Grillmair et al. (2013)
		$-69^{\circ} < \delta < -45^{\circ}$				
ATLAS stream	Pyxis?	$18^{\circ} < R.A. < 30^{\circ}$	20		-1.4?	Koposov et al. (2014)
		$-32^{\circ} < \delta < -25^{\circ}$				
PAndAS MW	dG?	$0^{\circ} < R.A. < 22^{\circ}$	17	127	-1.5?	-1.5? Martin et al. (2014)
Stream		$40^{\circ} < \delta < 48^{\circ}$				
Hermus	GC?	241° < R.A. < 254°	18.5		-2.3?	Grillmair (2014)
		$5^{\circ} < \delta < 50^{\circ}$				
Hyllus	GC?	245° < R.A. < 249°	20		-2.3?	Grillmair (2014)
		$11^{\circ} < \delta < 34^{\circ}$				
Ophiuchus stream	CC	241° < R.A. < 243°	8–9.5	290	-1.95	Bernard et al. (2014), Sesar et al. (2015)
		$-7.2^{\circ} < \delta < 6.7^{\circ}$				

 Table 4.2 Currently known halo clouds

			Distance V _{hel}	V_{hel}		
Designation	Progenitor	Progenitor Known extent	kpc	$\mathrm{km}\mathrm{s}^{-1}$	[Fe/H]	Selected references
Triangulum-	dG?	$-10^{\circ} < \text{R.A.} < 30^{\circ}$	20	(-200, -50)	9.0—	Majewski et al. (2004), Rocha-Pinto et al. (2004),
Andromeda (TriAnd1)		$20^{\circ} < \delta < 45^{\circ}$				Martin et al. (2007), Chou et al. (2011)
						Deason et al. (2014), Sheffield et al. (2014)
Hercules-Aquila	dG?	$0^{\circ} < l < 80^{\circ}$	10–25	(-130, -120)	(-2.2, -1.4)	10–25 (-130, -120) (-2.2, -1.4) Belokurov et al. (2007b), Watkins et al. (2009),
		$-50^{\circ} < b < 50^{\circ}$				Sesar et al. (2010a), Simion et al. (2014)
Virgo	dG?	See map in Fig. 4.3 $\sim 6-20$ (200, 360)	~6-20	(200, 360)	(-2.0, -1.0)	(-2.0, -1.0) Vivas et al. (2001), Newberg et al. (2002),
Overdensity						Jurić et al. (2008), Bonaca et al. (2012a),
						Carlin et al. (2012b), Duffau et al. (2014)
Triangulum	dG?	3° < R.A. < 23°	28	(-200, -50) -0.6	9.0—	Martin et al. (2007), Sheffield et al. (2014)
-Andromeda 2 (TriAnd2)		$28^{\circ} < \delta < 42^{\circ}$				
Pisces Overdensity	dG?	$350^{\circ} < R.A. < 360^{\circ} 80-100 -75$	80–100	-75	-1.5	Sesar et al. (2007), Watkins et al. (2009),
		$-1.3^{\circ} < \delta < +1.3^{\circ}$				Kollmeier et al. (2009), Sesar et al. (2010b),
						Sharma et al. (2010), Vivas et al. (2011)

after rivers in Greek mythology (Acheron, Lethe, Cocytos, Styx, Alpheus, Hermus, and Hyllus).

Progenitor: This column provides the name of the progenitor, if known or suspected. Where there is a question mark, readers are referred to the references for the source of the uncertainty. If the progenitor is listed as dG? (dwarf galaxy) or GC? (globular cluster), the actual progenitor is unknown, but its likely nature is conjectured based on the strength or morphology of the stream. Extensive, broad (FWHM > 500 pc), or hot streams ($\sigma_v > 10 \,\mathrm{km \, s^{-1}}$) presumably arose from more massive systems such as dwarf galaxies, whereas narrower (FWHM $< 200 \,\mathrm{pc}$), less populous, and colder streams ($\sigma_v < 5 \,\mathrm{km \, s^{-1}}$) most likely arose from globular clusters. This latter conclusion is based primarily on the similarity in the cross-sectional widths of such streams (~100 pc) to those of known globular cluster streams (Pal 5, NGC 5466). On the other hand, Carlberg (2009) has shown that streams should be heated by encounters with other Galactic constituents, and that initially narrow streams should become hotter and broader with time. Our division between globular cluster and dwarf galaxy streams must therefore be regarded with some skepticism until more observational evidence can be brought to bear (e.g. progenitor identifications, α -element ratios, etc.).

Known Extent: To help researchers to identify structures they may come across in the course of their work, we provide the maximum extent of the streams on the celestial sphere, as determined either in the discovery paper or in subsequent investigations. While the positions and trajectories of some features are shown in Figs. 4.1, 4.2, 4.3, 4.4, 4.5, and 4.6, readers are generally referred to the discovery or follow-up papers for more detailed maps of the streams. In some cases the

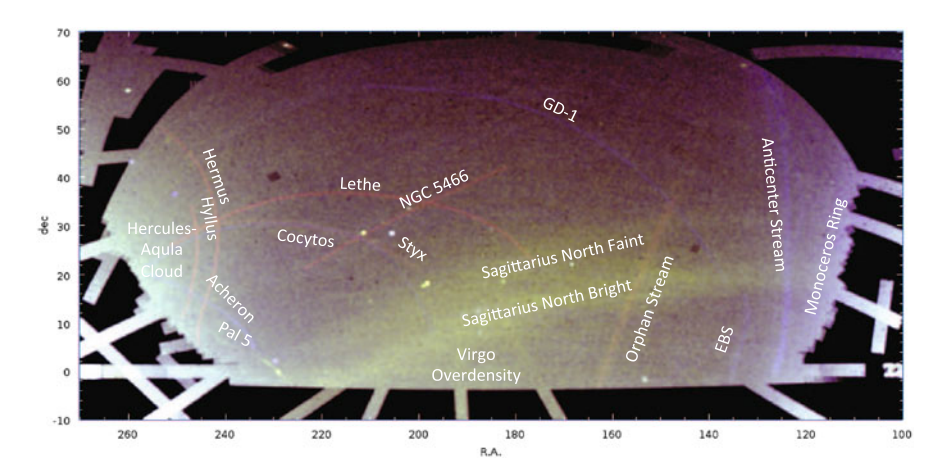


Fig. 4.1 A matched-filter surface density map of the northern footprint of the Sloan Digital Sky Survey. The filter used here is based on the color-magnitude distribution of the metal poor globular cluster M 13. The stretch is logarithmic and all but the Sagittarius streams have been enhanced using arbitrarily scaled Gaussians to make them visible at this stretch. Bluer colors correspond to more nearby stars (\leq 15 kpc) while redder colors reflect the distribution of more distant stars

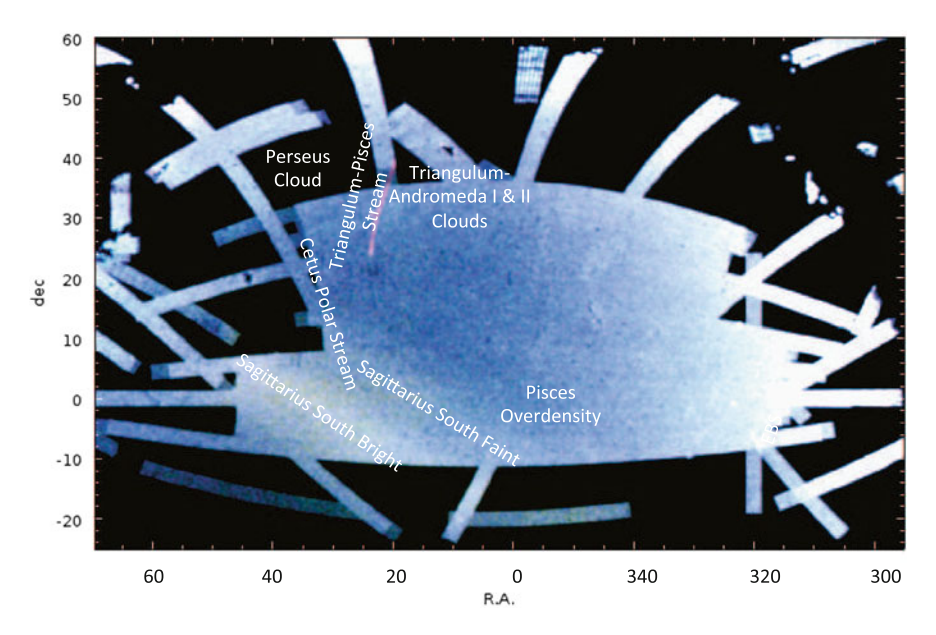


Fig. 4.2 As in Fig. 4.1, but for the southern footprint of the SDSS

streams evidently extend beyond the discovery survey regions. For these features we simply provide the R.A. and Dec limits of the survey used.

Distance: This column provides the range of heliocentric distances for different portions of streams. Where different distances are estimated by different authors, we provide only the most recent estimates. These distance estimates will undoubtedly be refined as deeper surveys are carried out, spectroscopic metallicities are obtained, proper motions and Galactic parallaxes are measured, or RR Lyrae can be physically associated with streams. As distances can vary greatly from one portion of a given stream to another, readers are referred to discovery and follow-up papers for estimates of distance with position.

 V_{hel} : If radial velocities have been measured for one or more portions of a stream, the range of velocities is given here. This range can be quite large (e.g., Sagittarius or GD-1), where the length of the stream, combined with the Sun's motion, can produce very substantial gradients over the length of the stream. Once again, readers are referred to the references for more specific information.

[Fe/H]: Metallicity estimates can be based on the color-magnitude locus of stream stars, on the metallicity of the matched filter that yields the highest signal-to-noise ratio, or on spectroscopy of individual stars. Estimates based solely on photometry can have fairly large uncertainties and are consequently flagged with question marks.

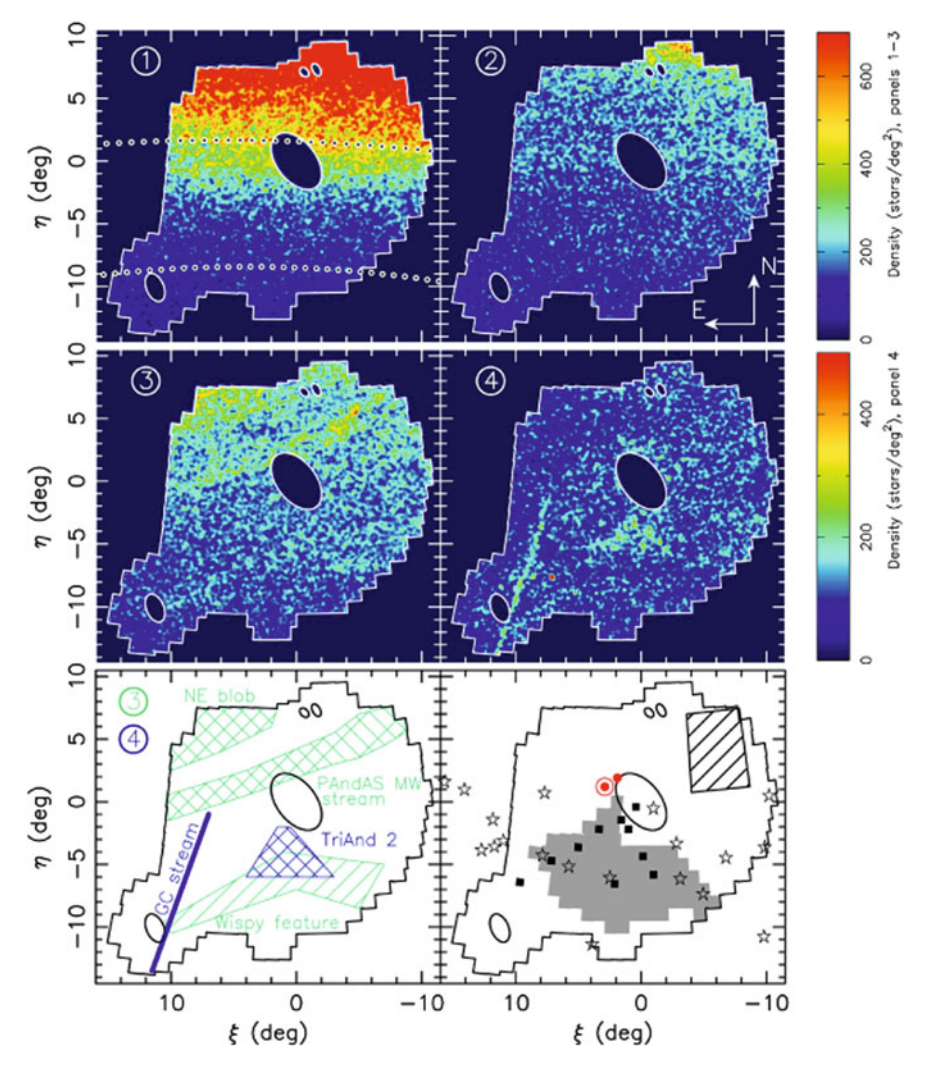


Fig. 4.3 Stellar density in the PAndAS survey in the foreground of M31 (coordinates are relative to the M31 center, with north *upward* and east toward the *left*). Panels *I*–4 show smoothed stellar density maps for CMD-filtered stars at mean distances of 7, 11, 17, and 27 kpc from the Sun, respectively. The *lower left panel* shows the Milky Way substructures identified by Martin et al. (2014) in this so-called "PAndAS Field of Streams." [Figure 2 from Martin et al. (2014)]

Selected References: We provide a selected set of references for each stream. These include the discovery paper(s) and subsequent works that demonstrably extend the stream, provide additional spectroscopic or proper motion measurements, examine stream morphology, RR Lyrae content, model the orbits of the streams, or use the streams as probes of the Galactic potential.

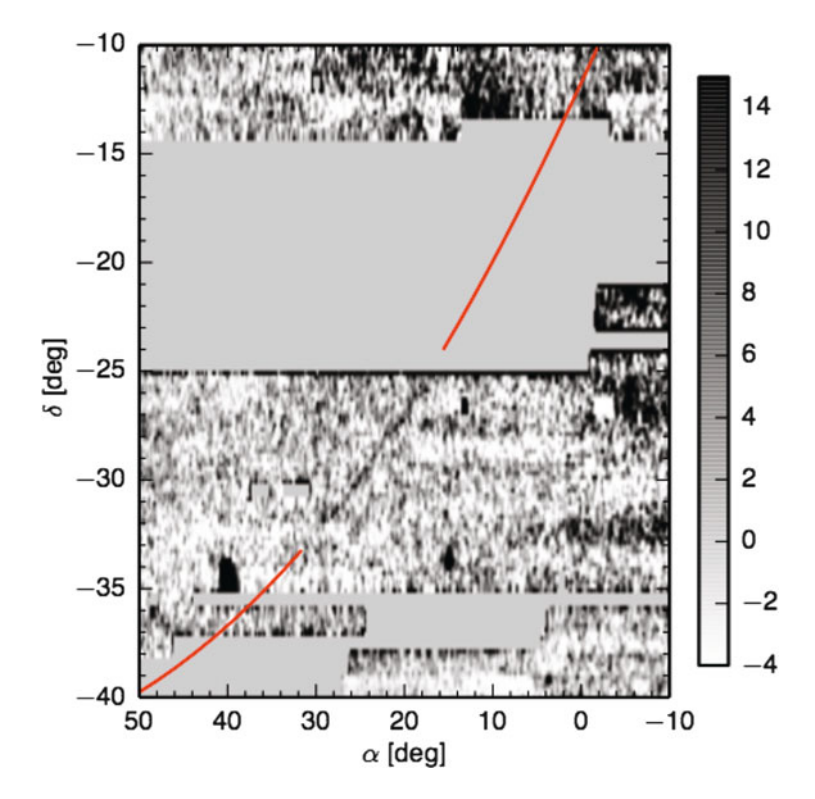


Fig. 4.4 Surface density map of the ATLAS stream, using a filter optimized for a stellar population with [Fe/H] = -2.1, an age of 12.5 Gyrs, and a distance of 20 kpc. *Darker shades* correspond to higher surface densities. [Figure 1 from Koposov et al. (2014)]

Clouds are listed in Table 4.2, and are distinguished from streams by their more diffuse, non-localized nature. These features are also likely to be the result of tidal stripping or disruption, but determining their nature and origin may have to await future radial velocity and proper motion surveys.

The locations and extent of many of the structures in Tables 4.1 and 4.2 are shown in Figs. 4.1 and 4.2. The PAndAS MW, ATLAS, and Ophiuchus streams are shown separately in Figs. 4.3, 4.4, and 4.5.

In the remainder of this chapter we discuss some of the particulars of individual streams listed in Tables 4.1 and 4.2. As the Sagittarius and Monoceros/Anticenter streams are the subject of much study and controversy, they merit more detailed discussion, and we refer the reader to Chaps. 2 and 3 for more on these systems.

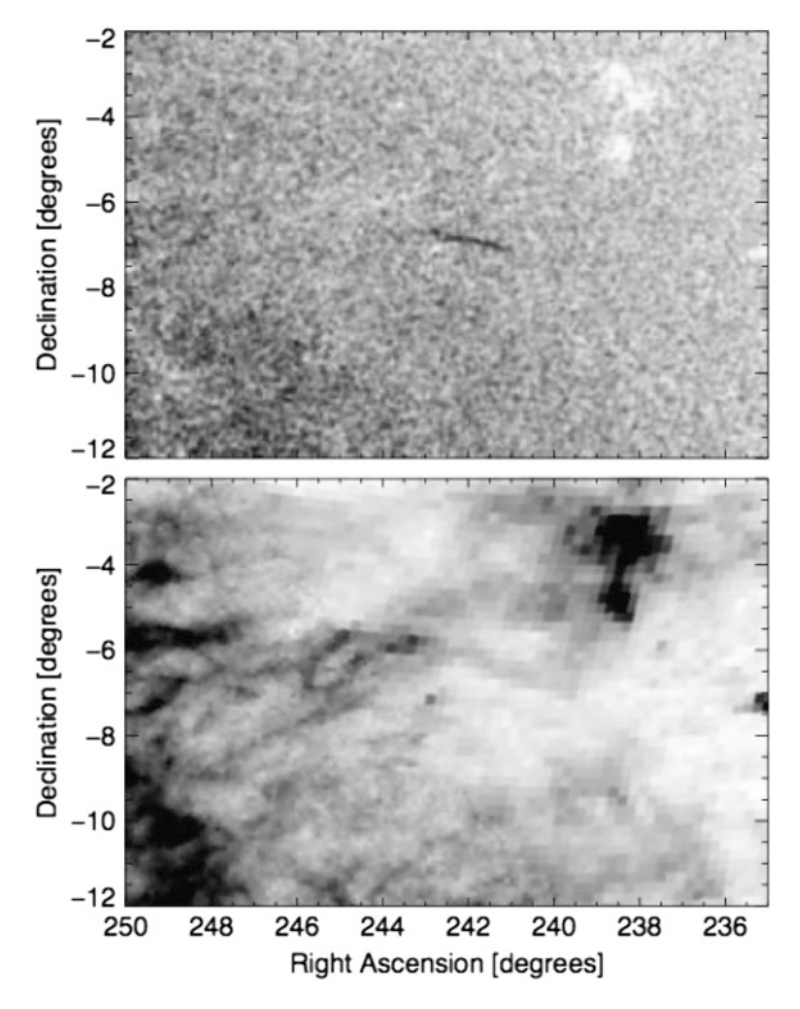


Fig. 4.5 Surface density map of the Ophiuchus stream, optimized for old and metal-poor stars at a distance of 8–12 kpc. *Darker shades* correspond to higher surface density. The *lower panel* shows a reddening map of the same region. [Adapted from Fig. 1 of Bernard et al. (2014)]

4.2.1 Streams with Known or Likely Globular Cluster Progenitors

Pal 5 The stream associated with the globular cluster Palomar 5 (Pal 5) is one of the most striking examples among the known tidal streams. The stream is clearly visible as a narrow ribbon of stars arcing across the corner of SDSS starcount maps such as Fig. 4.1 and the "Field of Streams" from Belokurov et al. (2006b, also reproduced in Chap. 1 of this volume). As it is clearly associated with the cluster, is a well-defined, kinematically-cold stream, and is at a distance (\sim 23 kpc) close enough to be studied

in detail, this stream has been the object of intense scrutiny. Indeed, as it can be studied in such exquisite detail, the Pal 5 stream has become something of a test case for models of tidal disruption (e.g., Dehnen et al. 2004; Mastrobuono-Battisti et al. 2012) and evolution of the tidal tails in the Galactic halo. The stream is clearly defined over $>25^{\circ}$ on the sky, with radial velocity members now identified over at least $\sim 20^{\circ}$ of its extent (e.g., Odenkirchen et al. 2009; Kuzma et al. 2015). As it is robustly detected above the background stellar density, the Pal 5 stream has been used to explore gaps in streams and their implications for the density of dark matter subhalos (Carlberg et al. 2012, see also Chap. 7). As much of the stream is still in the vicinity of Pal 5, with a rather periodic distribution of clumps near the cluster, there remains some controversy concerning the extent to which these gaps may be a product of epicyclic motions of stars within the stream (Küpper et al. 2008, 2012) rather than the result of encounters with subhalos.

NGC 5466 The tidal stream associated with the globular cluster NGC 5466 has been suggested (Lux et al. 2012) to have strong implications for the shape of the Galactic dark matter halo. Though this stream is quite strong near the cluster (Belokurov et al. 2006a), its more distant reaches are very much more tenuous (Grillmair and Johnson 2006). The analysis by Lux et al. (2012) suggested that the trajectory of the northern tip of the stream may have important consequences for the inferred shape of the dark matter halo. More definitive results await the identification of tracers with which to derive velocity and distance to the stream at large separations from the main body of the cluster.

GD-1 Now traced to over 80° across the northern SDSS footprint, the "GD-1" stream (Grillmair and Dionatos 2006b) is the longest of the cold streams discovered to date. At a mean distance of \sim 9 kpc, the stream's narrow \sim 0.5° width corresponds to only \sim 70 pc in cross section, suggesting that the GD-1 progenitor was (or is) a globular cluster. The orbit of this stream has been well established using SDSS velocity measurements by Willett et al. (2009), who found a best-fitting orbit with pericenter of \sim 14 kpc, apocenter of \sim 28 kpc, and low inclination ($i \sim 35^{\circ}$). Koposov et al. (2010) explored the constraints that this system places on the shape and strength of the Galactic potential, and were able to put tight limits on the circular velocity at the Sun's radius ($V_c = 224 \pm 13 \,\mathrm{km \, s^{-1}}$). Constraints on the shape of the halo are comparatively weak owing to the relatively low orbital inclination and the strong influence of the Galactic disk. Its relatively high surface density over a large angular swath, kinematically cold population, presumed great age, and lack of a nearby progenitor make GD-1 an excellent candidate to search for the perturbing effects of dark matter subhalos (see Chap. 7). The measurement of 8 ± 3 stream gaps over ~8 kpc of GD-1's extent by Carlberg and Grillmair (2013) suggest that the Milky Way contains some 100 dark matter subhalos with $M > 10^6 \,\mathrm{M}_{\odot}$ within the apocenter of the GD-1 orbit. Verifying and refining this estimate will require both deeper photometric surveys and better radial velocity sampling of GD-1.

EBS The Eastern Banded Structure (EBS) is a \sim 18°-long stellar overdensity discovered in the SDSS by Grillmair (2006a). Because of its proximity and similar

distance (\sim 10 kpc) to the Anticenter Stream (ACS), the EBS was originally thought to be associated with the ACS/Monoceros structures. Grillmair (2011) and Li et al. (2012) showed that EBS is distinct both in metallicity and kinematics from the ACS. Furthermore, Grillmair (2011) associated two velocity structures (ECHOS) of Schlaufman et al. (2009) with EBS and determined that its orbit is likely to be highly eccentric, unlike that of the ACS. A \sim 2°-wide overdensity of stars within the EBS was also noted by Grillmair (2011), who suggested that this object, dubbed Hydra I, may be the remains of EBS's progenitor. Deeper and wider surveys of the EBS are currently in progress and will hopefully shed more light on the nature and origin of this stream.

Pisces/Triangulum The Pisces/Triangulum Stellar Stream is a narrow ($\sim 0.2^{\circ}$) stream that was found as a \sim 5.5 kpc-long photometric overdensity by Bonaca et al. (2012b), who dubbed it the "Triangulum Stream" based on its proximity to M33. It was detected independently as a kinematically coherent feature among SDSS spectra by Martin et al. (2013), who called it the "Pisces Stellar Stream" because it resides in Pisces. While Bonaca et al. (2012b) estimated a distance of 26 ± 4 kpc to the stream based on fitting isochrones of metallicity [Fe/H] = -1.0 to stars in the structure, Martin et al. (2013) were able to estimate a spectroscopic metallicity of [Fe/H] ≈ -2.2 , and revised the distance estimate to the Pisces stream to 35 \pm 3 kpc. This stream is prominent in stellar density maps of the PAndAS survey (Martin et al. 2014, reproduced here as Fig. 4.3, see panels 4 and 5), extending the stream several degrees northward of the SDSS footprint. Interestingly, Martin et al. (2014) found that the stream ends abruptly, suggesting either a physical truncation or a sharp distance gradient at the northern end. As no progenitor has yet been identified, and as kinematical data exist only for only one point along the stream, an orbit has not been estimated.

Acheron, Cocytos, Lethe, Hermus, and Hyllus These stream candidates are long, narrow, but relatively low signal-to-noise overdensities of low-metallicity stars in the northern footprint of the SDSS survey. No velocity information has yet been gleaned for these streams, but efforts are underway to associate tracers such as blue horizontal branch stars and RR Lyrae with one or more of them.

Alpheus This nearby ($<2\,\mathrm{kpc}$) stream candidate was discovered by combining the WISE All-Sky and 2MASS catalogs (Grillmair et al. 2013). These authors suggest that, by virtue of distance and orientation, the stream could plausibly have originated in the globular cluster NGC 288 some 20° away. Deeper surveys and velocity information will be required to test this hypothesis.

Ophiuchus This stream is somewhat unique among our current sample of streams in that it is apparently highly foreshortened, and is seen nearly end-on from our vantage point. It was detected (Bernard et al. 2014) as an overdensity of metal-poor stars in the Pan-STARRS1 3π survey. Though only 2.5° long, Sesar et al. (2015) subsequently determined that the Ophiuchus stream is actually \sim 1.6 kpc in length, appearing foreshortened due to our nearly end-on viewing angle. Their velocity and proper motion measurements indicate that the stream is kinematically cold and

on a fairly eccentric orbit with peri- and apocentric distances of 3.5 and 17.5 kpc, respectively. To explain the rather short length of the stream given its inferred orbit, Sesar et al. suggested that the progenitor must have suffered a substantial change in its orbit and become disrupted only rather recently (\sim 250 Myr ago).

4.2.2 Streams with Presumed Dwarf Galaxy Progenitors

Orphan Stream The Orphan stream is a roughly 1–2°-wide stellar stream spanning nearly the entire vertical (declination) extent of the SDSS northern Galactic hemisphere footprint. This stream, so called because its progenitor has not been identified, was discovered at about the same time by Grillmair (2006a) and Belokurov et al. (2007b). Because the stream has fairly low surface brightness, determining the distance and velocity of stream members along its extent is difficult. However, some such measurements have been done, and a few attempts have been made to derive orbits. The first of these, by Fellhauer et al. (2007a), explored the possibility that two objects spatially coincident with the stream—the Ursa Major II (UMaII) dwarf spheroidal and the HI cloud known as Complex A—are physically associated with the stream. They concluded that UMaII is likely the progenitor of the Orphan stream, and predicted a strong velocity gradient along the stream. In contrast, Sales et al. (2008) modeled the disruption of a massive two-component dwarf galaxy on the Orphan stream orbit, and found that UMaII is not likely to be the progenitor, and indeed the progenitor is likely to be almost completely disrupted. A more extensive characterization of the stream from SDSS was conducted by Newberg et al. (2010), who then used the data to derive an orbit for the structure and produce an N-body model of a disrupting satellite on this orbit. Their models suggest that the SDSS debris is part of the leading tail of a disrupting satellite on an eccentric ($e \sim 0.7$) orbit that carries the dwarf out to Galactocentric distances of \sim 90 kpc.

The Orphan stream has been traced with RR Lyrae stars to a distance of 55 kpc by Sesar et al. (2013), who also identified a strong metallicity gradient along the stream. These authors could not identify members beyond 55 kpc, and suggest that this is either because the leading stream actually ends at that point, or the tracers are lost due to survey incompleteness or low metallicity. The large metallicity spread seen among these RR Lyrae bolsters the case that this is a dwarf galaxy remnant. The low velocity dispersion and large metallicity spread have been confirmed by Casey et al. (2013), and high-resolution spectroscopy (Casey et al. 2014) shows abundances consistent with dwarf spheroidal chemical evolution.

It is unclear whether any of the satellites (UMaII and the Segue 1 dwarf galaxy) or Complex A are associated with the Orphan stream. Further exploration in the southern celestial hemisphere to identify the path of the stream, its stellar density, and possibly a progenitor, is currently underway. We note that this stream is likely to be a particularly good tracer of the Galactic potential, since it is well traced over a large swath (constraining its orbit quite well) and traverses a large range of Galactic

radii. The combination of the orbit fit to the Orphan stream by Newberg et al. (2010) and distance constraints from RR Lyrae (Sesar et al. 2013) suggest a fairly low mass for the Galactic halo (\sim 3 × 10¹¹ M $_{\odot}$ within 60 kpc).

Cetus Polar Stream This structure was identified in a study of the Sagittarius (Sgr) stream (see Chap. 2) with SDSS data by Yanny et al. (2009) as a set of BHB stars with velocity and metallicity distinct from that of Sgr. Newberg et al. (2009) followed this up by tracing the stream with BHB stars from SDSS DR7, finding a stream aligned roughly along constant Galactic longitude in the south Galactic cap. The authors showed that the ratio of blue straggler stars (BSSs) to BHBs is higher in Sgr than the Cetus Polar Stream (CPS), and that most of the BHB stars in this region of the sky (at distances of $\sim 30 \,\mathrm{kpc}$) are associated with the CPS and not Sgr. This was confirmed by Koposov et al. (2012), who used the offset between BHBs and BSSs to separate Sgr and the CPS in the South. The distance and velocity trends seen in this work imply that the CPS progenitor is (or was) on an orbit that counter-rotates relative to that of Sgr, as had also been found via orbit-fitting by Newberg et al. (2009). Interestingly, Newberg et al. (2009) determined that the massive globular cluster NGC 5824 lies very close to their computed orbit, at nearly the predicted distance, and with almost exactly the predicted radial velocity. Moreover, the tidal extensions found by Grillmair et al. (1995) and Leon et al. (2000) for NGC 5824 also lie along the predicted orbit of the CPS.

The most extensive examination of the CPS was that of Yam et al. (2013). This group used the additional data available in SDSS DR8 to refine the kinematic signature and the distances to the CPS. The newly-available contiguous sky coverage of DR8 photometry was exploited to map the density of BHB stars along the stream and fit the stream width. Yam et al. then used all of this new information to fit an orbit to the stream, and found a low-eccentricity ($e \approx 0.2$), highly inclined $(i \approx 87^{\circ})$ orbit with apo- and pericentric distances of ~ 36 and ~ 24 kpc from the Galactic center. N-body models of $10^8 M_{\odot}$ satellites (assuming mass follows light) on this orbit were found to reproduce the stream velocities and their dispersions, along with the width of the stream, as a function of position. However, matching the density profile of the stream requires a lower mass satellite of $10^6 M_{\odot}$. This suggests that mass does not (or did not) follow light in the progenitor of the CPS. In other words, the stream must originate from a low-mass, dark matter-dominated satellite similar to the "ultra-faint dwarf spheroidals" found in SDSS. This is corroborated by the low metallicity ([Fe/H] ~ -2.2) of CPS stars, which would place the CPS progenitor among typical metallicities of ultra-faint dwarfs.

PAndAS MW Stream This stream, seen in panels 3 and 5 of Fig. 4.3, was found by Martin et al. (2014) in the PAndAS photometric survey of the area around M31. There is a wealth of Galactic substructure along the line of sight to M31 in this survey, including both TriAnd 1 and TriAnd 2, the Monoceros structure, and the Pisces/Triangulum stream. The width and velocity dispersion estimated by Martin et al. (2014) suggest a dwarf galaxy progenitor for the PAndAS stream. Stellar populations suggest that this is an old, metal-poor structure, and it follows an orbit that is roughly parallel to the Galactic plane at a distance of ∼17 kpc from the Sun.

Styx Styx is at a distance of \approx 46 kpc and is presumed to be a relic of a dwarf galaxy solely by virtue of its fairly substantial girth (\sim 1°) (Grillmair 2009). A sparse but significant overdensity (Boötes III) is situated near the stream at a nearly identical distance, and Grillmair (2009) suggested that this overdensity might be the remains of the stream's progenitor. However, subsequent velocity measurements of Boötes III (Carlin et al. 2009) yielded $V_{hel} = 197 \, \mathrm{km \, s^{-1}}$, which appears to be at odds with the near perpendicularity of Styx to our line of sight. No velocities have yet been measured for the stream itself.

4.2.3 Clouds and Other Diffuse Stellar Structures

Overdensities in Virgo The nature and number of the substructure(s) in the Virgo constellation is uncertain. Main sequence turnoff (MSTO) stars from SDSS in this region of the sky have been used to show enhanced stellar densities spanning a huge sky area that have become known as the "Virgo Overdensity (VOD)." This was initially seen in a single stripe of SDSS imaging data at a distance of ~20 kpc by Newberg et al. (2002). Subsequent SDSS studies have mapped an overdensity (relative to neighboring regions of sky) spanning distances of at least $10 < d < 20 \,\mathrm{kpc}$ over $> 1000 \,\mathrm{deg^2}$ (Jurić et al. 2008), and subsequently over 3000 deg² (Bonaca et al. 2012a). Overdensities of RR Lyrae stars are seen in the same region of sky, but in much smaller numbers. However, the much more precise distances that can be derived for RR Lyrae have led numerous authors to point out substructures localized in distance rather than in a large cloud-like structure as seen in MSTO stars. The first of these was the discovery by Vivas et al. (2001) of 5 RR Lyrae from the QUEST survey at a distance of $\sim 20 \,\mathrm{kpc}$; this was followed by a \sim 19 kpc clump in Vivas and Zinn (2003), and a detection at 12 < d < 20 kpc by Vivas and Zinn (2006), also from QUEST. Subsequent RR Lyrae studies from the SEKBO survey by Keller et al. (2008, 2009) have seen similar overdensities at \sim 16–20 kpc distances. Additionally, Keller et al. (2010) detected an overdensity between distances of 12 < d < 18 kpc from the Sun using subgiants from SDSS.

While none of the photometric detections of Virgo substructures (see map in Fig. 4.6) are completely inconsistent with each other, the patchiness among RR Lyrae detections suggests that there is at the very least some density variation within a single large structure, and perhaps a superposition of multiple structures that makes up the overall VOD. It is only with kinematics that this possibility can be explored. Follow-up spectroscopy of QUEST RR Lyrae initially showed (Duffau et al. 2006) that six stars apparently form a cold peak at $V_{\rm gsr} \approx 100\,{\rm km\,s^{-1}}$, which the authors dubbed the "Virgo Stellar Stream." Subsequent studies of this general region of sky (e.g., Newberg et al. 2007; Vivas et al. 2008; Prior et al. 2009; Brink et al. 2010; Carlin et al. 2012b) have variously found RV peaks between 100 and 250 km s⁻¹ (see Fig. 4.6), with some of these appearing to be localized in both distance and velocity. For example, Duffau et al. (2014) identified at least three peaks at distances ranging from \sim 10 to 20 kpc and velocities between

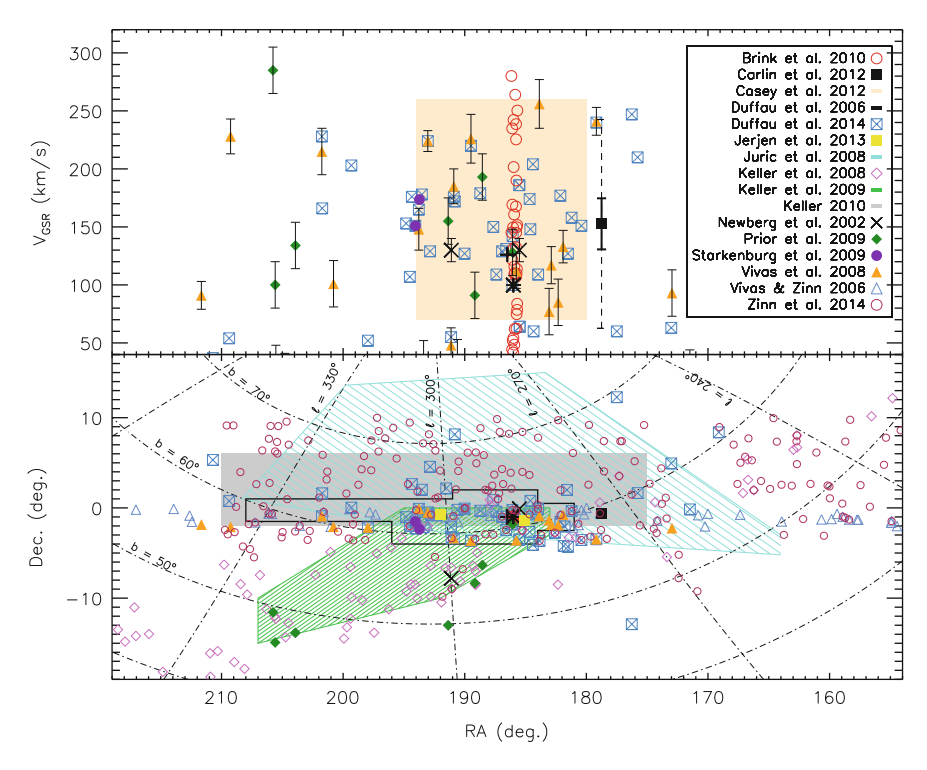


Fig. 4.6 Map of positions and velocities of stars that have been associated with the Virgo substructure(s) in the literature. The *upper panel* gives GSR-frame velocities as a function of right ascension, while the *lower panel* shows RA/Dec positions on the sky. Sources of the data are given in the legend; those with filled areas on the plot are given as *horizontal lines* of the same color as the fill. While there are many "excess" stars in this region of sky at velocities higher than expected for Milky Way populations, there is no clear spatial overdensity or kinematically cold peak visible in this figure

 \sim 120 and 220 km s⁻¹. On the basis of such detections, it has been argued that the substructure in Virgo in made up of many tidal remnants overlapping in phase space. (Note, however, that Casey et al. (2012) found velocity peaks at $V_{\rm GSR} \sim 120$ and \sim 200–240 km s⁻¹. These authors identified the lower-velocity peak as the VSS, and speculate that the high-velocity feature may be related to the Sagittarius trailing tail.) Regardless of the origin, the radial velocities (see Fig. 4.6) alone make it clear that the Virgo substructure is, on average, moving too rapidly away from the Galactic center to be a "cloud" of debris piling up at orbital apocenter as discussed in Chap. 6.

An important clue to the nature of the Virgo substructures came from the measurement of an orbit for Virgo stars in a single pencil-beam. Initially, Casetti-Dinescu et al. (2009) determined the orbit of a single RR Lyrae star known to be a Virgo member. Their combined proper motions and radial velocity yield a rather eccentric orbit that suggests this star recently passed the pericenter of its orbit. This work was expanded by Carlin et al. (2012b), who measured proper

motions and radial velocities of 17 stars consistent with VOD membership. This orbit confirms that the Virgo substructure results from an object on an eccentric orbit that recently made its closest approach. Indeed, Carlin et al. were able to qualitatively reproduce the large spatial extent (both on the sky and in distance) and velocity spread of the Virgo Overdensity by modeling a massive dwarf spheroidal disrupting on their measured orbit. This suggests that the entire structure may be a "puffed-up" dwarf galaxy that just passed its pericenter rather near the Galactic center. However, it is unclear how to reconcile the apparent clumpiness within the larger structure; this may be substructure related to group infall or structure within the progenitor satellite. Alternatively (as suggested by, e.g., Duffau et al. 2014), the entire structure may be a superposition of tidal structures overlapping each other on the sky, similar to the overlapping remnants that fell in along "preferred" directions in the simulations of Helmi et al. (2011). More observations and modeling are needed to understand the structures in this complicated region of the sky.

TriAnd1 and 2 Rocha-Pinto et al. (2004) identified an overdensity of 2MASS color-selected M-giant candidates between roughly $100^{\circ} < l < 150^{\circ}$, $-40^{\circ} < b < -20^{\circ}$. This feature, dubbed the "Triangulum-Andromeda" (TriAnd) structure, is at heliocentric distances of $\sim 18-30\,\mathrm{kpc}$. Rocha-Pinto et al. (2004) spectroscopically confirmed that TriAnd is a kinematically cold structure, and found a metallicity of $\langle \mathrm{[Fe/H]} \rangle = -1.2$ with ~ 0.5 -dex scatter. These authors also noted a trend of line-of-sight velocity with Galactic longitude that looks like an extension of the Monoceros velocity trend; however, TriAnd was thought to be too distant to be an extension of Monoceros. At nearly the same time, this same substructure was seen by Majewski et al. (2004) as a clear main sequence in the foreground of combined CMDs from their photometric survey of M31. These authors estimated the distance to be $\sim 16-25\,\mathrm{kpc}$ from the Sun, with $\sim 20\,\%$ higher distance at the furthest region from the Galactic plane compared to the lowest latitudes. The stellar density is roughly constant over the region surveyed, and is used to estimate a total luminosity over $\sim 1000\,\mathrm{deg^2}$ of $\sim 5 \times 10^5\,L_{\odot}$.

A much deeper and larger-area survey of the M31 outskirts presented by Martin et al. (2007) revealed the existence of a second main sequence in the same region of the sky. This study, which covered $\sim 76\,\mathrm{deg^2}$ between $\sim 115^\circ < l < 130^\circ, -30^\circ < b < -25^\circ$, associated the brighter of the two MSTO features with TriAnd, and the fainter as a new structure dubbed "TriAnd2" (with the original structure called TriAnd1). These two features were found to be at heliocentric distances of ~ 20 and $\sim 28\,\mathrm{kpc}$, and both show fairly narrow main sequences consistent with $\sim 2\,\mathrm{kpc}$ line-of-sight depth. TriAnd1 shows stellar densities at the lowest latitudes (i.e., nearest the plane) and lowest longitudes in the region covered that are $2-3\times\mathrm{higher}$ than at the opposite side of the survey footprint. The surface brightness ($\Sigma_{\mathrm{V}}\sim 32\,\mathrm{mag}\,\mathrm{arcsec}^{-2}$) found by Martin et al. (2007) is similar to that derived by Majewski et al. (2004) for this very diffuse stellar substructure.

Sheffield et al. (2014) undertook an extensive spectroscopic survey of over 200 M giant stars selected to be consistent with TriAnd membership. These authors found two distinct RGB features in 2MASS that correspond to the TriAnd1 and TriAnd2

MSTO features from Martin et al. (2007). Interestingly, even though the two features are separated by more than 5 kpc in line-of-sight distance, their trends in line-of-sight velocity with Galactic longitude are indistinguishable. The nearer of these features (TriAnd1) is found by Sheffield et al. to have mean metallicity of [Fe/H] = -0.57, while TriAnd2 has [Fe/H] = -0.64. A possible origin for the two features is shown by these authors via an *N*-body model of a dwarf galaxy disrupting in the Milky Way halo. In this scenario, the two TriAnd features are debris that were stripped from a single satellite on consecutive pericentric passages of its orbit. The fairly large satellite mass required in this model is consistent with the metal-rich (relative to most dwarf galaxies) stellar populations in TriAnd; in order to enrich to such a level, the progenitor must have been fairly massive.

The PAndAS deep photometric survey of the M31 vicinity has apparently resolved some wispy substructure on smaller scales in this region of sky. Martin et al. (2014) mapped stars from PAndAS in different distance slices, and found a narrow stream at a distance of \sim 17 kpc, another wedge-shaped feature at \sim 27 kpc that is likely associated with TriAnd2, and wispy stellar structure throughout the 17-kpc slice that is attributed to TriAnd1 suffusing the entire field of view. Clearly there is a complex web of substructures intermingling in this region of the sky. Indeed, based on positional and kinematical similarities, Deason et al. (2014) argued in a recent analysis of spectroscopic data in this sky area that the PAndAS stream, TriAnd overdensities, and the Segue 2 ultrafaint dwarf galaxy are associated remnants of a group infall event. This scenario posits that the comparatively more metal-rich TriAnd represents the group-dominant central galaxy, with Segue 2 and the PAndAS structure remnants of TriAnd satellites. Finally, we note that Xu et al. (2015) recently suggested that TriAnd results from the oscillation of the midplane of the disk below $b = 0^{\circ}$, and that the apparent stellar overdensity is part of a disk that extends out to 25 kpc or more. There is clearly much more work needed to understand the nature of the TriAnd features.

Hercules-Aquila Cloud This structure was originally discovered as an overdensity of MSTO stars in the SDSS DR5 database at heliocentric distances of \sim 10–20 kpc by Belokurov et al. (2007b). The cloud covers an enormous area of the sky, apparently extending to at least \pm 40° in Galactic latitude, centered on longitude of $l \sim 40^\circ$. Belokurov et al. attempted to identify the kinematical signature of the Cloud using SDSS spectra of RGB stars, and suggested that a peak at $V_{\rm gsr} \sim 180\,{\rm km\,s^{-1}}$ represents the velocity of Hercules-Aquila stars. Due to its similarity in the CMD to the SDSS ridgeline of the globular cluster M92 ([Fe/H] = -2.2), the stellar population of the Hercules-Aquila was suggested to be rather metal poor (perhaps slightly more metal-rich than M92).

In a series of papers, Larsen et al. (2008, 2011) extensively mapped a nearby structure between \sim 1–6 kpc from the Sun that was dubbed the "Hercules Thick Disk Cloud." The authors (Larsen et al. 2011) suggest that the overdensity seen by Belokurov et al. (2007b) was actually an artifact of the background-subtraction method used in that work, and that the true stellar overdensity is actually much more nearby. However, subsequent studies with unambiguous standard candles such as RR Lyrae have confirmed that there is a structure at $d_{\text{hel}} \sim 20 \,\text{kpc}$. It remains

unclear whether the more distant Hercules-Aquila cloud is related to the apparent thick disk extension.

Hercules-Aquila has been extensively mapped with RR Lyrae stars. Sesar et al. (2010a) used RR Lyrae from SDSS Stripe 82 (on the celestial equator in the south Galactic cap) to show that the Hercules-Aquila cloud contains at least 1.6 times the stellar density of the halo at \sim 15–25 kpc. Photometric metallicity estimates from this work suggest that the cloud's mean metallicity is similar to that of the Galactic halo. Watkins et al. (2009) also studied the RR Lyrae in SDSS Stripe 82, using the proper motions of Bramich et al. (2008). Watkins and colleagues find 237 RR Lyrae that are likely associated with the Hercules-Aquila cloud; these actually make up the majority of their RR Lyrae star sample. The mean distance to the cloud in Stripe 82 is estimated to be \sim 22 kpc, but with dispersion (standard deviation) of \sim 12 kpc. Watkins et al. estimate a mean photometric metallicity of [Fe/H] = -1.43 for the Hercules-Aquila stars. This study additionally presents the most reliable estimate of the velocity of this substructure. Stars with Hercules-Aquila cloud metallicities separate from the thick disk at $300^{\circ} < RA < 320^{\circ}$ in velocity—the mean velocity is centered around $V_{\rm gsr} \approx 25 \, {\rm km \, s^{-1}}$, with a long tail to lower velocities (and blending with the disk at higher velocities).

Simion et al. (2014) mapped the Hercules-Aquila cloud using RR Lyrae from the Catalina Sky Survey (Drake et al. 2014). After subtracting off the contribution of the underlying halo populations, this group concluded that the cloud is more prominent in the southern Galactic hemisphere than in the north, peaking at a heliocentric distance of \sim 18 kpc. It is unclear whether the structure is truly asymmetric about the Galactic plane, or whether higher extinction in the north has affected the completeness of the RR Lyrae sample. The Hercules-Aquila RR Lyrae are predominantly of Oosterhoff class I; thus the stellar populations in the cloud are similar to those of the Galactic halo. The luminosity of the progenitor is estimated to be between $-15 < M_V < -9$, which would place it in the range of the brightest "classical" Milky Way dwarf galaxies.

Pisces Overdensity The Pisces Overdensity is one of the most distant stellar overdensities known in the Galactic halo. This structure was originally found in a study of Stripe 82 RR Lyrae by Sesar et al. (2007) as a grouping of 26 stars (denoted by the authors as "clump J") at a mean distance of 81 kpc from the Sun. This structure was confirmed by Watkins et al. (2009) in a separate analysis of RR Lyrae from SDSS Stripe 82. Watkins et al. dubbed the group of 28 stars at \sim 80 kpc mean distance the "Pisces Overdensity," and suggested that the total stellar mass of this substructure is \sim 10⁴-10⁵ M $_{\odot}$, with mean metallicity of [Fe/H] \sim -1.5. Kollmeier et al. (2009) obtained follow-up spectra of a handful of RR Lyrae stars in Stripe 82, and found five stars tightly clumped in velocity, confirming its identification as a coherent substructure that the authors suggested was a (possibly disrupted) dwarf galaxy. Additional spectra of RR Lyrae observed by Sesar et al. (2010b) complicated this picture by resolving the overdensity into two peaks separated in velocity by \sim 100 km s $^{-1}$. Thus the Pisces Overdensity may actually consist of more than one tidal debris feature overlapping in space. Sharma et al. (2010) subsequently found

a much larger extended structure (dubbed "A16") in the same region of sky using 2MASS-selected M-giant candidates. In this work, the candidates are at distances of $\sim 100\,\mathrm{kpc}$. The large spatial extent (including another possibly associated structure, "A14," at similar distances about 30° away) and somewhat metal-rich (as evidenced by the presence of M-giants) nature of this structure was suggested to indicate an unbound satellite.

While the origin and nature of the Pisces Overdensity remains unclear, it is evident that there are tidal debris structures at distances of more than 80 kpc in the halo. Further kinematical and chemical analysis will be essential to relate the Pisces substructure to other known satellites or structures in the halo.

Perseus Cloud Another poorly studied apparent substructure is the Perseus Cloud, originally isolated among 2MASS-selected M-giant candidates by Rocha-Pinto et al. (2004). Though it appears to be an extension of the TriAnd structure on the sky, and is at a similar distance, Rocha-Pinto et al. argue that their spectroscopic velocities show the two structures to be unrelated. The nature of this stellar structure remains undetermined.

Canis Major and Argo There are other purported stellar overdensities in the Milky Way that we have not discussed here because their nature (as an actual overdensity and/or as a tidal debris structure) is still undetermined. These include the Canis Major overdensity, which was originally seen as a low-latitude excess of 2MASS-selected M giants by Martin et al. (2004a). This feature has been suggested to be a recently accreted dwarf galaxy (Martin et al. 2004a,b; Bellazzini et al. 2006a), and perhaps even the progenitor of the Monoceros Ring (e.g., Peñarrubia et al. 2005). Others (including Momany et al. 2006; Moitinho et al. 2006) have attributed this apparent stellar overdensity to the warp and flare of the Galactic disk. The Argo stellar overdensity (Rocha-Pinto et al. 2006) is near the Canis Major feature in 2MASS M giants, and is also poorly studied. As the focus of this review is on known tidal substructures, and the nature of these structures is still under debate, we will not discuss them further. Some discussion of Canis Major and its possible relation to the low-latitude Monoceros structure can be found in Chap. 3 of this volume.

4.3 Future Discoveries

Given that the currently available, large-area digital sky surveys do not cover the entire sky, we expect that a significant number of strong streams remain to be discovered within 50 kpc. The Pan-STARRS survey (Kaiser et al. 2002), which covers considerably more sky area than the SDSS, will presumably yield additional streams, and extend at least some of the streams whose known extent is currently limited by the SDSS footprint. In the southern hemisphere, the ATLAS (Shanks et al. 2013), Skymapper (Keller et al. 2007), and Dark Energy Surveys (Rossetto et al. 2011) remain to be completed. Covering regions of the sky that have been largely unexplored to date, they will almost certainly yield a number of new streams,

in addition to extending some of the streams and clouds in Tables 4.1 and 4.2. We note that extending known streams is at least as important as finding new ones, as longer streams both reduce the uncertainty in orbit shape and tighten the possible constraints on the Galactic potential.

Further progress in finding cold or tenuous streams in the SDSS and other surveys will almost certainly result from simultaneously combining photometric filtering with velocity and proper motion measurements. Spectra are now available for $\sim 7 \times 10^5$ stars in the SDSS DR10. Newberg et al. (2009) combined photometric measurements with velocities and metallicities to detect the Cetus Polar Stream, a structure which had eluded prior discovery through photometric means alone. Several spectroscopic surveys either planned or in progress (e.g., LAMOST) will almost certainly make contributions in this area, particularly in detecting streams that are highly inclined to our line of sight (e.g., ECHOS, Schlaufman et al. 2009).

The Large Synoptic Survey, expected to begin early in the next decade, will greatly extend the reach of current photometric (e.g., matched filter) methods of stream detection. Even a single pass over the visible sky will be significantly deeper than the SDSS, and the end-of-survey photometric depth is expected to reach r=27.5 (Grillmair and Sarajedini 2009). On the other hand, background galaxies will vastly outnumber stars at this depth, and significant improvements will need to made in the area of star-galaxy separation if we are to take full advantage of the data. If this can be achieved, then applying matched-filter techniques to upper main sequence stars should enable us to photometrically detect streams out to as much as $500\,\mathrm{kpc}$. RR Lyrae will enable us to probe even more deeply into the halo (e.g. Sesar et al. 2013); even with fairly conservative single-pass detection limits, LSST should enable us to detect RR Lyrae out to more than $700\,\mathrm{kpc}$.

Distance estimates are currently the largest source of uncertainty in the use of tidal streams as probes of the potential. The Gaia survey will clearly have an enormous impact here, providing trigonometric distances for giant branch stars out to tens of kpc. In addition, a number of synoptic surveys have detected many thousands of RR Lyrae, some of which have been associated with known streams (e.g. Sesar et al. 2013), and whose distances can now be measured to $\simeq 2\%$ using infrared photometry. On the other hand, the coldest streams may have very few giant branch stars or RR Lyrae. Distances for these have often been estimated photometrically, using filter matching or upper main sequence fitting. However, the ages and metallicities of the stream stars are only poorly known, and the distance uncertainties due to inappropriate filter templates are correspondingly large. Eyre and Binney (2009) and Eyre (2010) have described and demonstrated an alternative method of finding distances by using proper motions to measure "Galactic parallax." This technique relies on the premise that any net proper motion component of stars perpendicular to a stream must be a consequence of the sun's reflex motion. The accuracy of the method is currently on par with photometric distances, limited primarily by the quality of the available proper motions. The Gaia survey should enable very significant improvements in the application of this technique.

Proper motions can also be used to verify and even detect streams, and both Gaia and LSST are expected to make significant contributions to the field. With

expected end-of-mission proper motion accuracies of \leq 200 micro-arcseconds to 20th magnitude, the Gaia survey will enable us to push well down the stream mass function out to perhaps tens of kpc. Beyond that, the end-of-survey proper motion uncertainties for LSST will be on the order of $100\,\mathrm{km\,s^{-1}}$ at $100\,\mathrm{kpc}$. With suitable averaging and the application of Bayesian techniques, this should be sufficient to detect the remote and particularly high-value, extended tidal tails of many of the dwarf galaxies.

Acknowledgements JLC gratefully acknowledges support from the NSF under grants AST 09-37523 and AST 14-09421.

References

Alard, C. 1996, ApJ Lett, 458, L17

Bellazzini, M., Ibata, R., Martin, N., Lewis, G. F., Conn, B., & Irwin, M. J. 2006a, MNRAS, 366, 865

Bellazzini, M., Newberg, H. J., Correnti, M., Ferraro, F. R., & Monaco, L. 2006b, A&A, 457, L21

Belokurov, V., Evans, M. W., Irwin, M. J., et al. 2006a, ApJ, 637, L29

Belokurov, V., Zucker, D. B., Evans, N. W., et al. 2006b, ApJ Lett, 642, L137

Belokurov, V., Evans, N. W., Irwin, M. J., et al. 2007a, ApJ, 658, 337

Belokurov, V., Evans, N. W., Bell, E. F., et al. 2007b, ApJ Lett, 657, L89

Bernard, E. J., Ferguson, A. M. N., Richardson, J. C., et al. 2014, MNRAS, 443, 84

Bonaca, A., Jurić, M., Ivezić, Ž., et al. 2012a, AJ, 143, 105

Bonaca, A., Geha, M., & Kallivayalil, N. 2012b, ApJ Lett, 760, L6

Bramich, D. M., Vidrih, S., Wyrzykowski, L., et al. 2008, MNRAS, 386, 887

Brink, T. G., Mateo, M., & Martínez-Delgado, D. 2010, AJ, 140, 1337

Carlberg, R. G. 2009, ApJ Lett, 705, L223

Carlberg, R. G., Grillmair, C. J., & Hetherington, N. 2012, ApJ, 760, 75

Carlberg, R. G. & Grillmair, C. J. 2013, ApJ, 768, 171

Carlin, J. L., Grillmair, C. J., Muñoz, R. R., Nidever, D. L., & Majewski, S. R., 2009, ApJ, 702, 9

Carlin, J. L., Majewski, S. R., Casetti-Dinescu, D. I., Law, D. R., Girard, T. M., & Patterson, R. J. 2012a, ApJ, 744, 25

Carlin, J. L., Yam, W., Casetti-Dinescu, D. I., et al. 2012b, ApJ, 753, 145

Casetti-Dinescu, D. I., Girard, T. M., Majewski, S. R., et al. 2009, ApJ Lett, 701, L29

Casey, A. R., Keller, S. C., & Da Costa, G. 2012, AJ, 143, 88

Casey, A. R., Da Costa, G., Keller, S. C., & Maunder, E. 2013, ApJ, 764, 39

Casey, A. R., Keller, S. C., Da Costa, G., Frebel, A., & Maunder, E. 2014, ApJ, 784, 19

Chou, M.-Y., Majewski, S. R., Cunha, K., et al. 2007, ApJ, 670, 346

Chou, M.-Y., Majewski, S. R., Cunha, K., Smith, V. V., Patterson, R. J., & Martinez-Delgado, D. 2011, ApJ, 731, L30

Cui, X.-Q., Zhao, Y.-H., Chu, Y.-Q., et al. 2012, Research in Astronomy and Astrophysics, 12, 1197

Deason, A. J., Belokurov, V., Hamren, K. M., et al. 2014, MNRAS, 444, 3975

Dehnen, W., Odenkirchen, M., Grebel, E. K., & Rix, H.-W. 2004, AJ, 127, 2753

Deng, L.-C., Newberg, H. J., Liu, C., et al. 2012, Research in Astronomy and Astrophysics, 12, 735

Drake, A. J., Graham, M. J., Djorgovski, S. G., et al. 2014, ApJS, 213, 9

Duffau, S., Zinn, R., Vivas, A. K., et al. 2006, ApJ Lett, 636, L97

Duffau, S., Vivas, A. K., Zinn, R., Méndez, R. A., & Ruiz, M. T. 2014, A&A, 566, 118

Eyre, A. 2010, MNRAS, 403, 1999

Eyre, A., & Binney, J. 2009, MNRAS, 399, L160

Fellhauer, M., Belokurov, V., Evans, N. W., et al. 2006, ApJ, 651, 167

Fellhauer, M., Evans, N. W., Belokurov, V., et al. 2007b, MNRAS, 375, 1171

Fellhauer, M., Evans, N. W., Belokurov, V., Wilkinson, M. I., & Gilmore, G. 2007a, MNRAS, 380, 749

Grillmair, C. J., 2006a, ApJ, 645, L37

Grillmair, C. J., 2006b, ApJ, 651, L29

Grillmair, C. J. 2009, ApJ, 693, 1118

Grillmair, C. J. 2011, ApJ, 738, 98

Grillmair, C. J. 2014, ApJ, **790**, 10

Grillmair, C. J., Freeman, K. C., Irwin, M., & Quinn, P. J. 1995, AJ, 109, 2553

Grillmair, C. J., & Johnson, R. 2006, ApJ, 639, L17

Grillmair, C. J., & Dionatos, O. 2006a, ApJ, 641, L37

Grillmair, C. J., & Dionatos, O. 2006b, ApJ, 643, L17

Grillmair, C. J., Carlin, J. L., & Majewski, S. R. 2008, ApJ, 689, L117

Grillmair, C. J., & Sarajedini, A. LSST Science Book, LSST Corporation, Tucson (2009)

Grillmair, C. J., Cutri, R., Masci, F. J., et al. 2013, ApJ, 769, 23

Helmi, A., Cooper, A. P., White, S. D. M., et al. 2011, ApJ Lett, 733, L7

Ibata, R. A., Gilmore, G., & Irwin, M. J. 1994, Nature, 370, 194

Ibata, R., Lewis, G. F., Irwin, M., Totten, E., & Quinn, T. 2001a, ApJ, 551, 294

Ibata, R., Irwin, M., Lewis, G. F., & Stolte, A. 2001b, ApJ Lett, 547, L133

Ibata, R. A., Irwin, M. J., Lewis, G. F., Ferguson, A. M. N., & Tanvir, N. 2003, MNRAS, 340, L21

Irwin, M., & Hatzidimitriou, D. 1995, MNRAS, 277, 1354

Jurić, M., Ivezić, Ž., Brooks, A., et al. 2008, ApJ, 673, 864

Kaiser, N., Aussel, H., Burke, B., et al. 2002, SPIE, 4836, 154

Keller, S. C., Schmidt, B. P., Bessell, M. S., et al. 2007, PASA, 24, 1 Keller, S. C., Murphy, S., Prior, S., Da Costa, G., & Schmidt, B. 2008, ApJ, 678, 851

Keller, S. C., da Costa, G. S., & Prior, S. L. 2009, MNRAS, 394, 1045

Keller, S. C., Yong, D., & Da Costa, G. S. 2010, ApJ, 720, 940

Kollmeier, J. A., Gould, A., Shectman, S., et al. 2009, ApJ Lett, 705, L158

Koposov, S., Rix, H-W, & Hogg, D. W. 2010, ApJ, 712, 260

Koposov, S., Irwin, M., Belokurov, V., Ganzalez-Solares, E., Kupcu, Y.A., Lewis, J., Metcalfe, N., & Shanks, T. 2012, ApJ, 750, 80

Koposov, S. E., Irwin, M., Belokurov, V., et al. 2014, MNRAS, 442, L85

Küpper, A. H. W., MacLeod, A., & Heggie, D. C. 2008, MNRAS, 387, 1248

Küpper, A. H. W., Lane, R. R., & Heggie, D. C. 2012, MNRAS, 420, 2700

Kuzma, P. B., Da Costa, G. S., Keller, S. C., & Maunder, E. 2015, MNRAS, 446, 3297

Larsen, J. A., Humphreys, R. M., & Cabanela, J. E. 2008, ApJ Lett, 687, L17

Larsen, J. A., Cabanela, J. E., & Humphreys, R. M. 2011, AJ, 141, 130

Law, D. R., Majewski, S. R., & Johnston, K. V. 2009, ApJ Lett, 703, L67

Law, D. R., & Majewski, S. R. 2010, ApJ, 714, 229

Leon, S., Meylan, G., & Combes, F. 2000, A&A, 359, 907

Li, J., Newberg, H. J, Carlin, J. L, et al. 2012, ApJ, 757, 151

Luo, A.-L., Zhang, H.-T., Zhao, Y.-H., et al. 2012, Research in Astronomy and Astrophysics, 12, 1243

Lux, H., Read, J. I., Lake, G., & Johnston, K. V. 2012, MNRAS, 424, 16

Majewski, S. R., Skrutskie, M. F., Weinberg, M. D., & Ostheimer, J. C. 2003, ApJ, 599, 1082

Majewski, S. R., Ostheimer, J. C., Rocha-Pinto, H. J., et al. 2004, ApJ, 615, 738

Martin, C., Carlin, J. L., Newberg, H. J., & Grillmair, C. J., 2013, ApJ, 765, 39

Martin, N. F., Ibata, R. A., Bellazzini, M., Irwin, M. J., Lewis, G. F., & Dehnen, W. 2004a, MNRAS, 348, 12

Martin, N. F., Ibata, R. A., Conn, B. C., Lewis, G. F., Bellazzini, M., Irwin, M. J., & McConnachie, A. W. 2004b, MNRAS, 355, L33 Martin, N. F., Ibata, R. A., & Irwin, M. 2007, ApJ, 668, L123

Martin, N. F., Ibata, R. A., Rich, R. M., et al. 2014, ApJ, 787, 19

Martínez-Delgado, D., Gómez-Flechoso, M. Á., Aparicio, A., & Carrera, R. 2004, ApJ, 601, 242

Mastrobuono-Battisti, A., Di Matteo, P., Montuori, M., & Haywood, M. 2012, A&A, 546, L7

Mateo, M., Olszewski, E. W., & Morrison, H. L. 1998, ApJ Lett, 508, L55

Moitinho, A., Vázquez, R. A., Carraro, G., et al. 2006, MNRAS, 368, L77

Momany, Y., Zaggia, S., Gilmore, G., et al. 2006, A&A, 451, 515

Newberg, H. J., Yanny, B., Rockosi, C., et al. 2002, ApJ, 569, 245

Newberg, H. J., Yanny, B., Cole, N., et al. 2007, ApJ, 668, 221

Newberg, H. J., Yanny, B., & Willett, B. A. 2009, ApJ, 700, L61

Newberg, H. J., Willett, B. A., Yanny, B., & Xu, Y. 2010, ApJ, 711, 32

Odenkirchen, M., Grebel, E. K., Rockosi, C. M., et al. 2001, ApJ, 548, L165

Odenkirchen, M., Grebel, E. K., Dehnen, W., et al. 2003, AJ, 126, 2385

Odenkirchen, M., Grebel, E. K., Kayser, A., Rix, H.-W., & Dehnen, W. 2009, AJ, 137, 3378

Peñarrubia, J., Martínez-Delgado, D., Rix, H. W., et al. 2005, ApJ, 626, 128

Prior, S. L., Da Costa, G. S., Keller, S. C., & Murphy, S. J. 2009, ApJ, 691, 306

Rocha-Pinto, H. J., Majewski, S. R., Skrutskie, M. F., & Crane, J. D. 2003, ApJ, 594, L115

Rocha-Pinto, H. J., Majewski, S. R., Skrutskie, M. F., Crane, J. D., & Patterson, R. J. 2004, ApJ, 615, 732

Rocha-Pinto, H. J., Majewski, S. R., Skrutskie, M. F., Patterson, R. J., Nakanish, H., Munoz, R. R., & Sofue, Y. 2006, ApJ, 640, L150

Rockosi, C. M., Odenkirchen, M., Grebel, E. K., et al. 2002, AJ, 124, 349

Rossetto, B. M., Santiago, B. X., Girardi, L., et al. 2011, AJ, 141, 185

Sales, L. V., Helmi, A., Starkenburg, E., et al. 2008, MNRAS, 389, 1391

Schlaufman, K. C., Rockosi, C. M., Allende Prieto, C., et al. 2009, ApJ, 703, 2177

Sesar, B., Ivezić, Ž., Lupton, R. H., et al. 2007, AJ, 134, 2236

Sesar, B., Ivezić, Ž., Grammer, S. H., et al. 2010a, ApJ, 708, 717

Sesar, B., Vivas, A. K., Duffau, S., & Ivezić, Ž. 2010b, ApJ, 717, 133

Sesar, B., Grillmair, C. J., Cohen, J. G., et al. 2013, ApJ 776, 26

Sesar, B., Bovy, J., Bernard, E. J., et al. 2015, ApJ, submitted; arXiv:1501.00581

Shanks, D. J., Belokurov, V., Chehade, B., et al. 2013, The Messenger, 154, 38

Sharma, S., Johnston, K. V., Majewski, S. R., et al. 2010, ApJ, 722, 750

Sheffield, A. A., Johnston, K. V., Majewski, S. R., et al. 2014, ApJ, **793**, 62

Simion, I. T., Belokurov, V., Irwin, M., & Koposov, S. E. 2014, MNRAS, 440, 161

Slater, C. T., Bell, E. F., Schlafly, E. F., et al. 2014, ApJ, 791, 9

Starkenburg, E., Helmi, A., Morrison, H. L., et al. 2009, ApJ, 698, 567

Totten, E. J., & Irwin, M. J. 1998, MNRAS, 294, 1

Vivas, A. K., Zinn, R., Andrews, P., et al. 2001, ApJ Lett, 554, L33

Vivas, A. K., & Zinn, R. 2003, Memorie della Societa Astronomica Italiana, 74, 928

Vivas, A. K., Zinn, R., Gallart, C. 2005, AJ, 129, 189

Vivas, A. K., & Zinn, R. 2006, AJ, 132, 714

Vivas, A. K., Jaffé, Y. L., Zinn, R., et al. 2008, AJ, 136, 1645

Vivas, A. K., Sesar, B., Duffau, S., & Ivezic, Z. 2011, Revista Mexicana de Astronomia y Astrofisica Conference Series, 40, 261

Watkins, L. L, Evans, N. W., Belokurov, V., et al. 2009, MNRAS, 398, 1757

Willett, B. A., Newberg, H. J., Zhang, H., Yanny, B., & Beers, T. C. 2009, ApJ, 697, 207

Xu, Y., Newberg, H. J., Carlin, J. L., et al. 2015, ApJ, 801, 105

Yam, W., Carlin, J. L., Newberg, H. J., Dumas, J., O'Malley, E., Newby, M., & Martin, C. 2013, ApJ, 776, 133

Yanny, B., Newberg, H. J., Grebel, E. K., et al. 2003, ApJ, 588, 824

Yanny, B., Newberg, H. J., Johnson, J. A., et al. 2009, ApJ, 700, 1282

Zhao, G., Zhao, Y.-H., Chu, Y.-Q., Jing, Y.-P., & Deng, L.-C. 2012, Research in Astronomy and Astrophysics, 12, 723

Zinn, R., Horowitz, B., Vivas, A. K., et al. 2014, ApJ, 781, 22

Chapter 5 Kinematically Detected Halo Streams

Martin C. Smith

Abstract Clues to the origins and evolution of our Galaxy can be found in the kinematics of stars around us. Remnants of accreted satellite galaxies produce overdensities in velocity-space, which can remain coherent for much longer than spatial over-densities. This chapter reviews a number of studies that have hunted for these accretion relics, both in the nearby solar-neighborhood and the more-distant stellar halo. Many observational surveys have driven this field forwards, from early work with the Hipparcos mission, to contemporary surveys like RAVE and SDSS. This active field continues to flourish, providing many new discoveries, and will be revolutionized as the Gaia mission delivers precise proper motions for a billion stars in our Galaxy.

5.1 Introduction to Kinematic Streams

At first glance the kinematics of disk stars in the solar neighborhood might appear to be a smooth distribution, but upon closer inspection one can uncover a wealth of structure. The fact that this velocity distribution is clumpy has been known for over a century. The German astronomer J.H. von Mädler, while carrying out observations to measure the Sun's motion, noticed clumping in the distribution of proper motions (Mädler 1846). This collection of stars moving with the same velocity, what we now refer to as a "moving group", consists of members of the Pleiades open cluster, including stars several degrees from the centre of the cluster. This work was built on by Proctor (1869), who found a further two moving groups—Hyades and Sirius.

The dissection of the local stellar velocity distribution has told us a great deal about star formation and Galactic structure. Figure 5.1 presents a contemporary analysis of the velocity distribution, showing that it is rich in substructure. These moving groups can be attributed to young open clusters which have not yet dispersed, or could be due to dynamical effects such as stars trapped at resonance with the Galactic bar or spiral arms (e.g., Dehnen and Binney 1998; Bovy and Hogg

M.C. Smith (\boxtimes)

Key Laboratory for Research in Galaxies and Cosmology, Shanghai Astronomical Observatory, Chinese Academy of Sciences, 80 Nandan Road, Shanghai 200030, China e-mail: msmith@shao.ac.cn

114 M.C. Smith

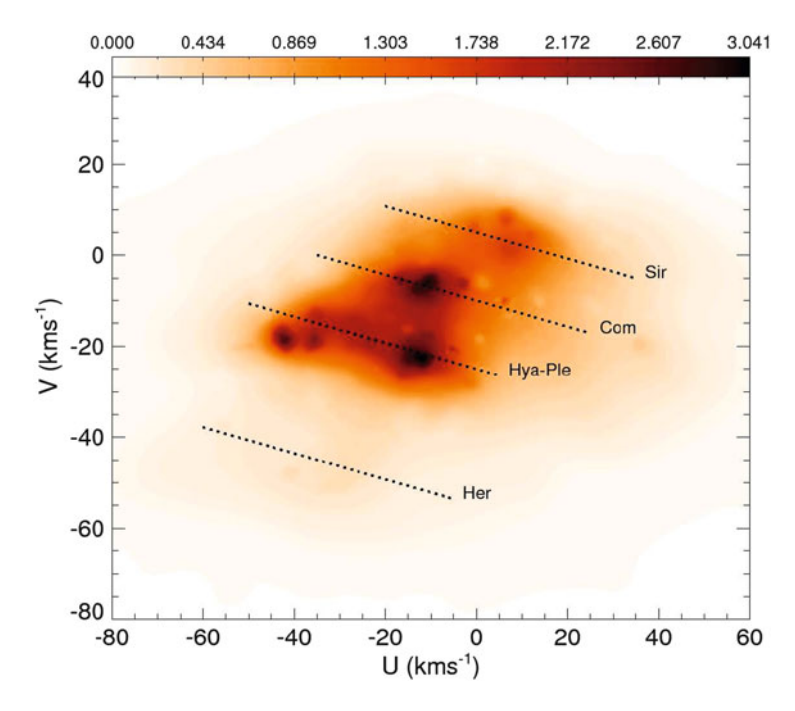


Fig. 5.1 The local stellar velocity distribution from a compendium of observational datasets. The two velocity components correspond to the cartesian in-plane velocities, with U increasing in the direction of the Galactic center and V in the direction of the Sun's rotation. The approximate locations of four moving groups are denoted by the *dotted lines*. Figure taken from Antoja et al. (2010)

2010; Sellwood 2010; McMillan 2011). However, neither of these will be explored in this chapter; interested readers are suggested to see Antoja et al. (2010) for a detailed and comprehensive review on the subject of moving groups. Instead we will here focus primarily on a third mechanism for creating moving groups, namely the accretion of extra-galactic systems.

As can be seen from the other chapters in this volume, we know of many tidal streams in the stellar halo of the Milky Way. However, more diffuse streams, which are created if the progenitor is less massive, is on a highly eccentric orbit, or was tidally disrupted in the distant past, are harder to identify as spatial over-densities on the sky. They can, however, be discovered by exploring higher-dimensional space; a stream can that has dispersed in configuration space may still remain coherent in phase space. In this chapter the many successful efforts to find fainter and more ancient accretion events will be reviewed, starting with the solar neighborhood (Sect. 5.2) and moving out to structures in the more distant halo (Sect. 5.3).

5.2 Local Kinematic Streams

5.2.1 The Helmi Stream

In the 150 years since Mädler made his initial discovery, many other studies have identified kinematic substructures. Some of these, such as the Arcturus or Kapteyn group, have been proposed to be extra-galactic in origin (we will return to these later). However, the first indisputable accretion remnant was found by Helmi et al. in their seminal 1999 paper (Helmi et al. 1999), which we will now discuss.

The first step to identifying clumping in velocity space is, by definition, obtaining a sample of accurate velocities. Large surveys have been crucial in propelling many fields in astronomy, from Kapteyn's visionary international survey of the early twentieth century (Kapteyn 1906; Kinman 2000; van der Kruit 2015), to the Sloan Digital Sky Survey in the early twenty-first century (York et al. 2000); for a review of many significant results from such surveys in the field of Milky Way science, see Ivezić et al. (2012). One of the most important surveys in the past 20 years in the field of stellar kinematics was the Hipparcos mission. This was a European-led satellite mission, launched in 1989 and operated until 1993, which measured the position of stars to unprecedented accuracy. This enabled a catalogue of proper motions and parallaxes to be constructed for over 100,000 stars (ESA 1997), although the complex nature of this task meant that the final definitive catalogue was only published in 2007 (van Leeuwen 2007a,b).

Possessing such accurate proper motion data for large numbers of stars enables statistically meaningful analyses to be done of rare types of stars. For arguably the first time researchers were able to construct significant samples of stars from the halo, which remember constitutes only around 0.5% of the stellar mass in the solar neighborhood (Jurić et al. 2008). With this sample, one could now begin to search for kinematic over-densities.

The groundwork for Helmi's discovery was laid in the 1999 paper entitled "Building up the stellar halo of the Galaxy" (Helmi and White 1999). This paper used a combination of numerical simulations and analytical techniques to investigate the disruption of satellite galaxies as they are accreted into the Milky Way, paying particular attention to the consequences for the local stellar halo. By analyzing the disruption of the satellite using action-angle variables, they studied how the tidal stream evolved over 10 Gyr, and showed that the system became phase mixed; at a particular location (for example in the solar neighborhood) one might detect multiple kinematic over-densities from the same progenitor. This is because one (large) progenitor can produce a tidal stream that wraps multiple times around the Milky Way, and can produce numerous separate clumps in phase space. A simple calculation shows that if the local stellar halo is entirely made up of debris from 10 to 100 accreted satellites (of luminosity 10^7 or $10^8 L_{\odot}$) then one would expect to find a few hundred separate kinematic streams in the solar neighborhood, although the individual stars in these streams would not necessarily be clumped in density.

116 M.C. Smith

Given the high quality data that were becoming available at that time, namely the aforementioned Hipparcos catalogue, Helmi et al. (1999) were able to construct a catalogue of 97 metal-poor red giants and RR Lyrae stars within 1 kpc of the Sun (using data compiled by Beers and Sommer-Larsen 1995 and Chiba and Yoshii 1998). With distances estimated from photometry (to \sim 20 %), radial velocities from spectroscopy (to \sim 10 km/s) and proper motions mainly from Hipparcos (to a few mas/yr), they were then able to analyze the phase-space distribution of this halo sample.

One then needs to determine the optimal space (combinations of x, y, z, v_x, v_y , and v_z) in which to identify accretion debris. To do this one normally identifies integrals of motion, i.e., quantities that are conserved (or approximately conserved) along an orbit (see Sect. 3.1.1 et seq of Binney and Tremaine 2008); stream stars are thus clumped in these quantities. For example, in a spherical potential we know that the total energy and the three components of angular momentum are all conserved along an orbit, leading to four integrals of motion. However, the Milky Way is not a spherical system, particular in the inner regions where the contribution of the disk to the total potential is important. Fortunately it is close to being axisymmetric (since we do not need to worry about the Galactic bar, which is restricted to the innermost few kpc). For an axisymmetric system, there are two integrals of motion: the energy, and the component of the angular momentum parallel to the symmetry axis (L_z) . It can also be shown that the total angular momentum, although not precisely conserved, varies only slightly for modest amounts of flattening and, importantly, shows no long-term evolution.

There are small complications to this picture. First, the stars of a satellite galaxy do not all follow the same precise orbit, due to the internal velocity dispersion of the system. This means that stars will have a finite volume in this space defined by the integrals of motion. Second, the potential of the Milky Way will undoubtedly be varying over the time-scales under discussion, for example from the build-up of the disk as gas settles into the equatorial plane of the Galaxy. This leads to an oft-used term in this field—adiabatic invariants (see Sect. 3.6 of Binney and Tremaine 2008). These are quantities that are constant for slowly-evolving potentials, i.e., potentials that vary on time-scales longer than typical orbital periods.

For their analysis, Helmi et al. (1999) chose to use the two-dimensional space of L_z and $L_\perp = \sqrt{L_x^2 + L_y^2}$. They did this as the former is conserved for an axi-symmetric potential and, since $L^2 = L_\perp^2 + L_z^2$ and both L and L_z are approximately constant for stars in a particular tidal stream, the latter is not expected to vary significantly. These two quantities were selected because they are trivial to determine for their sample, unlike the energy which, although conserved, requires one to assume a model for the gravitational potential. The distribution of L_z and L_\perp for the solar neighborhood sample of Helmi et al. (1999) is shown in Fig. 5.2. For a local sample of stars $L_z \approx R_\odot * v_\phi$, where v_ϕ is the azimuthal component of the velocity. Since the stellar halo shows no significant signs of rotation (e.g., Smith et al. 2009b), one would expect that the distribution should be symmetric about $L_z = 0$; clearly this is not the case at high L_\perp , where there is a significant

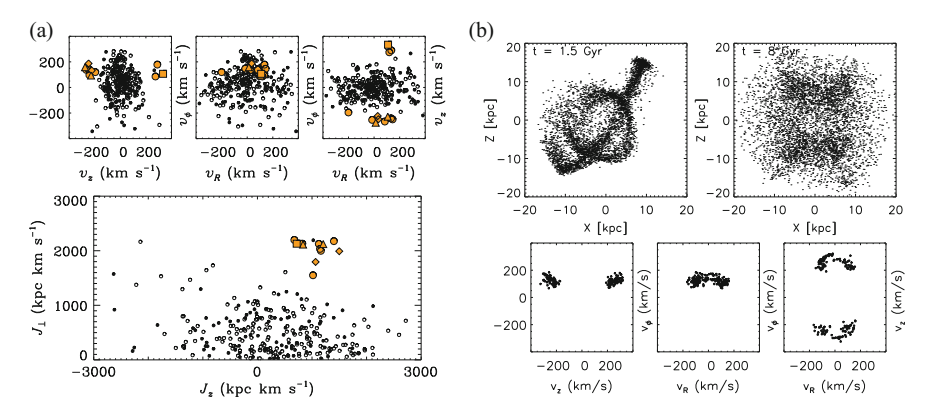


Fig. 5.2 The discovery of kinematic substructure in the solar neighborhood, from Helmi et al. (1999). The *left panel* shows the observational discovery, which was based on analysis of stars from the Hipparcos mission. The *lower panel* shows the distribution in angular momentum space (in their notation J = L), while the *upper panels* show the kinematics. *Yellow filled dots* are the candidate members of the substructure. The *right panels* show an *N*-body model of the stream, which is almost entirely phase mixed after 8 Gyr. This panel was taken from Helmi (2008)

cluster of stars in the region (L_z , L_\perp) = (1000, 2000) kpc km/s. The probability of such a clump of seven stars occurring by chance is estimated to be less than 1%. Although their original halo sample contained only 97 stars, they augmented it with more distant and more metal-rich stars, obtaining a total of 12 stars that belong to this overdensity.

Helmi et al. (1999) also investigated the velocity distribution of stars from this system (top panels of Fig. 5.2; see also Fig. 1.1 of Chap. 1 which shows a subset of the sample in a slightly different coordinate system). Note that in Helmi's coordinate system, positive L_z implies v_{ϕ} is in the same direction as Galactic rotation, so these stars have azimuthal velocities similar to the Sun, but with very high vertical velocities (as can be seen from the top-left panels of Fig. 5.2, v_z is around 200 km/s). It is also interesting to see that v_z is split into two separate clumps—one moving downward and one upward. This is most likely a manifestation of the aforementioned phase-mixing, where one progenitor can produce multiple streams in phase-space. So although there are two streams, these stars are all from the same accretion event. Helmi and collaborators constructed an N-body simulation of this system, which provides a very good representation of the observed velocity distribution (Fig. 5.2, right-hand panels). This shows how the progenitor can be almost completely disrupted in configuration space, yet remain coherent in velocity space. The two separate clumps in v_z are reproduced, as is the spread in v_R . The simulation also allows them to estimate the properties of the progenitor, which they concluded was likely to be similar in size to the Fornax dwarf spheroidal.

Subsequent studies have confirmed the Helmi stream and increased the number of member stars, though somewhat reducing the fraction of the halo it comprises (for example Chiba and Beers 2000; Re Fiorentin et al. 2005; Dettbarn et al. 2007;

Kepley et al. 2007). Later surveys containing fainter stars have enabled us to identify halo subdwarfs in this system (Klement et al. 2009; Smith et al. 2009b), bringing the total number of members to over 30 out to distances of a few kpc. The reported fraction of local stellar halo made of Helmi stream debris varies from reference to reference, probably due to differences in search techniques, but is most likely around 5%. The chemistry of 12 of these stars has been investigated by Roederer et al. (2010). They find a spread in [Fe/H] from -3.4 to -1.5, with detailed abundances similar to those of the general halo population, concluding that star formation in the progenitor was truncated before the products of Type Ia supernovae or AGB stars enriched the inter-stellar medium.

The Kepley et al. (2007) study also introduces a novel way to estimate the age of accretion. They utilize the fact that once the progenitor has become completely phase-mixed, the total number of stars in the positive and negative v_z clumps would be the same. The observed fraction with positive v_z is actually 28 %, which means it is not entirely mixed. By analyzing an N-body simulation of the accretion (similar to the right-panel of Fig. 5.2), they can tentatively say that it was likely to have been accreted between 6 and 9 Gyr ago, i.e., not too recently (otherwise the ratio would be more lopsided) and not too long ago (otherwise the ratio would be closer to unity).

5.2.2 Other Early Discoveries

As pointed out in the introduction, moving groups have been studied for many years, but definitively determining their origins is not easy. As a consequence, finding halo streams in the solar neighborhood can be a precarious venture. Over-densities, as their name suggests, can only be identified as an excess on top of a background population. However, in this case the background population in question (the Milky Way disk) is far from a simple homogenous population; lumps and gradients can often masquerade as coherent structures and so great care has to be taken in their classification. This problem has afflicted many potential stream discoveries and, as can be seen in this chapter, ambiguities still remain for a number of these.

Various streams, such as Hyades-Pleiades, Hercules and Arcturus, are believed to be Milky Way stars brought together by resonances in the disk. Originally identified by Eggen (see his 1996 review), the broad metallicity or age spread of these three streams argues against disruption of a disk star cluster as the origin, and abundance patterns similar to disk stars disfavors the extragalactic scenario—hence the conclusion of a dynamical origin (e.g., Famaey et al. 2008; Bovy and Hogg 2010; Fuchs and Dettbarn 2011). Some of these are more controversial than others; the Arcturus stream has generated much debate (e.g., Navarro et al. 2004), but more-recent analyses have shown that the narrow velocity dispersion (Bovy et al. 2009) and chemical inhomogeneity (Williams et al. 2009; Bensby et al. 2014) favor a dynamical origin. Making definitive claims about the origins of such systems is not easy.

Another stream that has been studied extensively is the Kapteyn moving group, again named by Eggen. The name comes from the fact that the velocities of this group are similar to that of Kapteyn's star, which is a well-known very high proper motion star only 4 pc away from the Sun. This group is on a mildly retrograde orbit, moving at around $-50\,\mathrm{km/s}$.

Quite early it was speculated that this retrograde group might be related to the globular cluster Omega Centauri (Omega Cen; e.g., Eggen 1978), which is on a similar orbit. This cluster is interesting, as it appears to possess a broad spread in both chemistry and age, indicating that it could be the core of a disrupted dwarf galaxy (Lee et al. 1999). This might suggest that this retrograde moving group is in fact the stripped remnants of the galaxy. A number of works have pursued this hypothesis (see Majewski et al. 2012 for a nice overview of the current situation), including a detailed spectroscopic analysis of 16 stars by Wylie-de Boer et al. (2010). This latter reference confirms the similarity in chemistry between the cluster and the moving group, but provocatively questions whether the group may in fact be material stripped from the host galaxy of Omega Cen as it was disrupted. The argument against the association of this debris with Omega Cen is that one would need a significant amount of dynamical friction to bring the system onto its current orbit, something which would not be possible for an object as small as Omega Cen. However, the authors acknowledge that their hypothesis is currently unproven; if they are correct that Omega Cen and the Kapteyn moving group do not originate in the same dwarf galaxy progenitor, then why the close similarity in chemistry and why the age spread in the cluster? Clearly more work needs to be done to address this question and fully understand the connection, especially given that a large fraction of the inner halo could belong to this moving group (see, for example, Majewski et al. 2012; Fig. 5.3) and hence it could have played a significant role in the early development of our galaxy.

5.2.3 Streams in the Geneva-Copenhagen Survey

5.2.3.1 Pieces of the Puzzle

Although Hipparcos was (and still is) clearly a hugely important resource for studying the kinematics of stars in the solar neighborhood, it was hampered by a lack of radial velocities. What was needed was a systematic survey of radial velocities, providing a sample with a well-defined selection function. The Geneva-Copenhagen survey (Nordström et al. 2004; Holmberg et al. 2007, 2009; Casagrande et al. 2011) produced radial velocities and metallicities for 13,000 nearby stars. Combining these with proper motions and (for the majority of stars) distances from the Hipparcos mission, resulted in a complete sample of F- and G-type dwarfs within 40 pc and a larger, magnitude-limited sample to around 200 pc. Although this is a relatively local sample compared to the one analysed in Helmi's (1999) study,

120 M.C. Smith

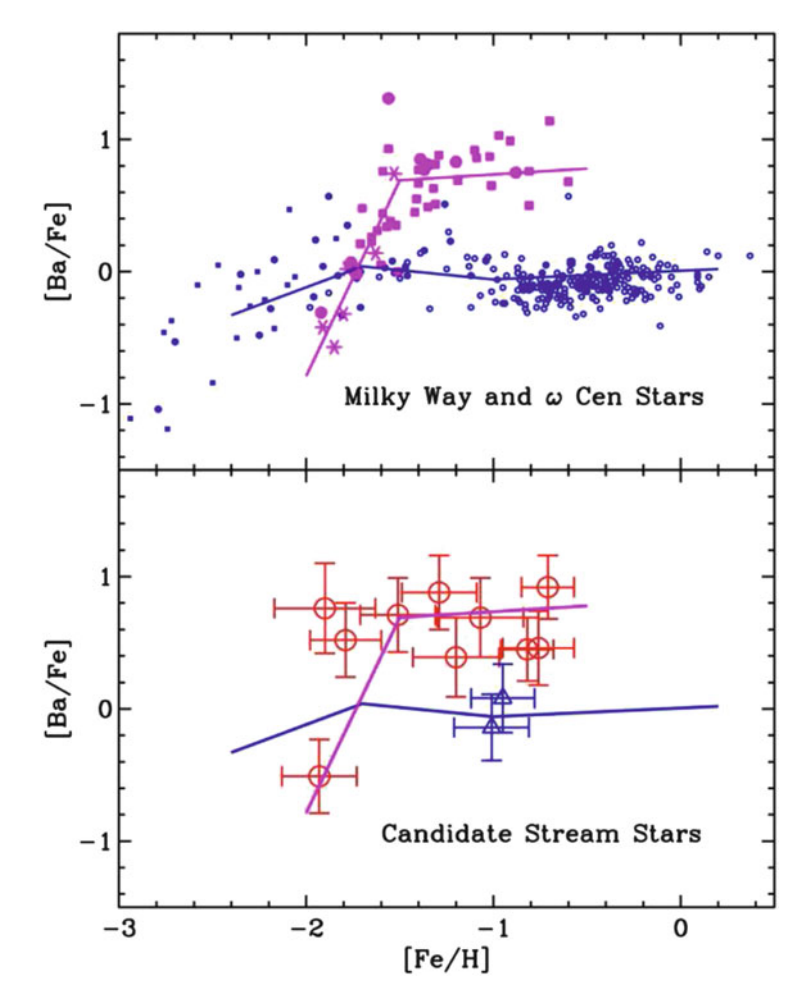


Fig. 5.3 *Top panel*: the distribution of [Ba/Fe] vs [Fe/H] for Milky Way stars (*blue points*) and a characteristic locus (*blue line*), overlaid with the same for Omega Cen (labeled ω Cen) stars (*magenta points* and *line*), where data for both are taken from the literature. *Bottom panel*: the distribution of barium abundances for ten stars in the retrograde kinematic stream discussed in Majewski et al. (2012; *red*), plus two retrograde stars not in the stream (*blue*). This retrograde stream is similar to the Kapteyn stream and is potentially associated to Omega Cen, a hypothesis which is supported by the close similarity in chemistry between the cluster stars in the *top panel* and the stream stars in the *bottom*. Taken from Majewski et al. (2012)

and contains only a handful of halo stars, the accurate 6D phase-space information allows a detailed analysis of the orbital properties of the stars.

In addition to the Helmi stream, which is the most prominent in the local stellar halo, a number of other candidate streams have been found. Helmi continued her analysis using this Geneva-Copenhagen survey (Helmi et al. 2006), choosing a different space to search for accretion debris than in their 1999 study. This time

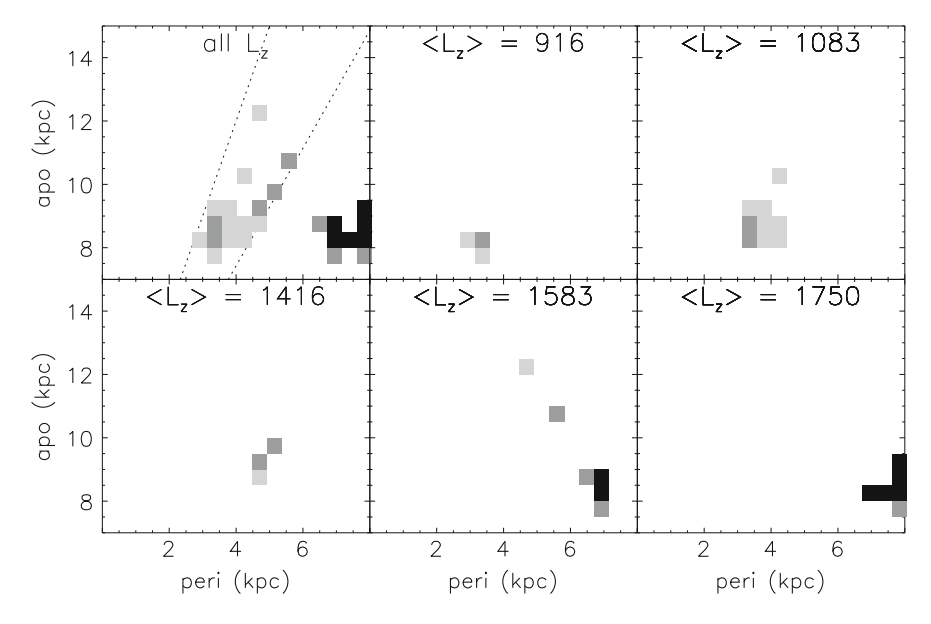


Fig. 5.4 Distribution of overdense cells in the apo-center/peri-centre/angular-momentum (APL) space. Each panel shows the distribution of stars in the space of apo- and peri-center (for different cuts in the L_z angular momentum). Darker colors correspond to higher statistical significance of an excess compared to the smooth background. Notice the group of stars confined within the dotted lines (corresponding to eccentricities between 0.3 and 0.5). As L_z increases, the orbits move outwards in radii. Taken from Helmi et al. (2006)

they chose three parameters, L_z (which, as mentioned above, will be conserved in an axisymmetric system) and the peri- and apo-center distances (the minimum and maximum distance that the star's orbit comes to the Galactic center). We will refer to this as the APL space (Fig. 5.4). Using simulations, they showed that disrupted satellites remain reasonably localized in this space, with the extent depending on the initial size of the satellite. When projected into the 2D space of apo- versus peri-center distance, debris remain contained within a band of constant eccentricity, implying that the stars approximately retain the eccentricity of their progenitor's orbit. Moreover, in this space one can see the different kinematic streams forming as the satellite becomes phase mixed, although the accuracy required to determine this is not feasible with current datasets.

One clear drawback of this method is that it relies on a knowledge of the gravitational potential in order to calculate apo- and peri-center distances. However, as the sample under investigation is located in such a small volume, the potential is approximately constant and hence the orbital parameters are determined by the kinematics, rather than their location. This means that although the apo- and pericenter distances may be slightly off due to an incorrectly chosen potential, this will result in a systematic shift in this space and will not work to smear out any coherent features.

By comparing the density of stars in this 3D space to Monte Carlo realizations of a smooth model, Helmi et al. (2006) were able to show that their distribution is significantly more structured than what one would expect from a smooth model. They went on to identify a group of stars with eccentricities around 0.4. This value is clearly inconsistent with the thin disk, although thick disk stars may possess such high eccentricities. Folding in metallicities appears to show that this group can be divided into three separate accretion events, with different trends in v_z and age.

The process of determining exactly how many distinct groups are contained in such a discovery is complex and open to interpretation. High-resolution follow-up studies have analyzed the elemental abundance patterns of these stars and suggested that there may actually be only two distinct groups (Stonkutė et al. 2012, 2013; Ženovienė et al. 2014); the common abundance patterns suggest that Groups 2 and 3 from the original (Helmi et al. 2006) paper may come from the same progenitor. Tentative ages for these stars show two populations, a relatively metal-rich one of around 8 Gyr and a more metal-poor one of around 12 Gyr, but the authors acknowledge that more work needs to be done as ages are notoriously difficult for main-sequence stars. They conclude by speculating that the similarity between the chemical composition of stars in these two kinematic groups and in the Milky Way's thick disk suggests that the progenitor of this system may be related to the formation of the thick disk.

The original authors revisited these streams in Helmi et al. (2014), obtaining high-resolution spectra for even more stars in this eccentricity range (0.3–0.5). Although they no longer focus on the division proposed in their original paper, they show that the properties of stars in this eccentricity range are not homogenous, with an apparent division around [Fe/H] = -0.4.

5.2.3.2 Arifyanto and Fuchs

In the same year as Helmi et al. were mining the Geneva-Copenhagen survey, a group in Germany (Arifyanto and Fuchs 2006) were searching for accretion debris in a sample of 742 stars based on a catalogue from Carney et al. (1994). This resulted in the detection of a number of streams, but none are believed to be due to accretion; three had been previously identified (Hyades-Pleiades, Hercules and Arcturus; discussed above) and there was a new discovery, again not conclusively extragalactic in origin (Ramya et al. 2012).

However, despite not identifying any bone-fide accretion remnants, this paper warrants discussion here for its approach to identify nearby streams. Using a Keplerian approximation for orbits developed by Dekker (1976), Arifyanto and Fuchs (2006) determine proxies for the total angular momentum and eccentricity, along with a third parameter corresponding to the inclination of the orbit (see Klement 2010 for a review of this method). They argue that this three dimensional space is ideal for dissecting velocity space, as evidenced by their success at finding the above disk streams. This method is simple to apply and unlike the previous APL approach does not require orbits to be calculated, but it is not perfect as it

relies on the aforementioned Keplerian approximation that only holds for spherical potentials. Despite these drawbacks it has proved a popular approach that has been used by numerous authors, mainly by employing the proxy for the eccentricity ($\sqrt{U^2+2V^2}$). Although the approximations behind this proxy break down for high eccentricities, overdensities should remain coherent, and so the simplicity of this approach has resulted in its widespread use.

Another early paper to adopt this technique was Dettbarn et al. (2007), who analysed the sample of Beers et al. (2000) and found a number of candidate halo streams, including existing groups (such as the Helmi stream) and some new ones (named S_1 , S_2 , and S_3).

5.2.4 The Modern Era

5.2.4.1 The RAVE Survey

It should be evident by now that progress in understanding the formation and evolution of our galaxy rests on large surveys. We will now discuss two influential surveys in this field from the past decade: the RAdial Velocity Experiment (RAVE) and the Sloan Digital Sky Survey (SDSS). Both of these have led to numerous discoveries, as can be seen from this and many other chapters in this volume.

Taking a kinematic census of large populations of the Milky Way requires both photometric and spectroscopic surveys. Many proper motion catalogues have been assembled, often by combining various existing ground-based astrometric surveys (e.g., the Hipparcos/Tycho catalogue, UCAC4, and PPMXL). Spectroscopic surveys are in some sense rarer as it requires significant telescope time to amass spectra for hundreds of thousands of stars. One of the largest such surveys is the RAVE survey (Steinmetz et al. 2006), which began in 2003 on the 1.2 m UK Schmidt Telescope at the Anglo-Australian Observatory. Despite not being particularly new (it was around 30 years old when the survey started) or having a large aperture, this telescope had a number of important assets: the field of view was very large (6° diameter field); it had relatively high multiplexing capabilities (150 fibers per plate); and, crucially, for most of the survey it had dedicated use of the telescope. The combination of these factors allowed RAVE to efficiently produce large catalogues of radial velocities and abundances, resulting in a final catalogue of around 500,000 stars in the Southern hemisphere with magnitude range 9 < I < 12 (the fourth public data release is presented in Kordopatis et al. 2013). By concentrating on a narrow window around the calcium triplet region (8410–8795 Å) with reasonable resolution (R \sim 7500), the radial velocity accuracy is excellent, at around a couple of km/s (see Fig. 29 of Kordopatis et al. 2013). Furthermore, stellar parameters can be derived at a level of around a few tenths of a dex for log g and metallicity (see Table 2 of Kordopatis et al. 2013). For the higher signal-to-noise spectra it is even possible to estimate abundances for a number of individual elements, such as Mg, Al, Si, Ca, Ti, Fe, and Ni (Boeche et al. 2011; Kordopatis et al. 2013). If we are interested in learning

about the kinematics of stars, the final piece of information is distances, which can be estimated by combining the observed stellar parameters with stellar models. This was first undertaken by Breddels et al. (2010) and subsequently refined by Zwitter et al. (2010) and Binney et al. (2014a).

With all this information in hand, RAVE has proved to be a hugely important survey for understanding the kinematics of the solar neighborhood, for example Binney et al. (2014a). In terms of streams, the first attempt to investigate this was Seabroke et al. (2008). By looking at stars from a couple of surveys, including RAVE, they came to the conclusion that there were no massive streams (with hundreds of stars) present in the dataset. They contrasted this to the situation in the outer halo (see Sect. 5.3 of this chapter, as well as other chapters in this volume), where the system is clearly far from relaxed and contains a number of streams and substructures. The results here are in agreement with previous studies, for example the work of Gould (2003), which used a sample of 4000 halo stars with proper motions to conclude that no more than 5% of the local halo can be made up of a single stream. At first glance this may appear to conflict with some estimates for the density of the Helmi et al. (1999) stream, but one should note that their discovery is made up of two separate kinematic streams due to the extensive phase-mixing (Fig. 5.2).

The first attempt to systematically search for small-scale clumping in velocity space in the RAVE survey was undertaken by Klement et al. (2008), who adopted the Keplerian approximation described in Sect. 5.2.3.2. One issue here is that 6D phase-space information is required and, back in 2008, distances had not yet been estimated for RAVE stars. To overcome this issue they made the naive assumption that the sample would be dominated by main-sequence stars and applied a simple monotonic color-magnitude relation suitable for dwarf stars. Due to the bright magnitudes that RAVE probes, this assumption is rather weak and it was subsequently found that around half of the stars are likely to be giants or subgiants (e.g., Binney et al. 2014b). They later rectified this issue (Klement et al. 2011), basically finding that their results were unchanged. Despite this problem in their original paper, they were still able to recover a number of existing streams, calculating their significance by comparing to expectations from a smooth background model (Fig. 5.5). One new stream (dubbed "KFR08") was also detected at a level of 3-sigma. Despite being relatively metal-rich (-1 < [Fe/H] < 0) and on a prograde orbit (with v_{ϕ} of around 160 km/s), the high vertical velocity (vertical dispersion being around 100 km/s) indicates that this feature is unlikely to be associated with the disk and is therefore believed to be the remnant of an accreted satellite. This was later analyzed by Bobylev et al. (2010) in a sample constructed from Hipparcos stars with accurate trigonometric parallaxes (van Leeuwen 2007a) and metallicities and ages (Holmberg et al. 2007, 2009); by identifying additional giant stars in this stream they were able to identify the main sequence turnoff and, through isochrone fitting, determining this is likely to be a very old stream (likely 13 Gyr in age). We will return to this stream briefly in Sect. 5.2.4.2, as it is was subsequently confirmed using an independent data set.

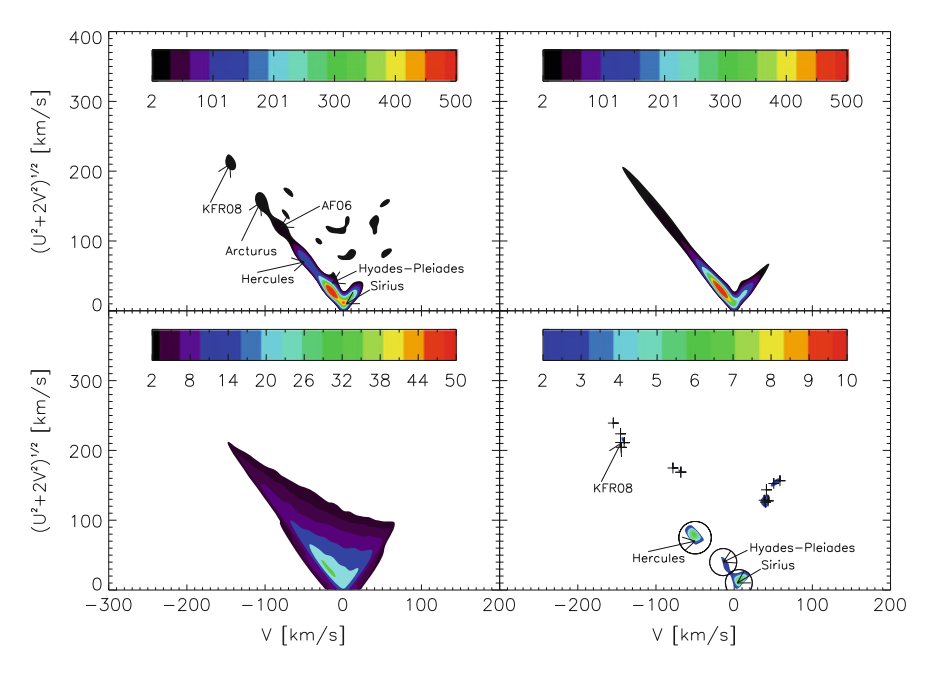


Fig. 5.5 Distribution of kinematic over-densities in RAVE, as presented by Klement et al. (2008). The *upper-left panel* shows the full distribution of the observed dataset, which can be compared to the expected distribution from a smooth model (*upper-right*) and its corresponding dispersion (*lower-left*). By subtracting the model from the data, normalized by the dispersion, one obtains the distribution of overdensities (*lower-right*). This reveals known substructures, such as Hercules, and new ones, such as KFR08. This figure is taken from the later analysis presented in Klement et al. (2011)

As discussed above, determining the origin of moving groups can be tricky due to the complex nature of the background in which they reside (i.e., the Milky Way disk). This difficulty is highlighted by another candidate stream identified by the RAVE survey, entitled the Aquarius Stream (Williams et al. 2011). It was discovered through its radial velocity offset from the surrounding population (Fig. 5.6)—a cluster of 15 stars localized on the sky and with very similar metallicities. This old stream was not connected to any other existing structures and Williams et al. concluded that it was likely recently stripped material from a globular cluster or dwarf galaxy. However, despite being relatively close by (most of the stars are within a few kpc), uncertainties in the distances and proper motions mean that the clumping in angular momentum space is inconclusive.

At this point detailed abundances are required to definitely determine the origin of this stream. Two teams took up this task, one led by Wylie-de Boer et al. (2012) using the AAT telescope and one led by Casey et al. (2014) using the Magellan Clay telescope. Unfortunately, instead of clarifying the issue, these studies raised more questions than they answered. The first analysis (Wylie-de Boer et al. 2012) looked at six member stars, concluding that the exceptionally tight metallicity spread

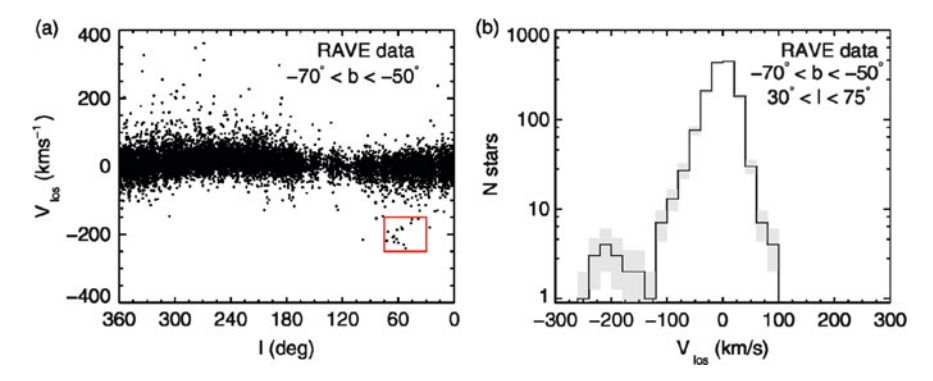


Fig. 5.6 These plots, from Williams et al. (2011), show the disputed Aquarius stream/group. Despite the strong signature in kinematics (which we see localized at $V_{\rm los} \sim -200\,{\rm km/s}$), it is still argued whether this is the remnant of a disrupted globular cluster (Wylie-de Boer et al. 2012) or just a perturbation in the disk (Casey et al. 2014)

 $(\sigma_{\rm [Fe/H]} = 0.1 \, {\rm dex})$ and abundance ratios unambiguously show that the Aquarius stream is a disrupted globular cluster. The second analysis (Casey et al. 2014), on the other hand, looked at 5 stars and unambiguously found that this system cannot be a disrupted globular cluster, giving their paper the unequivocal title "The Aquarius comoving group is not a disrupted classical globular cluster". After finding a wide metallicity spread ($\sigma_{\rm [Fe/H]} = 0.4 \, {\rm dex}$) that is inconsistent with a globular cluster and abundance ratios that are inconsistent with a dwarf galaxy, they conclude that the stars are indistinguishable from the Milky Way field population. The coherence in their kinematics may be a result of the perturbation of the disk when a satellite fell in, but this is just conjecture and their main conclusion is that the chemistry of these stars clearly shows that they are not the accreted remnants of either a globular cluster or dwarf galaxy. The fact that any two studies disagree is not surprising. What is surprising is that one cannot easily explain away this discrepancy on the grounds of small number statistics, since these two analyses have four stars in common! So the fact that very different conclusions have been reached is hard to reconcile, although the higher signal-to-noise of the spectra in the Casey et al. study certainly works in their favor and they consequently argue that the Wylie-de Boer et al. metallicities may be inaccurate. To conclude, the nature of the Aquarius stream/group is still open for debate.

5.2.4.2 The SDSS Survey

In terms of studies of the Milky Way, another major survey in the past decade has been the Sloan Digital Sky Survey (SDSS). The photometric part of the survey has led to the discovery of a host of new streams and dwarf galaxies, including a new population of ultra-faint dwarf galaxies (see Belokurov 2013 for a recent review). Furthermore it has spurred on many different analyses on the state of the disk both

through its photometry and spectroscopy (for example, see review articles by Ivezić et al. 2012 and Smith et al. 2012).

The sub-project dedicated to stellar spectroscopy, called the Sloan Extension for Galactic Understanding and Exploration (SEGUE; Yanny et al. 2009), was included in SDSS-II and SDSS-III and collected spectra for nearly 350,000 stars. There were also a large number of stars targeted in the other sub-projects (over 300,000) and although they have a very complex selection function, these stars are still useful for studies of the Milky Way. These SDSS spectra were taken at a much lower resolution than RAVE (with $R \approx 2000$) but with a much broader wavelength coverage (3800– 9200 Å). With these data the SDSS team were able to measure stellar parameters to precisions similar to those of RAVE, namely log g and [Fe/H] to around 0.3 dex (Lee et al. 2008). Alpha element abundances have also been obtained (Lee et al. 2011), but of course these are harder to determine and, at the time of writing (i.e., SDSS Data Release 12), are yet to be officially released as part of the SDSS survey. Despite not being officially released, a number of authors have used these alpha-element abundances, for example measuring the abundance "knee" of the Sagittarius stream (de Boer et al. 2014). The spectroscopy has also led to a variety of papers on the Milky Way disk, most provocatively the series of papers led by Jo Bovy arguing that the thick disk is not a separate entity from the thin disk (Bovy et al. 2012). The SDSS survey is still ongoing, with the stellar spectroscopy now undertaken by the ambitious APOGEE project, which will be discussed later in Sect. 5.4.

The search for phase-space substructures in SDSS was undertaken by Klement et al. (2009) and Smith et al. (2009b), using complimentary datasets and techniques. Klement et al. took the seventh data release from SDSS and applied the same methods as used during their search for overdensities in the RAVE survey. Since the SDSS stars are much fainter than the RAVE stars, proper motions are generally less precise. Therefore in order to reduce the corresponding uncertainties in tangential velocities, they decided to focus on stars within 2 kpc of the Sun. They were able to confirm their candidate overdensity from the RAVE survey (the KFR08 group, discussed above), further breaking this into two separate groups, one of which is likely to have a disk origin (R1) and one of which is likely accretion debris (R2). They also confirm one of the previously mentioned streams from Dettbarn et al. (2007), adding more members and arguing that this is actually smeared out in phase-space, resulting in multiple clumps in their analysis. As with most works, the Helmi stream was found with very strong significance. Finally, two additional candidate halo streams were identified (C1 and C3).

At the same time as Klement et al. (2009) were working on their paper, Smith et al. (2009b) were working on an independent study using SDSS data. Their approach was complimentary in that it was able to probe much greater distances thanks to precise proper motions from Bramich et al. (2008). These proper motions were constructed using the 250 square degree Stripe 82 region of SDSS, which was repeatedly monitored primarily for the purpose of detecting supernovae. However, the multiple epochs are also ideal for constructing proper motion catalogues. The fact that the proper motions come from a single survey avoids the problem of crossmatching data from separate telescopes with often very different conditions and

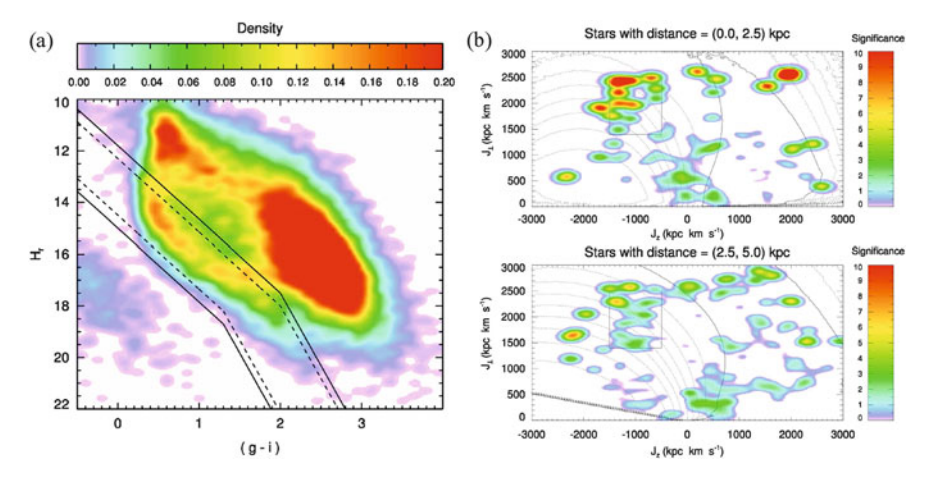


Fig. 5.7 Analysis of kinematic overdensities in SDSS subdwarfs. The *left panel* shows how the subdwarfs can be selected from a reduced proper motion diagram. The subdwarfs, which are located within the *dotted lines*, separate from the disk sequence owing to their fainter intrinsic magnitudes and greater velocities. The *two right panels* show the resulting distribution of subdwarfs in angular momentum space, after subtraction of a smooth halo model. Note the prominent Helmi stream, located around $J_z = -1000$ and $J_\perp = +2000$ kpc km/s. The *dotted lines* in these panels denote the detection efficiency, which has to be considered as these stars are kinematically selected. Figure taken from Smith et al. (2009b)

imaging systems, significantly reducing the systematic errors. Despite the relatively short baseline (7 years), proper motions were measured to a few mas/yr precision, even at faint magnitudes. Koposov et al. (2013) updated the catalogue using improved techniques, reducing the systematic errors even further and obtaining a precision of around 2 mas/yr per star. The stunning precision enabled the authors to detect the proper motion of the Sagittarius stream, even at a distance of 30 kpc.

These accurate proper motions allowed Smith et al. to investigate halo stars out to 5 kpc, with accuracy around 30–50 km/s for each component of the velocity. The halo stars were identified using a reduced proper motion diagram (Fig. 5.7). This technique, which uses the proper motion as a proxy for distance, is often used to separate (nearby) dwarfs from (distant) giants, but is a powerful technique to separate halo stars from disk stars, as halo stars are faster moving and hence have higher proper motions for a given distance. Although this selection is kinematically biased, it is easy to correct for this, as the cut in reduced proper motion corresponds to a cut in tangential velocity; from a simple model one can calculate the detection efficiency for stars of a given velocity without accurate distances or luminosity functions. An additional factor which helps to separate out halo stars is that metal-poor stars are bluer, meaning that (for a given color) metal-poor stars are intrinsically fainter than metal-rich ones by as much as a couple of magnitudes [see, for example, equation A2 of Ivezić et al. (2008); see also Bochanski et al. (2013)]. Once the halo stars were identified photometrically from the reduced proper motion

diagram, they were cross-matched with SDSS spectroscopy to provide metallicities and velocities. Distances were estimated by combining spectroscopic metallicities with the photometric distance relation of Ivezić et al. (2008), amended slightly to include a minor correction as one approaches the turn-off region [see Appendix B of Smith et al. (2009b) and the Appendix of Smith et al. (2012)]. Here also the Stripe 82 data were beneficial; the multiple epochs provide much improved photometric accuracy compared to the rest of the SDSS footprint (e.g., median (g - i) error was less than 10 mmag), enabling much more precise photometric distances.

This halo sample was exploited for a variety of studies, including measuring the tilt of the halo velocity ellipsoid out of the plane (Smith et al. 2009a) and investigating the global kinematics (Smith et al. 2009b). In the context of this chapter, the sample was also important for investigating halo substructures. By working in angular momentum space (L_z, L_\perp) , the sample shows clear evidence for the Helmi stream, for the first time detecting candidate members up to 5 kpc away (see Fig. 5.7). New candidate substructures were also found, dubbed Sloan Kinematic Overdensities (SKOs). The first one of these (SKOa) is particularly interesting—detected as a weak overdensity of stars with high L_{\perp} , it turned out that the feature coincides (in angular $L_z - L_{\perp}$ space) with a number of globular clusters taken from Dinescu et al. (1999). Figure 10 of Smith et al. (2009b) shows how these four clusters (NGC 5466, NGC 6934, NGC 7089/M2 and NGC 6205/M13) lie apart from the main distribution, raising the intriguing possibility that SKOa may be either the remains of tidal debris from one of these clusters or alternatively the remnant of a larger galaxy which hosted a number of smaller systems (i.e., these clusters, possibly including the progenitor of SKOa). Such hypotheses are difficult to test, but a detailed abundance analysis will be able to determine if its chemistry is consistent with any of these four globular clusters.

The remaining two over-densities, (SKOb and c) arose from a search for distant systems that are localized on the sky. The orientation of the Stripe 82 field (it is a long, thin stripe measuring $2.5 \times 100^{\circ}$ on the sky) means that coherent streams are likely to "cut through" this narrow stripe, and so Smith et al. (2009b) sliced the field along its length and searched for clumping in angular momentum space. Of the two overdensities, the most prominent is SKOb. This has been confirmed using data from MMT (Smith et al., in preparation; see Fig. 5.8), pinning down the distance to between 4 and 5 kpc. This structure is intriguing because, unlike most of the other halo moving groups mentioned in this chapter, it appears to be coherent, i.e. more like a stream than a moving group. As it is close enough to measure proper motions, this means that if we can trace an extension of this system across the sky it will become a 6D stream, which are very rare and important for modelling the halo (e.g., Koposov et al. 2010). As with SKOa (and, for that matter, the other overdensities found by Klement et al. in SDSS), detailed abundances would be useful to better understand the origins of this system. However, as SDSS photometric data extends to relatively faint magnitudes, high resolution follow-up studies are prohibitively expensive in terms of telescope time.

130 M.C. Smith

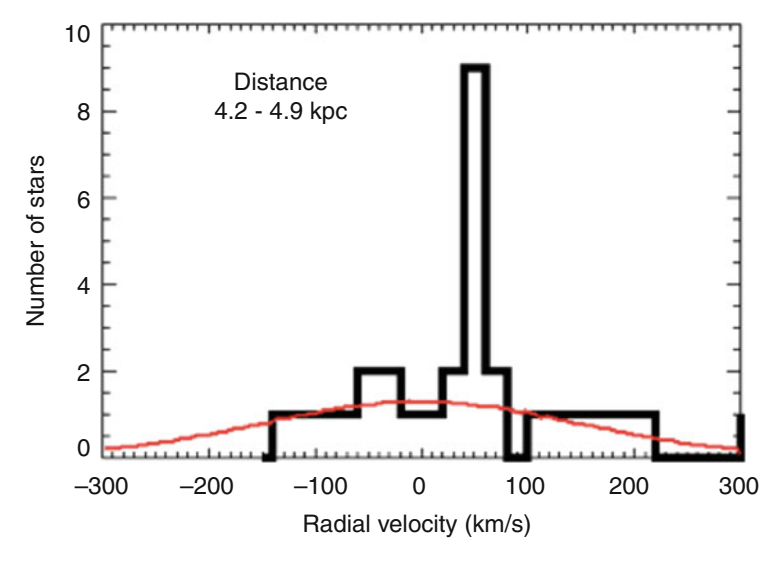


Fig. 5.8 Confirmation of the SKOb overdensity, which was initially discovered by Smith et al. (2009a). This figure shows the radial velocity distribution of stars with distances between 4.2 and 4.9 kpc, exhibiting a clear peak at +60 km/s. The *red curve* denotes the expected distribution for the smooth halo

5.3 Distant Halo Streams

The above discussion of local halo streams focused on those found using three-dimensional kinematics. However, once we move beyond the solar neighborhood, uncertainties in proper motions prohibit the use of tangential velocities. Tangential errors scale linearly with distance; for example, a proper motion error of 1 mas/yr at 1 kpc corresponds to a tangential velocity error of 4.7 km/s, but at 10 kpc this error will grow to 47 km/s. As a consequence, any detailed structure in phase-space is washed out. Fortunately, radial velocity uncertainties do not scale with distance and so these can be used to probe large volumes of the halo, with the caveat that it is now harder to interpret any identified substructures with two components of the velocity missing. Also working in our favor is that in the outer halo the mixing times are much longer, which allows ancient structures to remain coherent in configuration space for many Gyr.

The most spectacular and important discovery of halo substructure through radial velocities is that of the Sagittarius dwarf galaxy. For many years observers had found dwarf galaxies around the Milky Way, beginning with the Magellanic Clouds, but one lay hidden behind the bulge of the Milky Way and was only discovered in 1994 (Ibata et al. 1994). This was uncovered serendipitously during a radial velocity survey of stars towards the Galactic bulge. When analyzing the radial velocity distributions in certain fields, instead of the expected Gaussian distribution, a secondary peak was identified. This peak corresponded to the Sagittarius dwarf

galaxy, whose systemic radial velocity is offset from the bulge by around 150 km/s. Subsequent works have revealed that this dwarf is in the process of being devoured by our Galaxy, with tidal streams being discovered encircling the entire Milky Way (see Chap. 2).

At higher latitudes other streams have been identified by their coherent radial velocities, including the Cetus Polar Stream (Newberg et al. 2009), the cold metal-poor stream of Harrigan et al. (2010) and the high-velocity stream of Frebel et al. (2013).

One of the most impressive studies of radial-velocity selected substructures in the halo was led by Kevin Schlaufman in the "ECHOS" series of papers (Schlaufman et al. 2009, 2011, 2012). Their approach was to take each SDSS/SEGUE spectroscopic plate and determine, using robust statistics, whether the radial velocity distribution of the main-sequence stars matches what one expects for a smooth halo. This was done using two statistical tests, as described in Sect. 3.2 of Schlaufman et al. (2009) and illustrated in Fig. 5.9. The first test compared the radial velocity histogram to a similar histogram (with the same number of radial velocity measurements) drawn from a smooth model halo. This realization of the smooth halo was repeatedly resampled in order to test the significance of any peaks in the observed distribution. In the upper panel of Fig. 5.9, the grey shaded region shows the 95 % confidence interval from these realizations of the smooth halo model; the fact that the observation (black histogram) and its error bar do not overlap the grey shaded region implies that this is a robust detection of velocity substructure. The second test is based on the cumulative distribution of velocities, which retains more information than the previous approach (i.e., unlike the previous approach, it avoids any binning of the data). Again the observed distribution is compared to one drawn from a smooth model, but this time they compare the steepness of the cumulative distribution function. This is shown in the lower panel of Fig. 5.9, where one can see that the observed slope (given by the black curve) reaches into the high-significance regions (shown by the dark grey region).

Schlaufman et al. applied these techniques to observations of main-sequence halo stars out to 17.5 kpc on 137 individual spectroscopic plates of SEGUE data. In these 137 lines of sight, they identified a total of ten strong candidates (where the number of false positive detections is estimated to be less than 1) and a further 21 weaker candidates (estimated to have fewer than three false positives). A number of these are likely to be detections of existing substructures, such as the Monoceros stream, but seven of the strong candidates are new detections. Note that this does not translate to seven new independent halo substructures, as some streams could intersect multiple lines of sight, but it does show that the halo of the Milky Way is (at least in terms of its kinematics) lumpy, even in the inner halo where phase mixing should occur on relatively small time-scales. Schlaufman et al. quantify this "lumpiness," concluding that around 34% of the inner halo is in the form of elements of cold halo substructures (ECHOS) and estimate that there could be as many as 10³ individual kinematic groups in the entire inner halo.

The chemical composition of these ECHOS was investigated in the series' second paper (Schlaufman et al. 2011). They found that these ECHOS were

132 M.C. Smith

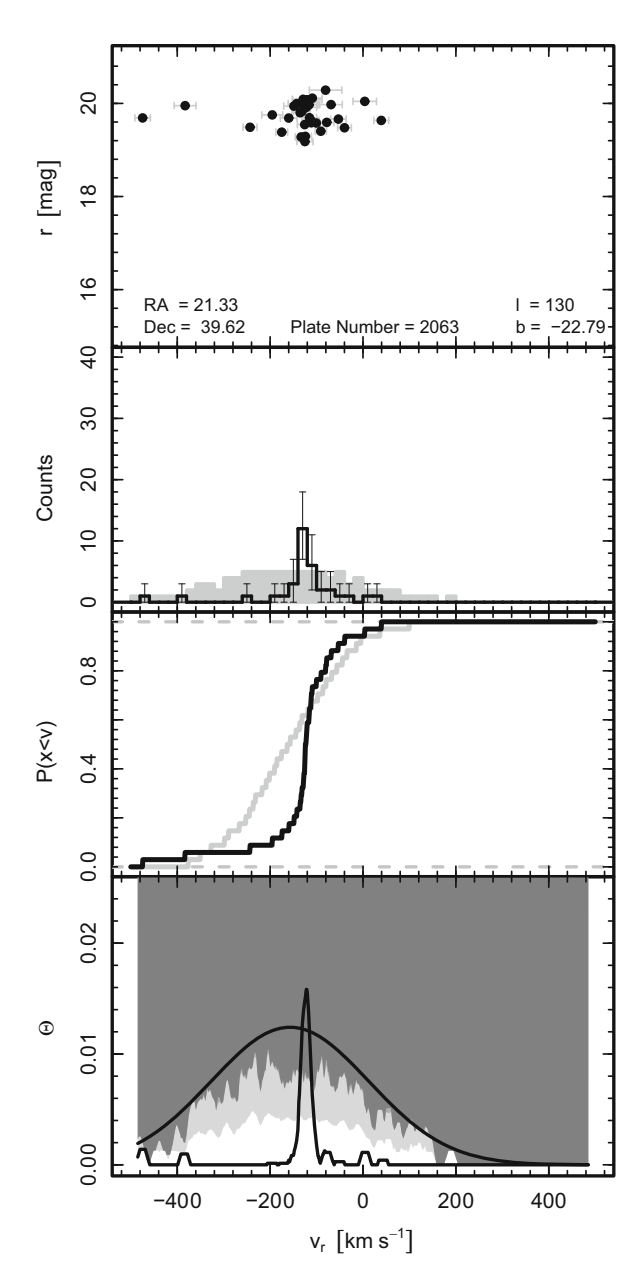


Fig. 5.9 Example of the search for an ECHOS from Schlaufman et al. (2009). The *upper panel* shows the radial velocity distribution (*black histogram* with error bars) and the 95 % confidence interval from the multiple realizations of the smooth halo model (*grey shaded histogram*). The *middle panel* shows the cumulative distribution function from the observed data (*black*) and mean from the realizations of the smooth halo model (*grey*). The *lower panel* shows their measure of the statistical significance Θ (*black line*), with the various significance levels denoted in *light* and *dark grey*. The wide Gaussian in this panel shows an envelope around the most significant region, which is included to remove any spurious detections due to small-scale fluctuations

more iron-rich and less alpha-enhanced than the smooth halo, concluding that the most-likely origin is that they were formed from the tidally disrupted debris of relatively massive dwarf galaxies ($M_{\rm tot} > 10^9 M_{\odot}$). In the final paper of this series (Schlaufman et al. 2012) the authors investigated the spatial coherence in [Fe/H] as a function of Galactocentric radius, concentrating only on main sequence turnoff stars from the kinematically smooth halo (namely SEGUE fields in which no ECHOS were detected). Although these fields are phase mixed and show no kinematic substructures, the chemistry of these stars can illuminate their origins. By studying the distributions of stars in the [Fe/H]–[α /Fe] plane they found that the accreted halo becomes dominant beyond around 15 kpc from the Galactic center, arguing that at smaller radii the halo is probably formed from a combination of in-situ star formation and dissipative major mergers at high redshift.

As the careful work of Schlaufman et al. has shown, statistical studies are important if we are to dissect the halo of the Milky Way beyond the solar neighborhood, especially when the sky coverage is not contiguous and the sampling of stars with spectra is sparse. Various tools have been developed, including the 4distance measure introduced by Starkenburg et al. (2009, see also the similar approach of Clewley and Kinman 2006). This technique, which is based around the separation of pairs of stars in four dimensions (angular position on the sky, distance and radial velocity), has proved influential for subsequent works (e.g., Cooper et al. 2011; Xue et al. 2011) and will undoubtedly continue to be used on surveys of distant halo stars where proper motions are unavailable.

5.4 Future Prospects

Despite extensive progress in identifying kinematic streams, the field is far from exhausted. On the contrary, this decade is likely to see a resurgence in this field, leading to unprecedented insights into the formation of our Galaxy.

From the current generation of spectroscopic surveys, we can expect significant progress in the coming years. In terms of sheer volume of spectra, the Chinese LAMOST survey is unsurpassed (Deng et al. 2012). By gathering over a million spectra each year, this spectroscopic survey has great potential. Already one new candidate kinematic overdensity has been identified (Zhao et al. 2014) and various works are analysing substructure in the local velocity distribution, for example the work of Xia et al. (2015) which is utilizing the extreme deconvolution technique (Bovy et al. 2011).

If we think about the accreted galaxies which built up our stellar halo, they will of course have a range of masses and accretion times. Their chemical composition will therefore vary since the amount of enrichment that can take place depends on these factors (see, for example, Lee et al. 2015). As a consequence, a detailed dissection of the accretion history of our halo will require both kinematics and chemistry. By combining dark matter simulations with semi-analytic prescriptions for the star formation and chemistry, it is possible to make predictions for what we may be able

134 M.C. Smith

to detect and how much we can infer about our Galaxy's accretion history from a given set of kinematic and chemical abundance data (e.g., Johnston et al. 2008).

There are a number of spectroscopic surveys that operate at resolutions sufficient to carry out detailed chemical abundance analyses, for example the SDSS project APOGEE (Holtzman et al. 2015), the GALAH survey (Freeman 2012), or the Gaia-ESO survey (Gilmore et al. 2012; Randich et al. 2013). These detailed abundances open up the possibility of "chemical tagging," whereby abundance ratios are used to disentangle the different formation sites for groups of stars (Freeman and Bland-Hawthorn 2002). Clearly these additional dimensions will be extremely valuable when attempting to identify kinematic substructures in the local disk, where groups may overlap if one looks at only the 6D phase-space. Although this technique is ideally suited to finding moving groups in the disk, chemistry will allow us to classify halo streams and understand their origins—in effect carrying out the discovery and follow-up in one step.

As the Gaia satellite begins to deliver scientific return, there is no doubt that we are on the cusp of a true revolution in this field. This mission, which is led by the European Space Agency, is collecting high precision astrometry of a billion stars in our galaxy. All stars in the sky brighter than 20th magnitude will be observed, leading to exquisite proper motions and parallaxes. The precision is so great that it will be able to measure distances (through trigonometric parallax) to less than 1% for ten million stars. In addition to the astrometry, Gaia will provide detailed photometric information (from spectrophotometry) including stellar parameters and, for stars brighter than around 17th magnitude, spectroscopic information including radial velocities. A description of the science capabilities can be found in de Bruijne (2012), although continually updated performance information can be found on the Gaia webpage. The final catalogue is expected in 2022, with interim releases before then.

Clearly such an unprecedented mapping of 6D phase space will open up an entirely new view of the local velocity distribution. While we wait for the first Gaia data to appear, many authors have attempted to estimate what we might be able to see. One example of this is Gómez et al. (2010), who modelled the Milky Way halo through the accretion of satellite galaxies, then convolved these with Gaia's observational errors. Figure 5.10 shows what we may be able to detect in a solar neighborhood realization; there are 10⁵ stellar halo particles within this sphere of 4 kpc radius, plus around 20,000 stellar disk particles. Upon applying a detection algorithm to identify substructure, Gómez et al. (2010) confirm 12 separate accretion events, corresponding to around 50% of all disrupted satellites in this volume. For some of these detections the authors find that it should be possible to directly estimate when these satellites were accreted, exploiting the fact that disrupting satellites form separate clumps in frequency space and the separation of these clumps relates to the time since accretion (McMillan and Binney 2008; Gómez and Helmi 2010). This remarkable feat requires a large enough sample of stars with

¹http://www.cosmos.esa.int/web/gaia/science-performance.

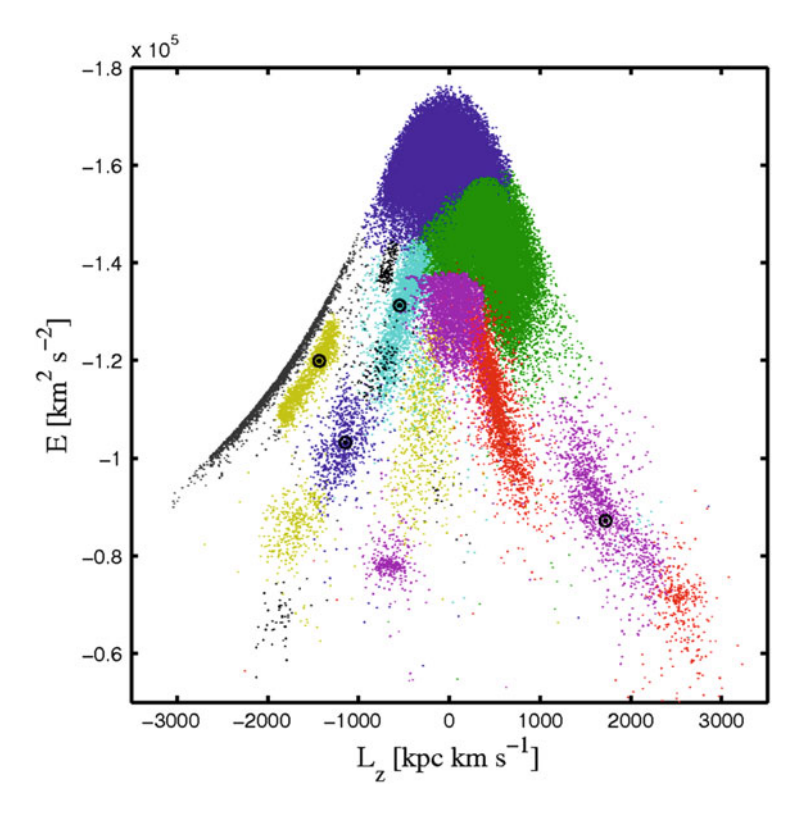


Fig. 5.10 An example of how Gaia might see the distribution of accreted satellites in the solar neighborhood. The *different colors* correspond to different satellites in the space of energy and the vertical component of the angular momentum. *Black circles* denote the four satellites for which it will be possible to estimate the time of accretion. Taken from Gómez et al. (2010)

accurate parallaxes (typically 50 or more stars with parallax error less than 2%), but in this realization Gómez et al. predict that it should be attainable for at least four of their detected satellites. Being able to determine the time of accretion, together with a detailed analysis of the chemistry of these stars, will undoubtedly teach us a great deal about the evolution of star formation in these earliest galaxies.

With Gaia in mind, a number of other studies have devised methods to search for substructures. One such work is that of Mateu et al. (2011), who utilize the fact that (for a spherical potential) streams will fall on great circles as viewed from the Galactic center. This is based on an earlier study (Johnston et al. 1996), but by extending the analysis to include data such that will be available from Gaia (i.e., parallaxes and kinematics) the method has much greater efficacy. Of course this technique still requires streams to be confined to orbital planes and, as such, is ill-suited to the inner halo where the shorter dynamical times lead to significant phase mixing. However, at intermediate distances in the halo where Gaia will still be able

136 M.C. Smith

to provide reasonable parallaxes (with distance accuracy of say 30 %), this technique will thrive.

Although Gaia will play a dominant role in the coming decades, it will not provide all of the answers. The onboard spectroscopy is limited to only the brightest stars and will not deliver detailed chemistry, meaning that a huge ground-based follow-up program is required. The realization that this limitation hampered the scientific return of the Hipparcos mission motivated the development of the Gaia-ESO survey, and also provides strong motivation for future instruments, such as Subaru's Prime Focus Spectrograph (Takada et al. 2014), 4-MOST (de Jong et al. 2014), WEAVE (Dalton et al. 2014) and the Maunakea Spectroscopic Explorer (Simons et al. 2014).

It is fascinating to see how, 150 years since Mädler and his contemporaries made their first discoveries, the analysis of kinematic substructures is still playing an important role in understanding the evolution of the Galaxy. Mädler couldn't have imagined that some moving groups could be the relics of other galaxies, but today these substructures are illuminating our knowledge of the earliest galaxies and hierarchical assembly. As new surveys are undertaken, the census of substructures becomes more complete. Perhaps in 150 years accretion events such as these will still be contributing new insights.

Acknowledgements The author acknowledges financial support from the CAS One Hundred Talent Fund, NSFC grants 11173002 and 11333003, the National Key Basic Research Program of China (2014CB845700) and the Strategic Priority Research Program "The Emergence of Cosmological Structures" of the Chinese Academy of Sciences (XDB09000000). This work is partially supported by the Gaia Research for European Astronomy Training (GREAT-ITN) Marie Curie network, funded through the European Union Seventh Framework Programme (FP7/2007–2013) under grant agreement No. 264895. This chapter uses data obtained through the Telescope Access Program (TAP), which has been funded by the Strategic Priority Research Program "The Emergence of Cosmological Structures" (Grant No. XDB09000000), National Astronomical Observatories, Chinese Academy of Sciences, and the Special Fund for Astronomy from the Ministry of Finance.

References

```
Antoja, T., Figueras, F., Torra, J., Valenzuela, O., & Pichardo, B. 2010, Lecture Notes and Essays
in Astrophysics, 4, 13
```

Arifyanto, M. I., & Fuchs, B. 2006, A&A, 449, 533

Beers, T. C., & Sommer-Larsen, J. 1995, ApJS, 96, 175

Beers, T. C., Chiba, M., Yoshii, Y., et al. 2000, AJ, 119, 2866

Belokurov, V. 2013, New Astronomy Reviews, 57, 100

Bensby, T., Feltzing, S., & Oey, M. S. 2014, A&A, 562, A71

Binney, J., & Tremaine, S. 2008, Galactic Dynamics: Second Edition (Princeton University Press)

Binney, J., Burnett, B., Kordopatis, G., et al. 2014a, MNRAS, 439, 1231

-.. 2014b, MNRAS, 437, 351

Bobylev, V. V., Bajkova, A. T., & Mylläri, A. A. 2010, Astronomy Letters, 36, 27

Bochanski, J. J., Savcheva, A., West, A. A., & Hawley, S. L. 2013, AJ, 145, 40

Boeche, C., Siebert, A., Williams, M., et al. 2011, AJ, 142, 193

Bovy, J., & Hogg, D. W. 2010, ApJ, 717, 617

Bovy, J., Hogg, D. W., & Roweis, S. T. 2009, ApJ, 700, 1794

Bovy, Jo, Hogg, D. W., & Roweis, S. T. 2011, Annals of Applied Statistics, 5, 1657

Bovy, J., Rix, H.-W., & Hogg, D. W. 2012, ApJ, 751, 131

Bramich, D. M., Vidrih, S., Wyrzykowski, L., et al. 2008, MNRAS, 386, 887

Breddels, M. A., Smith, M. C., Helmi, A., et al. 2010, A&A, 511, 90

Carney, B. W., Latham, D. W., Laird, J. B., & Aguilar, L. A. 1994, AJ, 107, 2240

Casagrande, L., Schönrich, R., Asplund, M., et al. 2011, A&A, 530, A138

Casey, A. R., Keller, S. C., Alves-Brito, A., et al. 2014, MNRAS, 443, 828

Chiba, M., & Yoshii, Y. 1998, AJ, 115, 168

Chiba, M., & Beers, T. C. 2000, AJ, 119, 2843

Clewley, L., & Kinman, T. D. 2006, MNRAS, 371, L11

Cooper, A. P., Cole, S., Frenk, C. S., & Helmi, A. 2011, MNRAS, 417, 2206

Dalton, G., Trager, S., Abrams, D. C., et al. 2014, in Society of Photo-Optical Instrumentation Engineers (SPIE) Conference Series, Vol. 9147, Society of Photo-Optical Instrumentation Engineers (SPIE) Conference Series, 0

de Boer, T. J. L., Belokurov, V., Beers, T. C., & Lee, Y. S. 2014, MNRAS, 443, 658

de Bruijne, J. H. J. 2012, Ap&SS, 341, 31

de Jong, R. S., Barden, S., Bellido-Tirado, O., et al. 2014, in Society of Photo-Optical Instrumentation Engineers (SPIE) Conference Series, Vol. 9147, Society of Photo-Optical Instrumentation Engineers (SPIE) Conference Series, 0

Dehnen, W., & Binney, J. J. 1998, MNRAS, 298, 387

Dekker, E. 1976, Phys. Rep., 24, 315

Deng, L.-C., Newberg, H. J., Liu, C., et al. 2012, Research in Astronomy and Astrophysics, 12, 735

Dettbarn, C., Fuchs, B., Flynn, C., & Williams, M. 2007, A&A, 474, 857

Dinescu, D. I., Girard, T. M., & van Altena, W. F. 1999, AJ, 117, 1792

Eggen, O. J. 1978, ApJ, 221, 881

—. 1996, AJ, **112**, 1595

ESA, ed. 1997, ESA Special Publication, Vol. 1200, The HIPPARCOS and TYCHO catalogues. Astrometric and photometric star catalogues derived from the ESA HIPPARCOS Space Astrometry Mission

Famaey, B., Siebert, A., & Jorissen, A. 2008, A&A, 483, 453

Frebel, A., Lunnan, R., Casey, A. R., et al. 2013, ApJ, 771, 39

Freeman, K. C. 2012, in Astronomical Society of the Pacific Conference Series, Vol. 458, Galactic Archaeology: Near-Field Cosmology and the Formation of the Milky Way, ed. W. Aoki, M. Ishigaki, T. Suda, T. Tsujimoto, & N. Arimoto, 393

Freeman, K., & Bland-Hawthorn, J. 2002, ARA&A, 40, 487

Fuchs, B., & Dettbarn, C. 2011, AJ, 141, 5

Gilmore, G., Randich, S., Asplund, M., et al. 2012, The Messenger, 147, 25

Gómez, F. A., Helmi, A., Brown, A. G. A., & Li, Y.-S. 2010, MNRAS, 408, 935

Gómez, F. A., & Helmi, A. 2010, MNRAS, 401, 2285

Gould, A. 2003, ApJ Lett, 592, L63

Harrigan, M. J., Newberg, H. J., Newberg, L. A., et al. 2010, MNRAS, 405, 1796

Helmi, A. 2008, A&A Rev., 15, 145

Helmi, A., & White, S. D. M. 1999, MNRAS, 307, 495

Helmi, A., White, S. D. M., de Zeeuw, P. T., & Zhao, H. 1999, Nature, 402, 53

Helmi, A., Navarro, J. F., Nordström, B., et al. 2006, MNRAS, 365, 1309

Helmi, A., Williams, M., Freeman, K. C., Bland-Hawthorn, J., & De Silva, G. 2014, ApJ, 791, 135

Holmberg, J., Nordström, B., & Andersen, J. 2007, A&A, 475, 519

-... 2009, A&A, 501, 941

Holtzman, J. A., Shetrone, M., Johnson, J. A., et al. 2015, ArXiv e-prints, arXiv:1501.04110

Ibata, R. A., Gilmore, G., & Irwin, M. J. 1994, Nature, 370, 194

Ivezić, Ž., Sesar, B., Jurić, M., et al. 2008, ApJ, **684**, 287

138 M.C. Smith

Ivezić, Ž., Beers, T. C., & Jurić, M. 2012, ARA&A, 50, 251

Johnston, K. V., Hernquist, L., & Bolte, M. 1996, ApJ, 465, 278

Johnston, K. V., Bullock, J. S., Sharma, S., et al. 2008, ApJ, 689, 936

Jurić, M., Ivezić, Ž., Brooks, A., et al. 2008, ApJ, 673, 864

Kapteyn, J. C., ed. 1906, Plan of Selected Areas, Astronomical Laboratory at Groningen

Kepley, A. A., Morrison, H. L., Helmi, A., et al. 2007, AJ, 134, 1579

Kinman, T. D. 2000, in Astrophysics and Space Science Library, Vol. 246, Astrophysics and Space Science Library, ed. P. C. van der Kruit & K. van Berkel, 213–228

Klement, R., Fuchs, B., & Rix, H.-W. 2008, ApJ, 685, 261

Klement, R., Rix, H.-W., Flynn, C., et al. 2009, ApJ, 698, 865

Klement, R. J. 2010, A&A Rev., 18, 567

Klement, R. J., Bailer-Jones, C. A. L., Fuchs, B., Rix, H.-W., & Smith, K. W. 2011, ApJ, 726, 103

Koposov, S. E., Rix, H.-W., & Hogg, D. W. 2010, ApJ, 712, 260

Koposov, S. E., Belokurov, V., & Wyn Evans, N. 2013, ApJ, 766, 79

Kordopatis, G., Gilmore, G., Steinmetz, M., et al. 2013, AJ, 146, 134

Lee, D. M., Johnston, K. V., Sen, B., & Jessop, W. 2015, ApJ, 802, 48

Lee, Y. S., Beers, T. C., Sivarani, T., et al. 2008, AJ, 136, 2022

Lee, Y. S., Beers, T. C., Allende Prieto, C., et al. 2011, AJ, 141, 90

Lee, Y.-W., Joo, J.-M., Sohn, Y.-J., et al. 1999, Nature, 402, 55

Mädler, J. H. 1846, Astronomische Nachrichten, 24, 213

Majewski, S. R., Nidever, D. L., Smith, V. V., et al. 2012, ApJ Lett, 747, L37

Mateu, C., Bruzual, G., Aguilar, L., et al. 2011, MNRAS, 415, 214

McMillan, P. J. 2011, MNRAS, 418, 1565

McMillan, P. J., & Binney, J. J. 2008, MNRAS, 390, 429

Navarro, J. F., Helmi, A., & Freeman, K. C. 2004, ApJ Lett, 601, L43

Newberg, H. J., Yanny, B., & Willett, B. A. 2009, ApJ Lett, 700, L61

Nordström, B., Mayor, M., Andersen, J., et al. 2004, A&A, 418, 989

Proctor, R. A. 1869, Royal Society of London Proceedings Series I, 18, 169

Ramya, P., Reddy, B. E., & Lambert, D. L. 2012, MNRAS, 425, 3188

Randich, S., Gilmore, G., & Gaia-ESO Consortium. 2013, The Messenger, 154, 47

Re Fiorentin, P., Helmi, A., Lattanzi, M. G., & Spagna, A. 2005, A&A, 439, 551

Roederer, I. U., Sneden, C., Thompson, I. B., Preston, G. W., & Shectman, S. A. 2010, ApJ, 711, 573

Schlaufman, K. C., Rockosi, C. M., Allende Prieto, C., et al. 2009, ApJ, 703, 2177

Schlaufman, K. C., Rockosi, C. M., Lee, Y. S., Beers, T. C., & Allende Prieto, C. 2011, ApJ, 734, 49

Schlaufman, K. C., Rockosi, C. M., Lee, Y. S., et al. 2012, ApJ, 749, 77

Seabroke, G. M., Gilmore, G., Siebert, A., et al. 2008, MNRAS, 384, 11

Sellwood, J. A. 2010, MNRAS, 409, 145

Simons, D. A., Crampton, D., Côté, P., et al. 2014, in Society of Photo-Optical Instrumentation Engineers (SPIE) Conference Series, Vol. 9145, Society of Photo-Optical Instrumentation Engineers (SPIE) Conference Series, 15

Smith, M. C., Wyn Evans, N., & An, J. H. 2009a, ApJ, 698, 1110

Smith, M. C., Evans, N. W., Belokurov, V., et al. 2009b, MNRAS, 399, 1223

Smith, M. C., Okamoto, S., Yuan, H.-B., & Liu, X.-W. 2012, Research in Astronomy and Astrophysics, 12, 1021

Starkenburg, E., Helmi, A., Morrison, H. L., et al. 2009, ApJ, 698, 567

Steinmetz, M., Zwitter, T., Siebert, A., et al. 2006, AJ, 132, 1645

Stonkutė, E., Tautvaišienė, G., Nordström, B., & Ženovienė, R. 2012, A&A, 541, A157

—. 2013, A&A, **555**, A6

Takada, M., Ellis, R. S., Chiba, M., et al. 2014, PASJ, 66, 1

van der Kruit, P. C., ed. 2015, Astrophysics and Space Science Library, Vol. 416, Jacobus Cornelius Kapteyn

van Leeuwen, F., ed. 2007a, Astrophysics and Space Science Library, Vol. 350, Hipparcos, the New Reduction of the Raw Data

van Leeuwen, F. 2007b, A&A, 474, 653

Williams, M. E. K., Freeman, K. C., Helmi, A., & RAVE Collaboration. 2009, in IAU Symposium, Vol. 254, IAU Symposium, ed. J. Andersen, Nordströara, B. m, & J. Bland-Hawthorn, 139–144

Williams, M. E. K., Steinmetz, M., Sharma, S., et al. 2011, ApJ, 728, 102

Wylie-de Boer, E., Freeman, K., & Williams, M. 2010, AJ, 139, 636

Wylie-de Boer, E., Freeman, K., Williams, M., et al. 2012, ApJ, 755, 35

Xia, Q., Liu, C., Xu, Y., et al. 2015, MNRAS, 447, 2367

Xue, X.-X., Rix, H.-W., Yanny, B., et al. 2011, ApJ, 738, 79

Yanny, B., Rockosi, C., Newberg, H. J., et al. 2009, AJ, 137, 4377

York, D. G., Adelman, J., Anderson, Jr., J. E., et al. 2000, AJ, **120**, 1579 Ženovienė, R., Tautvaišienė, G., Nordström, B., & Stonkutė, E. 2014, A&A, **563**, A53

Zhao, J. K., Zhao, G., Chen, Y. Q., et al. 2014, ApJ, **787**, 31

Zwitter, T., Matijevič, G., Breddels, M. A., et al. 2010, A&A, 522, A54

Chapter 6 Origins and Interpretation of Tidal Debris

Kathryn V. Johnston

Abstract The stellar debris structures that have been discovered around the Milky Way and other galaxies are thought to be formed from the disruption of satellite stellar systems—dwarf galaxies or globular clusters—by galactic tidal fields. The total stellar mass in these structures is typically tiny compared to the galaxy around which they are found, and it is hence easy to dismiss them as inconsequential. However, they are remarkably useful as probes of a galaxy's history (as described in this chapter) and mass distribution (covered in a companion chapter in this volume). This power is actually a consequence of their apparent insignificance: their low contribution to the overall mass makes the physics that describes them both elegant and simple and this means that their observed properties are relatively easy to understand and interpret.

6.1 Introduction

Figure 6.1 contrasts internal and external views of two examples of debris structures seen in numerical simulations: streams from the disruption of a satellite along a mildly eccentric orbit (lower panels) and shells from the disruption of the same satellite along a much more eccentric orbit (upper panels; see Sect. 6.2 for a more detailed description of these simulations). This chapter first outlines our understanding of the formation of such debris structures (Sect. 6.3) and then goes on to explore what we can learn about dying and long-dead satellites from observations of their debris (Sect. 6.4) and the implications of the cosmological context for properties of the combined system of all debris structures that form our stellar halo (Sect. 6.5).

The following chapter discusses what debris structures can tell us about the tidal field—i.e. the mass distribution of the galaxy that destroyed them.

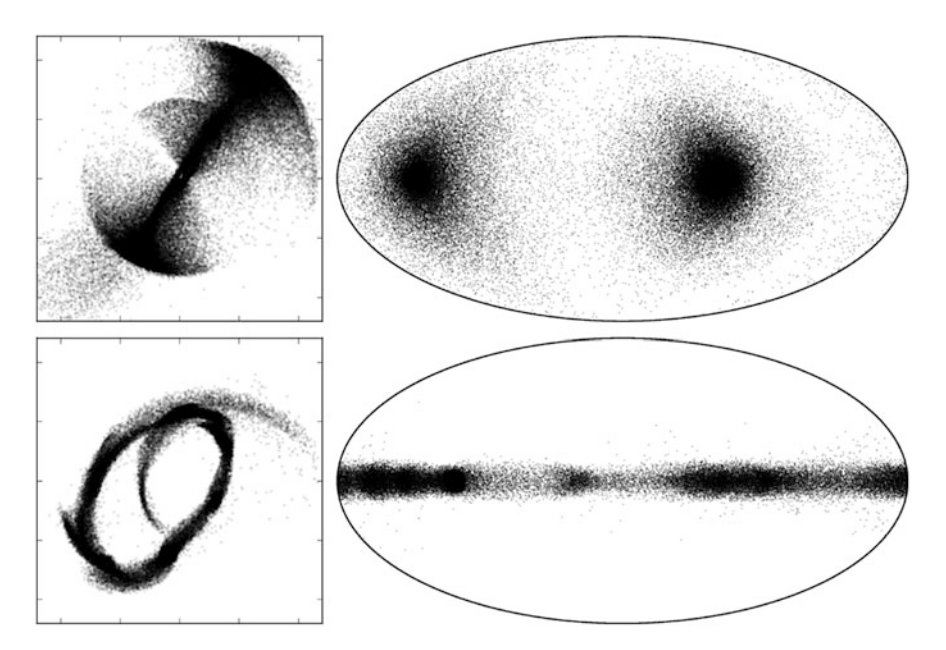


Fig. 6.1 External (*left panels*) and internal (i.e. all-sky projections—*right panels*) views of two examples of debris structures seen in numerical simulations described in Sect. 6.2. Both debris structures were formed along orbits with the same energy as a circular orbit at radius 25 kpc in the parent potential. The *top panels* are for a $6.5 \times 10^8 M_{\odot}$ satellite falling in along a highly eccentric orbit (angular momentum $L/L_{\rm circ} = 0.1$) and the *bottom panels* are for the same satellite on a more mildly eccentric orbit ($L/L_{\rm circ} = 0.9$)

6.2 Illustrative N-Body Simulations

The descriptions of debris evolution in this chapter are illustrated with a set of N-body simulations (see Dehnen and Read 2011, for a review of techniques) of satellite disruption presented in Hendel and Johnston (2015). The self-gravity of the satellite in these simulations was calculated with the Self-Consistent Field (SCF) code, which uses basis function expansions to represent the mutual influence of the particles on each other (Hernquist and Ostriker 1992). In each simulation, a 10^5 particle NFW-profile (Navarro et al. 1996) satellite was inserted at the apogalacticon of its orbit in a static, spherical host halo, with characteristics of dark matter halos thought to host Milky-Way-sized galaxies (NFW profile with a virial mass of $M = 1.77 \times 10^{12} M_{\odot}$ and a scale radius of 24.6 kpc, see Navarro et al. 1996). The satellite was evolved first in isolation, then the host potential was turned on slowly over ten satellite internal dynamical times to reduce artificial gravitational shocking. Total energy is conserved to better than $\sim 1\%$ of the satellite internal potential energy during all simulations.

Our figures illustrate the results of simulations for satellites with masses $m = 6.5 \times 10^6 M_{\odot}$ to $m = 6.5 \times 10^8 M_{\odot}$ (where m is the mass enclosed within 35 NFW

scale radii, the radius out to which particles were realized in the NFW distribution). The scale radius r_0 was adjusted for each mass so that their density was the same with a base value of $0.86\,\mathrm{kpc}$ for the $6.5\times10^6M_\odot$ satellite. These satellites were allowed to evolve for 8 Gyrs along orbits with the same energy as a circular orbit at $R=25\,\mathrm{kpc}$ in the host potential, but with angular momenta between 10 and 90% of that of a circular orbit (i.e. $L/L_\mathrm{circ}=0.1-0.9$) to contrast evolution on a near-circular to a highly-eccentric orbit.

6.3 Basic Principles of Debris Formation and Evolution

By definition, the tidal disruption of a satellite causes stars that used to be orbiting the satellite (which is in turn orbiting the parent galaxy) to become unbound and follow their own orbits around the parent galaxy. Figure 6.2 shows that, following disruption, the stars spread out through configuration space (i.e. they *phase-mix*, roughly along the satellite's orbit) as the distribution of orbital properties in debris corresponds to a distribution in orbital time-periods (described in Sect. 6.3.1). The rate at which the debris disperses reflects the scales over which debris orbital properties are distributed—which are set by the nature of tidal disruption (described in Sect. 6.3.2). The combination of tidal disruption and phase-mixing leads to phase-space morphologies for the debris that are primarily influenced by the mass of the satellite, its orbital path (which is in turn influenced by the parent galaxy potential), and the time since the debris became unbound. The scales of these morphologies can be broadly described by analytic formulae (Sect. 6.3.3.1) and represented by simple generative models (Sect. 6.3.3.2).

6.3.1 Debris Spreading: Phase-Mixing

The term *phase-mixing* beautifully encapsulates the physics of the evolution of debris structures. The nature of tidal disruption ensures that debris initially starts at the same *phase* (or position) along the orbit as the satellite from which it came, but with small offsets in its orbital properties (see Sect. 6.3.2). These offsets mean that the typical orbital frequency and time-periods in the debris differ systematically from those of the satellite, and hence that the debris will increasingly trail or lead the satellite in orbital phase as time goes by, *mixing* along the orbit to form streams and shells.

6.3.1.1 Intuition from Spherical Potentials

Figure 6.3 illustrates how and why phase mixing occurs for the idealized case of orbits in the spherical NFW potential used in our simulations. The top-left and

144 K.V. Johnston

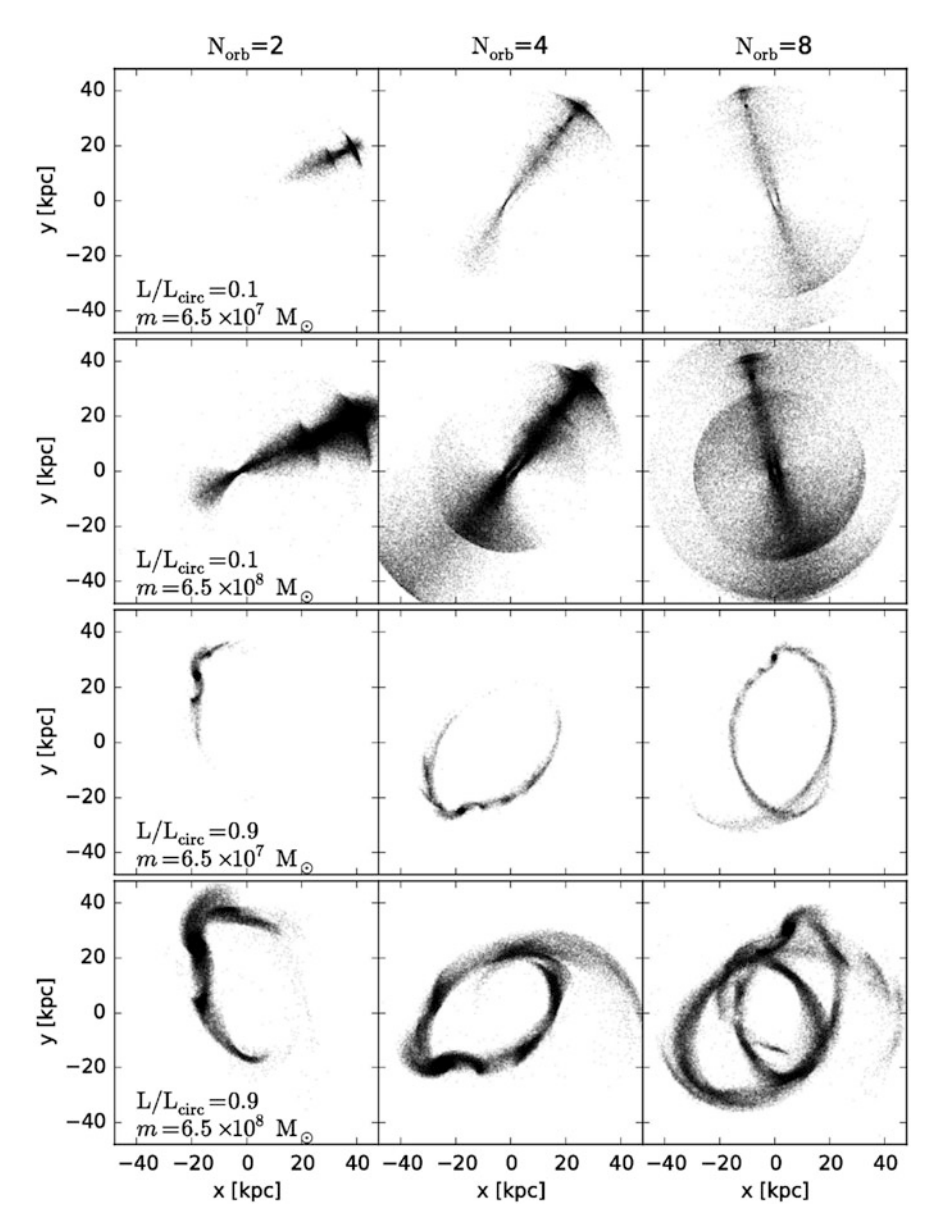


Fig. 6.2 Evolution of debris along highly (*top panels*) and mildly (*bottom panels*) eccentric orbits for two different mass satellites (labelled in *left-hand panel*). Note that highly eccentric orbits produce shells, while more circular orbits form streams

upper-right-hand panels contour the radial time periods (time between successive apocenters or pericenters) and precession rate (angle between successive apocenters or pericenters) for orbits of a given energy and angular momentum per unit mass.

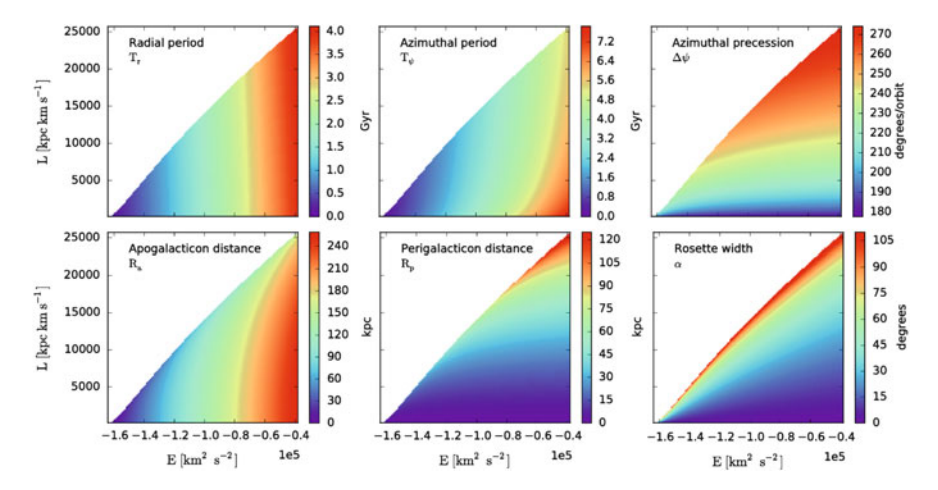


Fig. 6.3 Orbital properties in the spherical potential used in the N-body simulations as a function of energy (represented by the radius of a circular orbit of that energy) and angular momentum. The maximum angular momentum at a given energy is that of a circular orbit. The rosette width, α , is the angle the orbit travels through during half a radial period, centered around apocenter

While the radial time periods depend much more strongly on energy than angular momentum, the precession angle depends more strongly on angular momentum, though to some extent on energy as well.

Figure 6.4 shows how a set of moderately eccentric orbits that have a small range of orbital energies (left panel) or angular momenta (right panel) diverge in phase over just a few orbits. In particular note that: orbits with the same angular momenta but different energies spread in radial phase (i.e. positions along their oscillation in radius between apocenter and pericenter), while those with the same energies but different angular momenta spread in precession angle; the physical spread is much more striking for energy differences than for the equivalent angular momentum differences because the precession rate is a much weaker function of orbital properties than the orbital frequencies; and there is little dependence on orbital phase of these observations.

Figure 6.5 applies this intuition to one of our simulations, by color-coding particles with their differences in energy (first and third rows) and angular momentum (second and fourth rows) relative to the satellite from which they came. The sorting in energy along the orbital path and angular momentum around the orbital path is striking for both highly (top two panels) and mildly (lower two panels) eccentric orbits. It is also clear that the angular extent of the shells that form for the highly eccentric orbit is driven by differences in angular momenta, while the angular extent of streams is dominated by differences in energy.

Overall, these simple experiments give us an intuitive understanding of not only why phase-mixing occurs, but also the role that orbital properties play in determining whether debris is likely to form stream-like or shell-like morphologies.

146 K.V. Johnston

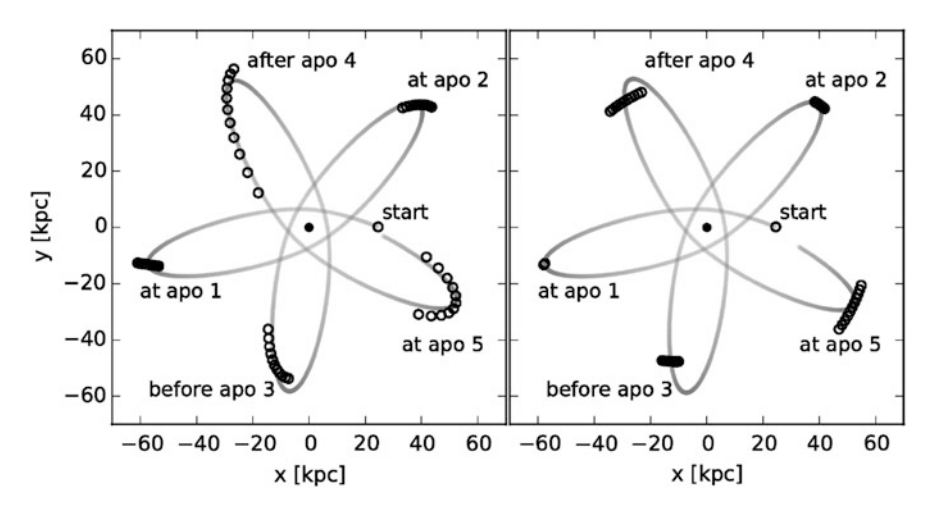


Fig. 6.4 Evolution of 11 particles that started at the same place along an orbit, but with a small spread in energy at fixed angular momentum (*left hand panel*) or angular momentum at fixed energy (*right-hand panel*). The orbit of a galactic satellite is shown by the *solid line*, and the galaxy's center is shown by the *solid dot*. The particles are shown at five subsequent times, one time for each petal of the orbit. Note that the positions of the particles diverge in phase in just a few orbits

6.3.1.2 Action-Angle Formalism

The description in the previous section is useful for developing an intuitive understanding of debris evolution since it employs familiar orbital descriptors (i.e., energy and angular momentum) that can be written down analytically for any potential and any point in phase-space. However, this description does not work for non-spherical potentials where angular momentum is not conserved and cannot be used to label orbits. Debris evolution can be described elegantly for more general (but integrable—see below) potentials using the action-angle variables of Hamiltonian dynamics. A formal development of this description is given in Helmi and White (1999) (and summarized in Binney and Tremaine 2008). We restrict ourselves here to a summary of the key ideas and equations.

Any point in phase-space can be located using the traditional spatial and velocity co-ordinates (x, \mathbf{v}) . For regular (i.e. non-chaotic) orbits in *integrable* potentials, any phase space point can be equivalently labelled by conjugate variables (θ, \mathbf{J}) where: (1) the actions, \mathbf{J} , are conserved orbital properties which fully specify the path of the orbit through phase-space; and (2) the angles, θ , represent the position along the orbit at which the point lies. The actions and angles can be related through *Hamilton's equations*:

$$\dot{\mathbf{J}} = -\frac{\partial H}{\partial \boldsymbol{\theta}}, \quad \dot{\boldsymbol{\theta}} = \frac{\partial H}{\partial \mathbf{J}},$$
 (6.1)

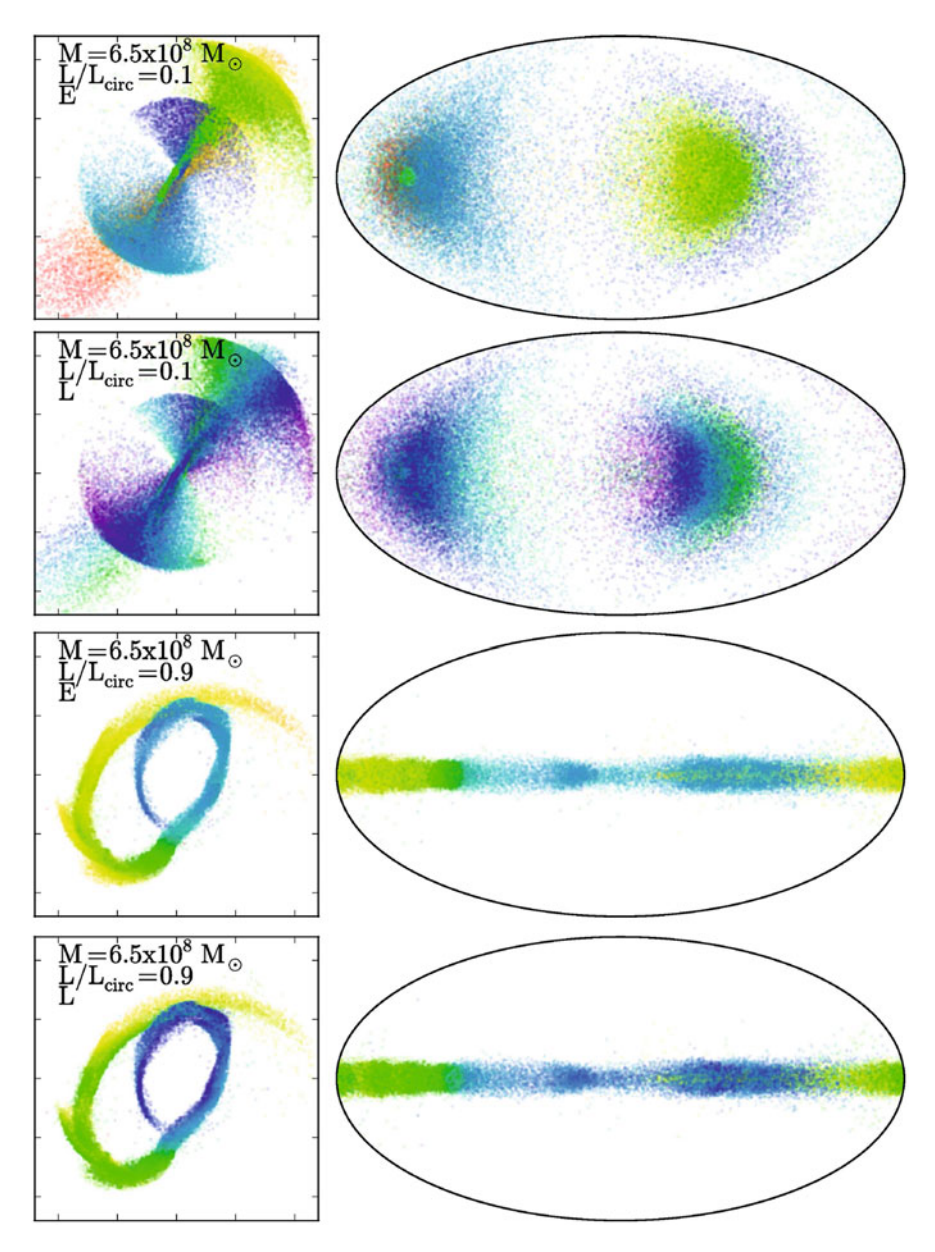


Fig. 6.5 Same as Fig. 6.1 but color-coded by differences between the satellite and debris in energy (first and third rows) and angular momenta (second and fourth rows)

where the function H (the *Hamiltonian*) is the energy of the orbit. Since the actions are conserved along an orbit $(\dot{\mathbf{J}} = 0)$, $\partial H/\partial \theta = 0$ and hence the Hamiltonian H can only be a function of the actions, $H = H(\mathbf{J})$. Then the Hamiltonian defines three

148 K.V. Johnston

unique orbital frequencies associated with each angle,

$$\mathbf{\Omega} \equiv \dot{\boldsymbol{\theta}} = \frac{\partial H}{\partial \mathbf{J}},\tag{6.2}$$

which are also conserved along the orbit since they are only functions of J. Equation (6.2) can be trivially integrated to give the position along the orbit at any time:

$$\boldsymbol{\theta} = \boldsymbol{\theta_0} + \boldsymbol{\Omega} t. \tag{6.3}$$

Note that these Hamiltonian angles are not trivially related to the angular position along an orbit derived from position (x, y, z): Eq. (6.3) shows that they increase linearly with time at a rate that is not orbital-phase dependent (i.e. with constant frequency), unlike, e.g., the angular coordinate along an eccentric orbit in a spherical potential, where the angular velocity is greater at pericenter than apocenter.

In this framework, the small range of orbital properties in tidal debris (illustrated with energy and angular momentum differences in Fig. 6.3) can be represented by small changes to the actions, ΔJ , which in turn lead to a range in orbital frequencies,

$$\Delta\Omega_i = \Delta \mathbf{J} \frac{\partial\Omega_i}{\partial \mathbf{J}} = \Delta J_j \frac{\partial^2 H}{\partial J_i \partial J_i}.$$
 (6.4)

This equation can also be trivially integrated to describe debris spreading (i.e. phase-mixing)

$$\Delta \boldsymbol{\theta} = \Delta \boldsymbol{\theta}_0 + \Delta \boldsymbol{\Omega} t. \tag{6.5}$$

This action-angle description allows a re-statement of our understanding of the origins of debris morphology in terms of the properties of the *Hessian* matrix— $\partial^2 H/\partial J_i\partial J_i$ in Eq. (6.4)—which governs how orbital frequencies change in response to perturbations in the actions. This is a real symmetric matrix, which can be diagonalized and from which eigenvalues and eigenvectors can be derived. Assuming an isotropic distribution in actions (i.e. ΔJ the same in every dimension—not strictly true, see Sect. 6.3.2 and Bovy 2014) the eigenvectors of the Hessian define the principal directions (in angle) into which debris spreading occurs and the eigenvalues define the rates at which this occurs. For realistic galactic potentials for which the Hessian has been derived, one eigenvalue has typically been found to dominate, indicating preferential spreading in just one dimension to form a tidal *stream*.

While action-angle variables offer an elegant description of debris dispersal, their versatility and applicability are not unlimited. Action-angles can be found for any spherical potential, but are only known for one family of non-spherical potentials: the triaxial Stäckel potentials (see Binney and Tremaine 2008). Otherwise, they cannot generally be written down nor exactly derived numerically. This means

that the transformation from (θ, \mathbf{J}) to the more familiar co-ordinates (\mathbf{x}, \mathbf{v}) is non-trivial and hampers the development of a simple intuitive understanding of how they correspond to each other. Moreover, this description breaks down entirely for chaotic regions of non-integrable potentials. Approaches to tackle these limitations typically involve approximating general potentials in which the actions are unknown with ones in which they *are* known. Examples include representing a general potential using an expansion in Stäckel potentials (Sanders 2012) or calculating actions for an orbit in a general potential from the actions derived for a set of orbits in a slightly perturbed potential (Bovy 2014; Sanders and Binney 2014).

6.3.2 Orbital Properties of Tidal Debris

The previous section attributed the dispersal of stars stripped from satellite disruption to the range in orbital time-periods within the debris. This section examines what sets that range.

Suppose a satellite of mass $m_{\rm sat}$ is following a circular orbit of radius R around a galaxy of mass M_R enclosed within R, with speed $V_{\rm circ} = \sqrt{GM_R/R}$. Moving to a frame co-rotating with the orbit allows the definition of a time-independent *effective* potential, $\Phi_{\rm eff}$, and the conserved Jacobi integral, $E_J = v^2/2 + \Phi_{\rm eff}$. The tidal radius, $r_{\rm tide}$, at which the size of the satellite is limited by the gravitational influence of the parent can be estimated from the saddle points (the inner and outer Lagrange points) in $\Phi_{\rm eff}$ as:

$$r_{\text{tide}} = \left(\frac{m_{\text{sat}}}{3M_R}\right)^{1/3} R \tag{6.6}$$

(see Binney and Tremaine 2008, Sect. 8.3 for derivation), which also defines a limiting E_J for escape from the satellite. However, since the escape of a star from the satellite depends on both its position and velocity, the tidal radius should not be considered as a solid boundary between bound and unbound stars. Moreover, it is not possible to define a strict tidal radius or E_J for satellites on non-circular orbits as there is no steadily-rotating frame in which the joint potential appears static. Nevertheless, numerical experiments have repeatedly demonstrated that the *tidal scale*,

$$s = \left(\frac{m_{\text{sat}}}{M_R}\right)^{1/3} \tag{6.7}$$

suggested by Eq. (6.6) captures much of the physics that creates debris distributions from satellites of a variety of masses and on a variety of orbits (Johnston 1998; Helmi and White 1999; Eyre and Binney 2011; Küpper et al. 2012; Bovy 2014).

Figure 6.6 illustrates this understanding with plots of the orbital distributions produced in our numerical simulations (see Sect. 6.2), for satellites on orbits from

150 K.V. Johnston

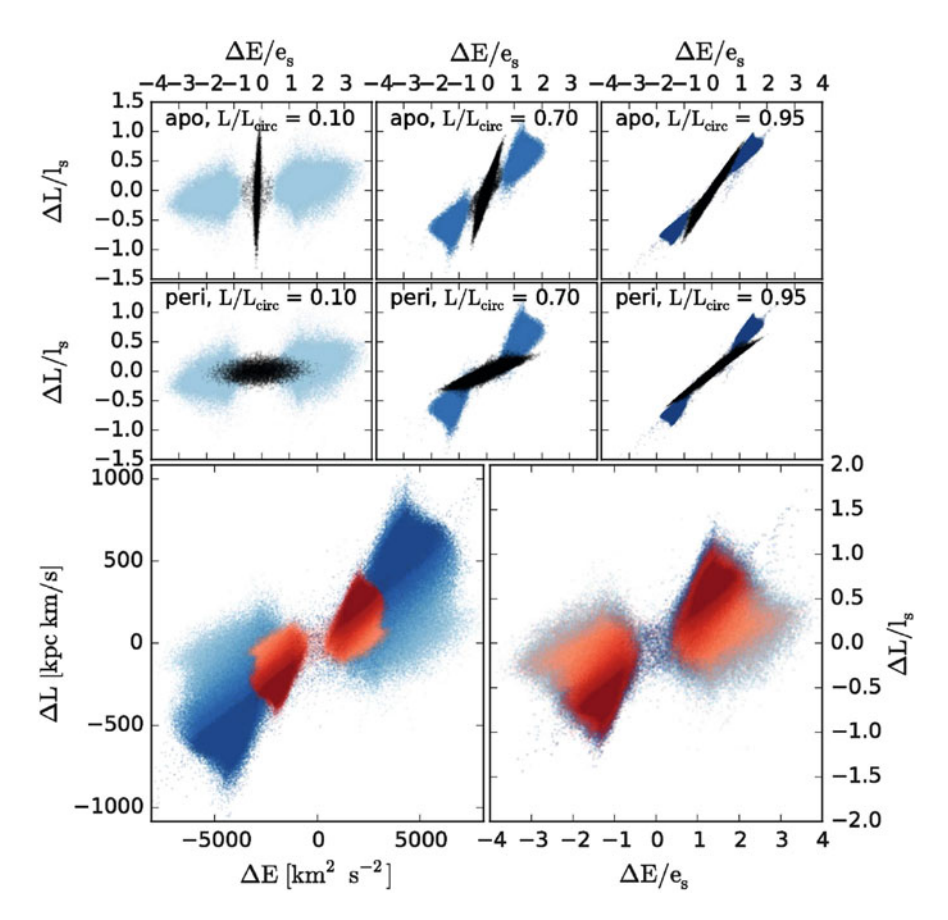


Fig. 6.6 Distribution in orbital properties for debris (*blue*) and satellite (*black*), relative to the satellite's orbit at apocenter (*top row*) and pericenter (*second row*). The illustrated orbits are for a $6.5 \times 10^7 M_{\odot}$ satellite on orbits with $L/L_{\rm circ} = 0.1, 0.7, 0.95$. Left panels show the most eccentric orbits, and the most circular are on the right, with each case color-coded with a particular shade of blue. The axes in the top two rows are scaled by the expected energy and angular momentum scales given in Eq. (6.8). The blue points representing the debris are distributed similarly at apocenter and pericenter, for a given eccentricity. The bottom panels combine the energy and angular momentum distributions for all eccentricities and for two different masses $(6.5 \times 10^7 M_{\odot})$ in blue and $6.5 \times 10^6 M_{\odot}$ in red) and plot them in physical units (bottom left) and scaled units (bottom right). Material that is still bound to the satellite is not shown in the lower two panels. Note that in scaled units (bottom right panel), the width of the leading/trailing distributions as well as the gap between them are similar across a wide range of eccentricities

highly eccentric to nearly circular (top panels, left to right). Each panel plots the energies (ΔE) and angular momenta (ΔL_z) of escaped particles (in blue) relative to the satellite's own (i.e. at origin in each plot—bound particles are shown in black). The axes have been scaled by simple estimates for the energy and angular momenta

ranges over which the particles are expected to be distributed,

$$e_s = r_{\text{tide}} \frac{d\Phi}{dR}$$
 and $l_s = sL_z$, (6.8)

where Φ is the potential of the parent galaxy.

Each panel in Fig. 6.6 shows paired distributions of unbound particles corresponding to debris leading/trailing the satellite along its orbit at negative/positive values of ΔE corresponding to systematically larger/smaller frequencies and shorter/longer orbital time periods. There is a distinct gap in orbital properties between the debris distributions for tidally stripped stars which is occupied by particles still bound to the satellite. (On the last pericentric passage, when all the particles become unbound the debris distribution will fill in this gap, see Johnston 1998.) While the boundary between bound and unbound is not exact in configuration space, the separation between black and blue points in orbital properties is clear. The bottom panels contrast the debris distributions for all orbits (overplotted on each other) and two different satellite masses in physical (left-hand panel) and scaled (right-hand panel) units. All together, the figures show that both the width of the leading/trailing distributions and the gap between them are similar in these scaled units across a wide variety of eccentricities. Similar scaled distributions can be plotted for orbital actions and frequencies (see, e.g., Bovy 2014, for a discussion).

This uniformity in orbital properties for orbits with a range of eccentricities, when normalized with a single physical scaling, is one of the factors that enables the very simple descriptions of subsequent evolution outlined below in Sects. 6.3.3.1 and 6.3.3.2. Since the satellite is typically small, the global potential is dominated by the (nearly static) parent galaxy and the debris orbital properties can be assumed not to evolve with time. Of course this assumption is a simplification—the gravitational influence of the satellite does not just turn off when a particle crosses the tidal radius but actually shapes the final distribution of debris orbital properties (see Choi et al. 2009; Gibbons et al. 2014, for some discussions of this).

6.3.3 Application: Models of Streams

6.3.3.1 Estimating Physical Scales in Debris

The understanding of distributions of orbital properties in tidal debris (Sect. 6.3.2) can be combined with the behavior of orbits (i.e. the azimuthal time periods, T_{Ψ} , for increasing the azimuthal angle by 2π and precession angles between turning points, Ψ , see Fig. 6.3 and Sect. 6.3.1) to make simple predictions for the physical scales and time-evolution of the debris. Exploiting the fact that orbital time periods in spherical potentials are largely independent of angular momenta (as illustrated in Fig. 6.3) the azimuthal time period for any orbit can be approximated by that of a circular orbit of the same energy T_{Ψ}^{circ} . Then, the angular extent of the debris at

152 K.V. Johnston

time t after disruption due to the characteristic energy scale over which it spreads ($\sim 4e_s$ —see Eq. (6.8) and Fig. 6.6) is of order:

$$\Psi_e = 4e_s \left(\frac{1}{T_{\psi}^{\text{circ}}} \frac{\partial T_{\psi}^{\text{circ}}}{\partial E} \right) \frac{2\pi t}{T_{\psi}^{\text{circ}}}$$
(6.9)

Similarly, given the angle Ψ between subsequent apocenters along the orbit of the parent satellite, the angular extent due to the spread in apocentric precession rates over the characteristic angular momentum scale ($\sim 4l_s$) can be estimated as:

$$\Psi_l = 4l_s \frac{\partial \Psi}{\partial L} \frac{t}{T_{tt}^{\text{circ}}}.$$
 (6.10)

Lastly, for a purely spherical potential, where the orbits are planar, the height h of debris perpendicular to the orbital plane is set by the range of orbital inclinations available to debris escaping at the Lagrange (i.e. saddle) points in the effective potential with the characteristic ranges in energies and angular momenta. It has been shown to be of the same order as the tidal radius,

$$h \sim sR \sim r_{\text{tide}}.$$
 (6.11)

These simple formulae can be used to characterize the length Ψ_e and width Ψ_l in and height h above the orbital plane for debris from a satellite of any mass disrupting along any orbit in any spherical potential (e.g. as confirmed with N-body simulations in Johnston et al. 2001). Note that, since both Ψ_e and Ψ_l are proportional to time, the ratio Ψ_e/Ψ_l is constant in time, and typically much greater than 1. This explains the tendency for debris to form streams (as also suggested by the unequal eigenvalues of the Hessian in the action-angle description). This ratio decreases for more eccentric orbits, which contributes towards the more shell-like appearance of debris in these cases (see Sect. 6.4.1 for a more complete description).

6.3.3.2 Generating Predictions for Density Distributions Along Streams

The understanding of orbits and orbital distributions in debris can also be combined to build more detailed predictions for the full phase-space distribution along tidal streams. One approach is to first integrate only the orbit of the satellite and subsequently calculate at each phase along the orbit the centroid, width and density of debris that material tidally stripped over time must have under some assumptions for the mass-loss history of the disrupting object. This was first done using approximate, analytic expressions for debris morphology, derived from energy and angular momenta considerations alone (as outlined above and in more detail in Johnston 1998; Johnston et al. 2001). Helmi and White (1999) instead followed how the density of a single packet of debris (i.e. unbound at the same point in time and at the same orbital phase) evolved using an action-angle formalism. More

recently, Bovy (2014) and Sanders and Binney (2014) have built models in actionangle space, where the full phase-space distribution of a stream can be predicted by calculating the expected offset in angles at a given orbital phase from a single orbit integration. These latter models have the advantage over models built around energy and angular momenta in that they are also applicable to non spherical potentials and rely on a precise mapping rather than approximate scalings to calculate widths and offsets. However, they do rely on having methods to calculate actions and angles in arbitrary potentials, which introduce an additional layer of both complications and approximations (see Bovy 2014; Sanders and Binney 2014).

A second approach, slightly more computationally expensive but applicable to arbitrary potentials, is to integrate the satellite orbit and, at each time-step, release a set of particles to represent the stars lost at that time. At the point of release, the positions and velocities of the debris particles relative to the satellite are chosen to collectively reproduce the orbital distributions seen in full N-body simulations (e.g. as illustrated in Fig. 6.6). The particles' subsequent orbital paths in the combined field of the host and satellite can then be simply calculated using test-particle integration. At any point in time the integration can be stopped and the phase-space distribution of the particles be used to trace the resultant shells and streams. This simple approach has been used both for debris modeling (Yoon et al. 2011; Küpper et al. 2012) and potential recovery (Varghese et al. 2011; Gibbons et al. 2014).

6.4 Morphologies of Individual Debris Structures in Observable Co-ordinates

A broad summary of the dependencies of debris structures can be drawn from the physical models outlined in the previous section (and by inspection of Fig. 6.2):

- The *orbit* of the progenitor satellite sets the large-scale morphology of the debris structure.
- The *mass* of the satellite sets the scales over which debris is distributed.
- The *time* since the satellite starts losing stars determines the degree to which the debris is phase-mixed.

Armed with these descriptions we can now go on to interpret observations of debris structures in terms of the history of the progenitor satellite. There is a rich literature with exact models (typically based on N-body simulations) of individual structures (Johnston et al. 1995; Velazquez and White 1995; Helmi and White 2001; Peñarrubia et al. 2005). Here we instead discuss in principle how and why these models are uniquely sensitive to progenitor properties.

Note that the potential of the parent galaxy also affects debris properties, so debris can also be used to constrain the mass distribution in the Milky Way. This will be discussed in Chap. 7.

154 K.V. Johnston

6.4.1 Young Debris

As debris ages, it spreads further and further apart in orbital phase away from the progenitor along its orbit, overall decreasing in density over many orbits. The debris is considered *fully phase-mixed* once it fills the configuration-space volume defined by the progenitor's orbit. For example, for an eccentric orbit in a spherical potential, fully phase-mixed debris would be a spread over a (near-planar) annulus with inner and outer radii corresponding to the pericenter and apocenter of the parent satellite's orbit. For a loop orbit in a potential where the orbital plane precesses, the debris would fill a three-dimensional donut shape. For a given orbit, debris becomes fully phase-mixed much more rapidly for more massive progenitor objects.

The term "young debris" is used to refer to structures that have *not* had time to fully phase-mix and are apparent as distinct spatial overdensities in star-count maps, such as the Sagittarius and Orphan streams, and the GD-1 and Pal 5 globular cluster streams. These have been found at distances of 10–100 kpc from the Sun where the background stellar density is low enough for such low surface brightness features to be apparent and orbital timescales sufficiently long for mixing not to have proceeded far during the lifetime of the Galaxy.

As illustrated in Fig. 6.1, streams result from satellite destruction along mildly eccentric orbits. In these cases, the spreading due to differences in turning point precession (Ψ_l , see Eq. (6.10)) is much smaller than the initial angular width of the stream (of order $sR \sim r_{\rm tide}$) for many orbits and always less than the spreading along the orbit due to differences in orbital time (Ψ_e , see Eq. (6.9)). Hence the *width* of a stream is an indication of the progenitor mass. Once the mass is known, the age of the debris (or time since the satellite first started losing stars) can be estimated from the *length* of the streams.

Shells result from destruction along more eccentric orbits. There have been extensive studies of the properties and interpretation of shell systems seen around external galaxies (Quinn 1984; Sanderson and Helmi 2013), though these have largely concentrated on structures formed along almost radial orbits. The transition between conditions that produce stream-like or shell-like morphologies primarily depends on orbital eccentricity (e.g. Johnston et al. 2008, found this to occur on orbits where $L/L_{\rm circ} \sim 0.3-0.5$), but also depends on satellite mass and time since disruption. Both stream-like and shell-like morphologies can occur in the same structure in this transition region. For a given mass and orbit, streams are most apparent in the early stages of evolution as the spreading along the orbit that produces them (i.e. as estimated by Ψ_e in Eq. (6.9)) typically occurs more rapidly than the differential precession of the apocenters that gives rise to shells (i.e. as estimated by Ψ_l in Eq. (6.10)). However, along the more eccentric orbits, the rapid passage of debris through pericenter significantly reduces the density at these orbital phases and the apparent angular extent of contiguous streams can be effectively limited by the angular size subtended by the region around the apocenter of the orbit where debris spends most of its time (estimated in Hendel and Johnston 2015, as the angle centered on apocenter where the satellite orbit spends half of its time, α

in Fig. 6.3). Under these circumstances, a single disruption event can produce what appear to be distinct structures, centered at two or more orbital apocenters with orbital precession becoming the dominant effect that dictates the apparent angular spread around each one. The time at which these structures start taking on shell-like characteristics can be estimated by finding when Ψ_l is greater than α . (See also Amorisco 2015, for an independent discussion of these effects.)

6.4.2 Fully Phase-Mixed Debris

Despite the low density and lack of spatial coherence of fully phase-mixed debris, its presence can often still be detected. For example, Liouville's theorem states that the flow of points through phase-space is *incompressible*: that the phase-space density of debris remains constant in time even as it evolves to form streams and shells. An inevitable consequence is that debris must become locally more concentrated in velocity space even as it becomes more diffuse in configuration space (Helmi and White 1999). Hence, signatures of the disruption of satellites can remain apparent in catalogues of stellar velocities even if no spatial structures remain detectable. This idea was first conjectured by Olin Eggen (for a summary see Eggen 1987), who proposed that nearby moving groups of stars could be the remnant of long-dead star clusters. In Chap. 5 the more recent work on velocity substructure in the stellar halo (e.g. Xue et al. 2011; Schlaufman et al. 2009) is discussed in more detail.

Surveys with full phase-space information can exploit the fact that the orbital properties of the debris (e.g. their actions or frequencies) remain constant in a static potential. Helmi et al. (1999) were the first to apply this idea to data using the Hipparcos catalogue of proper motions and parallaxes to derive angular momenta and estimate energies for giant stars within 1 kpc of the Sun. They found $\sim\!10\,\%$ of the stars in their sample to be clumped in orbital-property space and concluded that $10\,\%$ of the local halo must be formed from an object similar to the dwarf galaxy Sagittarius being disrupted in the distant past.

Once larger samples with more accurate orbital properties are found in near-future surveys, Gómez and Helmi (2010) have shown how the ages of these structures might also be determined by looking for substructure in orbital properties within a group (see also McMillan and Binney 2008). To develop some intuition for this idea, consider the (incorrect) model of debris spreading exactly along a single orbit. In the early stages of mixing the local volume will contain just one wrap of the debris stream at one orbital phase. As the debris spreads, the local volume will gradually fill with more and more wraps. The spreading itself is caused by the debris having a range of orbital properties. Hence, each wrap of the debris within the local volume will have different orbital properties and the degree and spacing of substructure within the orbital properties of the group gives an estimate of the age.

The beauty of using orbital properties to identify debris members is that stars can be connected even if they have no clear association in velocity or configuration space alone. For example, looking to the future, combining a distance indicator with *Gaia*'s assessment of proper motions and radial velocities suggests that satellite remnants throughout the inner 100 kpc of the Milky Way might be identified using this method even if their members are spread on disparate planes and a wide range of radii.

6.5 Debris in a Cosmological Context: Modeling and Interpreting Properties of Stellar Halos

Within the current cosmological paradigm for structure formation, galaxies are thought to form, at least in part, hierarchically, with small galaxies forming first within small dark matter halos and gradually agglomerating to form larger galaxies within larger dark matter halos. Gas from this agglomeration process can dissipate and fall towards the center of the main halo to form a new generation of stars in the combined object. Unlike the gas, stellar orbits are dissipationless, so, once stripped, the stellar populations of infalling galaxies can be left behind orbiting in the halo of the galaxy. Of course, the orbits of infalling galaxies are affected by dynamical friction. For those that are more massive than a few percent of the parent this can lead to significant evolution within a few orbital periods so stars from these objects can potentially make a minor addition to the central stellar galactic components that are forming from the in situ gas (i.e. spheroid or disk, as seen in the hydrodynamic simulations of Abadi et al. (2006)). In contrast to the spheroid and disk, stellar halos are a great place to look for stars that have been accreted from other objects. Current models and data favor a picture where a significant fraction—and possibly all—of the stars in the halo originally formed in other objects.

The accreted nature of at least a significant fraction of stars in galactic halos suggests their observed properties can be used to address a number of questions. Cosmological parameters dictate the nature of hierarchical clustering: the frequency and epoch of infall of dark matter halos of different mass-scales and their orbital properties. In other words, the cosmology sets the parameters discussed in Sect. 6.4 that fully specify the type and number of tidal disruption events that have occurred. Hence, adopting a given cosmology (with the addition of some assumptions for how stars occupy different dark matter halos) leads to specific expectations for the level of substructure due to accretion within stellar halos (Sect. 6.5.1) as well as chemical trends between substructure and field stars (Sect. 6.5.2.2). These understandings can be exploited now and in the future to understand to what extent the distribution on the Milky Way's stellar halo matches our expectations (Sect. 6.5.3.1), and what we can learn about our accretion history from the extent and properties of substructure (Sect. 6.5.3.2). In turn—identifying stars that were originally formed in other objects at much higher redshift offers a unique perspective on the stellar populations in these galactic progenitors (Sect. 6.5.3.3).

6.5.1 Cosmological Simulations of Stellar Halo Formation

Stellar halos are hard to observe because they contain a tiny fraction of stars (and an even tinier fraction of the total mass) in a galaxy, spread out over a large volume. Moreover, surveys need to be sensitive to even smaller fractions of stars to learn about substructure within these halos, and the presence of this substructure makes it challenging to characterize the global characteristics of the halo itself. Early discussions were largely restricted to global properties and formations scenarios (e.g. see classic works by Eggen et al. 1962 and Searle and Zinn 1978) extrapolated from either local studies of high-velocity stars, larger volume surveys with tracer populations where distances could be estimated, or pencil beam surveys. The field has been revolutionized in the last two decades with the emergence of large-scale stellar surveys covering a significant fraction of the sky, such as the Sloan Digital Sky Survey (Abazajian et al. 2003) and the Two Micron All Sky Survey (e.g. Majewski et al. 2003).

Models of stellar halos face the same challenges as the observations in resolving such a tiny component of the galaxy, as well as substructure within it. One approach is to restrict attention to only stars that have been accreted from other systems and hence avoid the need to follow gas physics and ongoing star formation explicitly. Bullock et al. (2001) presented a first attempt by combining a semi-analytic, generative model of tidal disruption events (developed in Johnston 1998, and outlined in Sect. 6.3.3.2 above) with merger histories for Milky-Way like galaxies predicted in a cosmological context using the Press-Schechter formalism (Lacey and Cole 1993). These models showed abundant substructure in the model halos, which was coincidentally being mapped by SDSS in the real stellar halo. Bullock and Johnston (2005) made the next step to a more sophisticated approach by replacing the simple generative model of each disruption event with an N-body simulation to represent the dark matter evolution of the infalling object. Stars were "painted" onto the purely dark matter satellites by assigning a variable weight or mass-to-light ratio to each N-body particle. The weights were chosen in such a way that the properties of the latest infalling objects matched the internal spatial and velocity distributions observed for stars in nearby dwarf galaxies. The Bullock and Johnston (2005) models were limited in that the parent galaxy was represented by (slowly evolving) analytic functions and the results of the separate simulations were superposed only at the present time to make a stellar halo model. Hence they did not include either the influence of the accreting objects on the parent or on each other. Nor did they represent the cosmological context (such as preferential infall along filaments or global tidal influences due to nearby neighboring structures). Computational power is now such that full self-consistent N-body simulations of the formation of a Milky Way sized dark-matter halo are sufficiently resolved to address this limitation and there are now several example of stellar halo models made by painting stars onto these more realistic backdrops (De Lucia and Helmi 2008; Cooper et al. 2010; Lowing et al. 2015).

Of course, the ultimate goal is to simultaneously build a model of all components of a galaxy (dark matter along with stellar and gaseous components) using cosmological hydrodynamical simulations of structure formation capable of following the baryonic as well as dark matter physics. There are several examples already in the literature where the stellar halo components have been resolved in these models and their characteristics and history discussed (Abadi et al. 2006; Zolotov et al. 2009; Font et al. 2011; Tissera et al. 2013). In particular, these models drop the assumption that all stars in the halo come from accretion events and allow an exploration of how much of the stellar halo might have instead formed in situ. However, the properties of the stellar halos vary systematically between the simulations, as prescriptions for star formation and feedback also vary, so the results at this point seem indicative rather than conclusive.

For the remainder of this section we concentrate solely on the accreted component of the stellar halo and illustrate some general results common to all the models using the Bullock and Johnston (2005) simulations.

6.5.2 General Results of Cosmological Accretion Models

6.5.2.1 Accreted Phase-Space Structure in Halos

Figure 6.7 shows one of the Bullock and Johnston (2005) purely-accreted stellar halo models from external viewpoints, in space and velocity. The simplicity of the model permits sensitivity to both small as well as low surface brightness substructures within the halo. Generic features of this (and other) models are: a smooth, fully phase-mixed inner region; abundant substructure in the outer parts, detectable both in space and velocity; and an increasing prevalence of the substructure with Galactocentric radius. Beyond the phase-mixed inner regions, such model halos typically appear dominated by a handful of striking shells and streams, with shells tending to be more prevalent at the largest distances and streams in the intermediate parts (Johnston et al. 2008).

These generic features can broadly be explained in the context of the current cosmological expectations which suggest a history for the Milky Way where: (1) the majority of accretion events occurred more than 7–8 Gyrs ago; (2) the events had a range of luminosities associated with them; and (3) the accretions occurred on a mixture of orbits. Figure 6.8 illustrate this with external views of model halos, constructed by Johnston et al. (2008), that are instead built entirely from: (1) ancient or recent accretion events (left panels); (2) high or low luminosity events (middle panels); and (3) events evolving on high or low eccentricity orbits (right panels). The consequences of these differences are obvious with a simple visual comparison of the panels and can be easily explained with the physical intuition developed in Sects. 6.3 and 6.4: younger/older halos are more/less substructured because of the time available for phase-mixing; larger/smaller substructures correspond to higher/lower luminosity events because the total mass sets the tidal scales

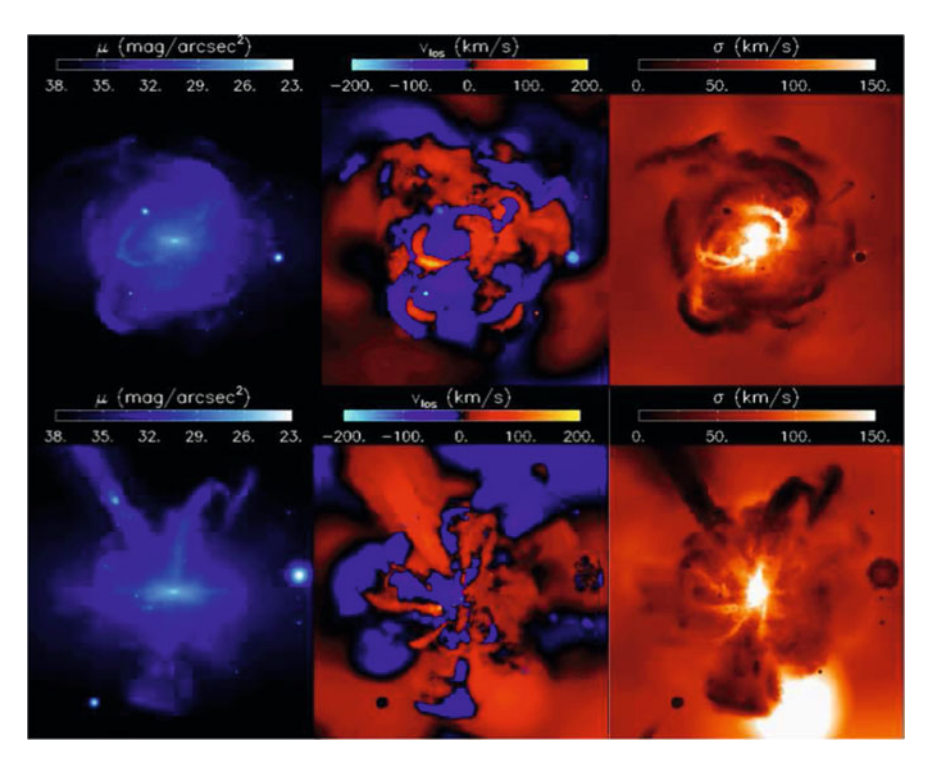


Fig. 6.7 Surface brightness (*left*), line-of-sight velocity (*middle*) and velocity dispersion (*right*) from external views of two stellar halo models built entirely from accretion events drawn from a merger history consistent with our current expectations (from Bullock and Johnston 2005; Johnston et al. 2008). Each box is 300 kpc on a side. Only the stellar halo component is shown. Image credit: Sanjib Sharma

at distruption; and the orbit distribution dictates the debris morphology because more/less eccentric orbits tend to produce shells/streams.

6.5.2.2 Accreted Stellar Populations in Halos

Figure 6.9 shows an alternative visualization of the model stellar halos shown in Fig. 6.7, but with the grid points color coded by the average metallicity and $[\alpha/\text{Fe}]$ abundance ratio along the line-of-sight. These were derived by assigning a simple star formation history to each infalling dwarf and running a leaky-accreting box model to estimate the associated chemical evolution (Robertson et al. 2005; Font et al. 2006). The parameters of the chemical evolution models were tuned to reproduce known properties of dwarf galaxies in the Local Group today—the observations that more luminous dwarfs tend to be more metal rich (e.g. Grebel et al. 2003), and that all nearby objects contain α -poor populations (e.g. Venn et al. 2004). Star formation was truncated in each dwarf at the time when it was

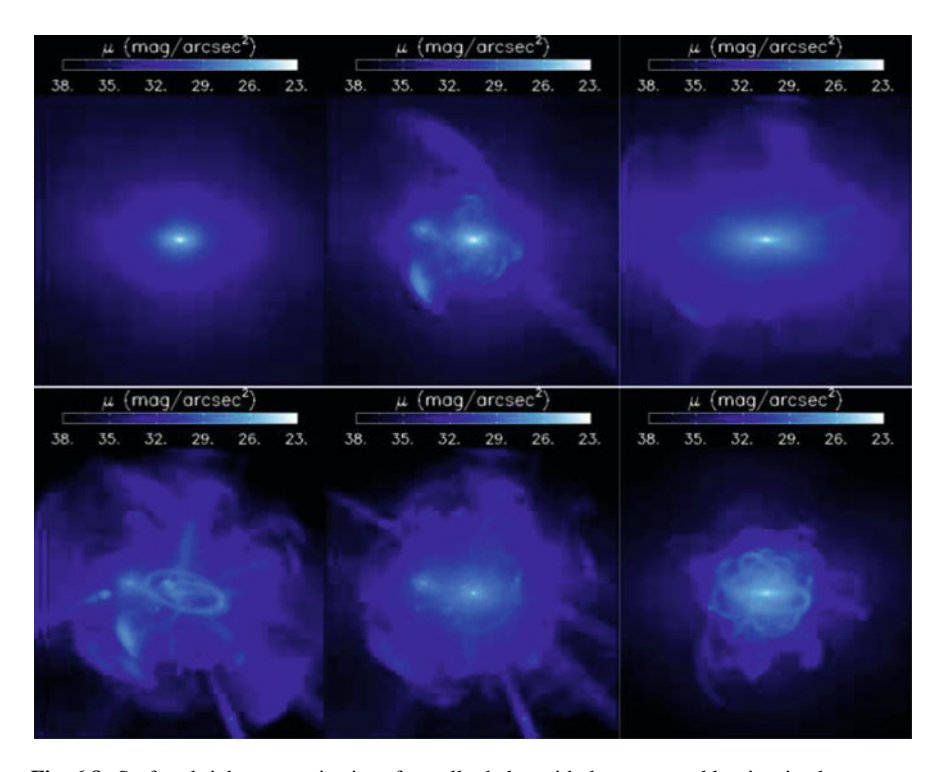


Fig. 6.8 Surface brightness projections for stellar halos with the same total luminosity, but merger histories that were artificially constrained to be dominated by different types of accretion events (following Johnston et al. 2008). In the *left panels*, the events had the same luminosity and orbit distributions, but were either all accreted a long time ago (*upper panel*) or recently (*lower panel*). In the middle panels, the events had the same accretion time and orbit distributions, but were either all of high (*upper panel*) or low (*lower panel*) luminosity. In the *right panels*, the events had the same accretion time and luminosity distributions, but were either all on near-radial (*upper panel*) or near-circular (*lower panel*) orbits. Image credit: Sanjib Sharma

accreted onto the Milky Way, as might be expected given that dwarfs near larger galaxies are observed to be quenched relative to their field counterparts (Grebel et al. 2003; Geha et al. 2012). The last attribute of the model effectively means that the cosmological framework also influences the nature of the stellar populations in accreted components of galactic stellar halos, setting the characteristic time over which star formation can occur.

In the left-hand panels of Fig. 6.9 the mass-metallicity relation is apparent, as the largest and most dominant debris structures tend to be the most metal rich. The influence of the cosmological background is apparent in the right-hand panels; the smooth stellar halo component is α -enhanced relative to both surviving satellites and the brighter debris features. Physically this trend can be attributed to the relative delay expected following star formation of Type Ia Supernovae (SNe) compared to Type II SNe. The progenitors of Type II SNe are massive stars, whose deaths

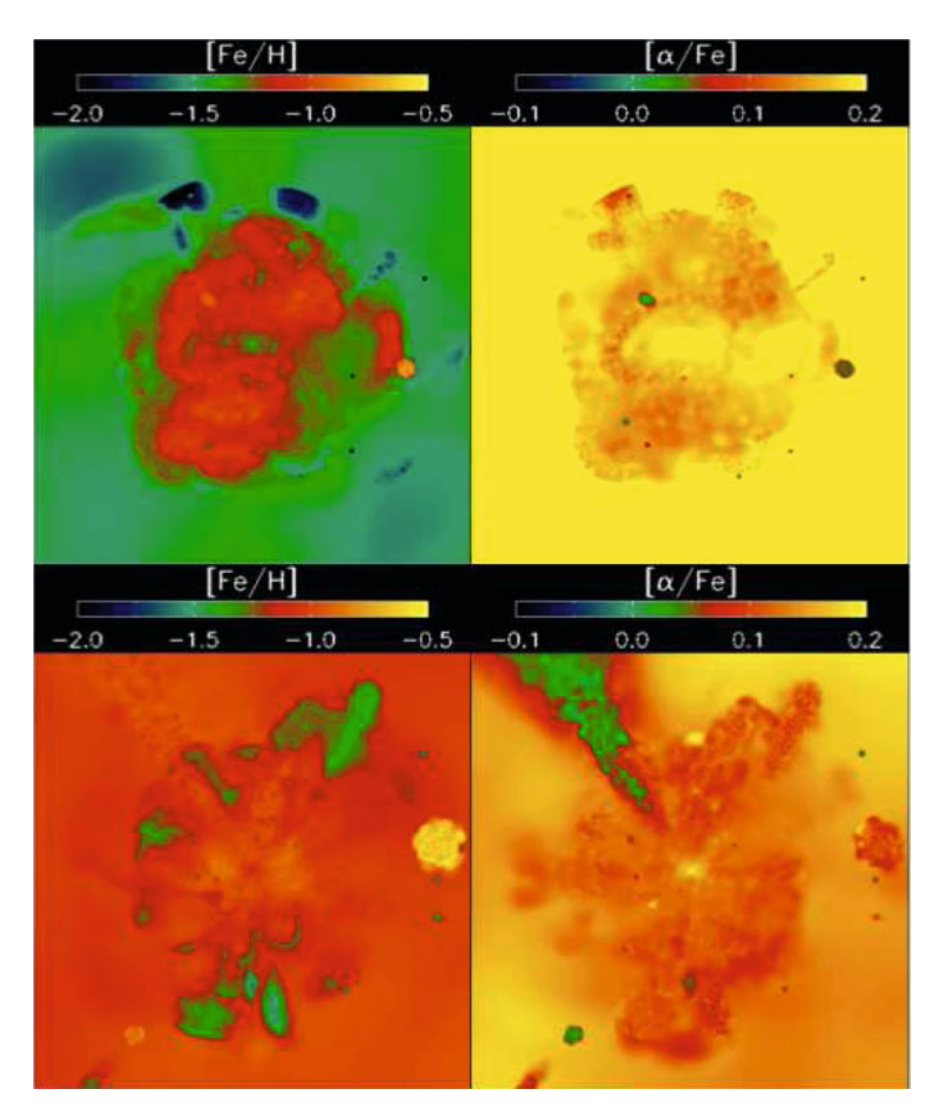


Fig. 6.9 Average [Fe/H] and $[\alpha/\text{Fe}]$ projected along the line-of-sight for the two stellar halo models shown in Fig. 6.7 (using chemical model developed in Robertson et al. 2005; Font et al. 2006). Image credit: Sanjib Sharma

produce both iron and α -elements, within a few million years of a star formation event. In contrast, Type Ia SNe, producing mainly iron, arise from the explosion of an accreting white dwarf star—objects which will not form for hundreds of millions of years after a star formation event. Hence, the oldest stellar populations in infalling dwarf galaxies are not expected to have been polluted by SNe Type Ia and should be rich in α elements, while younger populations will be relatively α -poor. In our accreted halo model, the smooth, fully phase-mixed portion of the

halo comes from early infalling objects that do not have a chance to ever make the younger populations. In contrast, these younger populations are apparent in more recently destroyed objects or surviving satellites that generally fell in even more recently. Zolotov et al. (2010) points to analogous trends in α element patterns when contrasting hydrodynamic simulations of the formation of galaxies with differing merger histories.

Distinctions between the chemical properties of field stars in the halo and satellite galaxies that have been known about for some time (Unavane et al. 1996; Venn et al. 2004) can naturally be explained within this cosmological context (Robertson et al. 2005; Font et al. 2006). Moreover, studies of stellar populations in the satellites, stellar halo and debris around M31 suggest this scenario can also be applied to understand variations there (see, e.g., Font et al. 2008; Gilbert et al. 2009, and Chap. 8).

6.5.3 Implications and Applications

6.5.3.1 Statistical Comparisons with Observations

As discussed in the previous section, combining our cosmological picture of how structures form in the Universe with tidal disruption and chemical evolution models leads to some specific expectations for phase-space and stellar population characteristics of debris structures as well as some general trends. Both the characteristics and trends are broadly consistent with current observational surveys. However, the stochastic nature of hierarchical structure formation means that there is large variation about the average properties among the stellar halo models produced and more quantitative comparisons employing a statistical approach are just starting.

The average spatial structure of the stellar halo, as well as the level of substructure within it, can be assessed using large scale photometric catalogues of stars. For example: Bell et al. (2008) fitted triaxial, power-law models to star counts of mainsequence turnoff stars selected from SDSS and also quantified the level of deviations around these smooth models; and Sharma et al. (2010) exploited the distinct colors of metal-rich, evolved stars in the 2MASS filters (following Majewski et al. 2003) to select distant M-giant stars and ran a group-finding algorithm on the selection in the space defined by their angular position and apparent magnitude (from Sharma and Johnston 2009). In both studies, the analyses were repeated on equivalent synthetic stellar samples generated from the simulated stellar halos of Bullock and Johnston (2005). The results (both numbers and scales of groups and level of deviations from a smooth model) varied significantly between the eleven different simulated stellar halos, with the results from the analysis of real data sitting within this spread. While this agreement is encouraging, when Helmi et al. (2011) repeated the Bell et al. (2008) analysis on the Cooper et al. (2010) model stellar halos (which were derived by "painting" stars in the "Aquarius" self-consistent dark matter simulations), they found systematically larger deviations from a smooth background than the prior

work at a level that was inconsistent with the observations. Recent work by Bailin et al. (2014) contrasting simulations with and without Galactic disk components suggest that this inconsistency with both observations and the Bullock and Johnston (2005) work might be attributed to the Aquarius simulations lacking the extra potential structure due to the disk.

Following photometric surveys with spectroscopic surveys allows assessments of the level of spatially correlated velocity substructure (e.g., using K-giants in the *Spaghetti Survey*, metal-poor MSTO stars from SEGUE, or BHBs from SDSS, see Starkenburg et al. 2009; Schlaufman et al. 2009; Xue et al. 2011). Currently, comparisons to models seem consistent, but again not conclusive (Xue et al. 2011).

Stellar populations in accreted halos are expected to exhibit spatial variation. These spatial variations have been found photometrically (by looking at the ratio of MSTO to BHB stars across the sky in the SDSS catalogue, see Bell et al. 2010) and spectroscopically (Schlaufman et al. 2012). In particular, Schlaufman et al. (2011, 2012) looked at the Fe- and α - element abundances of the velocity substructures they had found, and concluded that they tended to be chemically distinct from the smooth stellar halo, having systematically higher metallicity and lower [α /Fe], as might be expected for more recently accreted objects (Font et al. 2008). Analogous studies have also found these variations in M31 (Richardson et al. 2008; Gilbert et al. 2009; Bernard et al. 2015).

6.5.3.2 Recovering Accretion Histories

If stars, which may now spread throughout our dark matter halo, can be connected in such a way as to reassemble their original associations with infalling satellites, then the understanding of debris evolution outlined in Sect. 6.3 might be applied to learn about the original masses, orbits and infall times of those satellites. Collectively, these reconstructed groups might tell us the accretion history of our Galaxy from the stellar halo.

Several approaches have been proposed to attempt this reconstruction. Conceptually, the simplest is to take a sample of a single type of star (i.e. with restricted absolute magnitude range) from a large-scale photometric catalogue (e.g. M-giant stars from 2MASS or MSTO and BHB stars from SDSS) and search for groups in the 3-D space of angular position and apparent magnitude (e.g. Sharma et al. 2010). This approach is only effective for more recent accretion events (last several billion years) since earlier events have time to phase-mix and are not apparent as separate spatial groups. Exactly how far back in time, and the lowest luminosity of objects that might be recovered depends on the scale and depth of the survey as well as the stellar population that it is sensitive to Sharma et al. (2011a).

Helmi and White (2001) proposed a much more powerful approach to recovering stars from early events, but also one that requires rather more data dimensions. If the full six dimensions of phase-space can be measured for stars, then (within a given potential) their orbital properties can be calculated. In a static potential, while they spread out over time in phase-space, they will conserve their orbits and

hence remain as a group in the space of orbital characteristics (e.g. energy and actions) indefinitely. Several studies have analyzed prospects for *Gaia* in this context (Gómez et al. 2010; Sharma et al. 2011b; Gómez et al. 2013).

One limitation to identifying satellite members by using observed orbital properties is defining what those properties are: it is as yet unclear whether the Milky Way can be represented by an integrable mass distribution in which actions can be derived. Moreover, the potential of the Milky Way is time-evolving and this can scatter debris stars away from their original orbits. However, stars can also "remember where they came from" in other ways: their chemical abundances reflect the gas cloud in which they are born. Freeman and Bland-Hawthorn (2002) proposed that, given a large enough sample of high-resolution spectra of disk stars, this chemical memory could be exploited to measure the history of star formation in the disk: while stars might be spread throughout the six-dimensional phase-space volume occupied by the disk, those born in the same cluster would all lie at a single location in the *N*-dimensional space of chemical abundances. These distinct chemical abundance patterns could be used to regroup them in their original birth clusters—an approach that Freeman and Bland-Hawthorn (2002) dubbed *chemical tagging*.

While stellar populations in satellite galaxies are spread out over a range of abundances (i.e. a small volume in *N*-dimensional chemical abundance space), the trends with satellite mass and assumed accretion time already seen in observations and simulations suggest that an analogous *chemical tagging* might work in the halo—perhaps not to reconstruct the exact objects from which stars came, but at least to look at the numbers of satellites of a given luminosity that might have accreted onto the Milky Way at different times. And, since the composition of a star cannot be erased by any dynamical evolution, this approach might work to recover the luminosity function of the very earliest infalling objects. Preliminary studies of how feasible this idea is to implement in practice are only just coming to fruition (Lee et al. 2015).

6.5.3.3 Accreted Populations as a Window on Galaxy Formation over Cosmic Time

Reconstructing the accretion history of our Galaxy is an exciting goal in itself, but it also opens up other possibilities. If we can find the stars—or at least identify the stellar populations—from similar-mass, long-dead objects infalling into the Milky Way at earlier epochs, this can give us a unique window on what baryons were doing in galaxies over cosmic time. In particular we can study baryons in the high-redshift progenitors of Milky-Way-type galaxies that may be impossible to see in situ even with the next generation of space telescopes (Okrochkov and Tumlinson 2010). In fact, the stellar populations in the Milky Way's halo today were originally formed in potential wells of many different depths (from the expected mass-spectrum of infalling dark matter halos) and that formed stars for different lengths of times (dictated by the spread in accretion times for those smaller halos onto the main

Milky Way halo). Moreover, these infalling halos may have formed in a variety of environments as later infalling objects are expected to be spread out over a larger volume at early times compared to earlier infalling objects (see Corlies et al. 2013). Indeed, the difference between the abundance patterns in low-metallicity stars in the halo and those observed in several ultra-faint dwarf satellites of the Milky Way can be attributed to differences in the degree to which they evolved in chemical isolation in the early Universe (see Lee et al. 2013, for a discussion). Hence, the study of detailed chemical abundances of stars in the halo can tell us not just about our own Galaxy, but about the properties of stellar populations in many smaller galaxies over cosmic time.

6.6 Summary of Status and Prospects

Overall, the discovery (over the last two decades) of debris structures encircling our Galaxy has motivated the development of a fairly sophisticated understanding of and tools for modeling debris structures. Putting these models and observations in a cosmological context has led to a dramatic, local confirmation of the hierarchical contribution to structure formation on small-scales: there is broad agreement between the models and data with the picture that a large fraction of our stellar halo results from the accretion of smaller systems. However, the wide variety of possible accretion histories means that this demonstration itself, while interesting, does not place strong constraints on cosmological models.

Two aspects of studies of debris around the Milky Way remain ripe for further exploration with near-future data. First, we can use stars from disrupted satellites to recover the accretion history of our Galaxy. The unbound structures apparent in current data sets represent the most dominant events accreted in the last several billion years. Data sets that will be available in the near future will enable the identification of debris that is either older (i.e. more fully phase-mixed) and from lower luminosity objects, both because of the large numbers of stars that will be catalogued (e.g. by Gaia) and because of the additional data dimensions that will have accurate measurements (e.g. proper motions from Gaia and detailed chemical abundances from the GALAH survey). Most importantly, the additional data dimensions will allow the calculation of quantities that are likely to be conserved during the lifetime of the stars (e.g. orbital properties such as energy and actions as well as chemical composition), which will further enable the "tagging" of these stars into the groups in which they originally formed. We can look forward to using these approaches to look much further back to the very earliest epochs of galaxy formation using stellar surveys.

While the accretion history of our Galaxy will play a key part in understanding the specific story of its formation and evolution, it is unlikely to have broader implications for the histories of other Milky-Way-sized galaxies, which are expected to have accretion histories that vary widely. However, a by-product of the accretion history will be the luminosity function of smaller infalling galaxies, along with 166 K.V. Johnston

the identification of stellar populations associated with these different mass objects looking back to the higher redshifts at which they were accreted. Such small galaxies will be very hard (if not impossible) to observe at higher redshift even with the next generation of telescopes. Hence the second aspect of debris studies that should be further explored is what we can learn about the evolution of dwarf galaxies over cosmic time from our stellar halo. In particular, what can the stellar populations tell us about the baryonic physics of galaxy formation within small dark matter halos—the processes of gas inflow, star formation, and feedback that remain key challenges in understanding galaxies in the Universe today?

Acknowledgements KVJ gratefully acknowledges David Hendel's work in generating the simulations and related figures used in Sect. 6.3 of this chapter. KVJ thanks her postdocs and graduate students for invaluable discussions through out the year (Andrea Kuepper, Allyson Sheffield, Lauren Corlies, Adrian Price-Whelan, David Hendel and Sarah Pearson). Her work on this volume was supported in part by NSF grant AST-1312196.

References

Abadi, M. G., Navarro, J. F., & Steinmetz, M. 2006, MNRAS, 365, 747

Abazajian, K., Adelman-McCarthy, J. K., Agüeros, M. A., et al. 2003, AJ, 126, 2081

Amorisco, N. C. 2015, MNRAS, 450, 575

Bailin, J., Bell, E. F., Valluri, M., et al. 2014, ApJ, 783, 95

Bell, E. F., Zucker, D. B., Belokurov, V., et al. 2008, ApJ, 680, 295

Bell, E. F., Xue, X. X., Rix, H.-W., Ruhland, C., & Hogg, D. W. 2010, AJ, 140, 1850

Bernard, E. J., Ferguson, A. M. N., Richardson, J. C., et al. 2015, MNRAS, 446, 2789

Binney, J., & Tremaine, S. 2008, Galactic Dynamics: Second Edition, by James Binney and Scott Tremaine. ISBN 978-0-691-13026-2 (HB). Published by Princeton University Press, Princeton, NJ USA, 2008.

Bovy, J. 2014, ApJ, 795, 95

Bullock, J. S., Kravtsov, A. V., & Weinberg, D. H. 2001, ApJ, 548, 33

Bullock, J. S., & Johnston, K. V. 2005, ApJ, 635, 931

Choi, J.-H., Weinberg, M. D., & Katz, N. 2009, MNRAS, 400, 1247

Cooper, A. P., Cole, S., Frenk, C. S., et al. 2010, MNRAS, 406, 744

Corlies, L., Johnston, K. V., Tumlinson, J., & Bryan, G. 2013, ApJ, 773, 105

Dehnen, W., & Read, J. I. 2011, European Physical Journal Plus, 126, 55

De Lucia, G., & Helmi, A. 2008, MNRAS, 391, 14

Eggen, O. J., Lynden-Bell, D., & Sandage, A. R. 1962, ApJ, 136, 748

Eggen, O. J. 1987, NATO ASIC Proc. 207: The Galaxy, 211

Eyre, A., & Binney, J. 2011, MNRAS, 413, 1852

Font, A. S., Johnston, K. V., Bullock, J. S., & Robertson, B. E. 2006, ApJ, 638, 585

Font, A. S., Johnston, K. V., Ferguson, A. M. N., et al. 2008, ApJ, 673, 215

Font, A. S., McCarthy, I. G., Crain, R. A., et al. 2011, MNRAS, 416, 2802

Freeman, K., & Bland-Hawthorn, J. 2002, ARAA, 40, 487

Geha, M., Blanton, M. R., Yan, R., & Tinker, J. L. 2012, ApJ, 757, 85

Gibbons, S. L. J., Belokurov, V., & Evans, N. W. 2014, MNRAS, 445, 3788

Gilbert, K. M., Font, A. S., Johnston, K. V., & Guhathakurta, P. 2009, ApJ, 701, 776

Gómez, F. A., & Helmi, A. 2010, MNRAS, 401, 2285

Gómez, F. A., Helmi, A., Brown, A. G. A., & Li, Y.-S. 2010, MNRAS, 408, 935

Gómez, F. A., Helmi, A., Cooper, A. P., et al. 2013, MNRAS, 436, 3602

Grebel, E. K., Gallagher, J. S., III, & Harbeck, D. 2003, AJ, 125, 1926

Helmi, A., & White, S. D. M. 1999, MNRAS, 307, 495

Helmi, A., White, S. D. M., de Zeeuw, P. T., & Zhao, H. 1999, Nature, 402, 53

Helmi, A., & White, S. D. M. 2001, MNRAS, 323, 529

Helmi, A., Cooper, A. P., White, S. D. M., et al. 2011, ApJ Lett, 733, L7

Hendel, D. & Johnston, K. V. 2015, accepted for publication in MNRAS

Hernquist, L., & Ostriker, J. P. 1992, ApJ, 386, 375

Johnston, K. V. 1998, ApJ, 495, 297

Johnston, K. V., Spergel, D. N., & Hernquist, L. 1995, ApJ, 451, 598

Johnston, K. V., Sackett, P. D., & Bullock, J. S. 2001, ApJ, 557, 137

Johnston, K. V., Bullock, J. S., Sharma, S., et al. 2008, ApJ, 689, 936

Küpper, A. H. W., Lane, R. R., & Heggie, D. C. 2012, MNRAS, 420, 2700

Lacey, C., & Cole, S. 1993, MNRAS, 262, 627

Lee, D. M., Johnston, K. V., Tumlinson, J., Sen, B., & Simon, J. D. 2013, ApJ, 774, 103

Lee, D. M., Johnston, K. V., Sen, B., & Jessop, W. 2015, ApJ, 802, 48

Lowing, B., Wang, W., Cooper, A., et al. 2015, MNRAS, 446, 2274

Majewski, S. R., Skrutskie, M. F., Weinberg, M. D., & Ostheimer, J. C. 2003, ApJ, 599, 1082

McMillan, P. J., & Binney, J. J. 2008, MNRAS, 390, 429

Navarro, J. F., Frenk, C. S., & White, S. D. M. 1996, ApJ, 462, 563

Okrochkov, M., & Tumlinson, J. 2010, ApJ Lett, 716, L41

Peñarrubia, J., Martínez-Delgado, D., Rix, H. W., et al. 2005, ApJ, 626, 128

Quinn, P. J. 1984, ApJ, 279, 596

Richardson, J. C., Ferguson, A. M. N., Johnson, R. A., et al. 2008, AJ, 135, 1998

Robertson, B., Bullock, J. S., Font, A. S., Johnston, K. V., & Hernquist, L. 2005, ApJ, 632, 872

Sanders, J. 2012, MNRAS, 426, 128

Sanders, J. L., & Binney, J. 2014, MNRAS, 441, 3284

Sanderson, R. E., & Helmi, A. 2013, MNRAS, 435, 378

Schlaufman, K. C., Rockosi, C. M., Allende Prieto, C., et al. 2009, ApJ, 703, 2177

Schlaufman, K. C., Rockosi, C. M., Lee, Y. S., Beers, T. C., & Allende Prieto, C. 2011, ApJ, 734, 49

Schlaufman, K. C., Rockosi, C. M., Lee, Y. S., et al. 2012, ApJ, 749, 77

Searle, L., & Zinn, R. 1978, ApJ, 225, 357

Sharma, S., & Johnston, K. V. 2009, ApJ, 703, 1061

Sharma, S., Johnston, K. V., Majewski, S. R., et al. 2010, ApJ, 722, 750

Sharma, S., Johnston, K. V., Majewski, S. R., Bullock, J., & Muñoz, R. R. 2011a, ApJ, 728, 106

Sharma, S., Bland-Hawthorn, J., Johnston, K. V., & Binney, J. 2011b, ApJ, 730, 3

Starkenburg, E., Helmi, A., Morrison, H. L., et al. 2009, ApJ, 698, 567

Tissera, P. B., Scannapieco, C., Beers, T. C., & Carollo, D. 2013, MNRAS, 432, 3391

Unavane, M., Wyse, R. F. G., & Gilmore, G. 1996, MNRAS, 278, 727

Varghese, A., Ibata, R., & Lewis, G. F. 2011, MNRAS, 417, 198

Velazquez, H., & White, S. D. M. 1995, MNRAS, 275, L23

Venn, K. A., Irwin, M., Shetrone, M. D., et al. 2004, AJ, 128, 1177

Xue, X.-X., Rix, H.-W., Yanny, B., et al. 2011, ApJ, 738, 79

Yoon, J. H., Johnston, K. V., & Hogg, D. W. 2011, ApJ, 731, 58

Zolotov, A., Willman, B., Brooks, A. M., et al. 2009, ApJ, 702, 1058

Zolotov, A., Willman, B., Brooks, A. M., et al. 2010, ApJ, 721, 738

Chapter 7 Tidal Debris as a Dark Matter Probe

Kathryn V. Johnston and Raymond G. Carlberg

Abstract Tidal debris streams from galaxy satellites can provide insight into the dark matter distribution in halos. This is because we have more information about stars in a debris structure than about a purely random population of stars: we know that in the past they were all bound to the same dwarf galaxy; and we know that they form a dynamically cold population moving on similar orbits. They also probe a different region of the matter distribution in a galaxy than many other methods of mass determination, as their orbits take them far beyond the typical extent of those for the bulk of stars. Although conclusive results from this information have yet to be obtained, significant progress has been made in developing the methodologies for determining both the global mass distribution of the Milky Way's dark matter halo and the amount of dark matter substructure within it. Methods for measuring the halo shape are divided into "predictive methods," which predict the tidal debris properties from the progenitor satellite's mass and orbit, given an assumed parent galaxy mass distribution; and "fundamental methods," which exploit properties fundamental to the nature of tidal debris as global potential constraints. Methods for quantifying the prevalence of dark matter subhalos within halos through the analysis of the gaps left in tidal streams after these substructures pass through them are reviewed.

7.1 Introduction

Understanding how matter is distributed in galaxies is a fundamental problem in astronomy. In particular, cosmological simulations of structure formation within the standard Λ CDM model of the Universe suggest that the stars we see collected together as galaxies are surrounded by much more massive and extended dark matter halos. The simulations outline expectations for the average properties of halos, including their characteristic density profiles (Navarro et al. 1997) and triaxial

K.V. Johnston (⊠)

Columbia University, New York, NY, USA

e-mail: kvj@astro.columbia.edu

R.G. Carlberg

University of Toronto, Toronto, ON, Canada

shapes and orientations as a function of radius (Jing and Suto 2002). They also suggest that each Milky-Way-sized dark matter halo encompasses a swarm of satellite subhalos in numbers far greater than the number of observed satellite dwarf galaxies in the Milky Way halo (traditionally referred to as the "missing satellites" problem, see Moore et al. 1999; Klypin et al. 1999). While it is possible that the observed dwarf galaxies account for all of the largest of these satellite subhalos (though this is far from clear, see Boylan-Kolchin et al. 2011), a multitude of smaller halos (masses of order $10^7 M_{\odot}$ or less) are still predicted to exist for which observed counterparts have not been identified (see Sect. 7.3 for a more complete discussion).

The expectations for the structure of and substructure within dark matter halos from the cosmological simulations are in general hard to test with great accuracy since we currently observe dark matter only by its gravitational effects on stars, and the dark matter extends well beyond where the majority of the stars in any galaxy lie. Tracer populations such as planetary nebulae and globular clusters have been used to estimate global masses beyond the visible components of galaxies (Côté et al. 2003), while satellite systems are thought to provide some accounting of the substructure though it remains far from clear how complete and unbiased that accounting is (Tollerud et al. 2008). Some progress on the projected shapes, total masses and largest substructures within dark matter halos has come from gravitational lensing (Vegetti et al. 2010). This chapter outlines why tidal debris is considered a promising and sensitive probe of dark matter halos as well as the subhalos they are expected to contain. In particular, this chapter concentrates on debris around our own Milky Way galaxy since this is the one place in the Universe where we might hope to measure the three-dimensional structure of a dark matter halo, as well as be sensitive to the proposed multitude of lower mass subhalos that may not contain gas or stars.

Historically, the knowledge that stars in disk systems are moving on near-circular orbits has been exploited to sensitively measure their mass distributions—indeed, the first systematic studies of the rotation curves of galaxies promoted the idea that galaxies were dominated by dark matter rather than baryonic matter (Rubin and Ford 1970). Although the nature of the dark matter particles themselves has yet to be determined, the idea that the majority of the mass in the Universe is composed of particles that are so far not observed because they do not interact with light is generally accepted in the field.

Stars in tidal debris structures make excellent probes of the matter distribution around galaxies for analogous reasons to disk stars. Like disk stars, we know more about their orbits than we would know for a purely random population—we know that the stars in tidal streams were once all part of the same parent satellite galaxy, and consequently have a small range of orbital properties about the progenitor satellite's orbit. Moreover, to be detectable in a photometric study, these debris structures must lie well outside the bulk of the stars in the parent galaxy and hence typically probe a very different region of the dark matter halo than the bulk of the stars in a galaxy.

Images of *streams* of debris in particular suggest that stars lie close to a single orbit, and this gives some simple insight into why they are such sensitive potential probes. If the stars were actually on *exactly* the same orbit and you could measure

the positions \mathbf{x} and velocities \mathbf{v} of each, then the potential (up to the unknown, constant energy E of the orbit) would simply be $\Phi(\mathbf{x}) = E - v^2/2$. A more detailed discussion of methods for measuring the global potential is presented in Sect. 7.2.

The dynamical *coldness* of streams, as determined from the small velocity dispersions and narrow spatial cross sections observed for many streams, also provides simple insight into their use as substructure probes. This low temperature means that discontinuities in the debris on much smaller scales than the apparent orbital path can arise due to asymmetries in the potential that are also on much smaller scale than the global potential. This leads to the exciting possibility of using debris to detect substructures within the potential, such as those arising from the thousands of dark matter subhalos that are expected to be orbiting within the main halo. Direct evidence of a large number of dark subhalos would *solve* the missing satellite problem. The characteristic signatures that substructure may leave in streams are discussed in Sect. 7.3.

7.2 Using Tidal Debris to Probe the Global Potential

As indicated in the introduction, adopting the simplifying (but ultimately incorrect) assumption that debris *exactly* traces a single orbit allows us to develop some intuition for how this data might be used. We can expand this intuition a little more by considering properties of orbits in different potentials. For example:

- 1. Orbits in a *spherical* potential are purely planar, while in *oblate* potentials, the orbital plane itself precesses with time. Figure 7.1 illustrates this by showing the orbital path (in red) and orbital pole (i.e., direction of angular momentum, in blue) in 3-D (top panels) and projected onto the plane of the sky (as viewed from the center of the parent galaxy—bottom panels) for the same orbit in spherical (left panels) and oblate (right panels) potentials. In the spherical case, the orbit aligns with a single plane on the sky and the pole appears as a single point. In the oblate case, the precession of the orbital plane is apparent as the orbital path not aligning with a single great circle and the direction of the pole evolving in time.
- 2. Within the orbital plane, the precession of the angular position of apocenters reflects the radial density profile of the parent potential. Figure 7.2 (from Belokurov et al. 2014) shows this precession angle calculated for a variety of potentials and orbital eccentricities, with zero precession corresponding to the point-mass, Keplerian potential in which orbits are ellipses and the apocenters are coincident.
- 3. The *eccentricity* (or ratio of apocenter to pericenter) of the orbit for a given pericentric velocity is set by the overall depth of the potential.

We are now in a position to measure the attributes listed above for observed streams. For example, using debris from the (ongoing) destruction of the Sagittarius (Sgr) dwarf spheroidal (see Chap. 2 of this volume), we know the precession of the orbital plane (Majewski et al. 2003), the trends of velocity along the stream

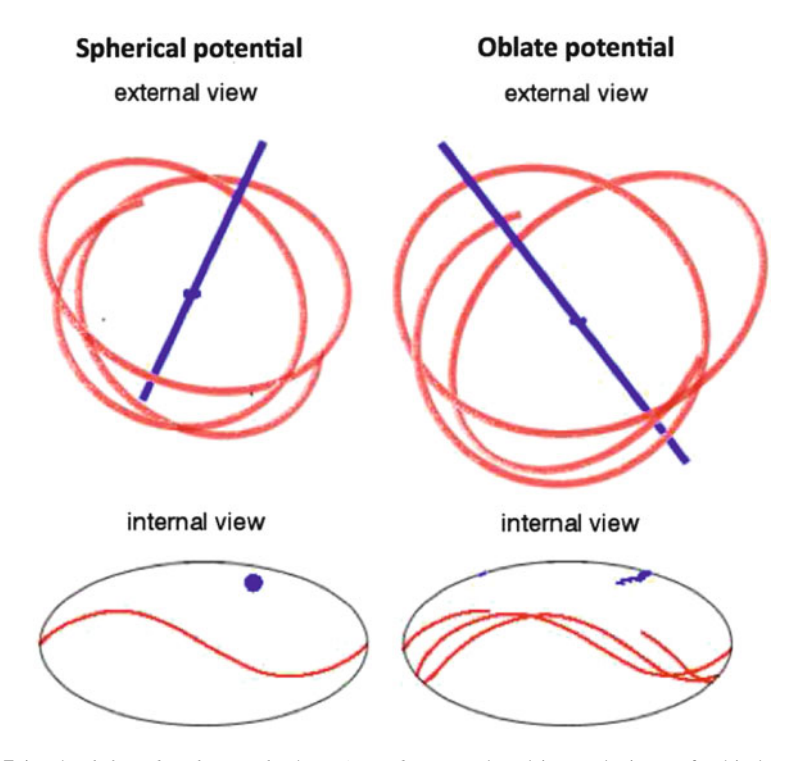


Fig. 7.1 The *left and right panels* show (*in red*) external and internal views of orbital paths in spherical and oblate potentials respectively. External views are as seen from outside the galaxy; the center of the galaxy is shown by a *small blue dot*. Internal views are Aitoff projection all-sky maps, as seen from the galaxy center. The direction of the orbital pole is shown by the *blue line* in external views and *blue dots* (in the oblate case a moving dot) in the internal views. The position of the pole changes over time for the oblate case due to the precession of the orbital plane, but the position of the pole does not change for the spherical case

(Majewski et al. 2004), as well as the angular separation between successive apocenters (Belokurov et al. 2014). It is this level of detailed data that has enabled the first attempt to reconstruct the three-dimensional shape and orientation of our Galactic dark matter halo (Law and Majewski 2010), or indeed of any galaxy in the Universe. However, significant controversy remains over what this reconstruction means, and this is inspiring a thorough and rigorous examination of how debris can robustly be used to measure potentials.

A multitude of approaches to exploiting our rich debris data sets to measure potentials have been proposed. They can be very broadly divided into two categories:

Predictive models predict the exact six-dimensional phase-space position and density of tidal debris from the progenitor's properties, orbit and parent galaxy potential. It is trivial to project the predictions of these models from phase-space to observables and hence to perform the comparison of data and model in coordinates where error distributions are well-understood. Hence these methods

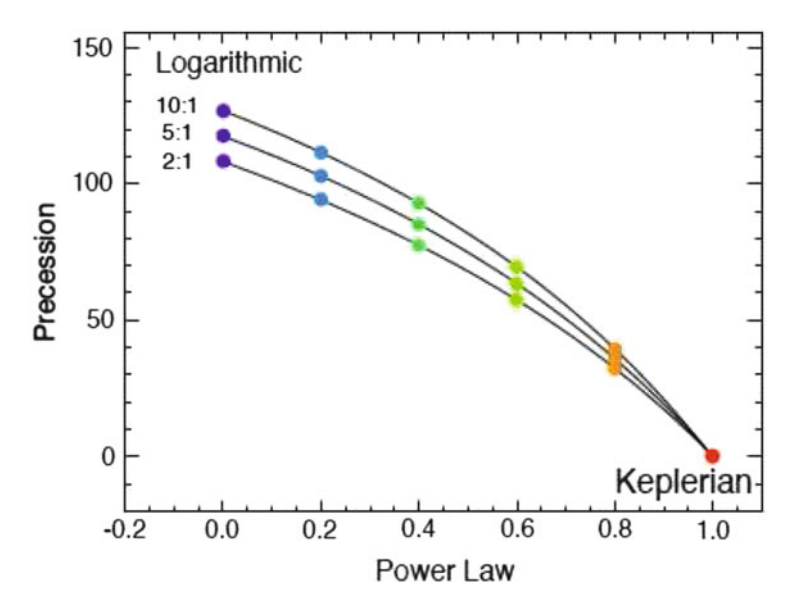


Fig. 7.2 Potential profile dependence of the precession of turning points. The plot shows the angle between successive apocenters for potentials varying from logarithmic to Keplerian. The *colors* are for orbits of different eccentricity. Reproduced from Belokurov et al. (2014)

are the easiest for which to account for the effect of errors (or even missing dimensions of information) on any parameter estimates. However, they are also the most sensitive to biases that may result from incorrect assumptions in the model—in particular in how stars are distributed in the satellite. For example, a rotating satellite can produce tidal streams with centroids systematically offset from those produced by a non-rotating satellite (Peñarrubia et al. 2010).

Fundamental methods exploit some more general intrinsic property that debris obeys rather than matching the full density distribution in phase-space. Typically, these methods require few (if any) assumptions about the satellite's internal structure and may be less prone to such biases than predictive models. On the other hand, they always involve a non-trivial transformation from observed coordinates to perform a comparison with model predictions, so correcting for systematic and random biases on parameter estimates due to errors in observables is difficult, if not impossible.

Methods in both categories are reviewed in more detail below.

7.2.1 Predictive Models

The most obvious example of a predictive model is an N-body simulation in which a ball of particles is allowed to evolve subject to its own gravity and the influence of external forces from the parent galaxy in which it is orbiting. These models naturally

include the physics of tidal stripping and are hence expected to generate the most physically realistic debris distributions for a satellite of a given mass and internal stellar distribution, orbiting in a given potential. Comparison of such models with data have been used most extensively in the case of the Sagittarius dwarf galaxy to measure the radial profile, depth and even triaxial shape of the Milky Way's potential (Helmi 2004; Law et al. 2005; Law and Majewski 2010). Nevertheless, the results for Sgr remain perhaps the most controversial, as the size and morphology of Sgr's streams suggest they might have been affected by additional physical effects beyond those incorporated in the current models (such as internal properties, orbital evolution due to a much larger primordial mass, or encounters with another satellite; see Chap. 2 of this volume for a more complete discussion).

The downside of a purely N-body approach is the computational cost of the models. Law and Majewski (2010) performed perhaps the most complete exploration of parameter space in any N-body study by identifying a modest region of parameter space using simple test-particle methods and then exploring this region with a grid of models to find a "best" fit by brute force. The ever-improving quality and quantity of data demands a more sophisticated, automated approach to exploring possible models, which in turn motivates exploration of how more approximate but computationally cheaper methods might be utilized.

The cheapest and most trivial example of a predictive model is to assume that a stream traces a single orbit (e.g., Johnston et al. 2005; Koposov et al. 2010; Deg and Widrow 2013). Note that Binney (2008) describes how this principle could be exploited even in the case of missing data dimensions. However, this approach cannot be used as anything more than broadly indicative of the behavior of the potential as studies have repeatedly revealed that debris occupies a range of orbits with properties systematically offset from the satellite (Johnston 1998; Helmi and White 1999; Johnston et al. 2001; Eyre and Binney 2011; Bovy 2014) and demonstrated that this offset leads to systematic biases in potential parameters (Sanders and Binney 2013a; Lux et al. 2013). Recent work in this area has taken the approach of instead using test-particle explorations to outline which streams (or which combination of streams) might be the most informative in measuring the Galactic potential assuming that these biases can be corrected for (Lux et al. 2013; Deg and Widrow 2014).

A number of methods have been proposed that move beyond the single-orbit approximation, without resorting to N-body simulations. All rely on our knowledge of scales in tidal debris gleaned from our understanding of the physics of tidal limitation and disruption as well as simulations of this process, as outlined in Sects. 6.3.2 and 6.3.3.1 of Chap. 6. For example, once lost from a satellite, the evolution of debris can be reasonably represented by test particle orbits (though care has to be taken in setting up the initial conditions for this unbound debris, see Gibbons et al. 2014), so an approach adopted by several authors is to follow many orbits with properties offset from the satellite's own over scales observed in full N-body simulations (Varghese et al. 2011; Küpper et al. 2012; Gibbons et al. 2014). In these methods, the satellite's own orbit is followed with additional, offset debris

orbits being initialized as the satellite loses mass, and subsequently integrated. The offset orbits represent the stream properties.

Section 6.3.3.2 of Chap. 6 outlines other predictive models for streams that also start from the orbit of the satellite, but do not rely on additional particles to represent the debris. Instead, these methods calculate the phase-space structure of stream populations offset from the satellite path given the orbital-phase and time since the material was lost using analytic approximations (Johnston 1998; Bovy 2014; Sanders 2014). These methods can also be used to search through trial potentials to find a good fit to stream data (Johnston et al. 1999b; Sanders 2014). However, they are limited by the extent to which the adopted analytic approximations apply, or are at least accurate enough for the purposes of recovering the potential. For example the model of Johnston (1998) is based on a description of debris scalings in energy and angular momenta and hence is only strictly applicable to purely spherical potentials. The methods proposed by Bovy (2014) and Sanders (2014) are instead formulated in action-angle space and hence provide elegant descriptions for a much wider range of some non-spherical potentials. ¹

7.2.2 Fundamental Methods

We use the term "fundamental methods" to refer to potential-measuring algorithms that do not generate full models of the phase-space distribution of debris structures, but rather exploit some basic principle that debris must obey.

For example, Helmi and White (1999) were the first to point out that the accreted nature of stars within a random population in the halo might be uncovered by looking at their orbital properties: stars accreted from a single object would be clustered around the original orbit of the parent satellite. Helmi and White (1999) used this idea to search for debris in energy and angular momenta in the Solar Neighborhood and Helmi and de Zeeuw (2000), Gómez et al. (2010) went on to explore how these clusters might appear in action-space for a *Gaia*-like survey of the halo. More recently, Sanderson et al. (2014) have noted that, since orbital properties (energies and actions) depend on the form of the Galactic potential, these same ideas could be used to constrain the mass distribution around our Galaxy. If a significant fraction of the stellar halo is composed from several long-dead satellites then the stars in a random survey should *not* appear random in orbital property-space, but rather clustered. However, if the orbital properties are calculated in a potential that is *not* a good representation of our Galaxy, then the clustering in orbital properties

¹As discussed in Chap. 6, while there are a very limited number of potentials for which exact analytic actions are known, there has been recent progress in various approximate techniques for finding actions more generally (Sanders 2012; Bovy 2014; Sanders and Binney 2015). These advances are promising, but the extent of their effectiveness for the purposes of generating accurate models of streams in realistic triaxial potentials has yet to be fully assessed.

will be less apparent: only in the correct potential is the clustering maximized. Peñarrubia et al. (2012) proposed an analogous approach using *entropy* as the test statistic to be minimized (equivalent to maximizing the clustering).

Equation (6.5) in Chap. 6 points to another fundamental property that debris must obey: in action-angle space, the angular offset ($\Delta\theta$) of debris from the satellite must lie along the same direction as the orbital frequency offset ($\Delta\Omega$) (Helmi and White 1999; Sanders and Binney 2013b). Since both the angles and the frequencies depend on the form of the potential, this requirement can be used as a potential measure with the correct potential being the one in which the vectors are most closely aligned in the same direction. (Note that this method implicitly assumes that the debris is distributed isotropically in action space, which is not strictly true—as pointed out by Bovy 2014.)

Finally, the common origin of debris can be exploited in another way—if the orbits of stars that are all part of the same debris structure are integrated backwards then their paths should all at some point coincide with the instantaneous phase-space position of the satellite from which they came. Only in the correct potential will this "recombination" happen (Johnston et al. 1999a; Price-Whelan and Johnston 2013; Price-Whelan et al. 2014).

In some ways, these methods are very powerful in that they require fewer (if any) assumptions about the properties of the satellite that created the debris. In addition, the statistical nature of the approaches of both Sanderson et al. (2014) and Peñarrubia et al. (2012) have the great advantage of not needing to have clear streams already identified in their data sets in order to work.

7.2.3 Summary: Status and Prospects

The many papers that have thus far used data on tidal debris to actually measure the properties of the Milky Way's dark matter halo are illustrative both of the potential power of this approach as a well as the extent of the data available (e.g., Johnston et al. 1999b; Ibata et al. 2001; Johnston et al. 2005; Koposov et al. 2010; Law and Majewski 2010; Newberg et al. 2010). However, these works have generally either used the data in very simplistic ways or employed debris models that have not been thoroughly tested.

The field is rapidly maturing with the prospect of much larger and more accurate data sets in the near future motivating the recent development of more sophisticated potential recovery algorithms (outlined above), many of which have been tested with N-body models. However, a number of other issues need to be more thoroughly explored:

• Most of the algorithms have only been tested on perfect data and only a couple have attempted to incorporate a rigorous treatment of observational errors (e.g., Koposov et al. 2010; Price-Whelan et al. 2014; Gibbons et al. 2014).

- Tests so far have typically asked how well parameters can be recovered for some assumed form for the Milky Way's potential. Ideally the Milky Way would be represented in a non-parametric way, allowing more flexibility in the representation of the underlying mass distribution. For example the mass distribution could be defined by a spatial grid of values or by the coefficients of a basis function expansion.
- Methods that have been formulated in action-space (Peñarrubia et al. 2012; Sanders and Binney 2013b; Bovy 2014; Sanders 2014; Sanderson et al. 2014) rely on being able to represent the Milky Way with an integrable potential in which actions can be found. Recent work has suggested ways of approximately recovering actions for any potential (Sanders and Binney 2015; Bovy 2014). For example, the true potential can be represented by the sum of a series of integrable potentials with known actions. However, the level of bias that these approximations introduce into potential-recovery have not yet been explored.
- All the algorithms have been developed and tested only for static, smooth and non-evolving potentials, while we know that the Milky Way has grown and contains many, moving substructures. In a preliminary investigation of these effects, Bonaca et al. (2014) show that individual stream measurements of the mass of the Milky Way in such an environment can vary by several tens of percent.
- None of the proposed algorithms have yet investigated the effect of the internal dynamical distribution in the progenitor satellite, which is known to affect the properties of streams (Peñarrubia et al. 2010).

Despite these current limitations, the promise of this approach provides ample incentive for further investigation. In particular, as noted above, while gravitational lensing studies are sensitive to the projected shapes of dark matter halos, the Milky Way is the one place in the Universe where we can look at the shape and orientation of a dark matter halo in three dimensions. As an illustration of this power, Fig. 7.3 shows some results of tests of the Rewinder algorithm (reproduced from Price-Whelan et al. 2014) applied to synthetic observations of just four particles drawn from an N-body simulation of satellite disruption. The observational errors were accounted for using a Bayesian approach during the recovery. The tests show that in the idealized case, where the form of the smooth and static potential is known, few percent errors on potential parameters are possible using even a very small sample with near-future data sets. For comparison, current estimates for the mass of the Milky Way differ by more than a factor of two (e.g., Barber et al. 2014). Since real sample sizes will be orders of magnitude larger than those used in the idealized experiment, the results suggest that there is ample room to introduce more flexible (and hence complex) and even time-dependent potentials that will provide a better representation of the true Milky Way mass distribution.

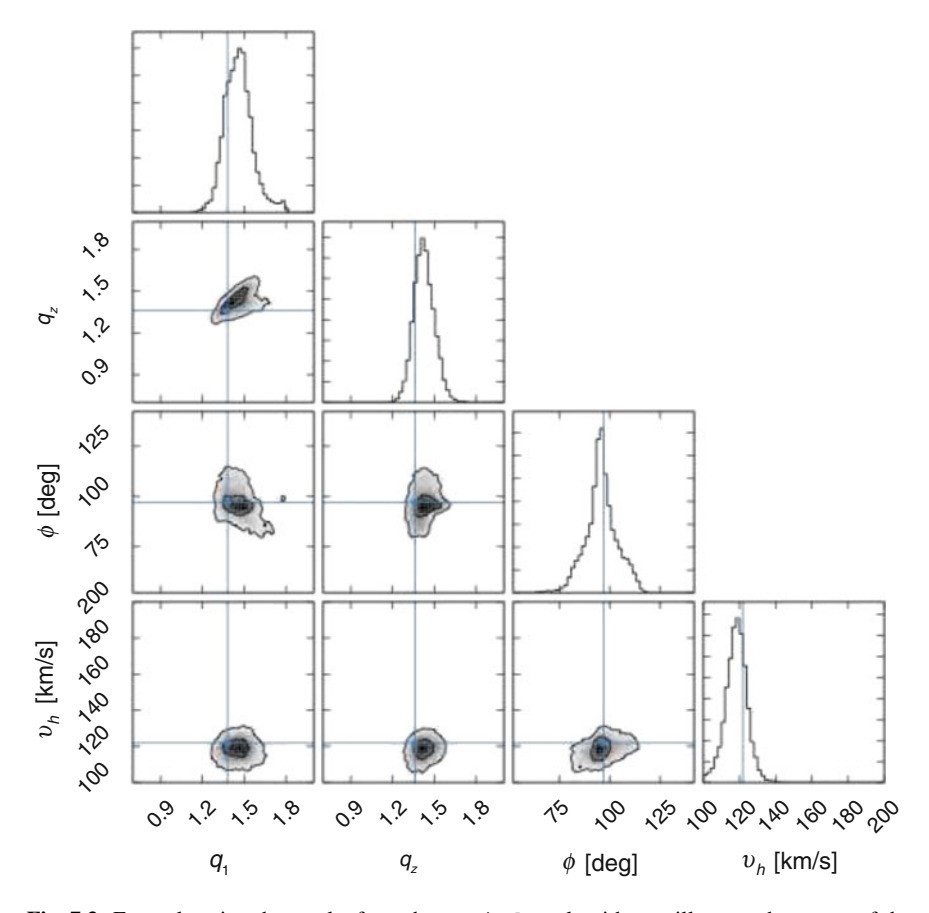


Fig. 7.3 Example using the results from the Rewinder algorithm to illustrate the power of the tidal tails as potential measures. A model galaxy containing a tidally disrupted dwarf galaxy was simulated. Four debris particles were then "observed" with errors expected for RR Lyrae stars surveyed with Spitzer (i.e., 2% distances from the mid-IR period-luminosity relation, see Madore and Freedman 2012), Gaia (i.e., very accurate proper motions) and ground-based radial velocity errors of $5\,\mathrm{km\,s^{-1}}$. In this case, four potential parameters (the velocity scale v_h , axis ratios q_1, q_z and orientation ϕ of the dark matter halo component in which the simulation was run) were recovered with few percent accuracies on each. Reproduced from Price-Whelan et al. (2014)

7.3 Using Tidal Debris to Probe Dark Matter Substructure

7.3.1 Cosmological Context

As discussed in the Introduction to this chapter, standard Λ CDM models of the Universe predict an order of magnitude more dark matter subhalos within the halos of typical galaxies than the number of known satellite galaxies orbiting the Milky Way (Klypin et al. 1999; Moore et al. 1999) This discrepancy can

partially be explained by accounting for the incomplete sky coverage of SDSS and the distance-dependent limit on this survey's sensitivity to low-surface brightness objects (Tollerud et al. 2008; Koposov et al. 2009). Indeed, models which take this into account and consider diffuse, (i.e., undetectable) satellite galaxies can reconcile the number counts for subhalos (Bullock et al. 2010). However, when they impose the suppression of stellar populations in low mass subhalos (which have masses below $5 \times 10^8 \, M_\odot$) the number of undetectable galaxies significantly declines and the prediction of numerous purely dark matter subhalos less massive than $5 \times 10^8 \, M_\odot$ remains. Proof of the existence (or lack) of these "missing satellites" could provide an important constraint on the nature of dark matter, which sets the minimum scale for the formation of dark matter subhalos.

In much the same way that there is predicted to be a *spectrum* of dark matter subhalos in orbits about the Milky Way, we know there is a *spectrum* of tidal debris structures; the dominant (more extended and hotter) structures (e.g., Sgr and the Orphan Stream) arise from the infall of the larger subhalos (i.e., the ones that contain stars) while the thinner and colder streams typically come from globular clusters. All will be disturbed by subhalo-induced fluctuations in the Milky Way's potential (as first investigated by Ibata et al. 2002; Johnston et al. 2002; Siegal-Gaskins and Valluri 2008).

The key question is which streams will be most sensitive to the "missing satellites"—in particular, the multitude of low mass $(M < 10^7 M_{\odot})$ subhalos that are predicted but whose existence has never been definitively proved. The more dominant streams have much larger cross sections and thus will encounter such subhalos more frequently, but they are also much thicker and hotter, making the effect of such individual encounters less apparent. Hence, to address this question, both the frequency of encounters of different mass subhalos as well as the size of the effect of those subhalos compared to the stream's own distribution must be accounted for (see Yoon et al. 2010, for explicit calculations). For the spectrum of subhalo masses predicted by Λ CDM, it has been found that hotter stellar streams, such as Sgr, are large enough to hide the signatures of the many encounters it suffers with smaller subhalos, though the (known) subhalos containing visible satellites could have an observable effect (Johnston et al. 2002). Thinner streams, such as Pal 5 and GD-1, should contain significant fluctuations in density and velocity at degree and sub-degree scales due to dozens of direct encounters with subhalos in the mass range $10^5 - 10^7 M_{\odot}$ over their lifetimes (Yoon et al. 2010; Carlberg 2012).

Given these results, in subsequent sections we restrict our attention to the case of direct encounters of lower mass subhalos with thin streams that are typically generated by the destruction of a globular cluster.

7.3.2 Dark Matter Encounters with Thin Stellar Streams

7.3.2.1 The Dynamics of Gaps in Stellar Streams

Star stream density variations on scales much smaller than the orbit of the stream are the result of encounters with perturbers (such as dark matter subhalos), the dynamics of the ejection of stars from the progenitor, and compression and expansion of a stream around an orbit.

The response of an infinitely thin stream to an encounter with a relatively low mass perturber is straightforward to calculate analytically using the impulse approximation, and the results can be generalized to streams with finite width. The results are in good agreement with numerical orbit integrations for streams with width to orbital radius ratios of 1:300, which includes the regimes of the two well studied thin streams (Pal 5 and GD-1). If a section of a stream encounters a massive satellite (e.g., the LMC), then that section of the stream will be completely pulled away and spread around the host galaxy.

Figure 7.4 introduces a coordinate system for calculating the effects of subhalos passing through a stream. A perturbing mass with a spherically symmetric gravita-

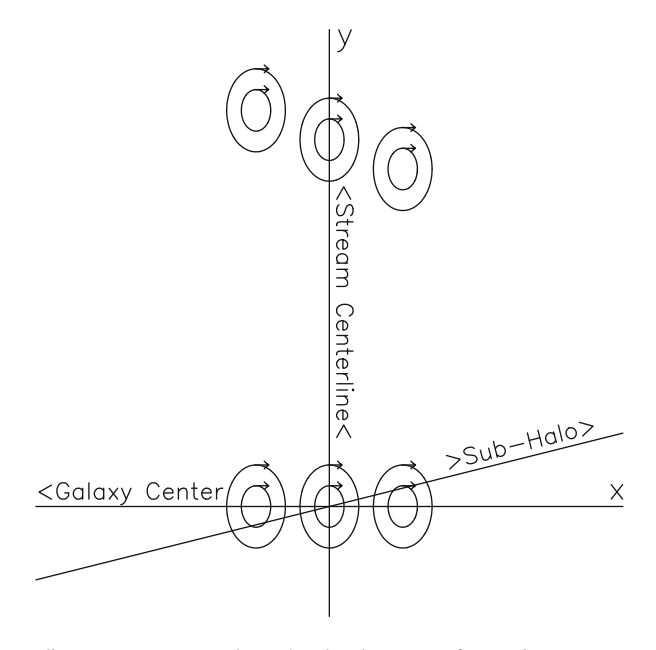


Fig. 7.4 A coordinate system to analyze the development of gaps in a stream. The stream is moving upward along the y axis. The guiding centers of three masses at different locations across the tidal stream are shown at y=0. At the top of the figure, the guiding centers of the same three masses are shown at a later time. The differential rotation of a galaxy means that the guiding centers of particles at larger radii drift backward. The width of the stream is determined by the combination of epicyclic motions and spread of guiding centers, the details of which depend on the orbit of the progenitor system (Carlberg 2013). In the text, we consider a subhalo that crosses the stream at y=0 at t=0. [Reproduced from Carlberg (2013)]

tional potential, $\Phi(r)$, induces a net velocity change, as a function of distance along the stream of:

$$\Delta \mathbf{v}(y) = -\int_{-\infty}^{\infty} \nabla \Phi(|\mathbf{d}(y,t)|) dt, \tag{7.1}$$

where $\mathbf{d}(y,t)$ is the distance along the stream from the stream crossing point at (x,y) = (0,0). Equation (7.1) are straightforward to numerically integrate for most radially symmetric density profiles.

To illustrate the behavior, Carlberg (2013) analytically integrated the velocity changes of Eq. (7.1) for a perturbing point mass, M, moving at speed (v_x, v_y) , and crossing a stream that is moving along the y axis at speed V_y . The velocity of the point mass relative to the stream is defined as $v_{\parallel} = v_y - V_y$ (the velocity parallel to the stream), and $v_{\perp} = v_x$ (toward the stream). The distance of closest approach of the mass to the stream is the impact parameter, b. The change in the v_{\parallel} component of the stream stars produces a change in the relative velocity of the stream and the subhalo given by:

$$\Delta v_{\parallel}(y) = \frac{-2GMv_{\perp}^{2}y}{v(v^{2}b^{2} + v_{\perp}^{2}y^{2})},$$
(7.2)

where $v=\sqrt{v_\parallel^2+v_\perp^2}$ is the speed of the perturbing mass relative to the stream stars. This equation has been previously derived in Yoon et al. (2010) with slightly different notation. For the direction of motion perpendicular to the stream, the velocity change is $\Delta v_\perp(y)=-(v_\parallel/v_\perp)\Delta v_\parallel(y)$. In the direction of smallest separation between the perturber and the stream (here called the z direction) the change is $\Delta v_z(y)=(v_\perp^2y/(v^2b))\Delta v_\parallel(y)$, which has the same sign at any location along the stream.

The effect of the perturber is to pull particles along the stream towards the crossing point, since $\Delta v_{\parallel}(y)$ is positive for negative y and negative for positive y. In addition, the displacement perpendicular to the stream has the same dependence on distance along the stream and is proportional to $-v_{\parallel}/v_{\perp}$; that is, the displacement is toward the incoming side below the crossing point (negative y) and away above it.

The velocity change was derived for a stream moving in a straight line; however, the velocity changes can be applied to a stream moving in a nearly circular orbit. For circular orbits, the particles travel along their guiding centers. The velocity changes along the stream are angular momentum changes which cause stars ahead of the crossing point (positive y) to have a reduced angular momentum and hence move to a smaller guiding center which always has a higher rate of angular rotation. Thus the stars ahead of the crossing point are pulled ahead. Similarly, the star behind the crossing point (negative y) are moved to lower angular rotation and fall behind. In this way, a gap is formed in the tidal stream.

The equations below are developed for the case of a perturber moving parallel to the orbital plane of the stream, so that the impact parameter is zero. For other orientations of the perturber, the direction of the response of the stream stars changes but the density profile of the resulting gap is essentially the same.

Stars behind the crossing point gain angular momentum and move to a larger guiding center, which has a lower rate of angular rotation, according to:

$$\Omega(y) = \frac{v_c}{X_0} \left[1 + \frac{\Delta v_{\parallel}(y)}{v_c} \right]^{-1}. \tag{7.3}$$

Hence, the stars begin to move apart, and a gap develops over a rotation period. The density profile of the gap can be derived from Eq. (7.3), which gives the change in angular position of the stars with time (see Carlberg 2013). The gap starts with a size comparable to the impact parameter or scale radius of the perturbing object, and continues to grow in length with time. The material that moves out of the gap piles up on either side and creates a characteristic "double horned" density profile. The infinitely narrow stream can be broadened to a finite width by introducing a Gaussian distribution of epicycles on the stream. Epicycles are often used to describe non-circular orbits as the combination of a guiding center with a circular orbit combined with the motion of an orbiting body on an "epicycle" orbit around the guiding center. In this case, the epicycles are introduced to give the stream width; the particles will wiggle back and forth around the center of the tidal stream. The cold stream density profile of a gap is then convolved with the appropriate Gaussian distribution along the stream. Numerical integrations show good agreement with this simple theory (Fig. 7.5). Recently Erkal and Belokurov (2015) have extended

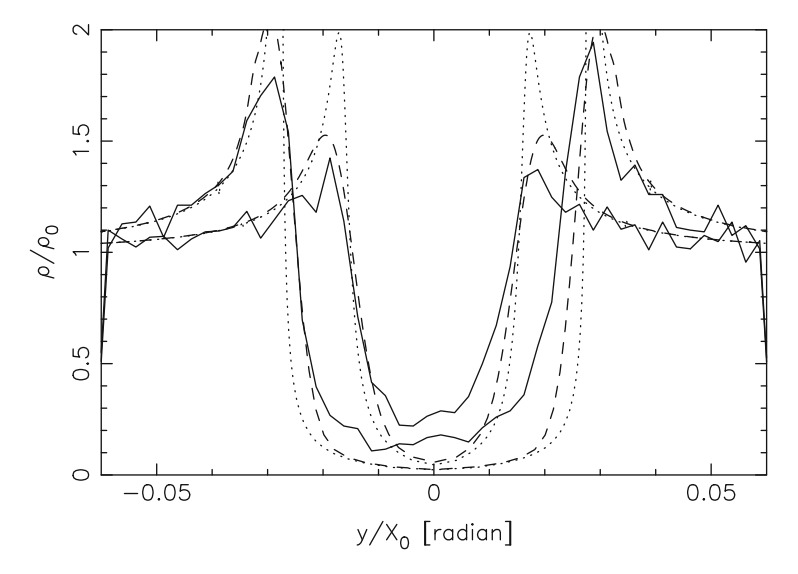


Fig. 7.5 The gap at two times (6.4 and 12.8 orbits after the encounter) in a detailed orbit integration (*jagged continuous line*) in a warm stream of width 0.005 relative to the orbital radius. The *dotted line* shows the predicted density profile for a cold stream and the *dashed line* is the prediction allowing for epicyclic motions. The simple theory is in good agreement with the simulation. [Reproduced from Carlberg (2013)]

this analysis into the mildly nonlinear regime, demonstrating that the folding of the stream leads to caustics in the density profile and that the growth in the width of the stream with time slows from t to \sqrt{t} .

More general simulations of the dissolution of a progenitor system in a realistic halo potential are essential to give a more realistic view of a stream. Because they contain no unseen dark matter to confuse the dynamical situation, disrupting globular clusters are the most straightforward systems to model. Nevertheless, even this fairly well defined situation is yet to be completely understood. This is largely a result of the range of orbits and potentials that need to be investigated as well as the details of how the progenitor is modeled. Kupper and collaborators have shown that when stars leave a globular cluster they stream through the Lagrange points with a fairly narrow spread of (primarily radial) velocities. Consequently the stars follow a cycloidal path. However, the dominant effect for clusters on non-circular orbits is that the mass loss varies around the orbit, leading to "spurs" which oscillate above and below the centerline of the stream at the epicyclic frequency.

One important outcome of a number of simulations is that the range of angular momentum within the streams from a globular cluster is quite small. This implies that there is an almost unique association between time since ejection from the globular cluster into the stream, and distance from the progenitor along the stream. Furthermore, there is very little shear present at any given distance along the stream, meaning that features in the stream are not blurred out significantly with time (Bovy 2014; Carlberg 2014).

Although in principle it is possible to work out the distribution of the number of gaps of a given size in a stream, the number of effects that need to be modeled mean that it is easier to do either a partially numerical integration, or a complete simulation. The basic idea is straightforward: small sub-halos cause small gaps (which subsequently grow with time). Therefore we expect that there will be a spectrum of gap sizes rising as a power law towards smaller gaps until the spectrum rolls over because random motions in the stream blur out gaps that are smaller than about the stream width. Carlberg and Grillmair (2013) presented a semi-analytic calculation of this spectrum. Two important effects are left out of the calculation. First, the gaps will overlap, meaning that the semi-analytic calculation is an upper limit. Second, some of the gaps might not be observable given a finite number of detected stars in the stream.

7.3.2.2 The Cumulative Effect of Sub-halos

Carlberg and Grillmair (2013) refined the cold-stream analysis of Carlberg (2012) to predict that the number of gaps created per unit time per unit length in the stream (the gap creation rate, R_{\cup}) as a function of galactocentric distance, r, in units of $30 \,\mathrm{kpc}$, and $M_8 = M/10^8 M_{\odot}$ of,

$$R_{\cup} = 0.00433 r^{0.26} M_8^{-0.36} \text{kpc}^{-1} \text{Gyr}^{-1}.$$
 (7.4)

At an encounter age of around 4 Gyr, sub-halos of mass M_8 create gaps of mean length ℓ ,

$$\ell = 9.57r^{0.16}M_8^{0.31}\text{kpc}. (7.5)$$

Eliminating M_8 between Eqs. (7.4) and (7.5), we find the gap creation rate as a function of gap size is:

$$\frac{dn(\ell)}{dt}d\ell = 0.060r^{0.44}\ell^{-1.16}\,\text{kpc}^{-1}\text{Gyr}^{-1}\frac{d\ell}{\ell}$$
(7.6)

for gaps of size ℓ , which is measured in kpc and the variable r is scaled to 30 kpc. If we evaluate this at 15 kpc for a stream of 4 Gyr age and integrate over all gap sizes larger than ℓ we find the fraction of the stream length that has gaps is

$$f(>\ell) = 1.1\ell^{-0.16} \frac{T}{4 \text{ Gyr}}.$$
 (7.7)

That is, for streams within about 30 kpc of the Galactic center, every position along a star stream of this age has been affected by a subhalo (Carlberg 2009). The dependence on gap size is very weak. The low mass subhalos heat the stream and to some degree frustrate and complicate the formation of subsequent small gaps. However, the stream remains intact. The larger subhalos that create gaps of several kpc in size cause sufficiently large perturbations perpendicular to the stream that it becomes possible for the orbits of stream segments to diverge, particularly if the overall potential is strongly triaxial (or more complicated) and/or time evolving (Figs. 7.6 and 7.7).

Work has begun on the dynamical modeling of streams in realistic cosmological halos. Cooper et al. (2010) examined streams already formed within a cosmological simulation which usefully illustrate the complicated time evolution of the stream shape. However, these simulations do not have the mass resolution to follow cool streams or globular cluster dissolution. Bonaca et al. (2014) have published a realistic, but approximate, approach to following a dissolving cluster in an evolving halo. One basic outcome is that streams that orbit in the outer parts of the galaxy halo are much less disturbed than those that orbit within the much more dynamic inner parts of the galaxy halo, as expected. The buildup of the visible stellar mass which dominates the potential field of the inner galaxy has yet to be modeled.

7.3.2.3 Detecting Gaps in Stellar Streams

The calculations of gap shapes above usefully predict that gaps should have a double-horned profile with an integral along their length of zero, meaning the mass displaced from the gap is simply piled up on either side of the stream. Gap finding then consists of running filters of all widths along the stream to find regions

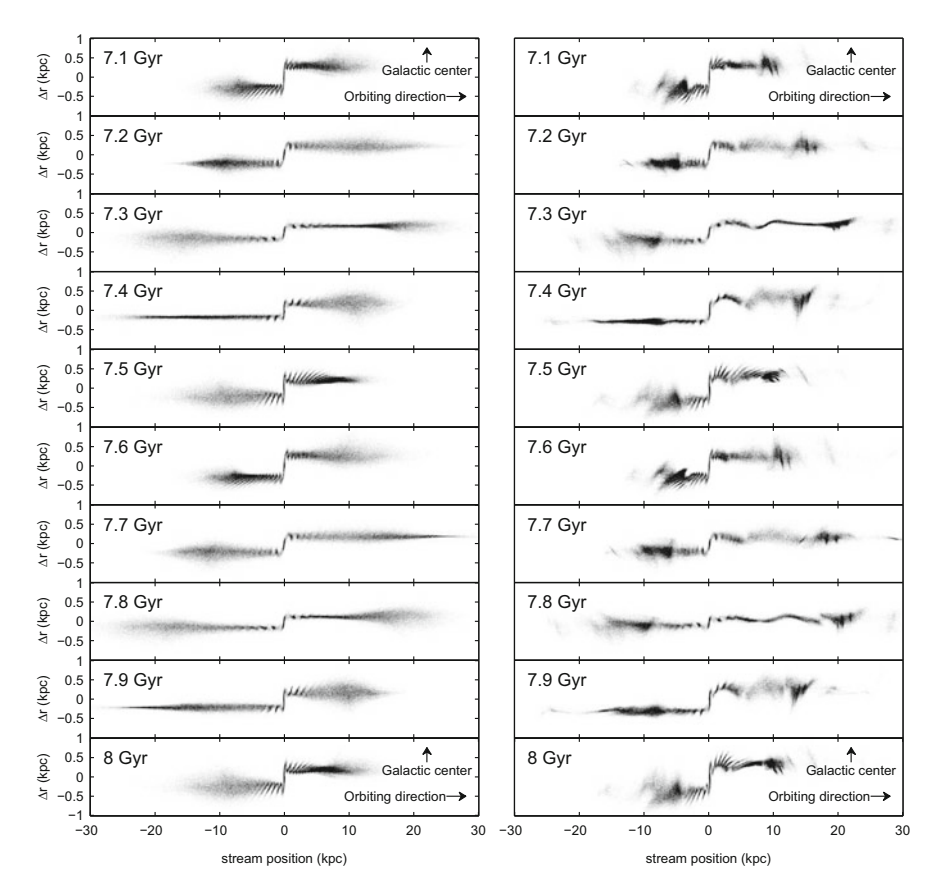


Fig. 7.6 Left panels: simulation of a stream that develops from a globular cluster, projected onto its orbital plane, and transformed to cartesian coordinates. Δr is the difference between the distance from the progenitor to the Galactic center and the distance from the stream debris to the Galactic center. Stream position is measured along the tidal stream. Right panels: same as the left column, but with subhalos included in the simulation, excluding subhalos above $10^8~M_{\odot}$

where there is a good match, identified as local peaks in the filtered distribution. To quantify the statistical confidence, the same filter is run through a density distribution with the same noise properties. The resulting distribution of peaks is sorted to identify what level constitutes 99 % confidence that a peak is not a false positive. Although this filtering procedure gives gap-finding a statistical foundation (Fig. 7.8), the current procedures could be improved. In particular, the rate of false positives is currently about 30 % of the peaks. This factor can be included as a correction, but reducing their number would be helpful. The shape of the gap filter is currently essentially an informed approximation and is not driven by the characteristics of the gaps in the data. That is, there is no current empirical approach to generate a gap spread function, comparable to the point spread function of a

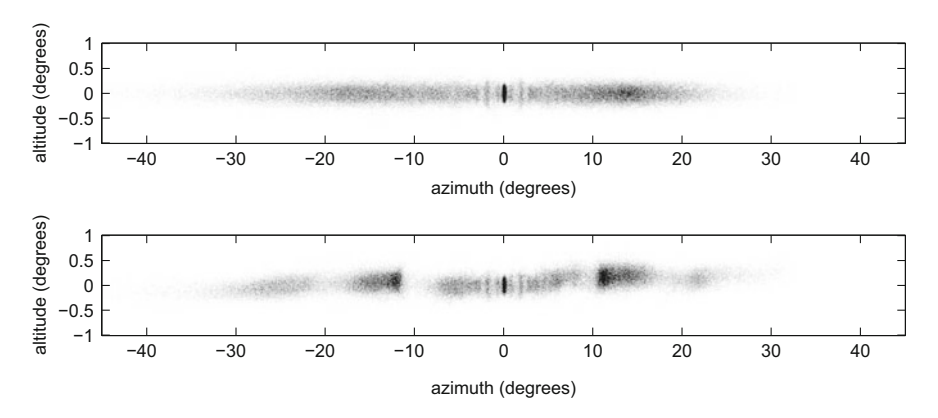


Fig. 7.7 The view from the center of the galaxy of the 7.5 Gyr timeslice of Fig. 7.6. The *top panel* shows the simulated tidal stream without subhalos, and the *bottom panel* includes a cosmologically motivated set of subhalos in the simulation. This projection is likely closer to a typical view of a stream outside the solar circle. The youngest part of the stream, close to the progenitor, contains epicyclic oscillations which phase mix away. The stream becomes older further away and is dominated by subhalo induced gaps

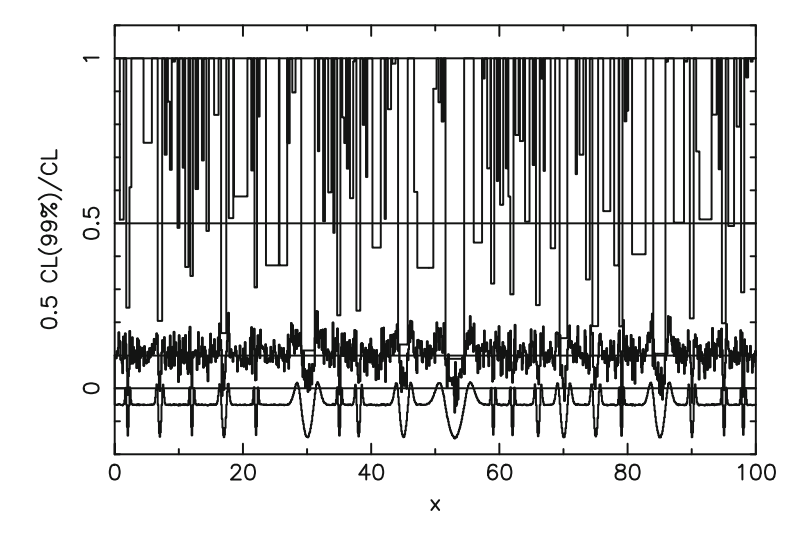


Fig. 7.8 A demonstration of the gap filter applied to artificial data with noise characteristics comparable to GD-1. The filter systematically over-estimates the number of gaps by about 44 %. The filter is a well-defined approach to finding and measuring gaps, but this version is subject to (calibratable) systematic errors

star that can be empirically determined in image data. Work is now beginning to undertake more extensive simulations; placing those results into a simulated sky will greatly improve the understanding of gap finding techniques.

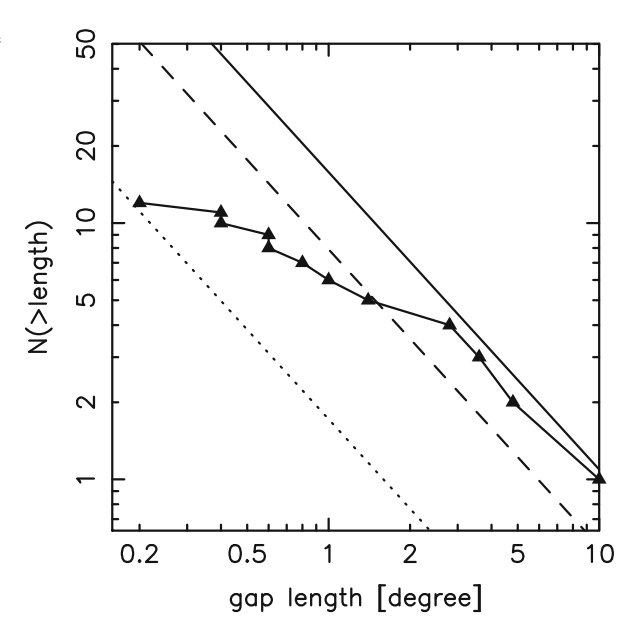
7.3.3 Current Observations and Future Prospects

Currently there are only two really well studied thin streams: the Pal 5 stream, emanating from the tidal lobes of the Pal 5 globular cluster, and the GD-1 stream, having no known progenitor.

There are three primary reasons for density variations in streams: the dynamics of mass loss from the progenitor, variations in velocity around the stream's orbit, and perturbations caused by encounters of the stream with any massive object. Massive objects range from baryonic structures to dark matter sub-halos, possibly containing visible stars or gas. The orbital effects are necessarily smooth variations around the orbit and hence on scales much larger than those which vary with the comparable size scales of the progenitors and the dark matter sub-halos of interest, which we review below (Fig. 7.9).

So far streams are detected through measurements of sky density, most often in the SDSS survey where the requirement for photometric colors precise to about 10% or better limits the data to about 21–22 magnitude in the SDSS system. Reaching large numbers of stars requires getting to at least the bottom of the red giant branch and ideally to main sequence turn off stars (or beyond) at absolute magnitudes of +5 or so. The outcome is that streams tend to be found at distances in the range of 10–20 kpc in the currently available data. Even with the very good optimal weighting procedures of Rockosi et al. (2002), which dramatically reduce the weight of background stars, the summed weight of stars in the stream is typically about 10–30% of the backgrounds. To obtain a local signal-to-noise of about one usually requires binning over the entire width of narrow streams, so no information

Fig. 7.9 A comparison of the recovered GD-1 cumulative distribution of gap sizes with the semi-analytic estimate of the expected numbers for various assumed mean stream ages



on 2D structure is available with current data. As deeper images, with more filters and eventually kinematic data become available, the local signal to noise will dramatically rise. Consequently, the currently available data is usually restricted to being a one dimensional density along the path of the stream.

Even a 60° long thin stream like GD-1 is expected to have only about a dozen or so detectable gaps over its visible length. Detecting more streams, which means going to larger Galactic radii, is a key element of the future of the field. In addition, more filter bands will allow improved optimal photometric matched filtering to include metallicity information to further suppress the foreground and background stars of the same temperature and luminosity. And finally, as better kinematic data slowly become available (note that Gaia will only reach about 20th magnitude, which is the regime where streams discovered in the SDSS pick up much of their signal), the use of improved distances and velocities for each individual star will allow us to more accurately identify which stars are in the stream, and will thus improve the detail with which models can be matched to the data. Moreover, it will then be possible to use kinematic signatures of gaps (a sideways S in velocity space) to find gaps and characterize the perturbers that caused them.

There is a vast array of planned all-sky imaging and spectroscopic surveys from both the ground and space that will transform our knowledge of stellar streams over the next decade. First, we will find new streams in the southern hemisphere, links with known streams in the north, and, in both hemispheres, find streams out to about 100 kpc with higher signal-to-noise than current data. Spectra will provide astrophysical information about the nature of the stream progenitors and stream kinematics, which will be particularly powerful in combination with proper motion and distance data. The challenge will then be to make use of these data, which will be somewhat noisy by theoretical standards, to put new and interesting constraints on the nature of both the smooth large scale potential of the galaxy, and the small scale variations in the potential expected in a Λ CDM universe.

Acknowledgements KVJ thanks her postdocs and graduate students for invaluable discussions throughout the year (Andreas Kuepper, Allyson Sheffield, Lauren Corlies, Adrian Price-Whelan, David Hendel and Sarah Pearson). Her work on this volume was supported in part by NSF grant AST-1312196. RGC thanks his graduate student Wayne Ngan and support from CIfAR and NSERC is gratefully acknowledged.

References

Barber, C., Starkenburg, E., Navarro, J. F., McConnachie, A. W., & Fattahi, A. 2014, MNRAS, 437, 959

Belokurov, V., Koposov, S. E., Evans, N. W., et al. 2014, MNRAS, 437, 116

Binney, J. 2008, MNRAS, 386, L47

Bonaca, A., Geha, M., Küpper, A. H. W., et al. 2014, ApJ, 795, 94

Bovy, J. 2014, ApJ, 795, 95

Boylan-Kolchin, M., Bullock, J. S., & Kaplinghat, M. 2011, MNRAS, 415, L40

Bullock, J. S., Stewart, K. R., Kaplinghat, M., Tollerud, E. J., & Wolf, J. 2010, ApJ, 717, 1043

Carlberg, R. G. 2009, ApJ Lett, 705, L223

Carlberg, R. G. 2012, ApJ, 748, 20

Carlberg, R. G., & Grillmair, C. J. 2013, ApJ, 768, 171

Carlberg, R. G. 2013, ApJ, 775, 90

Carlberg, R. G. 2014, arXiv:1412.2405

Cooper, A. P., Cole, S., Frenk, C. S., et al. 2010, MNRAS, 406, 744

Côté, P., McLaughlin, D. E., Cohen, J. G., & Blakeslee, J. P. 2003, ApJ, 591, 850

Deg, N., & Widrow, L. 2013, MNRAS, 428, 912

Deg, N., & Widrow, L. 2014, MNRAS, 439, 2678

Erkal, D., & Belokurov, V. 2015, MNRAS, 450, 1136

Eyre, A., & Binney, J. 2011, MNRAS, **413**, 1852

Gibbons, S. L. J., Belokurov, V., & Evans, N. W. 2014, MNRAS, 445, 3788

Gómez, F. A., Helmi, A., Brown, A. G. A., & Li, Y.-S. 2010, MNRAS, 408, 935

Helmi, A., & White, S. D. M. 1999, MNRAS, 307, 495

Helmi, A., & de Zeeuw, P. T. 2000, MNRAS, 319, 657

Helmi, A. 2004, ApJ Lett, 610, L97

Ibata, R., Lewis, G. F., Irwin, M., Totten, E., & Quinn, T. 2001, ApJ, 551, 294

Ibata, R. A., Lewis, G. F., Irwin, M. J., & Quinn, T. 2002, MNRAS, 332, 915

Jing, Y. P., & Suto, Y. 2002, ApJ, 574, 538

Johnston, K. V. 1998, ApJ, 495, 297

Johnston, K. V., Zhao, H., Spergel, D. N., & Hernquist, L. 1999a, ApJ Lett, 512, L109

Johnston , K. V., Majewski , S. R., Siegel, M. H., Reid, I. N., & Kunkel, W. E. 1999b, AJ, 118, 1719

Johnston, K. V., Sackett, P. D., & Bullock, J. S. 2001, ApJ, 557, 137

Johnston, K. V., Spergel, D. N., & Haydn, C. 2002, ApJ, 570, 656

Johnston, K. V., Law, D. R., & Majewski, S. R. 2005, ApJ, 619, 800

Klypin, A., Kravtsov, A. V., Valenzuela, O., & Prada, F. 1999, ApJ, 522, 82

Koposov, S. E., Yoo, J., Rix, H.-W., et al. 2009, ApJ, 696, 2179

Koposov, S. E., Rix, H.-W., & Hogg, D. W. 2010, ApJ, 712, 260

Küpper, A. H. W., Lane, R. R., & Heggie, D. C. 2012, MNRAS, 420, 2700

Law, D. R., Johnston, K. V., & Majewski, S. R. 2005, ApJ, 619, 807

Law, D. R., & Majewski, S. R. 2010, ApJ, 714, 229

Lux, H., Read, J. I., Lake, G., & Johnston, K. V. 2013, MNRAS, 436, 2386

Madore, B. F., & Freedman, W. L. 2012, ApJ, 744, 132

Majewski, S. R., Skrutskie, M. F., Weinberg, M. D., & Ostheimer, J. C. 2003, ApJ, 599, 1082

Majewski, S. R., Kunkel, W. E., Law, D. R., et al. 2004, AJ, 128, 245

Moore, B., Ghigna, S., Governato, F., et al. 1999, ApJ Lett, 524, L19

Navarro, J. F., Frenk, C. S., & White, S. D. M. 1997, ApJ, 490, 493

Newberg, H. J., Willett, B. A., Yanny, B., & Xu, Y. 2010, ApJ, 711, 32

Peñarrubia, J., Belokurov, V., Evans, N. W., et al. 2010, MNRAS, 408, L26

Peñarrubia, J., Koposov, S. E., & Walker, M. G. 2012, ApJ, 760, 2

Price-Whelan, A. M., & Johnston, K. V. 2013, ApJ Lett, 778, L12

Price-Whelan, A. M., Hogg, D. W., Johnston, K. V., & Hendel, D. 2014, ApJ, 794, 4

Rockosi, C. M., Odenkirchen, M., Grebel, E. K., et al. 2002, AJ, 124, 349

Rubin, V. C., & Ford, Jr., W. K. 1970, ApJ, 159, 379

Sanders, J. L. 2012, MNRAS, 426, 128

Sanders, J. L. 2014, MNRAS, 443, 423

Sanders, J. L., & Binney, J. 2013a, MNRAS, 433, 1813

Sanders, J. L., & Binney, J. 2013b, MNRAS, 433, 1826

Sanders, J. L., & Binney, J. 2015, MNRAS, 447, 2479

Sanderson, R. E., Helmi, A., & Hogg, D. W. 2014, IAU Symposium, 298, 207 (arXiv:1404.6534)

Siegal-Gaskins, J. M., & Valluri, M. 2008, ApJ, **681**, 40

Tollerud, E. J., Bullock, J. S., Strigari, L. E., & Willman, B. 2008, ApJ, 688, 277 Varghese, A., Ibata, R., & Lewis, G. F. 2011, MNRAS, 417, 198 Vegetti, S., Koopmans, L. V. E., Bolton, A., Treu, T., & Gavazzi, R 2010, MNRAS, 408, 1969 Yoon, J. H., Johnston, K. V., & Hogg, D. W. 2010, ApJ, 731, 58

Chapter 8 Substructure and Tidal Streams in the Andromeda Galaxy and its Satellites

Annette M.N. Ferguson and A.D. Mackey

Abstract Tidal streams from existing and destroyed satellite galaxies populate the outer regions of the Andromeda galaxy (M31). This inhomogeneous debris can be studied without of many of the obstacles that plague Milky Way research. We review the history of tidal stream research in M31, and in its main satellite galaxies. We highlight the numerous tidal streams observed around M31, some of which reside at projected distances of up to $\sim 120\,\mathrm{kpc}$ from the center of this galaxy. Most notable is the Giant Stellar Stream, a signature of the most recent significant accretion event in the M31 system. This event involved an early-type progenitor of mass $\sim 10^9\,\mathrm{M}_\odot$ that came within a few kpc of M31's center roughly a gigayear ago; almost all of the inner halo (R $\leq 50\,\mathrm{kpc}$) debris in M31 can be tied either directly or indirectly to this event. We draw attention to the fact that most of M31's outer halo globular clusters lie preferentially on tidal streams and discuss the potential this offers to use these systems as probes of the accretion history. Tidal features observed around M33, M32, NGC 205 and NGC 147 are also reviewed. We conclude by discussing future prospects for this field.

8.1 Introduction

Within the context of the cold dark matter paradigm, structure formation proceeds hierarchically and galaxies like the Milky Way and Andromeda (M31) are predicted to arise from the merger and accretion of many smaller sub-systems as well as from the smooth accretion of intergalactic gas (e.g., White and Rees 1978; White and Frenk 1991). Galaxy outskirts are of particular interest since the long dynamical timescales in these regions mean that coherent debris from past accretion events has the greatest longevity at such large radii. The discovery of the Sagittarius dwarf

A.M.N. Ferguson (⋈)

Institute for Astronomy, University of Edinburgh, Blackford Hill, Edinburgh EH9 3HJ, UK e-mail: ferguson@roe.ac.uk

A.D. Mackey

Research School of Astronomy & Astrophysics, Australian National University, Mount Stromlo Observatory, Cotter Road, Weston Creek, ACT 2611, Australia e-mail: dougal.mackey@anu.edu.au

galaxy and associated tidal stream (see Chap. 2) demonstrated beyond a doubt that satellite accretion played an important role in the growth of the Milky Way's halo, but the veracity of this aspect of the hierarchical model could not rest solely on a single event observed within a single galaxy. In this spirit, the late 1990s saw the quest begin to identify other galactic systems which were visibly in the process of devouring smaller satellites.

Our nearest giant neighbour, M31, provides the most obvious target for such studies. Lying at \sim 780 kpc, it is in many respects a sister galaxy to the Milky Way. It has a similar total mass (e.g., Diaz et al. 2014; Veljanoski et al. 2014), is of a similar morphological type, and it resides in the same low-density environment—one which is deemed typical for much of the present-day galaxy population. M31's proximity means that individual stars near the tip of the red giant branch (RGB) can be resolved from the ground; this offers a powerful method for probing very low effective surface brightnesses, such as those expected for tidal debris streams. Furthermore, its high inclination to the line-of-sight ($i \sim 77^{\circ}$) means that it is ideally suited for studies of its halo regions.

There are some disadvantages to studying tidal streams in M31 as opposed to our own Milky Way. Even with the world's largest telescopes, ground-based studies of M31's halo are limited to using luminous giant stars whereas Milky Way studies can harness the power of the much more numerous main sequence turn-off population (e.g., Belokurov et al. 2006). Additionally, in M31 we are mainly confined to analysis of projected positions on the sky (although occasionally some line-of-sight distance information is available), and we can only measure radial velocities. This can be contrasted with the situation in the Milky Way where it is possible to additionally determine line-of-sight distances¹ and proper motions, and thus probe the full six dimensional phase space. In effect, these differences imply that in M31 we are sensitive to tidal streams that are of higher surface brightness than those we can uncover in the Milky Way, and moreover typically only the subset retaining a high degree of spatial and/or kinematical coherence.

On the other hand, there are some clear advantages to studying an external system such as M31. Our vantage point largely alleviates complicated line-of-sight projection and extinction effects, such as must be endured in studies of the Milky Way. This means that we have a better understanding of the morphology of tidal features and where stellar substructures lie (at least in projection) with respect to each other, and with respect to additional halo tracers such as globular clusters (GCs) and dwarf satellites. Our bird's-eye view also makes it fairly straightforward to construct in situ samples of halo stars at various radii. Remarkably, we currently know more about the outer halo (R $\gtrsim 50\,\mathrm{kpc}$) of M31 than we do of the Milky Way. In the Milky Way, the outer halo is obscured by a dense veil of foreground stars making the robust identification of the low density population of outer halo

¹In practice, individual distances to large samples of stars in the Milky Way are crude at the moment. ESA's *Gaia* mission will change this when it starts to deliver data in 2016 but the most accurate distances will be limited to stars within roughly 10 kpc of the Sun.

stars difficult. In addition, while the main sequence turn-off method so extensively used by the Sloan Digital Sky Survey (SDSS) teams has probed out to distances of \sim 40 kpc, such stars are not detected in SDSS imaging at distances beyond this. While some outer halo substructures have been uncovered using other tracers (e.g., Newberg et al. 2003; Watkins et al. 2009), the inhomogeneous and sparse nature of these studies precludes any meaningful conclusions about the global properties of the Milky Way's outer halo. In M31, we also have a far clearer view of the low latitude regions of the galaxy, enabling discrimination between perturbed disk features and accreted substructures.

Over the last 15 years, a multitude of studies have targeted the outskirts of M31, and it can be readily argued that it is the system for which we currently have the most complete map of halo stars. This chapter reviews the tremendous progress and exciting results that have emerged from this work.

8.2 Historical Studies

While the first detailed studies of faint structure and substructure in M31 did not appear until the early 2000s, there were a number of studies prior to this which are of particular note.

Baade and Gaposchkin (1963) were the first to comment on the strong warp present in the outer parts of M31's stellar disk. Baade (p. 73) notes that the disk signature is still present at a major axis distance of 2° but that the opposing sides of the disk have "swirled" off in anti-symmetric directions by a radius of 2.25° —an observation he speculates could be due to the tidal action of the Milky Way on M31. The existence of the prominent stellar warp was further confirmed by Innanen et al. (1982) who stacked digitised Palomar Schmidt plates to reach surface brightnesses in M31 of $\mu_{V} \gtrsim 25.8$ mag arcsec⁻². Early H1 studies of M31 also revealed a strong warp in the neutral hydrogen disk (e.g., Roberts and Whitehurst 1975; Newton and Emerson 1977; Cram et al. 1980). While the stellar and H1 disks are warped in the same direction, the stellar warp appears to begin at a smaller radius than the H1 warp and it exhibits a greater deviation from the disk plane; this holds true along both major axes but seems especially apparent in the north-east.

Walterbos and Kennicutt (1988) conducted the definitive study of the light distribution in M31 before the era of wide-field resolved star mapping, including a first quantitative exploration of the peripheral disk. They constructed multi-band images from digitised Burrell Schmidt plates and analysed surface brightness and color profiles across the disk. They also detected a clear warp, but speculated that the north-eastern warp, due to its faintness and extreme bend, may actually be a galactic reflection nebula and not a stellar feature associated with M31. This issue was settled by Morris et al. (1994) who resolved the stellar populations in the north-eastern warp (which they termed the 'Spur') for the first time and showed they lay at the distance of M31. Figure 1 of Walterbos and Kennicutt (1988) shows beyond doubt that the north-eastern half of the disk is far more perturbed than the south-

western half, and, in hindsight, one can even see a slight luminosity enhancement in the direction of the Giant Stellar Stream.

Equally influential were the first studies of M31's resolved stellar halo. Mould and Kristian (1986), Crotts (1986) and Pritchet and van den Bergh (1988) all presented colour-magnitude diagrams (CMDs) of small regions located at several kpc along M31's minor axis, a region perceived at the time to be dominated by pure halo. These studies revealed a moderate metallicity population ([Fe/H] ~ -1) with a large metallicity spread, in stark contrast to the metal-poor halo of the Milky Way. The disparity of the halo populations in two galaxies that were otherwise considered rather similar remained a significant puzzle throughout the following decade.

8.3 Wide-Field Mapping Surveys of M31

The relative proximity of M31, while advantageous for detailed study, also poses a problem in that even the main body of the galaxy subtends a substantial angle on the sky. In the mid-to-late 1990s, wide-format CCD detectors became increasingly available on medium-sized telescopes and this development opened up new possibilities for surveying the faint outlying regions of M31. With a distance modulus of $m - M = 24.47 \pm 0.07$ (McConnachie et al. 2005), stars near the tip of M31's RGB ($M_I \approx -4$) have $I \approx 20.5$ and thus could be easily detected in modest exposures with a 2-m class telescope. As a result, it became feasible to contiguously map resolved stars at the bright end of the luminosity function over very large areas.

RGB stars are the evolved counterparts of low to intermediate mass (M $\sim 0.3\text{--}8\,M_\odot$) main-sequence stars with ages of at least 1 Gyr. While asymptotic giant branch stars and high mass main sequence stars can be even more luminous than RGB stars, RGB stars are the most interesting in the context of tidal stream research since they are long-lived and can be used to trace the old stellar components of galaxies, where signatures of hierarchical assembly are expected to be most prevalent. Additionally, for a fixed age, the colour of an RGB star depends almost entirely on its metallicity; thus, for a roughly uniform age stellar population, individual stellar metallicities can be derived purely from photometry.

Resolved star surveys map the spatial distribution of individual RGB stars which can in turn be used to infer the surface brightness distribution of the underlying light. This technique allows much lower surface brightness levels to be reached than typically achievable with conventional analyses of diffuse light. As a simplistic illustration of how the method works, consider a population of M31 RGB tip (TRGB) stars with $I_0 \sim 20.5$ and $(V - I)_0 \sim 1.5$. A surface density of 10^5 such stars per square degree corresponds to $\mu_V \approx 27$ mag arcsec⁻² while a surface density of 10^3 stars per square degree corresponds to $\mu_V \approx 32$ mag arcsec⁻². This calculation is crude since it neglects the fact that there is a range of RGB luminosities within a population, and also that some sizeable fraction of the total light will come from stars fainter than the magnitude limit, but these are corrections that can be easily calculated for any given survey (e.g., Pritchet and van den Bergh

1994; McConnachie et al. 2010). Nonetheless, it is sufficient to demonstrate that, in the low crowding outer regions of M31 (and external galaxies in general), the resolved RGB star technique is clearly the optimal means to search for and map very faint structures. The main challenges in using this method are to image to sufficient depth to detect a statistically significant population of RGB halo stars, and to disentangle genuine RGB stars from contaminating populations, which typically consist of foreground Milky Way dwarf stars and unresolved background galaxies (see left panel of Fig. 8.1).

The breakthrough in our ability to search for low surface brightness structure in the outskirts of M31 led to the discovery of a plethora of faint streams and substructure in the inner halo, including the dominant Giant Stellar Stream. The pioneering INT Wide Field Camera survey (e.g., Ibata et al. 2001; Ferguson et al. 2002; Irwin et al. 2005) mapped \approx 40 square degrees (163 contiguous pointings) around M31 in the *V* and *i* passbands, reaching to \sim 3 magnitudes below the TRGB (see right panel of Fig. 8.1). M31 was also targeted by the SDSS (Zucker et al. 2004a), where stars near the TRGB were mapped to large distances along the major axis. These surveys also uncovered several previously-unknown M31 dwarf satellites and globular clusters (e.g., Zucker et al. 2004b, 2007; Irwin et al. 2008; Huxor et al. 2008).

In parallel to these efforts to survey RGB stars, other groups began to explore the halo and outer disk populations using planetary nebulae (PNe) (e.g., Merrett

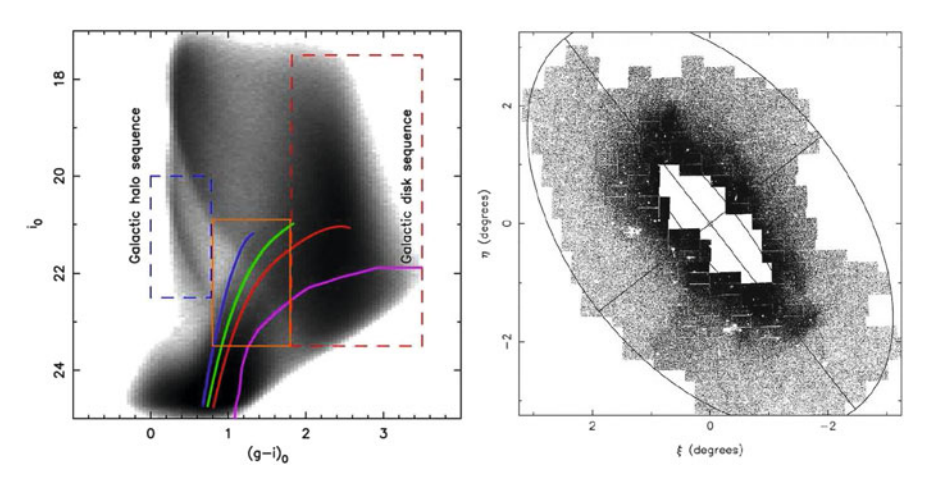


Fig. 8.1 (*Left*) A Hess diagram of the point sources in the PAndAS survey at distances beyond 2° of M31 (reproduced from Ibata et al. 2014). A series of fiducial tracks spanning [Fe/H]=-1.91, -1.29, -0.71 and -0.2 are superimposed on the RGB while contaminating Milky Way foreground disk and halo sequences are indicated by *dashed boxes*. Blueward of $(g-i)_0 \sim 1$ and fainter than $i_0 \sim 23$, unresolved background galaxies become the primary contaminant. The *orange box* shows the adopted colour-magnitude selection for M31 RGB stars. (*Right*) An early map of metal-poor RGB star counts around M31 from the INT/WFC survey (reproduced from Ferguson et al. 2002). The *outer ellipse* has a flattening of 0.6 and a semimajor axis length of 55 kpc

et al. 2003, 2006; Morrison et al. 2003; Kniazev et al. 2014). Although PNe offer some advantages over RGB stars as tracers of halo light (for example, they are more luminous, suffer much reduced sample contamination, and can provide simultaneous information on radial velocities), they are far rarer. From a survey of PNe in the M31 bulge, Ciardullo et al. (1989) found that the ratio between the number of PNe in the top 2.5 magnitudes of the luminosity function and the *V*-band luminosity was $\alpha_{2.5} \sim 30.8 \times 10^{-9}$ PNe per L_{\odot}. This leads to the expectation of \approx 50 PNe per square degree at $\mu_V \sim 24$ mag arcsec⁻² but only \approx 1 per square degree at $\mu_V \sim 28$ mag arcsec⁻². This makes surveys for resolved RGB stars far more efficient than those for PNe in the outer regions of M31. However, the situation changes for more distant galaxies, where RGB stars become too faint to resolve while PNe can still be detected (e.g., Coccato et al. 2013; Foster et al. 2014).

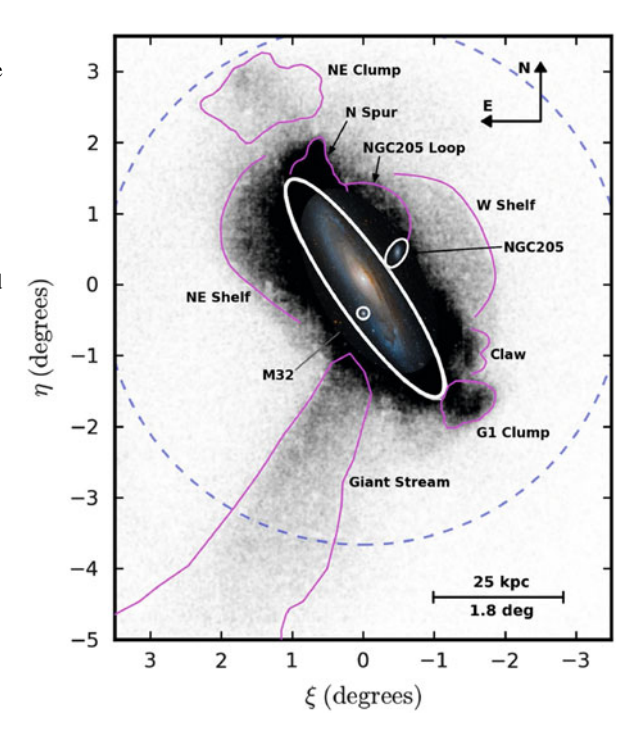
Based on the success of these early studies, exploration of the M31 *outer* halo began in the mid 2000s. Due to the lower stellar density in these parts, deeper photometry was required in order to sufficiently sample the RGB luminosity function and this in turn required larger telescopes. The Pan-Andromeda Archaeological Survey (PAndAS) was conducted using the MegaCam instrument on the 3.8-m CFHT to contiguously map over 380 square degrees around the M31-M33 region and detect stars to \sim 4 mag below the TRGB (e.g., Ibata et al. 2007; McConnachie et al. 2009; Ibata et al. 2014). Other wide-field ground-based work concentrated on deep pencil beam studies of the outer halo (e.g., Ostheimer 2003; Tanaka et al. 2010).

8.4 Major Tidal Features in the Halo of M31

Figures 8.2 and 8.3 show maps from the PAndAS survey of RGB stars in the inner and outer halo regions of M31, displayed to highlight prominent substructures. Additionally, Fig. 8.4 shows the distribution of RGB stars in four different metallicity bins, revealing how the morphology of the tidal debris changes as a function of metallicity. A striking feature of all of these visualisations is the non-uniformity of the stellar distribution in the outer regions. The most metal-poor map presented in Fig. 8.4 has a smoother appearance than the others, but it still exhibits a substantial degree of substructure.

The inner halo (R < 50 kpc) of M31 appears as a flattened structure (axis ratio \sim 0.5) in Fig. 8.2, around the edge of which bright tidal features (e.g., streams, clumps, spurs, shelves) can be seen. In the outer halo (R \geq 50 kpc), the most prominent features are a multitude of faint narrow streams and arcs. Based on their appearance in Fig. 8.4, these outer streams are also considerably more metal-poor than the substructures which dominate the inner halo. Lewis et al. (2013) searched for a correlation between the tidal structures seen in stars, and features in the H I gas around M31. Interestingly, they found a general lack of spatial correlation between these two components on all scales, with very few potential overlaps.

Fig. 8.2 The PAndAS map of metal-rich RGB stars in the inner halo of M31, upon which a typical textbook image of M31 is superposed. The map is constructed from stars with $i_0 \le 23.5$, having $-1 \le [Fe/H] \le 0$. The large white ellipse has a semi-major axis of 27 kpc and delineates the full extent of the bright disk; the dashed blue circle has a radius of 50 kpc. Prominent inner halo substructure is outlined and labelled, as are the dwarf satellites M32 and NGC 205



A brief description of some of the most prominent tidal features seen around M31 is given below:

- Giant Stellar Stream (GSS): Discovered in the first quadrant of M31 that was mapped by the INT/WFC survey, the GSS is the most prominent overdensity in M31's halo and covers a large fraction of its south-east quadrant (Ibata et al. 2001). It can be traced as a coherent structure to a projected galactocentric radius of ~ 100 kpc, and spans a width of ~ 25 kpc. The stream has a linear morphology with a sharp eastern edge and an estimated absolute V-band magnitude of $M_V \approx$ -14 (Ibata et al. 2001). However, this is a crude estimate based on only that part of the stream which is visible in the earliest INT maps. As the stream is now known to be more than twice as long as this, and other debris features have been identified as forward wraps of the structure, the total luminosity of the GSS could easily be 1-2 magnitudes higher. Ibata et al. (2007) show that there is a largescale stellar population gradient present, with the high surface brightness core region of the stream having relatively more metal-rich stars than the peripheral regions. Both photometric and spectroscopic studies reveal the core stream to have a moderately high metallicity of [Fe/H] ≥ -0.5 to -0.7, with the envelope dropping to [Fe/H] ~ -1.4 (Guhathakurta et al. 2006; Ibata et al. 2007; Gilbert et al. 2009).
- **G1 Clump:** This feature was first recognised in the INT map published by Ferguson et al. (2002) and appears as a rather round clump of stars located at a

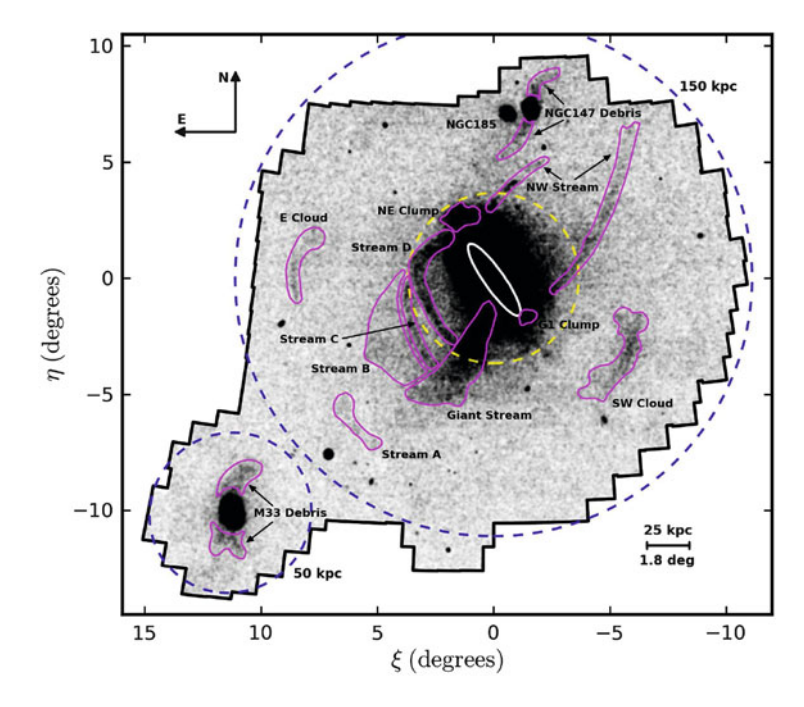


Fig. 8.3 A map of metal-poor RGB stars across the full extent of the PAndAS survey ($i_0 \leq 23.5$ and $-2.5 \leq [\text{Fe/H}] \leq -1.1$). The *white ellipse* is the same as in Fig. 8.2 while the *dashed circles* surrounding M31 have radii of 50 kpc (yellow) and 150 kpc (blue) respectively and that surrounding M33 has a radius of 50 kpc. Prominent outer halo substructure is outlined and labelled, as are tidal streams associated with the satellite galaxies M33 and NGC 147

projected radius of ~ 30 kpc along the south-western major axis of M31. It has dimensions of $0.5^{\circ} \times 0.7^{\circ}$, or 7×10 kpc at the distance of M31. Ferguson et al. (2002) estimate an absolute magnitude of $M_V \approx -12.6$ and a V-band surface brightness of ≈ 28.5 mag arcsec⁻². The feature was originally named because the luminous M31 globular cluster G1 lies nearby. This star cluster is notable because it has been argued to have both an internal metallicity spread as well as an intermediate-mass black hole, characteristics that suggest it could be the remnant core of a nucleated dwarf elliptical galaxy (e.g., Meylan et al. 2001; Gebhardt et al. 2005). While the detection of tidal debris in the vicinity of this enigmatic object was very exciting, subsequent observations of the properties of stars in the G1 Clump appear to rule out any association between the two (Rich et al. 2004; Reitzel et al. 2004; Ibata et al. 2005; Faria et al. 2007).

• North-East Clump (NE Clump): Located at a projected radius of \sim 40 kpc and near the north-eastern major axis, this substructure is one of the most nebulous features in the inner halo of M31. It subtends a diameter of \sim 1° or \sim 14 kpc at the distance of M31, and appears to connect to the main body of the galaxy by a faint filament. It is estimated to have an absolute *g*-band magnitude of $M_g \approx -11.6$

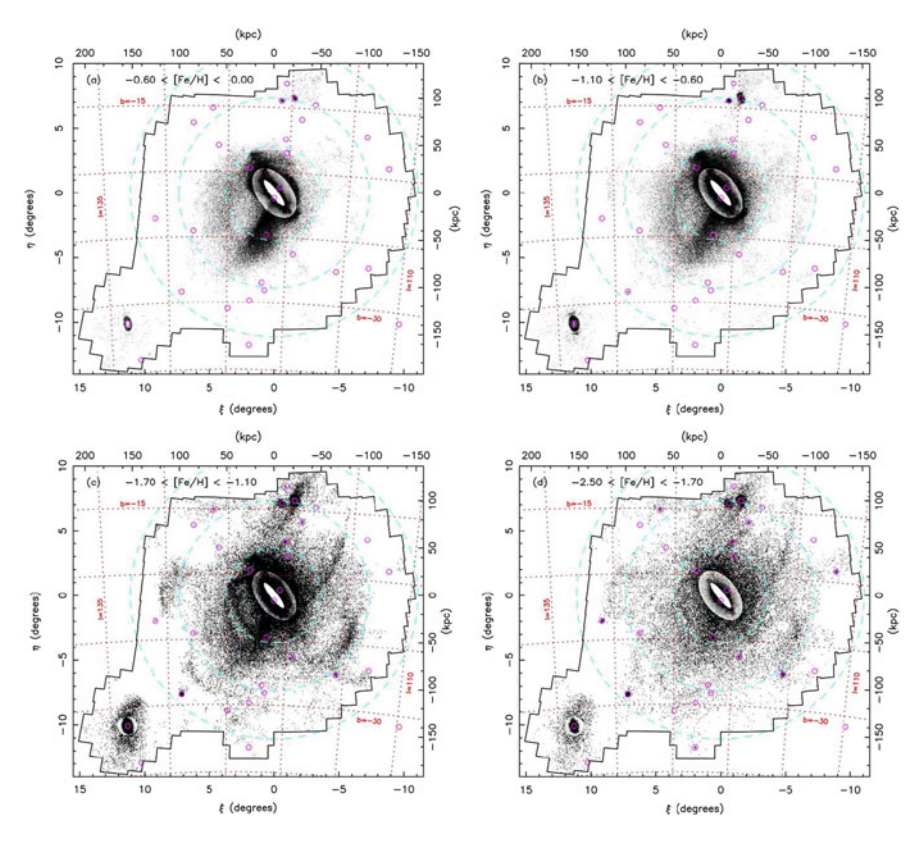


Fig. 8.4 The PAndAS map of RGB stars, as in Fig. 8.3, but presented this time as a function of metallicity. The two high metallicity bins (*top panels*) are dominated by the Giant Stellar Stream, although note that this structure changes morphology slightly between the two panels. While the low metallicity *bottom left panel* is dominated by numerous streams, the more metal-poor *right-hand panel* appears much smoother. [Reproduced from Ibata et al. (2014)]

and a *g*-band surface brightness of \approx 29.0 mag arcsec⁻² (Zucker et al. 2004a). Although it was initially suggested that the NE Clump was a disrupting dwarf satellite, subsequent observations have disfavoured this interpretation (Ibata et al. 2005; Richardson et al. 2008; Bernard et al. 2015a), since the stellar populations are more representative of the disk.

• North-Eastern (NE) and Western (W) Shelves: The NE Shelf is a diffuse but fairly sharp-edged extension lying north-east of M31's center, while the Western Shelf is a fainter feature of similar morphology and size on the opposite side of the galaxy. On the basis of their comparably high metallicities, Ferguson et al. (2002) suggested the NE Shelf could be an extension of the GSS. Using inferences from *N*-body simulations, Fardal et al. (2007) argued that both the NE and W Shelves were forward continuations of the stream, representing material stripped off during successive pericentric passages.

- Streams B, C, D: Identified by Ibata et al. (2007), Streams B–D are a series of approximately parallel tangential streams which cross the southern minor axis of M31 inside a radius of 100 kpc. Their metallicities are in the range −1.5 ≤ [Fe/H] ≤ −0.5. The eastern portions of Streams C and D appear to overlap in projection and all of the streams seem to terminate, or at least dramatically fade, once they reach the GSS. Stream C has been shown to be particularly complex, consisting of two distinct (but overlapping) metallicity and kinematic components (Chapman et al. 2008; Gilbert et al. 2009). Along with the GSS, the metal-rich component of Stream C is the only other outer halo feature visible in the most metal-rich maps of Fig. 8.4.
- Far Outer Halo Streams ($\mathbb{R} \gtrsim 100 \, \mathrm{kpc}$): Figs. 8.3 and 8.4 show that the outer halo is littered with various faint streams and clumps, including Stream A, the North-West (NW) Stream, the South-West (SW) Cloud and the Eastern (E) Cloud (Ibata et al. 2007; McConnachie et al. 2009; Richardson et al. 2011; Carlberg et al. 2011; Bate et al. 2014). With $\mu_{V} \geq 31.5 \, \mathrm{mag \ arcsec^{-2}}$, these streams represent the faintest spatially-coherent debris yet identified around M31. Stream A crosses the minor axis at a projected radius of $\sim 120 \, \mathrm{kpc}$ and aligns with the inner network of tangential streams. The E and SW Clouds appear as stellar arcs at slightly smaller radii on either side of Stream A. The NW Stream is a long ($\sim 100 \, \mathrm{kpc}$) and narrow ($\sim 3 \, \mathrm{kpc}$) radial feature; although there is no visible connection between the upper and lower branches of the stream, the fact that both trace out segments of a single ellipse and have a similar metallicity has supported the notion they are related (Carlberg et al. 2011). Part of the NW Stream was also seen in the deep pencil beam study of Tanaka et al. (2010) (their (Stream F); however, their Stream E was not recovered in the PAndAS survey.

8.5 Understanding the Nature and Origin of Tidal Features in M31

Following the initial discovery of tidal features in the M31 halo, concerted follow-up observations and detailed modelling have been carried out in order to develop a complete understanding of this material. In this section, we review and summarise some highlights from this work.

8.5.1 The Giant Stellar Stream

Over the last decade, the GSS has been the subject of intense study. On the observational side, efforts have concentrated on deriving quantities (e.g., distance, velocity) that can be used to model the orbit of the progenitor and on stellar population constraints that can be used to establish its nature. On the theoretical

side, work has focused on reconstructing the orbital history of the progenitor and using this knowledge to measure the halo mass of M31.

Line-of-sight distances to the stream are one of the key inputs for GSS orbit models. McConnachie et al. (2003) used measurements of the TRGB in a series of CFHT12K pointings to show that the GSS lies $\gtrsim 100\,\mathrm{kpc}$ behind M31 at a projected radial distance of 60 kpc and moves progressively closer to galaxy at smaller radii, with their distances being indistinguishable (within the uncertainties) at $\leq 10\,\mathrm{kpc}$. These authors were also able to detect the stream in two fields on the northern side of M31, where it lies $\sim 40\,\mathrm{kpc}$ in front of the galaxy, but no further, suggesting that the stream wraps fairly tightly around the M31 center towards the north-east.

Another key observable is the radial velocity distribution of stream stars. Individual RGB stars at the distance of M31 are sufficiently faint that an 8-m class telescope is required in order to measure their line-of-sight velocities; the DEIMOS multi-object spectrograph on the Keck II telescope has been the source of almost all the GSS radial velocity measurements to date (Ibata et al. 2004; Guhathakurta et al. 2006; Kalirai et al. 2006; Gilbert et al. 2009). These studies have shown that the radial velocity of the GSS becomes increasingly positive with increasing distance from the center of M31, ranging from $V_{helio} = -320 \,\mathrm{km \, s^{-1}}$ at a projected distance of 60 kpc to $V_{helio} = -524 \,\mathrm{km \, s^{-1}}$ at a projected distance of 17 kpc. In all fields studied so far, the velocity dispersion is quite narrow—in the range of 10–30 km s⁻¹. Intriguingly, a second cold kinematic component has been detected at several locations along the GSS (Kalirai et al. 2006; Gilbert et al. 2009). It has the same velocity gradient (and dispersion) as the primary GSS over the range in which the two have been mapped (\sim 7 kpc) but it has a radial velocity that is offset by $\sim +100 \, \mathrm{km \, s^{-1}}$. It is presently unclear whether this component is due to M31's disturbed disk or a forward wrap or bifurcation of the main stream.

The combination of line-of-sight distance and radial velocity measurements indicates that the GSS progenitor fell almost straight into M31 from behind. These data have motivated a variety of efforts to model the accretion of a dwarf satellite galaxy on a highly radial orbit (Ibata et al. 2004; Font et al. 2006; Fardal et al. 2006, 2008, 2013; Mori and Rich 2008; Sadoun et al. 2014). While these models differ in various aspects, they generally agree on the fact that the progenitor's initial stellar mass was in the range $1-5 \times 10^9 \, \rm M_{\odot}$ and that its first pericentric passage came within a few kpc of the M31 center less than $1-2 \, \rm Gyr$ ago. Some properties of the observed GSS, in particular the asymmetric distribution of stars along the stream cross section and the internal population gradient, are better reproduced in *N*-body models in which the progenitor possessed a rotating disk (e.g., Fardal et al. 2008; Sadoun et al. 2014).

In this near head-on collision, the progenitor experiences significant destruction at the first pericentric passage. Much of the satellite's mass is stripped off to form leading and trailing tidal streams, and a generic prediction is that much of M31's inner halo should be littered with this debris. Figure 8.5 shows the sky distribution of debris in a set of recent N-body models of the GSS's orbit within the M31 potential (Fardal et al. 2013). Each panel differs in the adopted values of M_{200} , the M31 mass inside a sphere containing an average density 200 times the closure density of the

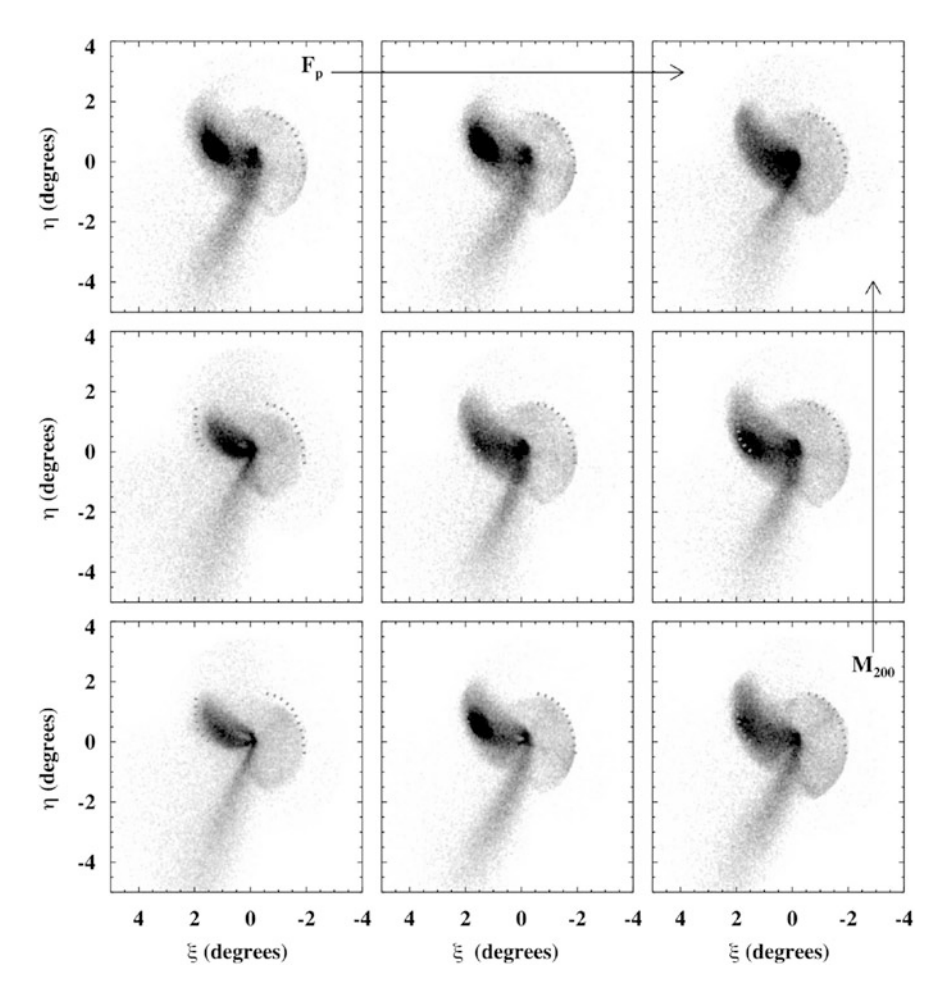


Fig. 8.5 Spatial distribution of stellar debris from the tidal disruption of the GSS progenitor, as predicted by a set of 9 N-body simulations. The *dashed lines* show the observed boundaries of the NE and W shelves. In each case, different combinations of M_{200} , the virial mass of M31, and F_p , the orbital phase of the progenitor at the present epoch, are adopted. While all panels share similar morphologies and resemble the main features seen in Figs. 8.2 and 8.3, some systematic differences can be seen as a function of the parameters. The present-day state of the progenitor varies from being tightly bound to highly dispersed; in all models shown here, it lies in the region of the NE shelf. [Reproduced from Fardal et al. (2013)]

universe, and F_p , the orbital phase of the progenitor at the present day. Although the exact pattern of debris depends on these (and a few other) parameters, all panels exhibit a similar morphology and show remarkable consistency with some of the features seen in Figs. 8.2 and 8.3. The GSS, the NE Shelf and the W Shelf are all naturally reproduced in this scenario, with the GSS representing the trailing stream of material torn off in the progenitor's first pericentric passage while the

NE and W shelf regions contain material torn off in the second and third passages, respectively. These predictions are in excellent agreement with observations of the stellar populations of these substructures — which show striking similarities in their star formation histories (SFHs) and metallicity distributions to those of the GSS (e.g. Ferguson et al. 2005; Richardson et al. 2008) — as well as with the observed kinematics of the shelves (e.g. Gilbert et al. 2007; Fardal et al. 2012). The extensive pollution of M31's inner halo by material stripped from the GSS progenitor provides at least a partial explanation for why this region is dominated by more metal-rich stellar populations compared to the Milky Way (e.g., Mould and Kristian 1986; Ibata et al. 2014).

Based on the projected positional alignment with the GSS, M31's luminous dwarf elliptical satellites M32 and NGC 205 were initially considered as prime candidates for the progenitor (Ibata et al. 2001; Ferguson et al. 2002). Indeed, both these systems possess unusual properties and, as will be discussed in Sect. 8.7, are tidally distorted in their outer regions (Choi et al. 2002; Ferguson et al. 2002). However, even the earliest attempts at orbit models ruled out a straightforward connection between the GSS progenitor and either of these two satellites (Ibata et al. 2004). Current models agree that any existing remnant should lie in the region of the NE Shelf, although thus far no candidate has been identified.

Although the location of the GSS progenitor remains a mystery, analysis of the stellar populations in the stream has provided important insight into its nature. Figure 8.6 shows deep HST CMDs of a variety of tidal debris fields in the inner halo of M31, including those associated with the GSS. One can clearly see two predominant CMD morphologies—those which contain a narrow tilted red clump and a prominent horizontal branch extending quite far to the blue (labelled 'SL' in Fig. 8.6), and those which contain a rounder red clump, a well-populated blue plume and exhibit no horizontal branch (labelled 'DL' in Fig. 8.6). Those pointings which directly sample material associated with the GSS progenitor uniformly exhibit the morphology of the former type (Ferguson et al. 2005; Richardson et al. 2008). A third category, labelled 'C', appears to be a composite of the previous morphologies.

Quantitative measures of the SFH and age-metallicity relation (AMR) of the GSS have been derived from deep CMDs using synthetic modelling techniques (Brown et al. 2006; Bernard et al. 2015a). The bottom panels of Fig. 8.7 show the most extensive analysis carried out to date, based on the 5 fields lying on GSS debris located throughout the inner halo. It appears that star formation in the progenitor got underway early on and at a fairly vigorous pace, peaking 8–9 Gyr ago. Star formation remained active until about 6 Gyr ago when there was a very rapid decline; this 'quenching' may indicate the time when the progenitor first entered the halo of M31. Roughly 50% of the stellar mass in the GSS fields was in place ~9 Gyr ago, and the metallicity had reached the solar value by 5 Gyr ago, consistent with direct spectroscopy constraints from RGB stars (e.g., Guhathakurta et al. 2006; Kalirai et al. 2006; Gilbert et al. 2009). In addition, all the GSS fields probed thus

²Meanwhile, Block et al. (2006) argue that a head-on collision between M31 and M32 about 200 million years ago could be responsible for the formation of two off-center rings of ongoing star formation seen in the M31 disk.

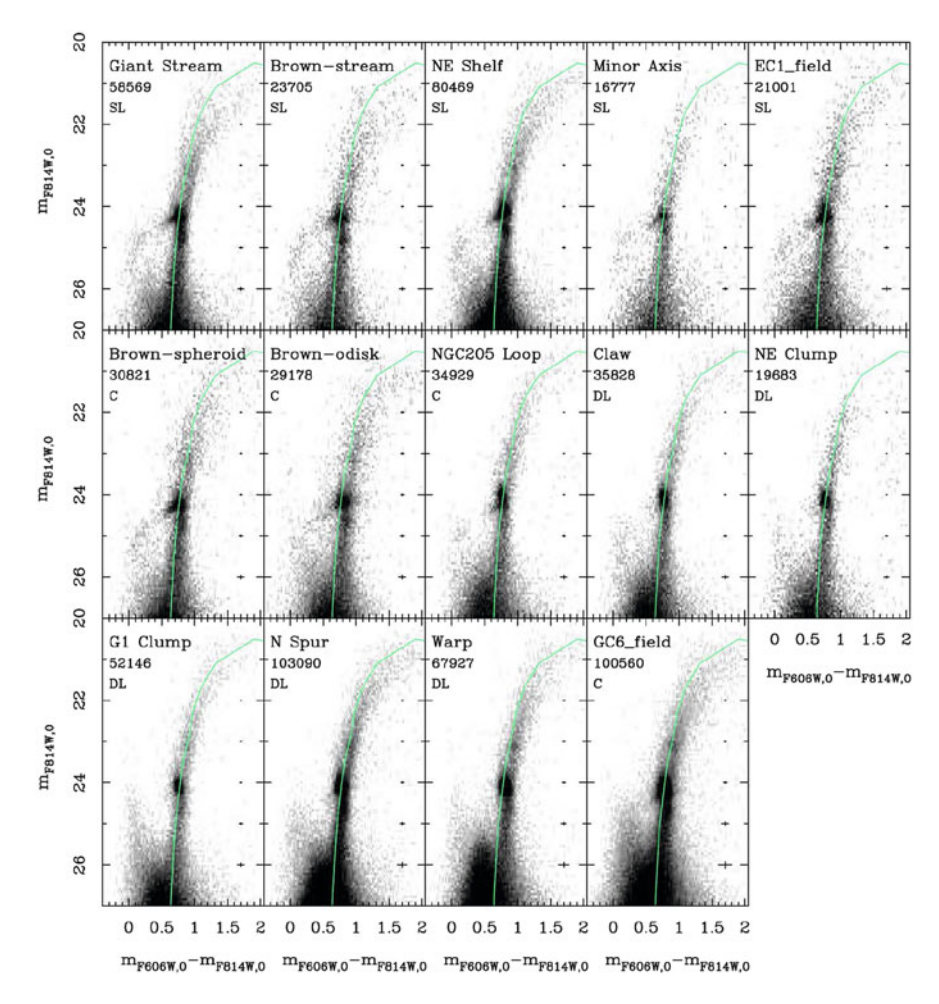


Fig. 8.6 HST/ACS Hess diagrams of 14 fields in the inner halo of M31, many of which lie on substructures seen in Fig. 8.2. The ridge line of 47 Tuc ([Fe/H]=-0.7 and age 12.5 Gyr) has been shifted to the distance of M31 and overlaid in each case. Based on their CMD morphologies, the fields can be segregated into two classes; stream-like (SL) fields with tilted red clumps and extended horizontal branches and disk-like (DL) fields with round red clumps and a population of blue plume stars. Composite (C) fields have features in common with both and likely represent cases where different material is projected along the line-of-sight. [Reproduced from Richardson et al. (2008)]

far reveal a large spread in metallicity (\geq 1.5 dex). Taken together, these properties suggest an early-type progenitor, such as a dwarf elliptical galaxy or spiral bulge. This further supports inferences from N-body modelling which suggest that the GSS progenitor was a fairly massive object with some degree of rotational support. Indeed, Fardal et al. (2013) argue it was likely the fourth or fifth most massive Local Group galaxy as recently as 1 Gyr ago.

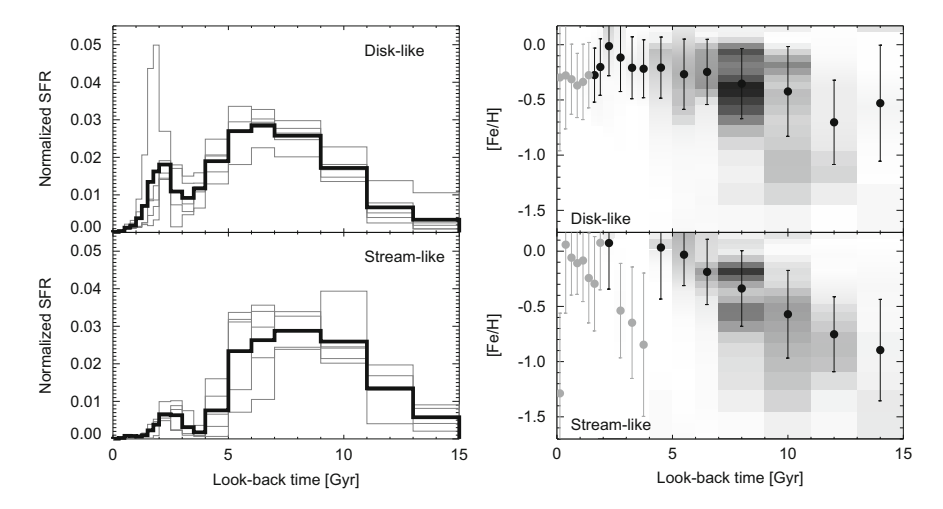


Fig. 8.7 (*Left*) The SFHs and (*right*) AMRs of M31 inner halo substructure fields, derived from quantitative fitting of the CMDs in Fig. 8.6. The SFHs for the individual fields are shown in *light grey* and are normalised to the total mass of stars formed in each field. Overlaid in bold are the average behaviours of the normalised SFHs. The *filled circles* in the AMRs show the median metallicity in each age bin, with *grey circles* indicating those bins which contain $\leq 1\%$ of the total stellar mass and hence carry significant uncertainties. There is more star formation at early (late) times in the stream (disk) fields and the stream fields also exhibit a more rapid early chemical evolution

8.5.2 Other Inner Halo Substructure

While tidal debris from the GSS progenitor can explain the origin of some of the M31 inner halo substructure, other features require a different origin. In particular, the substructures lying near the major axis—such as the NE and G1 Clumps and the Claw—do not arise naturally in models of the dissolution of the stream progenitor.

A first step to understanding this low latitude substructure was taken by Ibata et al. (2005) who analysed the kinematics of stars in numerous fields around M31, including the G1 and NE Clumps. They noted a strong signature of rotation in almost all fields out to a galactocentric radius of \sim 40 kpc, with some further detections out to 70 kpc. Stars are observed to move with velocities close to those expected for circular orbits in the plane of the M31 disk and with a typical velocity dispersion of $30\,\mathrm{km\,s^{-1}}$. Based on stacked spectra, Ibata et al. (2005) estimated the mean metallicity of these rotating outer populations to be [Fe/H] \sim -0.9.

The irregular morphology yet coherent rotation observed in the outer disk regions led Ibata et al. (2005) to speculate that a vast disk-like structure was being assembled as a result of multiple accretion events. However, this interpretation faced a number of challenges, such as the homogeneity of the constituent stellar populations and the need for the accreted satellites to be sufficiently massive so that dynamical friction could circularise their orbits before disruption.

An alternative explanation is that much of the inner halo substructure is material that has either been torn off of the M31 outer disk or dynamically heated from the disk into the halo. It has long been known that the accretion of a low mass companion can have rather a disruptive effect on a stellar disk (e.g., Quinn et al. 1993; Walker et al. 1996) and more recent work has quantified the way in which disk stars can get ejected into the halo through such events (e.g., Zolotov et al. 2009; Purcell et al. 2010). Kazantzidis et al. (2008) demonstrated how the accretion of a population of satellites with properties drawn from a cosmological simulation can produce distinctive morphological features in the host galaxy's disk, similar to the inner halo substructures seen in M31. Additionally, they confirmed earlier work that showed the final distribution of disk stars exhibits a complex vertical structure that can be decomposed into a thin and thick disk (see also Villalobos and Helmi 2008).

Examination of the constituent stellar populations in the non-GSS debris fields supports the idea that this material has originated in the disk (e.g., Ferguson et al. 2005; Brown et al. 2006; Richardson et al. 2008; Bernard et al. 2015a). The 'DL' fields in Fig. 8.6 are rather homogeneous in appearance, all displaying a round red clump with significant luminosity width, a well-populated blue plume and no apparent horizontal branch—features that indicate continuous star formation and a moderately young mean age. The quantitative SFHs and AMRs of the 'disk-like' debris fields further strengthen this assertion; roughly 65 % of the stars formed in the last 8 Gyr and chemical evolution proceeded at a modest pace, starting from a pre-enriched level (see top panels of Fig. 8.7). Most importantly, these trends are strikingly similar to those that have been measured for populations in the M31 outer disk (Bernard et al. 2012, 2015b).

It is also notable that both the stream-like and disk-like fields in Fig. 8.7 show evidence for an enhancement in the rate of star formation roughly 2 Gyr ago. This is surprising given that the constituent stellar populations in these fields have very different origins, and that many of them are substantially displaced from the main body (and the gas disk) of M31. There is now strong evidence that the M31 outer disk underwent a burst of star formation around this epoch, likely triggered by the relatively close passage of M33 (Bernard et al. 2012, 2015b). The existence of trace populations from this episode scattered throughout the inner halo, including up to 20 kpc along the minor axis, argues for a redistribution of disk material in the intervening time. It would thus appear that, in addition to being heavily polluted by GSS debris, the M31 inner halo also contains a widespread component of heated disk stars (Bernard et al. 2015a). This idea was independently raised by Dorman et al. (2013), who find that a non-negligible fraction of the inner halo stars identified kinematically in M31 show a luminosity function consistent with an origin in the disk.

Both the highly structured nature of the outer disk *and* the presence of displaced disk stars in the halo could be explained by one or more violent accretion events. Given the likely transitory nature of the outer disk substructures (Ibata et al. 2005) and the fact that stars as young as 2 Gyr have been displaced into the halo, the event responsible for disrupting the disk must have been rather a recent one and it

is tempting to speculate that it has been the head-on impact of the GSS progenitor roughly 1 Gyr ago (e.g., Mori and Rich 2008; Sadoun et al. 2014). If this scenario is correct, it implies that, in spite of its extremely messy appearance, all of M31's inner halo substructure can be traced to the direct and indirect effects of a single event.

8.5.3 Outer Halo Substructure

The outer halo debris features in M31 are much more poorly understood than those of the inner halo. While the inner halo is populated by tidal debris with a variety of morphologies and moderate metallicities, the outer halo is dominated by fairly narrow stellar streams and arcs which are, with the exception of the metal-rich component of Stream C, only apparent in maps constructed from metal-poor stars (see Fig. 8.3). The outer halo streams are of such low surface brightness that detailed characterisation of their stellar populations and kinematics has thus far been difficult. As will be discussed in the following section, GCs offer a very exciting way to probe the tidal features in these parts.

There are four main structures visible in the far outer halo—Stream A, the E Cloud, the SW Cloud and the NW Stream. All of these features lie at radii > 100 kpc from the center of M31 and subtend at least a few tens of kpc in length. Their CMDs indicate a similar metallicity of [Fe/H] ~ -1.3 (Ibata et al. 2007, 2014; Carlberg et al. 2011; Bate et al. 2014). The most luminous of the outer halo structures is the SW Cloud which Bate et al. (2014) estimate contains $\sim 5.6 \times 10^6 \, \rm L_{\odot}$ or equivalently $M_V \approx -12.1$. This luminosity is approximately 75 % of that expected for the feature on the basis of its measured metallicity and the Kirby et al. (2011) luminosity-metallicity relation. While this might indicate that a sizeable fraction of the luminosity of the parent object has been detected, it remains unclear at present whether these most distant halo features originate from distinct accretion events or material torn off from a single progenitor. Indeed, an interesting question is whether any of the outer halo debris can be traced to the accretion of the GSS progenitor. Although the metallicity of these features is considerably lower than that of the core of the GSS, it is a good match to that of the stream envelope (Ibata et al. 2007; Gilbert et al. 2009).

It is curious to note that the dwarf spheroidal satellite And XXVII appears projected on the upper segment of the NW Stream. Discovered by Richardson et al. (2011), this faint ($M_V \approx -7.9$) system is highly morphologically disturbed and it is tempting to speculate that it may be the source of the NW Stream debris. However, the metallicity of the stream stars appears somewhat higher than that of the dwarf galaxy which complicates the interpretation (Carlberg et al. 2011; Collins et al. 2013). Furthermore, Collins et al. (2013) note additional kinematic substructure in the vicinity of And XXVII which is not yet understood.

Ibata et al. (2014) have recently conducted a global analysis of the large-scale structure of the M31 halo using data from the PAndAS survey. Despite the presence

of copious substructures throughout, they find that the stellar halo populations closely follow power-law profiles that become steeper with increasing metallicity. The *smooth* metal-poor halo component (defined as the population with [Fe/H] < -1.7 that cannot be resolved into spatially distinct substructures with PAndAS), has a global (3D) power-law slope of $\gamma = -3.08 \pm 0.07$ and an almost spherical shape, but accounts for a mere \sim 5% of the overall halo luminosity. By far, most of the luminosity of the halo out to the edge of the PAndAS survey resides in moderatemetallicity substructure. Ibata et al. (2014) estimate that the total stellar mass of the M31 halo at distances beyond 2° is $\sim 1.1 \times 10^{10} \,\mathrm{M}_{\odot}$ and that the mean metallicity decreases from [Fe/H] = -0.7 at R = 30 kpc to [Fe/H] = -1.5 at R = 150 kpc for the full sample. An alternative approach to studying the outer halo in M31 has been taken by the SPLASH team who have obtained spectroscopy of RGB stars in many pencil-beam fields extending out to 175 kpc (Guhathakurta et al. 2006; Kalirai et al. 2006; Gilbert et al. 2006, 2012, 2014). In contrast to photometric studies, their approach allows them to identify and remove kinematic substructure in their fields, at least out to 90 kpc. Although it is not possible to directly compare the results of the PAndAS and SPLASH surveys, which are based on very different sample selections, their inferences on the global halo properties of M31 appear to be largely consistent (Ibata et al. 2014; Gilbert et al. 2014).

8.6 Globular Clusters as Probes of Tidal Streams in M31

An intriguing question regarding the substructures seen in the halo of M31 is whether they show any degree of spatial correlation with members of the M31 GC system. This is motivated in part by the long-held suspicion that a substantial number of the GCs in the Milky Way halo did not form in situ, but rather in small satellite dwarf galaxies that subsequently fell into the Galactic potential well and disintegrated. This idea was first suggested in the seminal paper by Searle and Zinn (1978) and was spectacularly verified in the early 1990s with the discovery of the disrupting Sagittarius dwarf, which is in the process of depositing *at least* five GCs into the outer halo of the Milky Way (e.g., Bellazzini et al. 2003; Law and Majewski 2010; see also Chap. 2 of this volume). Modern studies of the Galactic GC system have only served to add further weight to the assertion—it is now known that the abundances, velocities, ages, horizontal branch morphologies, and sizes of perhaps up to a third of Milky Way GCs are consistent with an external origin (e.g., Zinn 1993; Mackey and Gilmore 2004; Mackey and van den Bergh 2005; Marín-Franch et al. 2009; Forbes and Bridges 2010; Dotter et al. 2010, 2011).

Historically almost all work on the M31 GC system has been confined to regions comparatively close to the galactic center, typically within R \sim 20–25 kpc; however the situation has changed thanks to the aforementioned wide-field mapping surveys of M31. In particular, the INT/WFC and PAndAS surveys, but also to some extent the SDSS, have facilitated the first detailed and uniform census of the outer halo GC system of M31 (Huxor et al. 2005, 2008, 2011, 2014; Martin et al. 2006; di Tullio

Zinn and Zinn 2013, 2014). Remote clusters are abundant in M31; there are now more than 90 objects known to reside at projected radii beyond 25 kpc, 13 of which sit outside 100 kpc in projection, with the most distant at \sim 140 kpc in projection and up to 200 kpc in three dimensions (Mackey et al. 2010a, 2013b). This is many more than are seen in the outskirts of the Milky Way—while the disparity in the number of GCs in the Milky Way and M31 within \sim 25 kpc is roughly 3:1 in favour of M31, outside this radius it is more like 7:1 in favour of M31 (Huxor et al. 2014).

Figure 8.8 shows the positions of all known M31 GCs plotted on top of the PAndAS spatial density map of metal-poor RGB stars. In the outer parts of the halo, where large, coherent tidal debris streams are readily distinguished, there is a striking correlation between these features and the positions of a large fraction (\sim 50–80%) of the GCs. Substantial numbers of clusters are seen projected onto the

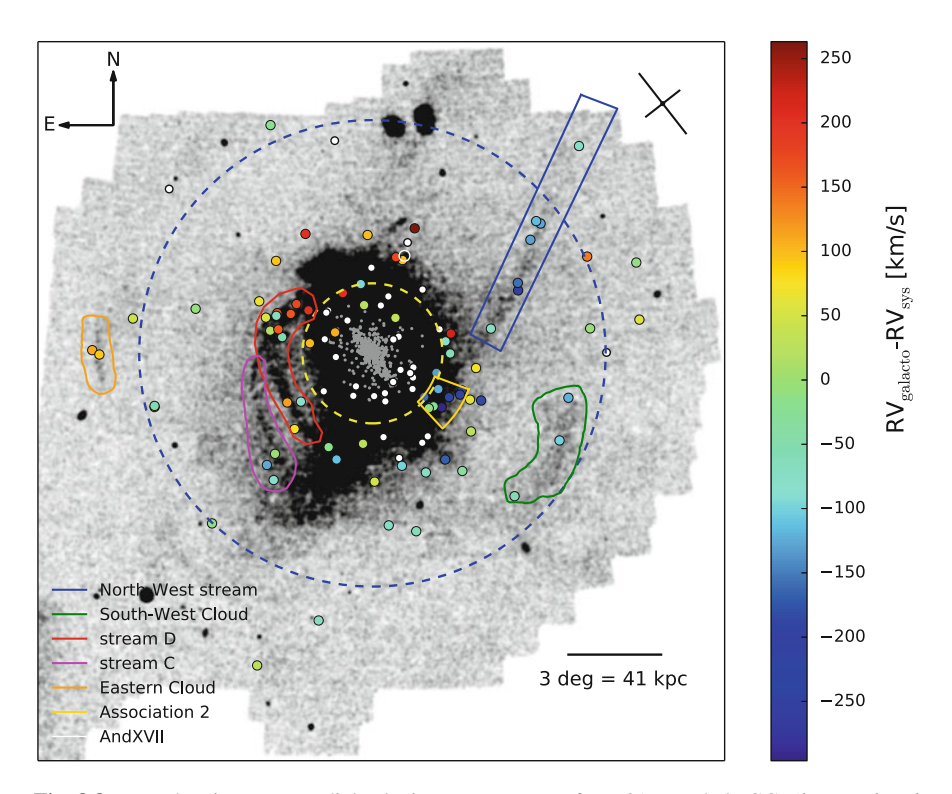


Fig. 8.8 Map showing extant radial velocity measurements for M31 outer halo GCs (*large colored dots*), projected on top of the PAndAS metal-poor RGB map. Most of the outer halo GCs can be seen to preferentially lie along stellar streams. Inner halo GCs from the Revised Bologna Catalogue are shown as *grey points*. The GCs are colour-coded by their radial velocity in the M31-centric frame (*white points* indicate those objects with no radial velocity measurement), and the *inner* and *outer dashed circles* correspond to radii of 30 and 100 kpc. A clear rotational signature is seen, with GCs in the NE side of the galaxy receding while those in the SW quadrant approach us. Additionally, coherent velocities are seen for GCs which lie along specific debris features, strongly suggesting that the GCs have been brought into M31 along with their host galaxies

NW Stream, the SW Cloud, the E Cloud, and the overlapping portion of Streams C and D. There is, in addition, a statistically significant overdensity of clusters ("Association 2") sitting near the base of the NW Stream, that cannot (as of yet) be identified with a visible tidal stream in the field halo.

Mackey et al. (2010b) have demonstrated that the probability of this global alignment between clusters and streams arising randomly is low—well below 1% for a GC system possessing an azimuthally uniform spatial distribution. This implies that the observed coincidence represents a genuine physical association and hence direct evidence that much of the outer M31 GC system has been assembled via accretion. Moreover, at least some of the properties of the accreted M31 GCs appear to be consistent with those exhibited by ostensibly accreted Galactic members—particular examples being those of younger ages (Mackey et al. 2013a) and extended structures (Huxor et al. 2011; Tanvir et al. 2012).

The argument made by Mackey et al. (2010b) is based entirely on statistical grounds; to determine on an object-by-object basis which GCs are associated (or not) with a given substructure requires kinematic information. The most extensive kinematic study of the M31 outer halo GC system to date is by Veljanoski et al. (2013, 2014), who acquired spectra for 71 clusters outside a projected radius of 30 kpc (representing 86% of the known population in these parts); the velocities of these objects in the M31-centric frame are color-coded in Fig. 8.8. It can be readily seen that GCs projected onto a given outer halo substructure tend to exhibit correlated velocities (see left panel of Fig. 8.9 for an example). Those objects on the NW Stream and SW Cloud reveal strong velocity gradients from one end of the substructure to the other, while clusters on the E Cloud form a close group in phase space. Members of the Stream C/D overlap area, and those in Association

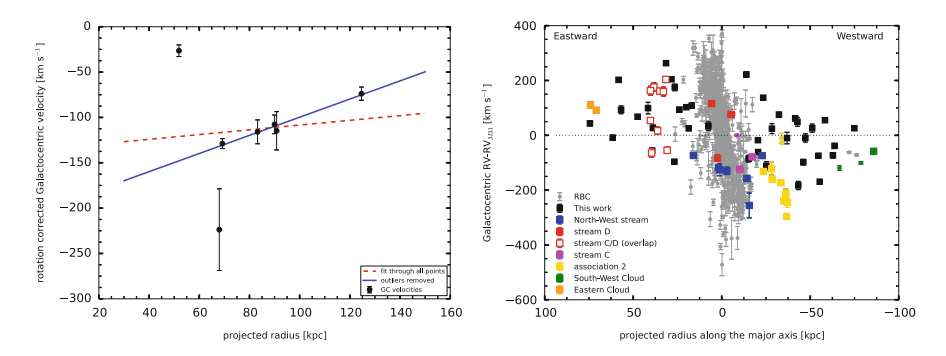


Fig. 8.9 (*Left*) Radial velocities for seven GCs that lie along the NW Stream. A clear signature of radial infall is evident. (*Right*) GC velocities, in the Galactocentric frame and corrected for the M31 systemic motion, versus distance along the M31 major axis. GCs which lie along specific debris features in the outer halo are colour-coded accordingly, while inner GC velocities taken from the literature are shown in *light grey*. The outer halo GCs rotate in the same sense as the inner GCs but with a somewhat smaller amplitude. The rotation is exhibited by the ensemble system of outer halo GCs and is not driven by specific stream features. Both panels are reproduced from Veljanoski et al. (2014)

2, split into additional sub-groups by velocity. A remarkable feature of many of the ensembles considered by Veljanoski et al. (2014) is the coldness of their kinematics, with all GC groupings exhibiting velocity dispersions consistent with zero given the individual measurement uncertainties. These results strongly reinforce the notion that a substantial fraction of the outer halo GC population of M31 has been accreted, and that these clusters trace the velocities of the tidal streams from their progenitor systems. Indeed, while definitive measurements have thus far only been possible for two substructures, the velocities of the GCs sitting on Stream C and on the SW Cloud have been shown to be in excellent agreement with those of the underlying stream stars (Collins et al. 2009; Mackey et al. 2014).

Figure 8.8 also demonstrates the surprising result that the M31 GC system as a whole possesses bulk rotation—those GCs to the west of M31 appear to systematically possess negative velocities in the M31-centric frame, while those to the east typically have positive velocities. Veljanoski et al. (2014) compared a variety of kinematic models to the data and found a rotation amplitude of $86 \pm 17 \,\mathrm{km \, s^{-1}}$ around an axis aligned with the M31 optical minor axis provided the best match. This rotation velocity is quite substantial—for comparison, Veljanoski et al. (2014) also found evidence that the velocity dispersion in the cluster system decreases from 129^{+22}_{-24} km s⁻¹ at 30 kpc to roughly 75 km s⁻¹ at 100 kpc. The right panel of Fig. 8.9 further elucidates this rotation by showing the GC velocities in the M31-centric frame as a function of projected radius along the major axis. It is apparent that the rotation of the outer halo GC system is in the same sense as for the inner halo clusters (and indeed the M31 disk), albeit with smaller amplitude. Importantly, the rotation does not seem to be driven purely by clusters that sit on the particular halo substructures nor by those sitting well away from any underlying halo feature—both groups apparently share in the pattern equally.

Understanding the origin of the angular momentum in the outer halo GC system of M31 presents a significant challenge. One possibility is if a large fraction of the halo GC system was brought into M31 by just one relatively massive host galaxy on a low inclination orbit. However, in this scenario it is difficult to explain the observed presence of distinct dynamically cold subgroups of GCs as well as the typically narrow stellar debris streams in the halo. Another possibility is that the outer halo GC system results from the assimilation of several dwarf galaxies, but that these were accreted onto M31 from a preferred direction on the sky. This scenario might well be related to the recent discovery that many dwarf galaxies, both in the Milky Way and M31, appear to lie in thin rotating planar configurations such that their angular momenta are correlated (Ibata et al. 2013; Pawlowski et al. 2012). In this context it is relevant that almost all of the dwarf galaxies thought to be members of the planes presently observed in both M31 and the Milky Way are insufficiently massive to host GCs, and furthermore that the rotation axes of the M31 outer halo GC system and the M31 dwarf plane are misaligned with each other by ~45°.

8.7 Tidal Streams from M31's Satellite Galaxies

M31 has a substantially richer satellite system than the Milky Way. Not only does it possess more dwarf companions, but it also possesses several moderately luminous ones: M33 with $M_{\rm V}=-18.8$ and the four dwarf ellipticals (dEs) M32, NGC 205, NGC 147 and NGC 185 with $M_{\rm V}=-15.5$ to -16.5 (McConnachie 2012; Crnojević et al. 2014). Tidal features are now known around nearly all of these systems, indicating that they are in the process of depositing tidally-stripped stars into the M31 halo.

The innermost satellites of M31 are M32 and NGC 205, which lie at M31-centric distances of 25 and 42 kpc, respectively (McConnachie 2012). These systems overlap the main body of M31 in projection, a fact that has greatly complicated detailed analyses of their outer structures. Nonetheless, diffuse light studies indicate that both systems exhibit breaks in their surface brightness profiles which are accompanied by sharp changes in isophotal ellipticity and position angle; such behaviour is consistent with expectations for systems undergoing tidal interaction and stripping (Choi et al. 2002; Johnston et al. 2002). Additionally, Ferguson et al. (2002) present isopheth maps from a scanned deep photographic plate which reveal the characteristic "S"-shape of tidal distortion in their peripheral regions. It is therefore curious that kinematic studies support the existence of unbound stars at large radii in NGC 205 but not in M32 (Geha et al. 2006; Howley et al. 2013).

Using resolved star count data from the INT/WFC survey, McConnachie et al. (2004) detected a 15 kpc long stellar arc that emanates from the northern side of NGC 205 before bending eastward back to the M31 disk. This discovery resulted from the fact that the stellar loop consists of RGB stars that are slightly bluer than the M31 inner halo stars and hence have enhanced contrast on metal-poor star count maps. Unfortunately, the true nature of this feature remains controversial. While McConnachie et al. (2004) detected a kinematic feature centered at $-160\,\mathrm{km\,s^{-1}}$ with a dispersion of $10\,\mathrm{km\,s^{-1}}$ that they attributed to the NGC 205 loop, subsequent re-examination of the data by Ibata et al. (2005) did not recover this cold component. Instead, they argued that the kinematic properties of this feature were consistent with the bulk motion of M31's disk. Furthermore, Richardson et al. (2008) and Bernard et al. (2015a) find that deep HST CMDs of this feature can be explained naturally by a combination of heated disk and GSS debris, without requiring any additional component of stars, while Howley et al. (2008) find the most likely orbit of NGC 205 to be incompatible with the location of the arc.

More recently, data from the PAndAS survey has been used to explore the outer regions of the dE satellites NGC 147 and NGC 185 to extremely faint surface brightness levels using resolved stars. Projected $\sim \! 100 \, \rm kpc$ north of M31, and lying at M31-centric distances of 120 kpc and 180 kpc, respectively (McConnachie 2012), these systems are sufficiently remote that contamination from M31 itself is minimal and the main complication is the presence of substantial foreground Galactic populations along their sightlines. Crnojević et al. (2014) trace both systems to $\mu_g \approx 32 \, \rm mag \, arcsec^{-2}$ and show that they have much greater extents than previously

recognized. As can be seen in Figs. 8.3 and 8.4, NGC 185 retains a regular shape in its peripheral regions while NGC 147 exhibits pronounced isophotal twisting due to the emergence of long symmetric tidal tails. Even neglecting these tails, NGC 147 appears more distended with an effective radius almost three times that of NGC 185. In contrast to NGC 185, it also exhibits no metallicity gradient. These differences in the structure and stellar populations of the dEs suggest that tidal influences have played an important role in governing the evolution of NGC 147 but not NGC 185. On the assumption that NGC 147, NGC 185 and nearby dwarf spheroidal CassII form a bound subgroup, Arias et al. (2015) show that it is possible to find orbits around M31 which result in substantial tidal disruption to NGC 147 but not the other two systems.

M31's most massive satellite is the low-mass spiral M33, lying almost 210 kpc away (McConnachie 2012). Although no unusual structure was detected around M33 in the early INT/WFC survey (Ferguson et al. 2007), the deeper PAndAS data led to the discovery of a gigantic "S"-shaped substructure that surrounds the main body of the galaxy (McConnachie et al. 2009, 2010). Traced to a projected radius of 40 kpc and $\mu_g \approx 33$ mag arcsec⁻², this feature coincides with a similar feature that was detected in H_I (Putman et al. 2009). McConnachie et al. (2009) used N-body simulations to conduct a preliminary exploration of the idea that this is the signature of M33's tidal disruption as it orbits around M31. They found that a relatively close recent encounter could explain the appearance of this low surface brightness substructure while satisfying the known phase space constraints of the two systems. Specifically, they suggest that M31 and M33 came within 40–50 kpc of each other roughly 2.5 Gyr ago, a hypothesis which is also consistent with the more recent Local Group orbit modelling work of van der Marel et al. (2012). This timescale is particularly interesting since the outer disks of both systems appear to have experienced strong bursts of star formation at this time and there is evidence to suggest the inflow of metal-poor gas (Bernard et al. 2012, 2015b). Thus, while more detailed modelling of this interaction is clearly required, there is tantalising evidence to suggest that it could explain a number of puzzling aspects about the M31-M33 system, such as the strong warps in both galaxies and the unusual synchronous burst of star formation.

8.8 Summary and Future Prospects

The vast amount of work on the M31 halo over the past 15 years has led to an exceptional situation where, in many ways, our knowledge of the peripheral regions of that system far exceeds our knowledge of those regions in our own Milky Way. Studies have been able to identify and characterise coherent debris streams in the M31 halo out to projected galactocentric distances of \sim 120 kpc, and detect and map the properties of the 'smooth' halo out to \sim 150–200 kpc. Even in the inner halo (\gtrsim 50 kpc), we have a much clearer understanding of the nature and origin of the tidal debris, thanks to our external perspective. This can be contrasted with the

situation in the Milky Way where many of the inner halo/outer disk structures are very poorly understood (e.g., the Monoceros, Hercules-Aquila, Tri-And, and Virgo overdensities; see Chaps. 3 and 4).

In comparison to the Milky Way, the M31 inner halo is littered with metal-rich debris. Some of this material has been stripped from the GSS progenitor, while the rest is likely to be material from the M31 disk heated by the recent impact of this satellite. M31 may also have more outer halo tidal streams than the Milky Way, although most Milky Way surveys to date have not had the sensitivity to detect substructures in these parts. Additionally, M31 (1) has a higher fraction of its total light in the halo component compared to the Milky Way (e.g., Ibata et al. 2014; Gilbert et al. 2012), (2) is characterised by a smooth density profile unlike the broken power-law of the Milky Way (Deason et al. 2013) and (3) has a substantially larger population of halo GCs, many of which lie along streams (Mackey et al. 2010b; Veljanoski et al. 2014). It is likely that these differences result from the unique accretion histories experienced by the two systems. M31 may have experienced more accretions than the Milky Way, or it may simply have experienced a more prolonged history of accretion. Indeed, there is a tantalising similarity between the properties of the Sagittarius dwarf and those inferred for the GSS progenitor—both are early-type galaxies with estimated initial stellar masses in the range $0.5-1 \times 10^9 \,\mathrm{M}_{\odot}$. The major building blocks of these halos may well have been comparable, but their orbits and accretion times rather different. In this spirit, it is worth speculating how the Milky Way and M31 halos would have compared to each other ~2 Gyr ago, before the GSS progenitor entered M31's inner halo.

A number of outstanding questions remain regarding the M31 system, and much exciting progress can be expected over the next decade. Some of the most pressing issues that remain to be addressed include:

- The development of a definitive understanding of M31's most significant recent accretion event: what was the true nature of the GSS progenitor and where is the remnant now? How did it come to be on such an extreme orbit and how did it survive in this state until ∼1 Gyr ago? What is the explanation for the second velocity component in the GSS and is there any connection between the GSS progenitor and the similarly metal-rich component of Stream C?
- Understanding the origin of the outer halo debris. What and where are the progenitors of the outer halo debris streams? Do these features result from one or many accretion events? The associated GCs are likely to play an important role in answering these questions, and also in using these streams to derive refined estimates of the mass and potential of M31. While line-of-sight distances to stream GCs are possible with HST observations, proper motion measurements may be possible for the most compact objects with Gaia.
- Understanding the origin of the coherent rotation in the outer GC population, and
 how it can be reconciled with the supposedly chaotic accretion of parent dwarf
 galaxies into the halo. Additionally, do the underlying debris streams and the
 smooth field halo also exhibit this rotation? Given the sparse nature of the stellar

populations in these parts, very large-scale spectroscopy campaigns covering a significant fraction of the halo will be required to answer these questions.

- Developing a holistic picture of M31's evolution that links its accretion history to its global evolution and current structure. There are fascinating hints that the recent interaction and accretion history of M31 can explain a variety of puzzling observations. The close passage of M33 could excite the strong asymmetric warps and bursts of star formation observed in both systems, while the accretion of the GSS progenitor could further disrupt the M31 outer disk, displace some fraction of the disk stars into the halo and deposit a substantial amount of metal rich debris in the inner halo. Much work is required to verify and fine-tune these ideas and there is a particular need for further detailed *N*-body modelling.
- Searching for the edge of the M31 stellar halo. Tidal streams, field stars and GCs have been found to the edge of the PAndAS survey, suggesting that they could extend yet further. New wide-field mapping facilities such as Hyper-Suprime Cam on the Subaru telescope will be required to efficiently explore beyond the limit of PAndAS and may benefit from the use of specialised filters to discriminate between foreground and M31 populations.

Acknowledgements We thank Edouard Bernard and Jovan Veljanoski for their help in creating Figs. 8.7 and 8.8. AMNF acknowledges support from an STFC Consolidated Grant (ST/J001422/1) and the hospitality of the Instituto de Astrofisica de Canarias while completing this chapter. ADM is grateful for support from the Australian Research Council through Discovery Projects DP1093431, DP120101237, and DP150103294.

References

Arias, V., Guglielmo, M., Nuwanthika, N., et al. 2015, MNRAS, submitted.

Baade, W., & Gaposchkin, C. H. P. 1963, Evolution of stars and galaxies., Cambridge, Harvard University Press.

Bate, N. F., Conn, A. R., McMonigal, B., et al. 2014, MNRAS, 437, 3362

Bellazzini, M., Ferraro, F. R., Ibata, R. A. 2003, AJ, 125, 188

Belokurov, V., Zucker, D. B., Evans, N. W., et al. 2006, ApJ, 642, L137

Bernard, E. J., Ferguson, A. M. N., Barker, M. K., et al. 2012, MNRAS, 420, 2625

Bernard, E. J., Ferguson, A. M. N., Richardson, J. C., et al. 2015a, MNRAS, 446, 2789

Bernard, E. J., Ferguson, A. M. N., Chapman, S. C. et al. 2015b, MNRAS, 453, L113

Block, D. L., Bournaud, F., Combes, F., et al. 2006, Nature, 443, 832

Brown, T. M., Smith, E., Ferguson, H. C., et al. 2006, ApJ, 652, 323

Carlberg, R. G., Richer, H. B., McConnachie, A. W., et al. 2011, ApJ, 731, 124

Chapman, S. C., Ibata, R., Irwin, M., et al. 2008, MNRAS, 390, 1437

Choi, P. I., Guhathakurta, P., & Johnston, K. V. 2002, AJ, 124, 310

Ciardullo, R., Jacoby, G. H., Ford, H. C., & Neill, J. D. 1989, ApJ, 339, 53

Coccato, L., Arnaboldi, M., & Gerhard, O. 2013, MNRAS, 436, 1322

Collins, M. L. M., Chapman, S. C., Irwin, M. J., et al. 2009, MNRAS, 396, 1619

Collins, M. L. M., Chapman, S. C., Rich, R. M., et al. 2013, ApJ, 768, 172

Cram, T. R., Roberts, M. S., & Whitehurst, R. N. 1980, A&AS, 40, 215

Crnojević, D., Ferguson, A. M. N., Irwin, M. J., et al. 2014, MNRAS, 445, 3862

Crotts, A. P. S. 1986, AJ, 92, 292

Deason, A. J., Belokurov, V., Evans, N. W., & Johnston, K. V. 2013, ApJ, 763, 113

Diaz, J. D., Koposov, S. E., Irwin, M., Belokurov, V., & Evans, N. W. 2014, MNRAS, 443, 1688

di Tullio Zinn, G., & Zinn, R. 2013, AJ, 145, 50

di Tullio Zinn, G., & Zinn, R. 2014, AJ, 147, 90

Dorman, C. E., Widrow, L. M., Guhathakurta, P., et al. 2013, ApJ, 779, 103

Dotter, A., Sarajedini, A., Anderson, J., et al. 2010, ApJ, 708, 698

Dotter, A., Sarajedini, A., & Anderson, J. 2011, ApJ, 738, 74

Fardal, M. A., Babul, A., Geehan, J. J., & Guhathakurta, P. 2006, MNRAS, 366, 1012

Fardal, M. A., Guhathakurta, P., Babul, A., & McConnachie, A. W. 2007, MNRAS, 380, 15

Fardal, M. A., Babul, A., Guhathakurta, P., Gilbert, K. M., & Dodge, C. 2008, ApJ Lett, 682, L33

Fardal, M. A., Guhathakurta, P., Gilbert, K. M., et al. 2012, MNRAS, 423, 3134

Fardal, M. A., Weinberg, M. D., Babul, A., et al. 2013, MNRAS, 434, 2779

Faria, D., Johnson, R. A., Ferguson, A. M. N., et al. 2007, AJ, 133, 1275

Ferguson, A. M. N., Irwin, M. J., Ibata, R. A., Lewis, G. F., & Tanvir, N. R. 2002, AJ, 124, 1452

Ferguson, A. M. N., Johnson, R. A., Faria, D. C., et al. 2005, ApJ Lett, 622, L109

Ferguson, A., Irwin, M., Chapman, S., et al. 2007, Island Universes - Structure and Evolution of Disk Galaxies, 239

Font, A. S., Johnston, K. V., Guhathakurta, P., Majewski, S. R., & Rich, R. M. 2006, AJ, 131, 1436 Forbes, D. A., & Bridges, T. 2010, MNRAS, 404, 1203

Foster, C., Lux, H., Romanowsky, A. J., et al. 2014, MNRAS, 442, 3544

Gebhardt, K., Rich, R. M., & Ho, L. C. 2005, ApJ, 634, 1093

Geha, M., Guhathakurta, P., Rich, R. M., & Cooper, M. C. 2006, AJ, 131, 332

Gilbert, K. M., Guhathakurta, P., Kalirai, J. S., et al. 2006, ApJ, 652, 1188

Gilbert, K. M., Fardal, M., Kalirai, J. S., et al. 2007, ApJ, 668, 245

Gilbert, K. M., Guhathakurta, P., Kollipara, P., et al. 2009, ApJ, 705, 1275

Gilbert, K. M., Guhathakurta, P., Beaton, R. L., et al. 2012, ApJ, 760, 76

Gilbert, K. M., Kalirai, J. S., Guhathakurta, P., et al. 2014, ApJ, 796, 76

Guhathakurta, P., Rich, R. M., Reitzel, D. B., et al. 2006, AJ, 131, 2497

Howley, K. M., Geha, M., Guhathakurta, P., et al. 2008, ApJ, **683**, 722

Howley, K. M., Guhathakurta, P., van der Marel, R., et al. 2013, ApJ, 765, 65

Huxor, A. P., Tanvir, N. R., Irwin, M. J., et al. 2005, MNRAS, 360, 1007

Huxor, A. P., Tanvir, N. R., Ferguson, A. M. N., et al. 2008, MNRAS, 385, 1989

Huxor, A. P., Ferguson, A. M. N., Tanvir, N. R., et al. 2011, MNRAS, 414, 770

Huxor, A. P., Mackey, A. D., Ferguson, A. M. N., et al. 2014, MNRAS, 442, 2165

Ibata, R., Irwin, M., Lewis, G., Ferguson, A. M. N., & Tanvir, N. 2001, Nature, 412, 49

Ibata, R., Chapman, S., Ferguson, A. M. N., et al. 2004, MNRAS, 351, 117

Ibata, R., Chapman, S., Ferguson, A. M. N., et al. 2005, ApJ, 634, 287

Ibata, R., Martin, N. F., Irwin, M., et al. 2007, ApJ, 671, 1591

Ibata, R. A., Lewis, G. F., Conn, A. R., et al. 2013, Nature, 493, 62

Ibata, R. A., Lewis, G. F., McConnachie, A. W., et al. 2014, ApJ, 780, 128

Innanen, K. A., Kamper, K. W., van den Bergh, S., & Papp, K. A. 1982, ApJ, 254, 515

Irwin, M. J., Ferguson, A. M. N., Ibata, R. A., Lewis, G. F., & Tanvir, N. R. 2005, ApJ Lett, 628, L105

Irwin, M. J., Ferguson, A. M. N., Huxor, A. P., et al. 2008, ApJ, 676, L17

Johnston, K. V., Choi, P. I., & Guhathakurta, P. 2002, AJ, 124, 127

Kalirai, J. S., Guhathakurta, P., Gilbert, K. M., et al. 2006, ApJ, 641, 268

Kazantzidis, S., Bullock, J. S., Zentner, A. R., Kravtsov, A. V., & Moustakas, L. A. 2008, ApJ, 688, 254

Kirby, E. N., Lanfranchi, G. A., Simon, J. D., Cohen, J. G., & Guhathakurta, P. 2011, ApJ, 727, 78

Kniazev, A. Y., Grebel, E. K., Zucker, D. B., et al. 2014, AJ, 147, 16

Law, D. R., & Majewski, D. R. 2010, ApJ, 718, 1128

Lewis, G. F., Braun, R., McConnachie, A. W., et al. 2013, ApJ, 763, 4

Mackey, A. D., & Gilmore, G. F. 2004, MNRAS, 355, 504

Mackey, A. D., & van den Bergh, S. 2005, MNRAS, 360, 631

Mackey, A. D., Ferguson, A. M. N., Irwin, M. J., et al. 2010a, MNRAS, 401, 533

Mackey, A. D., Huxor, A. P., Ferguson, A. M. N., et al. 2010b, ApJ Lett, 717, L11

Mackey, A. D., Huxor, A. P., Ferguson, A. M. N., et al. 2013a, MNRAS, 429, 281

Mackey, A. D., Huxor, A. P., Martin, N. F., et al. 2013b, ApJ Lett, 770, L17

Mackey, A. D., Lewis, G. F., Collins, M. L. M., et al. 2014, MNRAS, 445, L89

Marín-Franch, A., Aparicio, A., Piotto, G., et al. 2009, ApJ, 694, 1498

Martin, N. F., Ibata, R. A., Irwin, M. J., et al. 2006, MNRAS, 371, 1983

McConnachie, A. W. 2012, AJ, 144, 4

McConnachie, A. W., Irwin, M. J., Ibata, R. A., et al. 2003, MNRAS, 343, 1335

McConnachie, A. W., Irwin, M. J., Lewis, G. F., et al. 2004, MNRAS, 351, L94

McConnachie, A. W., Irwin, M. J., Ferguson, A. M. N., et al. 2005, MNRAS, 356, 979

McConnachie, A. W., Irwin, M. J., Ibata, R. A., et al. 2009, Nature, 461, 66

McConnachie, A. W., Ferguson, A. M. N., Irwin, M. J., et al. 2010, ApJ, 723, 1038

Merrett, H. R., Kuijken, K., Merrifield, M. R., et al. 2003, MNRAS, 346, L62

Merrett, H. R., Merrifield, M. R., Douglas, N. G., et al. 2006, MNRAS, 369, 120

Meylan, G., Sarajedini, A., Jablonka, P., et al. 2001, AJ, 122, 830

Mori, M., & Rich, R. M. 2008, ApJ Lett, 674, L77

Morris, P. W., Reid, I. N., Griffiths, W. K., & Penny, A. J. 1994, MNRAS, 271, 852

Morrison, H. L., Harding, P., Hurley-Keller, D., & Jacoby, G. 2003, ApJ Lett, 596, L183

Mould, J., & Kristian, J. 1986, ApJ, 305, 591

Newberg, H. J., Yanny, B., Grebel, E. K., et al. 2003, ApJ Lett, 596, L191

Newton, K., & Emerson, D. T. 1977, MNRAS, 181, 573

Ostheimer, J. C., Jr. 2003, Ph.D. Thesis

Pawlowski, M. S., Pflamm-Altenburg, J., & Kroupa, P. 2012, MNRAS, 423, 1109

Pritchet, C. J., & van den Bergh, S. 1988, ApJ, 331, 135

Pritchet, C. J., & van den Bergh, S. 1994, AJ, **107**, 1730

Purcell, C. W., Bullock, J. S., & Kazantzidis, S. 2010, MNRAS, 404, 1711

Putman, M. E., Peek, J. E. G., Muratov, A., et al. 2009, ApJ, 703, 1486

Quinn, P. J., Hernquist, L., & Fullagar, D. P. 1993, ApJ, 403, 74

Reitzel, D. B., Guhathakurta, P., & Rich, R. M. 2004, AJ, 127, 2133

Rich, R. M., Reitzel, D. B., Guhathakurta, P., Gebhardt, K., & Ho, L. C. 2004, AJ, 127, 2139

Richardson, J. C., Ferguson, A. M. N., Johnson, R. A., et al. 2008, AJ, 135, 1998

Richardson, J. C., Irwin, M. J., McConnachie, A. W., et al. 2011, ApJ, 732, 76

Roberts, M. S., & Whitehurst, R. N. 1975, ApJ, 201, 327

Sadoun, R., Mohayaee, R., & Colin, J. 2014, MNRAS, 442, 160

Searle, L., & Zinn, R. 1978, ApJ, 225, 357

Tanaka, M., Chiba, M., Komiyama, Y., et al. 2010, ApJ, 708, 1168

Tanvir, N. R., Mackey, A. D., Ferguson, A. M. N., et al. 2012, MNRAS, 422, 162

van der Marel, R. P., Besla, G., Cox, T. J., Sohn, S. T., & Anderson, J. 2012, ApJ, 753, 9

Veljanoski, J., Ferguson, A. M. N., Mackey, A. D., et al. 2013, ApJ Lett, 768, L33

Veljanoski, J., Mackey, A. D., Ferguson, A. M. N., et al. 2014, MNRAS, 442, 2929

Villalobos, Á., & Helmi, A. 2008, MNRAS, 391, 1806

Walker, I. R., Mihos, J. C., & Hernquist, L. 1996, ApJ, 460, 121

Walterbos, R. A. M., & Kennicutt, R. C., Jr. 1988, A&A, 198, 61

Watkins, L. L., Evans, N. W., Belokurov, V., et al. 2009, MNRAS, 398, 1757

White, S. D. M., & Rees, M. J. 1978, MNRAS, 183, 341

White, S. D. M., & Frenk, C. S. 1991, ApJ, 379, 52

Zinn, R. 1993, in Smith, G. H., Brodie, J. P., eds, ASP Conf. Ser. 48, The Globular Cluster-Galaxy Connection. Astron. Soc. Pac., San Francisco, p. 38

Zolotov, A., Willman, B., Brooks, A. M., et al. 2009, ApJ, 702, 1058

Zucker, D. B., Kniazev, A. Y., Bell, E. F., et al. 2004a, ApJ Lett, 612, L117

Zucker, D. B., Kniazev, A. Y., Bell, E. F., et al. 2004b, ApJ, 612, L121

Zucker, D. B., Kniazev, A. Y., Martínez-Delgado, D., et al. 2007, ApJ, 659, L21

Chapter 9 Stellar Tidal Streams in External Galaxies

Jeffrey L. Carlin, Rachael L. Beaton, David Martínez-Delgado, and R. Jay Gabany

Abstract In order to place the highly substructured stellar halos of the Milky Way and M31 in a larger context of hierarchical galaxy formation, it is necessary to understand the prevalence and properties of tidal substructure around external galaxies. This chapter details the current state of our observational knowledge of streams in galaxies in and beyond the Local Group, which are studied both in resolved stellar populations and in integrated light. Modeling of individual streams in extragalactic systems is hampered by our inability to obtain resolved stellar kinematics in the streams, though many streams contain alternate luminous kinematic tracers, such as globular clusters or planetary nebulae. We compare the observed structures to the predictions of models of galactic halo formation, which provide insight into the number and properties of streams expected around Milky Way like galaxies. More specifically, we discuss the inferences that can be made about stream progenitors based only on observed morphologies. We expand our discussion to consider hierarchical accretion at lower mass scales, in particular the observational evidence that substructure exists on smaller mass scales and the effects accretion events may have on the evolution of dwarf galaxies (satellite or isolated). Lastly, we discuss potential correlations between the presence of substructure in the halo and the structural properties of the disk. While many exciting discoveries have

J.L. Carlin (⊠)

Department of Physics, Applied Physics and Astronomy, Rensselaer Polytechnic Institute, 110 8th Street, Troy, NY 12180, USA

Earlham College, Richmond, IN, USA e-mail: jeffreylcarlin@gmail.com

R.L. Beaton

The Observatories of the Carnegie Institution for Science, Pasadena, CA, USA e-mail: rachael.l.beaton@gmail.com

D. Martínez-Delgado

Astronomisches Rechen-Institut (ARI), Zentrum für Astronomie der Universität Heidelberg (ZAH), Heidelberg, Germany

e-mail: delgado@ari.uni-heidelberg.de

R.J. Gabany

Black Bird Observatory II, Alder Springs, CA, USA

e-mail: rj2010@cosmotography.com

© Springer International Publishing Switzerland 2016 H.J. Newberg, J.L. Carlin (eds.), *Tidal Streams in the Local Group and Beyond*, Astrophysics and Space Science Library 420, DOI 10.1007/978-3-319-19336-6_9 been made of tidal substructures around external galaxies, the "global" questions of galaxy formation and evolution via hierarchical accretion await a more complete census of the low surface brightness outskirts of galaxies in and beyond the Local Group.

9.1 Introduction

Low surface brightness features, including "tails" and "bridges," are visible in highly disturbed galaxies that result from a major merger or strong encounter (Arp 1966; Toomre and Toomre 1972). Similarly, diffuse stellar streams and shells around massive elliptical galaxies have been known for decades, and are attributed either to the accretion of smaller disk galaxies (Quinn 1984) or to recent, "in-situ" star formation from gas that was already contained within the galaxy (Fabian et al. 1980). Schweizer and Seitzer (1988) extended these observations to early spiral galaxies, and suggested that the "ripples," as they called the shell-like features, were formed through mass transfer from nearby galaxies, in addition to wholesale mergers.

It has only been in recent years, with the advent of wide-area, deep photometric surveys, that the number and variety of stellar substructures (resulting from the tidal disruption of dwarf galaxies and globular clusters in "minor mergers") threading the halos of the Milky Way and Andromeda (M31) galaxies has become apparent. These stellar substructures can be studied in detail and together describe the hierarchical merging history of the two dominant galaxies in the Local Group. However, placing them in the broader context of cosmological galaxy formation models requires a more general picture of halo substructure only feasible via the exploration of a large number of more distant systems. Only with such a dataset in hand is it possible to determine whether the Milky Way and M31 have experienced 'typical' or 'atypical' merging histories (e.g., Mutch et al. 2011).

Models (e.g., Johnston et al. 2008; Cooper et al. 2010) predict that a survey reaching a surface brightness of \sim 29 mag arcsec⁻² around \sim 100 galaxies outside the Local Group should reveal many tidal features, perhaps as much as one detectable stream per galaxy. However, a suitably deep data set that is sensitive to low surface brightness features in a large number of galaxies does not yet exist, leaving the observational evidence needed to test these predictions incomplete. In the sections that follow, we will discuss the isolated discoveries of tidal debris structures in external galaxies and their overall utility for elucidating general stellar tidal features.

9.2 Stellar Streams: Detection Methods and Examples

Local Group galaxies, including the Milky Way and M31, can be dissected star by star, and thus provide a laboratory for understanding the details of hierarchical galaxy formation. However, it is unclear whether the Local Group galaxies represent typical evolution histories. To understand the place of the Milky Way and M31 in the larger context requires studying tidal substructures in galaxies beyond the Local Group, where resolving individual stars is difficult. In this section, we detail some of the methods used to discover tidal debris features, including resolved and unresolved stellar populations, and discuss the unique insights gleaned from some examples of these structures.

9.2.1 Resolved Stellar Structures in the Local Group

The era of massive, deep photometric surveys has enabled the detection of tidal debris structures within the Milky Way as stellar overdensities of carefully selected tracers. The famous "Field of Streams" image from SDSS (Belokurov et al. 2006; reproduced in Chap. 1) mapped substructure using main sequence turnoff (MSTO) starcounts to surface brightness limits of fainter than ~32 mag arcsec⁻². The identification of individual members of stellar streams enables extremely low surface brightness features to be detected. This can be achieved by kinematical selection of stream members (for example, via spectroscopic velocities), allowing features in the Galactic halo containing fewer than ~1 red giant branch (RGB) star per square degree to be identified. [For more on known substructures in the Milky Way, see Chapter 4 of this volume.]

Likewise, in M 31, photometric selection of metal-poor RGB candidates removes much of the contaminating background, and has allowed detections of features as faint as ~ 30 mag arcsec⁻², including the "giant stream" (Ibata et al. 2001) and other low surface brightness features (e.g., Ferguson et al. 2002; see Chap. 8 for more about M31). When individual stars can be resolved and spectroscopically vetted in M 31, the measurement of surface brightnesses as faint as ~ 32 mag arcsec⁻² is possible (see, e.g., Gilbert et al. 2012 and other results from the SPLASH survey). Thus, we are able to probe both the Milky Way and M 31 to depths of ~ 32 mag arcsec⁻², which is deep enough to sample most of the simulated halo substructures seen in simulations (discussed further in Sect. 9.4).

9.2.2 Detection Methods in and Beyond the Local Group

Current ground-based telescopes are unable to resolve stellar tidal streams around most galaxies beyond the Local Group into individual stars. Most of the streams that have been found in external galaxies thus appear as elongated, diffuse-light regions extending over several arcminutes on the sky. To map such tidal streams requires deep imaging that is also sensitive to extremely faint surface brightness features; the typical surface brightness of known stellar tidal streams is 27 mag arcsec⁻² or fainter, depending both on the luminosity of the progenitor and the time they were accreted (Johnston et al. 2008).

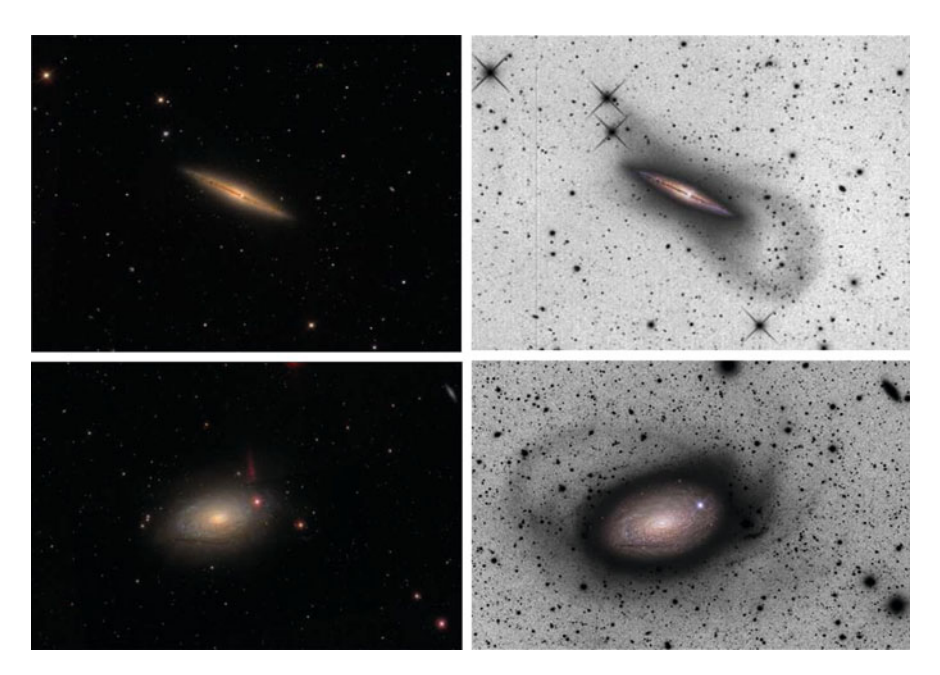


Fig. 9.1 *Left panels*: images from the Sloan Digital Sky Survey of the nearby galaxies NGC 4013 (*top*) and M 63 (*bottom*). These images do not show any obvious signs of tidal streams in the halos of these galaxies at the surface brightness limit of SDSS. Deep images of these same galaxies reveal a low-latitude stellar stream around NGC 4013 (*upper right panel*; Martínez-Delgado et al. 2009) and a giant tidal stream around the spiral galaxy M 63 (*lower-right*; Chonis et al. 2011). For reference, a color inset of each galaxy's central regions has been inserted atop the deeper images. These images illustrate the value of deep, sensitive imaging (i.e., beyond that of SDSS) for detecting the faint debris structures predicted by theoretical models in external galaxies [Figure credit: D. Martínez-Delgado/R.J. Gabany/SDSS.]

Faint tidal features can be identified on sky-limited archival photographic plates using a process called photographic amplification; the surface brightness limit is even fainter if photographically amplified derivatives of several plates are combined together (Malin 1981). Using these techniques (photographically or digitally) it is possible to detect extended features to 28 mag arcsec⁻² from existing photographic surveys (Malin and Hadley 1997). This depth is comparable to that achievable with SDSS in Fig. 9.1.

Small, fast (i.e., low focal-ratio) telescopes (e.g., Martínez-Delgado et al. 2010; van Dokkum et al. 2014) and modern CCD cameras are capable of imaging unresolved structures in external galaxies to $\Sigma_R \sim 29\,\mathrm{mag\,arcsec^{-2}}$. Detecting these faint features requires very dark sky conditions and images taken with exquisite flat-field quality over a relatively large angular scale. More specifically, stellar streams are typical found at large galactocentric distances (15 kpc < R < 100 kpc, or farther) and could be found out to a significant portion of the virial radius of the parent galaxy (for the Milky Way or M 31, $R_{\mathrm{virial}} \sim 300\,\mathrm{kpc}$). Thus, surveys for

stellar debris must produce images over large angular scales (from >30' for systems <10 Mpc to $\sim\!15'$ for systems $\sim\!50$ Mpc away). As an example, the survey strategy employed by Martínez-Delgado et al. (2010) uses stacks of multiple deep exposures of each target taken with high throughput clear "luminance" filters (transmitting 4000 Å < λ <7000 Å with a near-IR cut-off) with typical exposure times of 7–8 h.

Recent deep, wide-field imaging surveys have focused on nearby spiral galaxies that were suspected (based on existing data from, e.g., surveys such as POSS-II or SDSS, or from amateur astronomical imaging) to contain diffuse-light overdensities. To date, the combined observational efforts have revealed more than 50 previously undetected stellar structures in galaxies as distant as 80 Mpc. Figure 9.2 shows eight such galaxies from the survey of Martínez-Delgado et al. (2010), illustrating the variety of tidal debris features—both in their morphologies and in their projected radii. The central disks of the galaxies shown in Fig. 9.2 are of similar overall physical size, but the debris features can span large galactocentric

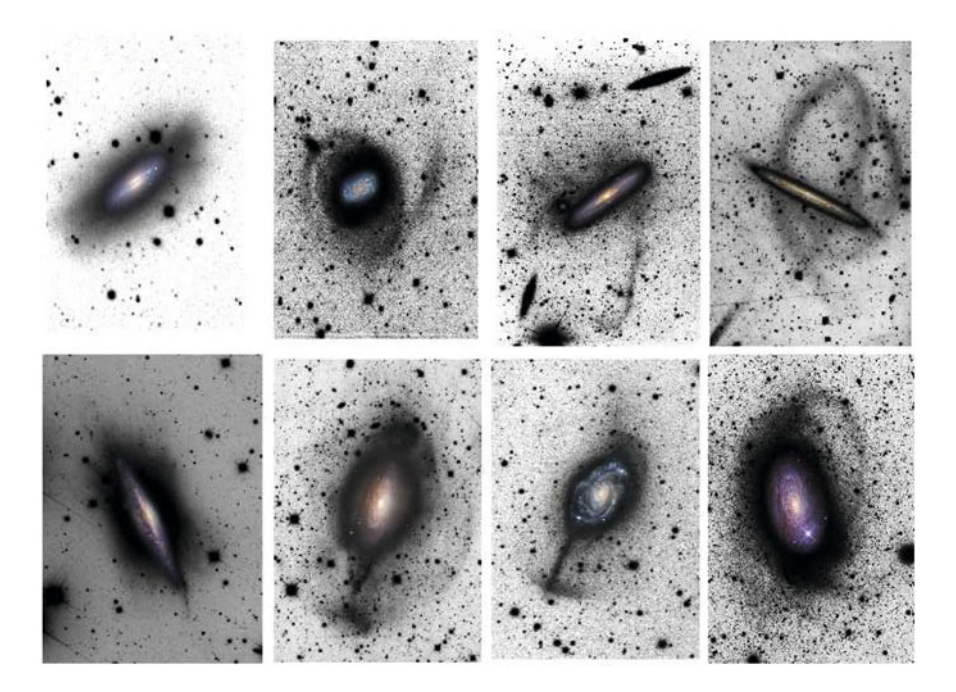


Fig. 9.2 Luminance filter images of nearby galaxies from the pilot survey of Martínez-Delgado et al. (2008, 2010) showing large, diffuse light structures in their outskirts. These include tidal streams similar to Sagittarius (*upper right panel*), giant plumes (*middle panels in the top row*), partially disrupted satellites (*top row, third panel from left*), umbrella-shaped tidal debris structures (*middle two panels in the bottom row*), enormous stellar clouds, prominent spikes, and large scale, complex inner halos sprinkled with several debris features. A color inset of the disk of each galaxy has been overplotted for reference. An illustrative comparison of these features to the surviving structures visible in cosmological simulations is given in Martínez-Delgado et al. (2010), their Fig. 2 [Figures reproduced by permission from Martínez-Delgado et al. (2008, 2010).]

distances. The morphologies of the features include great circle streams resembling the Sagittarius stream around our Galaxy (upper right panel of Fig. 9.2; Sagittarius is discussed in Chap. 2 of this volume), isolated shells, giant clouds of debris floating within galactic halos, jet-like features emerging from galactic disks, and large-scale diffuse structures that may be related to the remnants of ancient, already thoroughly disrupted satellites. The diversity in observed substructure morphology parallels that seen in simulations (e.g., Johnston et al. 2008; Cooper et al. 2010). In addition to the remains of satellites that are likely completely destroyed, there are a few examples (e.g., Martínez-Delgado et al. 2012; Martínez-Delgado et al. 2014; Amorisco et al. 2015) of surviving satellites caught in the act of tidal disruption, displaying long tails departing from the progenitor satellite (i.e., similar in spirit to observations in the Local Group). The extraordinary variety of morphological specimens provides strong evidence to support the hierarchical galaxy formation scenarios predicted by cosmological models (e.g., Cooper et al. 2010).

9.2.3 Unresolved Features Beyond the Local Group

Prior to recent dedicated CCD searches, only a few cases of extragalactic stellar tidal streams have been reported in nearby spiral galaxies. Malin and Hadley (1997) found two possible tidal streams surrounding the galaxies M 83 and M 104 by using special contrast enhancement techniques on plates obtained for wide-field photographic surveys. Shortly thereafter, a study of the nearby, edge-on galaxy NGC 5907 by Shang et al. (1998) employed deep CCD images to reveal an elliptical loop in the halo of this galaxy, which they believed to be the remains of a tidally disrupted galaxy similar in size to the Sagittarius dwarf galaxy (Sagittarius was at that time a recent discovery in the Milky Way halo). Shang et al. also identified another Sagittarius-like dwarf galaxy that they suggested might be interacting with the disk of NGC 5907, causing the observed warp in HI. Their photometry reached surface brightnesses of 28.6 and 26.9 mag arcsec⁻² in *R* and *I*-bands, respectively.

More recently, NGC 5907 was imaged by Martínez-Delgado et al. (2008, Fig. 9.3), revealing even fainter features of the stream. As shown in Fig. 9.3, this stream is prominently visible as an interwoven, rosette-like structure traversing nearly 720° around NGC 5907. Detailed *N*-body modeling suggests that *all* of the features can be reproduced from the accretion of a single, low-mass satellite galaxy, with the stream tracing two full orbits of its progenitor. The presence of such a long stream confirms that a stellar substructure can survive several gigayears, which though predicted by *N*-body simulations of tidally disrupted stellar systems around the Milky Way (e.g., Law et al. 2005; Peñarrubia et al. 2005) lacked direct confirmation. Interestingly, the *N*-body model of Fig. 9.3 was created using a progenitor with orbital parameters similar those found for Sagittarius in the Milky Way (Chap. 2). The model suggests that the fainter, outer loop material (blue points in Fig. 9.3) became unbound from its progenitor at least 3.6 Gyr ago. The

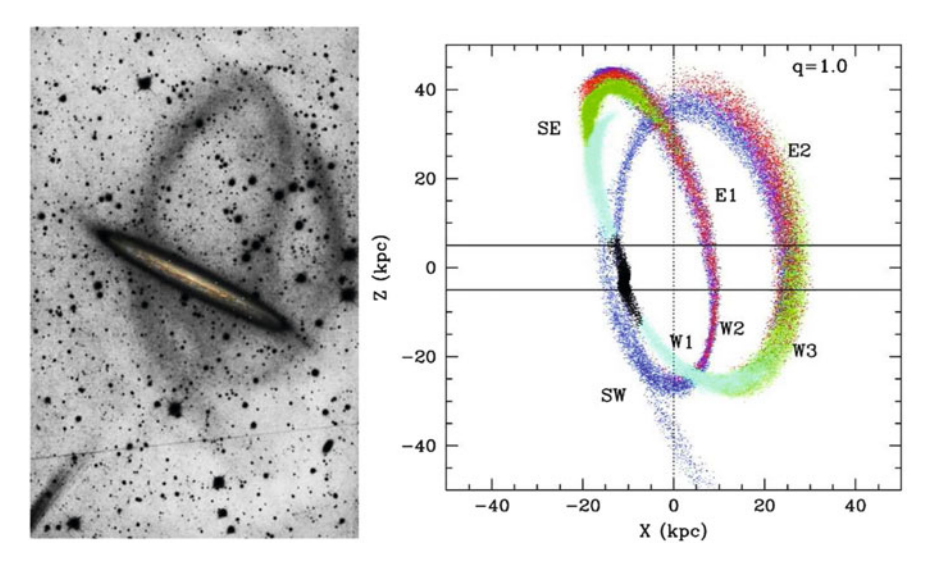


Fig. 9.3 *Left*: deep image of the stellar tidal stream around NGC 5907 obtained with the 0.5-m BBO telescope (Martínez-Delgado et al. 2008). The great-circle morphology of this system is likely very similar to that of the Sagittarius stream in the Milky Way. *Right*: *N*-body model of the NGC 5907 stellar stream. The satellite is realized as a King model with an initial mass, King core and tidal radii of $M = 2 \times 10^8 M_{\odot}$, $r_c = 0.39$ kpc and $r_t = 2.7$ kpc, respectively. Different colors denote particles that became unbound after different pericentric passages, whereas black particles are those that remain bound. The fainter, outer loop material (*blue points*) became unbound at least 3.6 Gyrs ago. For this particular model the orbital period is $T_r = 0.9$ Gyr [Figure reproduced by permission from Martínez-Delgado et al. (2008).]

substructure in NGC 5097 is one of the most striking examples of an external great-circle tidal stream to date.

While some galaxies have *great-circle* tidal streams that resemble the Sagittarius stream surrounding our Galaxy (e.g., in NGC 5907: Fig. 9.3, or NGC 4013 and M63: Fig. 9.1), others have enormous structures that resemble open umbrellas, and that extend over tens of kiloparsecs (e.g., the middle two panels in the bottom row of Fig. 9.2). These structures are often located on both sides of the host galaxy, and display long narrow shafts that terminate in a giant shell of debris (e.g., NGC 4651; Foster et al. 2014). Another umbrella-like feature, dubbed the "dog leg stream" (Amorisco et al. 2015), has a long narrow spoke (with an embedded progenitor) that stretches to a radius of \sim 150 kpc beyond the center of NGC 1097, terminating in a "dog-leg" that appears like an umbrella feature with one half of the shell missing (note that this system has other narrow plumes visible as well). With such examples, we are beginning to see real streams around galaxies in the local universe that resemble the menagerie of morphological features predicted by Λ -CDM hierarchical structure formation models (e.g., Johnston et al. 2008; Cooper et al. 2010; see also Chap. 6 of this volume).

While there have been numerous isolated discoveries of debris features around external galaxies, there have been few large-scale systematic surveys to build

a comprehensive census of halo substructures. Only such a survey can inform simulations by providing estimates of the prevalence of streams of different morphologies, and thus different progenitor masses, orbits, and infall times. One systematic search by Miskolczi et al. (2011) analyzed 474 galaxies in SDSS and found clear tidal features around 6% of the galaxies, with 19% exhibiting some features above the surface brightness limit of ~28 mag arcsec⁻². From imaging data in the Canada-France-Hawaii Telescope Legacy Survey, Atkinson et al. (2013) find tidal features (including both minor and major merger events) around 12% of the galaxies imaged. Given that the Λ -CDM paradigm predicts that we should see accretion relics around all Milky Way-sized galaxies, this ~10 % fraction from the SDSS/CFHT studies would seem to suggest a significant deficit of detected accretion events relative to predictions. However, as illustrated in Fig. 9.1 (see also Fig. 9.6), the surface brightness limits for most large scale surveys are simply too shallow to reveal the complex webs of substructure both predicted in simulations (e.g., Bullock and Johnston 2005) and observed locally in the Milky Way and M31 (i.e., where $\mu > 28$ mag arcsec⁻² can be attained using resolved stellar populations). However, it is puzzling that no tidal stream currently known in the Milky Way or M31 is remotely as bright as the "faint limits" of these large scale searches (Sagittarius—by far the brightest stream in the Milky Way—is only \sim 30 mag arcsec⁻² at about 30–40° from the core, according to Mateo et al. 1998).

9.2.4 Resolved Structures Beyond the Local Group

With large aperture facilities equipped with wide-field detectors, it is possible to resolve individual stars in some tidal debris structures beyond the Milky Way and M31. Perhaps the most spectacular example of this from ground-based observations is the Milky Way analog NGC 891, at a distance of \approx 10 Mpc, which was surveyed by Mouhcine et al. (2010) with Suprime-Cam on the 8.2 m Subaru telescope. With very long (>11-h) exposures, this study resolved stars to \sim 2 magnitudes below the RGB tip in NGC 891, covering a $\sim 90 \times 90$ kpc area around the galaxy down to i-band magnitudes fainter than 28th mag (see Fig. 9.4). Surface density maps of RGB stars show a complex of features looping throughout the halo of NGC 891, suggesting that the halo of this galaxy contains numerous accretion remnants. The disk of NGC 891 also appears to be "super-thick" (Mouhcine et al. 2010), providing further evidence of recent accretion. Another recent example of deep, ground-based observations is the study by Greggio et al. (2014), who mapped the density of RGB stars in the halo of the spiral galaxy NGC 253 at a distance of 3 Mpc using deep Zand J-band imaging from the VISTA telescope. As a whole, Greggio et al. found that the halo of NGC 253 is fairly homogeneous out to ~ 50 kpc, with the exception of a \sim 20 kpc wide shell roughly 28 kpc from the plane that is interpreted to be the result of a recent tidal interaction. While these ground-based studies are spectacular, the extremely deep, large-area observations required to resolve individual RGB stars

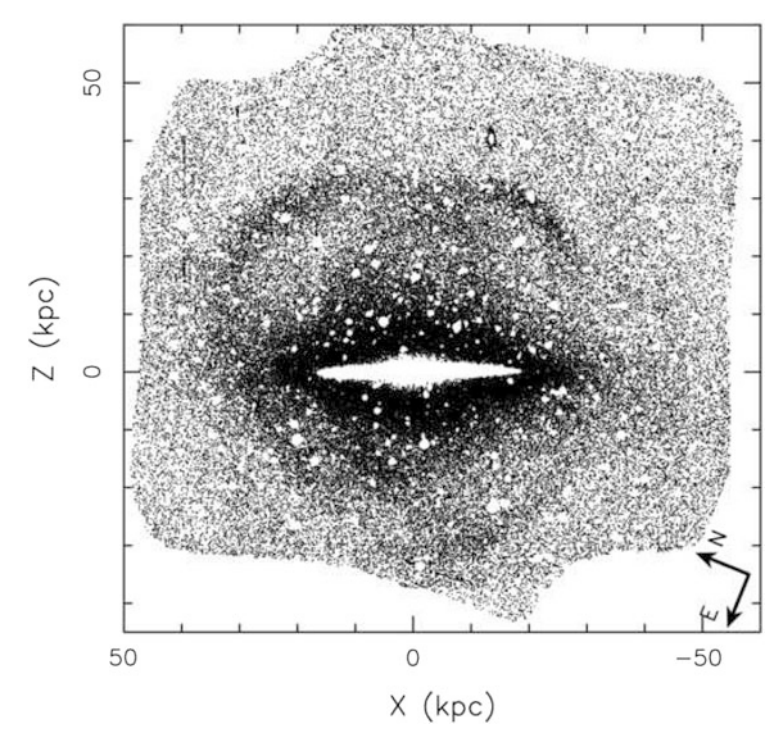


Fig. 9.4 Stellar density map of RGB stars with magnitudes $25.8 \le i_0 \le 27.0$ over a $\sim 90 \times 90$ kpc region surrounding the Milky Way analog galaxy NGC 891. Multiple interlocking loops and arclike ("great circle") features are visible over vast regions of the NGC 891 halo [Figure reproduced by permission from Mouhcine et al. (2010).]

in the accretion relics highlight the difficulty (or perhaps impossibility) of doing similar work for large numbers of Milky Way analogs.

Alternatively, space based telescopes can provide the necessary spatial resolution and depth to trace extra-galactic substructures with individual stars, albeit over significantly smaller angular scales than those on the ground (the HST+ACS field of view is \sim 4′). The HST+ACS GHOSTS survey (Radburn-Smith et al. 2011) resolved stars at the RGB tip and used them to map low surface brightness features (to $\Sigma_V \sim 30$ mag arcsec⁻²) in the outer regions of 14 disk galaxies out to distances of \sim 17 Mpc. Bailin et al. (2011) began with GHOSTS images from HST for the spiral galaxy NGC 253, and supplemented these with imaging over a much wider field of view with Magellan/IMACS, reaching well below the RGB tip. They estimated the total stellar luminosity of the NGC 253 halo to be roughly twice that of the Milky Way or M31, and fit profiles to stellar densities out to \sim 30 kpc from the galaxy center. The shelf-like feature to the south that had been seen by Malin and Hadley (1997) in photographic plates is clearly visible, as well as other substructure at the \sim kpc level. Thus, targeted follow-up, ground-based or

J.L. Carlin et al.

space-based, for stellar streams discovered in integrated light has the potential to build datasets complementary to those generated en masse for the Milky Way and M 31, reaching appropriate physical spatial scales and surface brightnesses.

9.3 *N*-Body Modeling of Streams

We now turn to discussion of what can be learned from the identification and subsequent theoretical modeling of tidal streams in galaxies beyond the Local Group. In many of the examples illustrated in this chapter, we have shown *N*-body models of disrupting satellites that roughly reproduce the observed morphology of detected streams. For example, for the great-circle tidal stream around NGC 5907 (Fig. 9.3), an *N*-body model that best replicates the morphology of the observed stream requires a massive Sgr-like galaxy that has spread debris over at least three orbits. If this is the case, then the complex stream structure seen around this galaxy can be entirely explained by a single accretion event. However, due to the difficulty in measuring kinematics for low surface brightness tidal streams (and, indeed, the impossibility of measuring kinematics of individual stars) at several Mpc away, models must be constrained solely by the observed morphology and the stellar density along the stream. While the panoramic perspective we are afforded of these systems offers many constraints on the properties of the progenitors and their orbits, kinematics will ultimately be needed to fully characterize each accretion event.

It is possible that carefully chosen spectroscopic observations can derive bulk kinematics of some tidal debris features around external galaxies. For example, Sanderson and Helmi (2013) outlined a method to do this for tidal caustics (or "shells") via careful choice of spectroscopic fiber positioning and identification of the tell-tale velocity signature. A much more promising avenue is to use intrinsically brighter point-like tracers such as globular clusters, planetary nebulae, or HII regions to elucidate debris structures. The densities of globular clusters have been used (D'Abrusco et al. 2015) to show large structures in the halos of Virgo cluster galaxies that may be evidence of recent accretion events.

An example of a stream in a distant galaxy for which kinematics have been measured and an orbit derived is that of the Umbrella Galaxy (NGC 4651). Foster et al. (2014) followed up the low surface-brightness imaging of Martínez-Delgado et al. (2010) with even deeper imaging from the Subaru/Suprime-Cam instrument. Figure 9.5 shows images from this study, which reveal a "stick" feature extending out to its terminus at a broad arc to the left of the main galaxy. On the opposite side of the disk (right side of the upper panel in Fig. 9.5), additional shell-like features are clearly seen. Foster et al. (2014) estimated the total stellar mass in the tidal debris to be $\sim 4 \times 10^8 M_{\odot}$, constituting about 1/50th the stellar mass of NGC 4651. In addition, Foster et al. (2014) obtained spectra of candidate globular clusters, planetary nebulae, and HII regions that are spatially coincident with the substructures, and distinguished the kinematical signature of the accreted debris (including a possible progenitor core) from the underlying galactic disk motions.

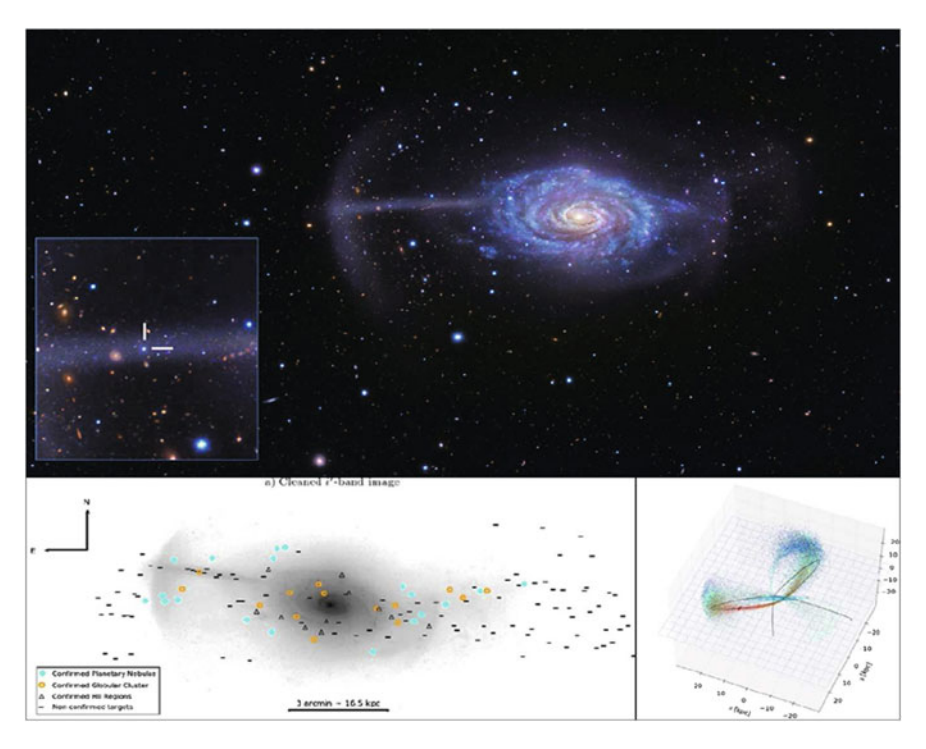


Fig. 9.5 The stellar stream in NGC4651. *Top*: color image of the extensive tidal features in NGC4651, including an "umbrella" and several shells of material. The stream has an exceptionally *blue color. Bottom left*: several globular clusters (*yellow circles*), planetary nebulae (*cyan diamonds*), and HII regions (*black triangles*) are found along the debris. These bright tracers permit kinematical probes that greatly enhance the ability of *N*-body modeling (*bottom right*) to elucidate the physical parameters of the accretion event [Lower panels reproduced from Foster et al. (2014), upper panel credit: R.J. Gabany, modified from Foster et al. (2014).]

The orbit derived from these is rather radial (as expected for an umbrella-like remnant; see Chap. 6 of this volume), with pericenter of only a few kpc, apocenter of \sim 40 kpc, and period of \sim 350 Myr. This implies that the ratio of total mass of the progenitor and the whole of NGC 4651 is \sim 0.15, making this minor merger event analogous to the Sgr accretion in the Milky Way (see Chap. 2) and the Giant Stellar Stream in M31 (Chap. 8). While detailed exploration of parameter space has yet to be achieved for this system, Foster et al. (2014) did adapt an existing *N*-body model to show that some inferences can be made from analysis of the surface brightness and velocities of the visible features and associated tracers.

As discussed in Chap. 7, the widths and surface brightnesses of streams that are traced over a long portion of their orbits provide constraints on the number and sizes of dark matter subhalos in the host galaxy's halo (see, e.g. Ibata et al. 2002; Johnston et al. 2002; Peñarrubia et al. 2006; Siegal-Gaskins and Valluri 2008). These authors show that the presence of dark matter subhalos in spiral galaxies would result in

progressive heating of tidal streams as a result of close encounters, and in fact gaps may be swept out of streams by interactions with subhalos (e.g., Yoon et al. 2011; Carlberg 2013; Erkal and Belokurov 2015; Ngan et al. 2015). As Peñarrubia et al. (2006) pointed out, the average number of dark matter substructures (and, thus, the likelihood of encounters) in a Milky Way-like galaxy decreases monotonically from $z \sim 2$ to the present, implying that "old" stream pieces like the ones visible in external galaxies are more likely to reveal perturbations than recently stripped ones. Tidal debris structures can also be used as kinematical tracers of the underlying gravitational potential in which they are produced (e.g., Johnston et al. 2001; see Chap. 7 for detailed discussion). This has been attempted in the Milky Way using the Sgr streams (e.g., Law et al. 2005; Peñarrubia et al. 2005; Law and Majewski 2010a; see Chap. 2 of this volume for more discussion of Sagittarius). The use of streams beyond the Local Group may ultimately become fruitful for this purpose, as they can be traced over multiple wraps, providing much stronger constraints on the level of stream precession due to the flattening of the halo. Finally, old stream pieces stretching over multiple orbital wraps allows us to study metallicity gradients in the stream (and thus within the progenitor galaxy), as has been done for the Sgr tidal stream (e.g., Bellazzini et al. 2006; Chou et al. 2007; Chap. 2 of this volume). All of these techniques, and likely many others, applied to external galaxies provide valuable constraints on the hierarchical process of galaxy growth and evolution beyond what can be gleaned from our embedded perspective in the Milky Way.

9.4 Stellar Tidal Streams as a Galactic Formation Diagnostic

One of the main objectives of stream surveys in nearby spiral galaxies is to compare the observations with cosmological simulations to ascertain whether the frequency and surface brightness of the detected stellar streams are consistent with those predicted by models. Observational modeling and theoretical understanding of such diffuse and intricate features requires specifically tailored cosmological numerical simulations. There are two main difficulties for these models: (1) sufficiently fine mass and spatial resolution is needed to recover complex and delicate tidal features around Milky Way mass halos; and (2) a sufficient volume is required to build a statistically meaningful sample of host galaxies. To simultaneously meet these two requirements, state-of-the-art cosmological simulations are needed. For this reason, there are still a limited number of models of the stellar halos of Milky Way-like galaxies. Examples include the models by Bullock and Johnston (2005, also described in Chap. 6 of this volume) and high resolution models of individual stellar halos for Milky Way-like galaxies based on the (dark matter only) Aquarius suite of simulations.

Numerical simulations (e.g., Johnston et al. 2008; Cooper et al. 2010) can be used as a guide to what we may expect; models suggest that remnants of recent (0–8 Gyr ago) accretion events, which correspond to the last few tens of percent of mass accretion for a Milky Way-like spiral, should remain visible as substructures

in presently observable stellar halos. These models also make predictions about what can be physically inferred from an external, "global" view of stellar halos. For example, from the shapes of debris remnants, we can infer the basic dynamical properties of the progenitor—Johnston et al. (2008) demonstrates that tidal debris of different morphologies each occupy different regions in the time of accretion vs. orbital eccentricity/energy plane (see their Fig. 9.3), and that surface brightness also gives evidence of both the time of accretion and the luminosity of a remnant's progenitor (see Fig. 4 of Johnston et al.). While this gives some general insight into properties of the accretion events, there is considerable degeneracy in the inference of such properties, which may best be thought of as providing reasonable estimates upon which to base specific modeling of the accretion events.

Figure 9.6 compares the predicted morphologies of model debris structures from Johnston et al. (2008) to observed structures in external galaxies, demonstrating that we see examples of the remnants predicted by the models in the local Universe.

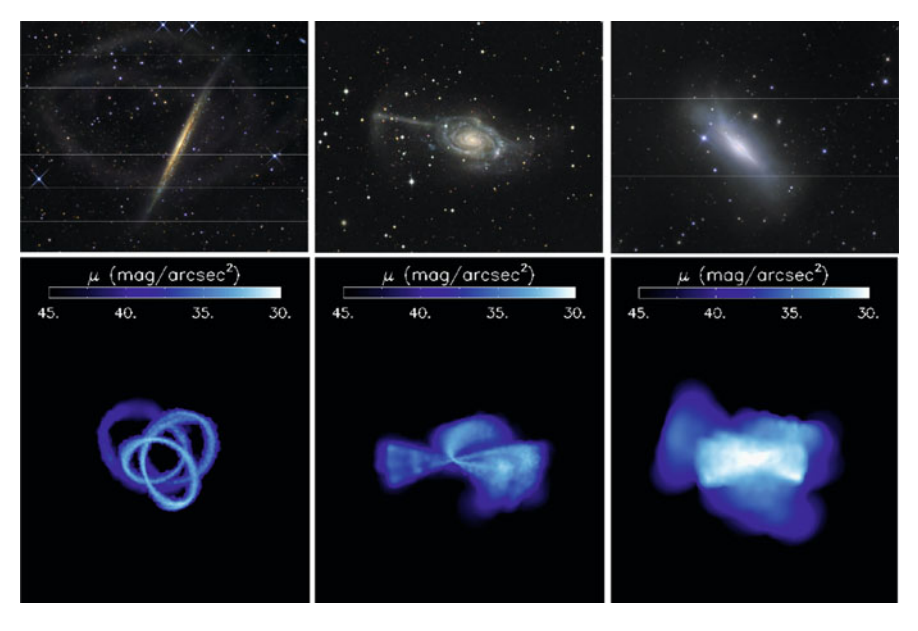


Fig. 9.6 Bottom row: externally-viewed snapshots showing the surface brightness of individual accretion relics in models of Milky Way-like stellar halos by Johnston et al. (2008). The three main morphological types identified in this study are illustrated: "great circle" streams (or "arcs"; left panel) arise from satellites accreted ~6–10 Gyr ago on nearly circular orbits; "cloudy" morphologies (also dubbed "shells" or "plumes"; middle panel) arise from accretion events within the past ~8 Gyr that fell in on eccentric orbits; and "mixed"-type tidal remnants (right) arise from ancient (more than 10 Gyr ago) accretion events that have had ample time to fully mix along their orbits. Top row: observational archetypes of each type of tidal debris from the survey by Martínez-Delgado et al. (2010): great circle stream in NGC 5907 (left), shell-like features around NGC 4651 (middle); and "mixed" debris near NGC 5866 (right panel) [Credit: D. Martínez-Delgado/R.J. Gabany, using data from Johnston et al. (2008).]

The classifications of debris structures suggested by Johnston et al. include: "great circles"—streams that arise from satellites on nearly circular orbits that were accreted ~6–10 Gyr ago; "cloudy" morphologies (also known as "shells" or "plumes") resulting from recently-accreted (less than ~8 Gyr ago) satellites that were on rather destructive, radial orbits; and "mixed"-type tidal remnants from ancient accretion events (more than ~10 Gyr ago) that have had time to phase mix and become nondescript. While these simulations make detailed predictions about the total number, frequencies, and specific properties of halo substructures, there is no analogous observational data set to which these simulations can be compared en masse. As demonstrated in Fig. 9.6, some observational examples of different stream morphologies have been identified in the local Universe, including "great circles" in NGC 5907 (Shang et al. 1998; Martínez-Delgado et al. 2008) and M 63 (Chonis et al. 2011; see also Fig. 9.1), the "plume"-like feature (or "umbrella") in NGC 4651 (Martínez-Delgado et al. 2010), and a feature of "mixed" morphology around NGC 1055 (Martínez-Delgado et al. 2010).

Generally, it is easiest to infer the physical properties of great circle streams, as the great circle is a reasonable tracer of the progenitor's orbit. Analytical relationships derived by Johnston et al. (2001) may be used to estimate the accretion time and total (dark matter+stellar+gas) initial mass of the progenitor of a stream on a great circle. Surface photometry across streams in multiple filters can be used to infer the stellar populations and total stellar mass for the stream (similarly to integrated light mapping of stellar mass surface density in external galaxies; e.g., Zibetti et al. 2009). Variations in the optical colors along the stream can be used to infer changes in the mean properties of the stellar populations, but are on the whole less diagnostic than similar studies using resolved stars in the Local Group. However, extraction of meaningful properties from the integrated light of streams requires S/N > 5-10 above the local background fluctuations over a sufficiently wide area to cover the full stream. Thus, not only must the image be deep, but the backgrounds need to be well characterized. This can be seen in Fig. 9.1, which shows that while hints of debris may be identifiable in SDSS imaging (e.g., Beaton et al. 2014), extraction of physical properties requires deep, well-characterized imaging.

Cooper et al. (2010) coupled the Aquarius simulations to a state-of-the-art semianalytic model known as GALFORM, which computes the properties (mass, size, star formation history and chemical abundance) of the galaxy forming in each dark matter halo. The GALFORM model is constrained through statistical comparisons to collective properties of the cosmological galaxy population (for example, optical and infrared luminosity functions), and by requiring that the surviving counterparts reproduce the observed size-luminosity relationship for Milky Way dwarfs. To meet these constraints, this technique demands fine-grained simulations such as Aquarius in order to adequately resolve the star-forming cores of satellite halos. This approach results in a set of dynamically self-consistent *N*-body realizations of stellar halos and their associated tidal streams at a resolution beyond the reach of current hydrodynamical simulations (e.g., Abadi et al. 2006), and without the need to invoke many of the approximations required by previous models (e.g., Bullock and Johnston 2005). The individual star formation history of each satellite (and hence properties such as stellar mass, luminosity and net metallicity) can be studied alongside the full phase-space evolution of its stars.

Current models have sufficient numbers of particles to resolve the main contributors of bright, coherent substructures that are similar to tidal features detected in the current imaging surveys (e.g., Martínez-Delgado et al. 2010). Thus it is possible to make sky-projected snapshots of these stellar halos from different viewing angles and a selected photometric band. Each model halo has experienced a unique merging history and provides predicted surface brightness, morphologies and overall distribution of the observable streams, survival of the progenitors and stellar populations (or mean colors), that can be compared with observational data. These snapshots can be used as the input source for creating a mock catalogue of synthetic images, which can be generated by adding simulated streams to real images including all the observational effects of the telescopes (e.g., typical sky noise, flat-field corrections, surface brightness limits, etc.) and contamination from other galactic substructures (e.g., the stellar disk that is not directly simulated by models of this type). An example of this technique using the Bullock and Johnston (2005) models as input is shown in Fig. 9.7. These mock observations give preliminary predictions for the level of substructure detectable in the stellar halo of a nearby spiral for the typical surface brightness limits of current imaging surveys. Moreover, additional observational properties, like chemical compositions (both [Fe/H], $[\alpha/\text{Fe}]$, can be explored as they relate to the other properties of substructure, the most significant being the time since accretion and luminosity (or stellar mass), as was done by, e.g., Font et al. (2006).

The Bullock and Johnston (2005) halos all have some structure visible at surface brightnesses of \sim 27–28 mag arcsec⁻². To surface brightnesses of \sim 29 mag arcsec⁻² there is ~ 1 visible stream in each simulated halo, and typically about 2 visible streams above ~ 30 mag arcsec⁻². The majority of the substructure, and thus the majority of the accretion history, is at surface brightnesses fainter than \sim 30 mag arcsec⁻². The degeneracy between the luminosity of the satellite, its accretion time, and its surface brightness is studied in depth by Johnston et al. (2008). Our inability to see the fainter streams, which were either accreted earlier or come from lower luminosity progenitors, implies that our view of halo substructure beyond the Local Group will be dominated by the most recent and/or most massive accretion event, and, in either case, the most metal rich populations (Johnston et al. 2008; Gilbert et al. 2009). Moreover, more massive accretion events tend to preferentially populate the innermost regions of the halo $(R_{\text{proj}} < 30 \,\text{kpc})$, as dynamical friction, which is more effective for more massive satellites, will cause the orbit of the progenitor to degrade (Johnston et al. 2008). Thus, our view of extragalactic tidal streams at relatively shallow surface brightness limits (i.e., those of POSS and SDSS) is highly biased to a specific subset of accretion events that are relatively rare for Milky Way sized galaxies.

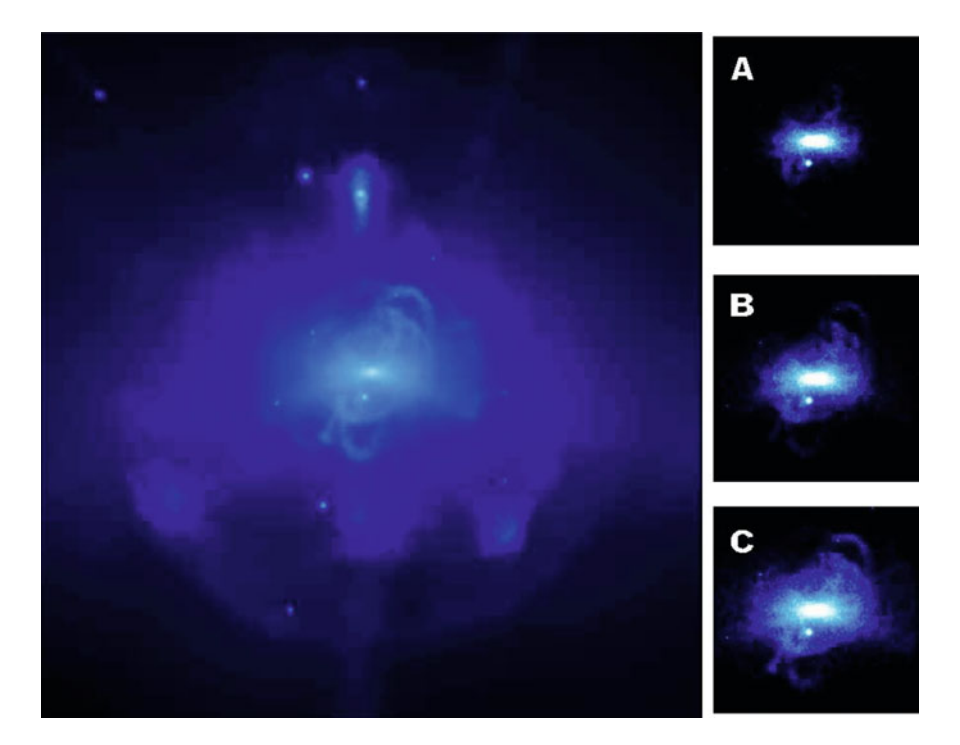


Fig. 9.7 Expected halo streams around a Milky Way-like galaxy from a simulation (Bullock and Johnston 2005). The figure shows an external perspective of one realization of a simulation within the hierarchical framework, with streams resulting from tidally disrupted satellites. The snapshot on the left is 300 kpc on a side (the virial radius for a Milky Way sized galaxy), and illustrates the result of a typical accretion history for a Milky Way-like galaxy. *Right panels*: theoretical predictions for the detectable tidal features in the same halo as the *left panel*, but assuming three different surface brightness (SB) detection limits: A: μ_{lim} =28, $B:\mu_{lim}$ =29 and $C: \mu_{lim}$ =30 mag arcsec⁻². Each snapshot is 100 kpc on a side. No discernible substructure is predicted for surveys with SB limits brighter than ~27–28 mag arcsec⁻² (e.g., POSS-II and SDSS). This result also shows as the number of tidal features visible on the outskirts of spirals depends dramatically on the SB limit of the observations. Moreover, the brightest substructures tend to be from the most massive satellites, which sample relatively rare accretion events (Johnston et al. 2008; Gilbert et al. 2009) [Figure credit: D. Martínez-Delgado. Left panel reproduced by permission from Bullock and Johnston (2005).]

9.5 The Role of Interactions Within Dwarf Galaxy Halos

Hierarchical formation models predict substructure should exist on all scales, not just around relatively massive galaxies like the Milky Way. Thus, exploration of the extended stellar structures of dwarf galaxies should reveal similar tidal features to those previously discussed. We first discuss the observational evidence for halos around dwarf galaxies and, in particular, for substructure in dwarf galaxy halos. Second, we discuss the impact that the creation of such substructures would have on dwarf galaxies. Understanding the formation and evolution of dwarf galaxies is

particularly vital to form realistic "initial conditions" for simulations and to make highly detailed predictions of substructure properties. For many reasons, extragalactic systems are best suited for these explorations.

9.5.1 Observational Evidence for Substructure at Dwarf Galaxy Scales

In the process of hierarchical structure formation, it is likely that some of the most massive satellite dwarf galaxies themselves host their own, even smaller satellites (dwarf spheroidals—"dSphs"—or globular clusters). In the Milky Way, we know that the most massive classical dwarf galaxies have globular clusters associated with them—specifically the Large Magellanic Cloud, the Small Magellanic Cloud, and the Fornax dSph (e.g., Forbes et al. 2000), as well as the Sagittarius tidal stream (e.g., Law and Majewski 2010b). The most massive Milky Way satellite, the Large Magellanic Cloud (LMC), is itself part of a bound pair of dwarf irregular galaxies (with the Small Magellanic Cloud, or SMC). Thus, we would expect to find evidence of tidal interaction around dwarf galaxies, analogous to the features we see in halos of more massive galaxies. The majority of the dwarf galaxies in the Local Group are satellites, which have experienced interactions with their more massive host. Thus, it can be difficult to disentangle effects on the dwarf created during the accretion by its parent from those it experienced before falling in. Studying external, isolated dwarf galaxies may prove a more effective means of understanding the role of hierarchical formation, including the role interactions may have in forming the Hubble sequence at low masses.

In fact, many of the unique features of the LMC-SMC pair can be explained by their binary interaction (e.g., Besla et al. 2012), including the spectacular 200° Magellanic Stream in HI (Nidever et al. 2010). Binary pairs are somewhat rare, as Robotham et al. (2012) find only two MW+LMC+SMC analog systems among the Galaxy Mass Assembly (GAMA) galaxies. While only 3.4% of GAMA galaxies are MW+LMC+SMC analogs, 12 % of SDSS galaxies have LMC-like companions (i.e., luminous satellite within 75 kpc; Tollerud et al. 2011), which suggests that about one in four LMC-like satellites have a smaller SMC-like companion. The relatively low fraction of LMC-SMC binary satellite systems supports a "transient" nature, as detailed numerical simulations of the LMC-SMC suggest they may not remain a bound pair for long (Besla et al. 2012). In fact, it has been suggested (e.g., D'Onghia and Lake 2008) that satellites should often fall in as pairs or in groups, rather than individually, and the dwarf galaxies found at the edge of the Local Group (representing future accretions) are grouped (e.g., Mateo 1998; McConnachie 2012). Thus, we would expect to find evidence of tidal interaction around dwarf galaxies, analogous to the features we see in halos of more massive galaxies.

Wide-field optical and near-infrared imaging has revealed stellar halos around many star-forming dwarf galaxies in and beyond the Local Group (see Stinson et al. 2009 for an extensive listing of many of these). While Stinson et al. determined that these extended stellar envelopes are not likely to arise due to tidal interactions with the (larger) host galaxies, it has not been determined whether they are the result of interactions with smaller satellites. Large area surveys of the most massive dwarf galaxies in the Local Group also indicate the presence of extended, "halolike" stellar populations at large effective radii, including M 33 (McConnachie et al. 2009), the LMC (Nidever et al. 2007), and the SMC (Nidever et al. 2011). Further characterization, including full kinematic profiles, is necessary to determine if these extended structures are lower mass versions of the halos found around Milky Way sized galaxies.

One of the many probable dwarf galaxies discovered by Karachentsev et al. (2007) was an elongated feature near the dwarf irregular galaxy NGC 4449 in Digitized Sky Survey (POSS-II) plates (denoted as object "d1228+4358" in their catalog). NGC 4449 is a dwarf starburst galaxy with an irregular morphology, with luminosity ($M_V = 18.6$) similar to that of the LMC, but with much stronger and more widespread ongoing star-formation activity. Its cold gas and HII regions exhibit peculiar kinematics (Hartmann et al. 1986; Hunter et al. 1998), suggesting that it may have recently interacted with another galaxy. Using deep, wide-field imaging around NGC 4449, Martínez-Delgado et al. (2012) definitively identified the Karachentsev et al. feature as a dwarf galaxy undergoing accretion by NGC 4449 (see Fig. 9.8). This new dwarf galaxy was also seen by Rich et al. (2012) in a similar deep-imaging survey, which revealed the dwarf (dubbed NGC 4449B) and its S-shaped morphology that is characteristic of disrupting satellites. After fitting and subtracting a halo model, Rich et al. showed additional arcs and possible disk ripple features in the residual stellar surface brightness maps, along with evidence for a break in the surface brightness profile of the NGC 4449 stellar halo. The morphology, size, luminosity, and surface brightness profile of the newly discovered stream/dwarf, along with evidence of tidal features in the NGC 4449 halo and outer disk, was suggested by Rich et al. (2012) to result from a dwarf (NGC 4449B) that is on its first passage, and passed near the center of its host $\sim 10^8$ yr ago. Thus, NGC 4449 is the first direct evidence of hierarchical structure formation similar to that seen in Milky Way-type galaxies, but on the mass scale of dwarf galaxies.

9.5.2 Implications of Dwarf-Dwarf Interactions

It is worth noting that the first stream from a dwarf-galaxy accretion event was found around one of the most intensely star-forming nearby galaxies. This leads one to wonder whether such accretion events are common among dwarf galaxies in recent epochs. It is possible that exact analogs to this stream have not been noticed in POSS or SDSS images because they are uncommon. However, another explanation is that the majority of such structures are fainter, more diffuse, or at a larger radius than the NGC 4449 stream, and thus await future detection. If streams as in NGC 4449 are common around dwarfs, they re-ignite classic ideas about galaxy interactions

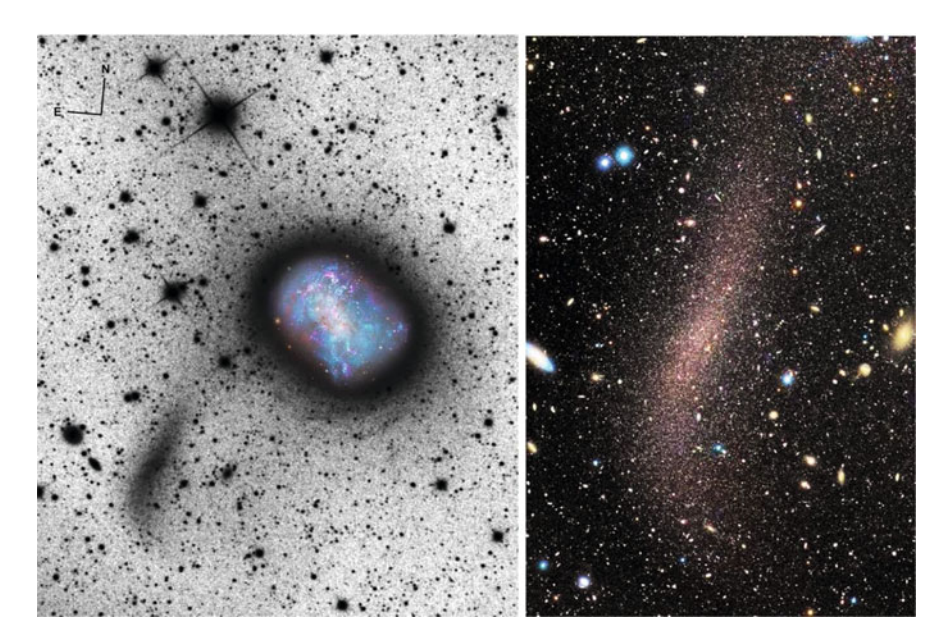


Fig. 9.8 The stellar stream around the dwarf galaxy NGC 4449. *Left*: greyscale image from Martínez-Delgado et al. (2012) with a color inset for the galaxy, which clearly indicates the presence of an S-shaped tidal stream approximately 7 kpc in length. There is no clear association with any of the existing HI gas features (Hunter et al. 1998). *Right*: Subaru telescope sub-arcsecond resolution image of the stellar stream (Martínez-Delgado et al. 2012). This is one of the few extragalactic stellar streams that has been resolved into individual stars, which provides direct probes of its stellar populations [Figure reproduced by permission from Martínez-Delgado et al. (2012).]

triggering starbursts. Given the high rates of star formation in dwarf galaxies, it is natural to ask if satellites are responsible. Surveys along these lines have produced mixed results (Noeske et al. 2001; Brosch et al. 2004; Li et al. 2008), but these studies were not looking for objects like the detected dwarf satellite of NGC 4449—a gas poor, low-surface brightness analog to the Local Group dSphs—and did not probe appropriate depths to find these objects. Regardless of the implications for starbursts, evidence from NGC 4449 and the Fornax dSph, which shows traces of having swallowed a smaller dSph (Coleman et al. 2005), suggests that accretion of even smaller building blocks is a viable avenue for direct assembly of dwarf galaxy stellar halos.

It has been proposed that dSphs orbiting massive galaxies such as the Milky Way may be the result of "pre-processing" which is a term for the effects of interactions within groups of dwarf galaxies (e.g., D'Onghia et al. 2009). More specifically, it has been suggested that the dSphs were once gas-rich, rotationally supported objects like the field galaxies (i.e., similar to NGC 4449) whose properties were modified into the gas-free, dispersion supported dSphs via interactions with companions. This is a compelling scenario for the class of dwarf galaxies in the Local Group known as "dwarf Transition" objects (see Mateo 1998; Grebel 1999; among others).

whose properties are intermediate between those of dIrrs and dSphs. Evidence of a dwarf-dwarf interaction in NGC 4449, in conjunction with the known HI streams around this dwarf galaxy, may thus demonstrate such a process in action. Moreover, Nidever et al. (2013) identified an HI filament associated with the M31 dwarf satellite IC 10. The dynamics and orientation of the stream are inconsistent with the orbital parameters of IC 10, and Nidever et al. (2013) suggest that the stream and other atypical HI features in the IC 10 disk could be explained via interaction with a "stealth" companion.

Wetzel et al. (2015) used the ELVIS simulations to explore the frequency of "pre-processing" for satellites within a simulated Milky Way host and found that nearly half of all satellites with stellar masses less than 10⁶ solar masses were preprocessed in a more massive satellite halo. More generally, satellites with lower stellar masses or those closer to their host are more likely to have undergone preprocessing. Recent observational work for the Milky Way and M 31 also provides hints of associated satellites or debris, including potential satellites with similar lineof-sight velocities (e.g., Chapman et al. 2007; Martin et al. 2009; Tollerud et al. 2012) and potential kinematic associations between substructures (e.g., Deason et al. 2014). While these initial probes are tantalizing, full phase space realizations of these objects that are only permitted via precision distances and proper motions are required to fully explore these associations locally. Moreover, though it is tempting to explain morphological transitions with dwarf-dwarf interactions, there is significant degeneracy with other physical processes that can alter HI morphologies even at large radius in a group environment; for instance the effects of ram pressure from the hot gaseous halo can be quite dramatic (see case studies in McConnachie et al. 2007; Kenney et al. 2014), and many isolated gas-poor dwarfs could be the result of "flyby" interactions with their host (see Teyssier et al. 2012). However, the HI debris created by dwarf-dwarf interactions and ram pressure are different, and finding more dwarf galaxies in "distress" will reveal the relative importance of these processes, which also have implications for their halo substructures.

A dramatic example of an ongoing dwarf-dwarf interaction was seen by Paudel et al. (2015), who found a pair of dwarf galaxies connected by a 15 kpc stellar bridge. The HI disk for one of the galaxies is "completely destroyed" and there are several knots of star formation that have global properties similar to either young globular clusters or ultra-compact dwarf galaxies. The Paudel et al. (2015) dwarfdwarf merger bears a striking resemblance to a scaled down version of equal mass mergers at larger total masses. The importance of dwarf interactions in shaping stellar populations of low-mass galaxies is highlighted in a recent systematic, multi-wavelength study of the relative star formation rates in interacting pairs of dwarf galaxies (TiNy Titans, or TNTs) by Stierwalt et al. (2015). This work found clear evidence of star formation enhancement (by a factor of $\sim 2.3 \pm 0.7$) among paired dwarfs relative to their unpaired counterparts. This enhancement occurs even in interacting pairs that are isolated by $D > 1.5 \,\mathrm{Mpc}$ from their nearest massive neighbor, showing that galaxy interactions are a frequent driver of enhanced star formation even outside the influence of larger galaxies. The Stierwalt et al. (2015) study also finds a factor of \sim 3 increase in the fraction of paired dwarfs that are starbursting relative to single dwarfs, further highlighting the role of interactions in triggering star forming episodes. Thus far, though, stellar tidal debris signatures of these dwarf-dwarf interactions have not been identified. [Note that this study is limited to pairs of mass ratio $(M_1/M_2)_* < 10$, while the disrupting companion to NGC 4449 has about 1/50th its stellar mass (Martínez-Delgado et al. 2012).]

9.6 Induced Star Formation, Disk Structure, and Tidal Streams

Simulations of structure formation on galactic scales in the prevailing ΛCDM paradigm predict that Milky Way-sized host galaxies should accrete several massive satellites from $z\simeq 1$ to the present. We now consider the effects of these interactions on the disk of the parent galaxy. Given the significantly shorter dynamical timescales in the disk, the potential effects of a even a minor accretion event could be profound. In particular, such events could incite abnormal structures in dissipational HI disks, either creating features after a pass through or creating large scale, global distortions in the HI structure. In the stellar component of the disk, the effects could be both more subtle and more long lived.

One example of a burst of star formation in a Milky Way-like galaxy with an associated recent accretion event is seen in NGC 5387 (Beaton et al. 2014; note that NGC 5387 can be considered a Milky Way analog based on its properties, but contains about an order of magnitude less mass than the MW). This system shows a low surface-brightness feature in SDSS imaging that was explored with deeper imaging by Beaton et al., who found a stellar stream extending over at least an entire orbital wrap, with median surface brightness of \sim 24.5 mag arcsec⁻² in Rband (see Fig. 9.9). This stream has a redder color than the typical stellar populations of NGC 5387, and contains a total stellar mass of $\sim 6 \times 10^8 M_{\odot}$. Coincident with the position of the stream's crossing of the NGC 5387 disk is a "blue overdensity" that is not only blue in optical colors, but is producing a large FUV flux as well. Evidence from the FUV flux as well as follow-up spectra obtained by Beaton et al. (2014) suggests a very recent (~8 Myr ago) star formation event of total stellar mass $2.5 \pm 1.3 \times 10^7 M_{\odot}$. Beaton et al. conclude that this blue overdensity is a complex of multiple HII regions produced by star formation either induced in the disk by the minor merger event, or in the dwarf galaxy progenitor of the stream itself. Whichever scenario is shown to be true, it is clear that the blue overdensity and its associated tidal stream represent star formation induced by the accretion of a satellite about 1/50th the mass of its host.

The presence of tidal streams encircling galaxies with warped disks (see, e.g., Martínez-Delgado et al. 2008) may suggest satellite galaxy perturbations as the origin of those disk features (e.g., Velazquez and White 1999; Weinberg and Blitz 2006). This suggests that promising galaxies to search for extragalactic tidal streams are those that display disk asymmetries in optical or HI images that may result from

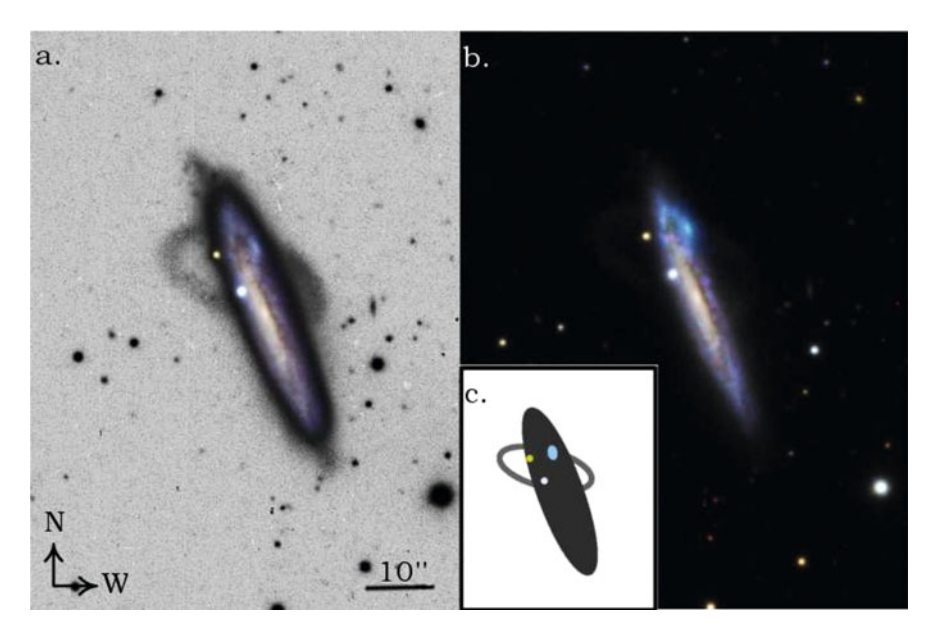


Fig. 9.9 Images of the stream and associated blue overdensity in NGC 5387. The *left panel* is the *R*-band image from the VATT, with the SDSS color image inlaid in the central regions, and clearly shows a full wrap of tidal debris about the disk of NGC 5387. The *right panel* shows a merged image composed of the SDSS, VATT, and *GALEX* FUV images, which more clearly highlights the blue overdensity near the northernmost edge of the disk of NGC 5387. The inset in the *right panel* is a schematic highlighting the disk in *dark gray*, the stream as a *lighter gray* loop, the blue overdensity as a *blue circle*, and two foreground stars [Reproduced from Beaton et al. (2014).]

gravitational interaction with the tidally disrupting companions. One striking case of such a system is NGC 4013, an isolated spiral galaxy with a prominent HI warp (Bottema et al. 1987) that has been revealed by deep imaging (Martínez-Delgado et al. 2009) to contain a faint loop-like stellar tidal stream at fairly low inclination to the disk (see the upper panels of Fig. 9.1). The sky-projected morphology of this structure displays a remarkable resemblance to an edge-on view of models of the Monoceros Ring feature (see Chap. 3) in the Milky Way as a tidal debris structure (Peñarrubia et al. 2005). This suggests that the progenitor system of the NGC 4013 stream may have been a low-mass satellite on a low-inclination, nearly-circular orbit that was accreted approximately ~2.8 Gyr ago. Stellar streams have also been discovered in the warped spiral galaxies NGC 5907 (Martínez-Delgado et al. 2008, see also Fig. 9.3) and M 63 (Chonis et al. 2011; see also Fig. 9.1), showing that disks that are apparently undisturbed as seen in the optical, but warped in HI maps, may reveal signatures of recent accretion events in deep imaging surveys

It has been shown that such accretion events should lead to strong warping, flaring, and thickening of an initially cold stellar disk (Kazantzidis et al. 2008), and to the generation of bars and spiral structure (e.g., Toomre and Toomre 1972; Gauthier et al. 2006; Dubinski and Chakrabarty 2009; Purcell et al. 2011). Such

perturbations may also lead to the formation of long-lived, ring-like stellar features in the outer reaches of the disk that may extend several kiloparsecs from the disk plane, and have surface brightnesses in the range of 25–30 mag arcsec⁻² (see Fig. 6 of Kazantzidis et al. 2008). Indeed, observations in the Milky Way are uncovering wave-like perturbations in the disk in stellar densities (Widrow et al. 2012; Yanny and Gardner 2013; Xu et al. 2015) and velocities (Gómez et al. 2012a,b; Carlin et al. 2013; Williams et al. 2013), with an accompanying array of simulations predicting the formation of such features (e.g., Chakrabarti and Blitz 2009; Michel-Dansac et al. 2011; Purcell et al. 2011; Gómez et al. 2013; Faure et al. 2014; Widrow et al. 2014). Evidence for dynamically heated populations is not unique to the Milky Way—Dorman et al. (2013) have identified a kinematically cold population in the halo of M31.

9.7 Future Prospects

While the study of tidal streams from major mergers/encounters (1:3 mass ratio) or even minor encounters (1:3-1:10 mass ratio) is an old field, the extension of these studies to those streams formed by satellite galaxies, a.k.a., micro-mergers (mass ratio <1:10), is a relatively new area of exploration. Study of mergers on this mass scale provide a direct way of addressing some open questions on galactic formation and evolution. In the last decade, the observational effort has yielded an unprecedented sample of bright stellar streams in nearby spiral galaxies, including the discovery of observational analogs to the canonical morphologies found in Nbody models of stellar halos (Johnston et al. 2008; see Chap. 6). This offers a unique opportunity to study in detail the apparently still dramatic last stages of galaxy assembly in the local universe and to probe the anticipated estimates of frequency of tidal stellar features from the Λ -CDM paradigm for MW-sized galaxies. Moreover, these discoveries demonstrate the need for deep, wide-field imaging that pushes fainter than current surveys in order to visualize external galaxy halos on par with the highly substructured portrait of our own Milky Way and M31. Such studies will address the following key questions (among others) on several aspects of hierarchical galaxy formation:

- How many tidal debris features still exist as recognizable substructures in nearby spiral galaxies?
- Is the abundant number of stellar streams exceptional in the Local Group spirals, and are tidal streams as common as predicted by cosmological models?
- At what rate are stellar streams still forming in the local Universe?
- Are the tidal stream properties (e.g., mean surface brightness) observed in the local Universe consistent with predictions from Λ-CDM simulations?
- What can we learn about baryonic processes within dark matter halos from observations of these stellar halo substructures?

• What is the (stellar) mass spectrum of the streams, and hence the mass spectrum of the progenitor satellites?

- What is the fraction of halo stars attributable (within data limitations) to distinct structures?
- Do all dwarf galaxies contain evidence of hierarchical accretion, and what is the role of such interactions in forming the progenitors of streams in larger galaxies?
- Do streams (or their progenitor satellites) contribute to disk heating and the formation of morphological perturbations observed in nearby galaxies?
- What is the incidence of low-inclination streams and what is their role in reshaping the outer disks of nearby spiral galaxies?

The study of external tidal streams also has the potential to tackle a significant number of other topics that are the focus of current astrophysical research (e.g., stellar populations of halos, the resilience of the disks involved with minor mergers, accretion of globular clusters, induced star formation in streams, nearfield cosmology, satellite dynamics, dark matter halo shapes, etc.). In particular, the interpretation of global properties of galaxy halos and outer disks from resolved stellar populations (from, e.g., the Hubble Space Telescope survey GHOSTS; Radburn-Smith et al. 2011, or the CALIFA high-resolution spectroscopy survey of nearby stellar systems; Sánchez et al. 2013) requires understanding the role and prevalence of tidal debris in galaxy halos. In addition, studying stellar population gradients along tidal streams via deep HST photometric data (see, e.g., Aloisi et al. 2005) will render important constraints on the effect of tides on the stellar formation history of dwarf galaxies. The panoramic view of tidal streams in external galaxies also offers an excellent opportunity to demonstrate tidal stripping of globular clusters formed in satellite galaxies, which may correspond to an important fraction of the globular cluster population of the host, as earlier proposed by Searle and Zinn (1978). Ultimately, the ideal scenario would require resolving stellar populations in large numbers of galaxies at distances of 10-20 Mpc, which will be feasible in the next one or two decades with 30-m class ground-based telescopes or the proposed suite of space-based instrumentation.

Finally, the future census of tidal streams and their properties will also provide an essential framework for exploring whether the Milky Way is a template for the archetypal spiral galaxy. The next generation of galactic surveys (LSST) and future astrometric space missions (Gaia) will dissect the structure and formation of the Milky Way with unprecedented detail, leading to a revolutionary improvement of our understanding of the Galaxy. In this regard, the study of these structures in external systems will be complementary in interpreting this local Galactic archaeological data in the context of galaxy formation and evolution, providing unique data in order to quantify how typical the Milky Way is with respect to other nearby galaxies of its type.

Acknowledgements JLC gratefully acknowledges support from the NSF under grants AST 09-37523 and AST 14-09421.

References

Abadi, M. G., Navarro, J. F., & Steinmetz, M. 2006, MNRAS, 365, 747

Aloisi, A., van der Marel, R. P., Mack, J., et al. 2005, ApJ Lett, 631, L45

Amorisco, N. C., Martinez-Delgado, D., & Schedler, J. 2015, arXiv:1504.03697

Arp, H. 1966, ApJ Supp, 14, 1

Atkinson, A. M., Abraham, R. G., & Ferguson, A. M. N. 2013, ApJ, 765, 28

Bailin, J., Bell, E. F., Chappell, S. N., Radburn-Smith, D. J., & de Jong, R. S. 2011, ApJ, 736, 24

Beaton, R. L., Martínez-Delgado, D., Majewski, S. R., et al. 2014, ApJ, 790, 117

Bellazzini, M., Newberg, H. J., Correnti, M., Ferraro, F. R., & Monaco, L. 2006, A&A, 457, L21

Belokurov, V., Zucker, D. B., Evans, N. W., et al. 2006, ApJ Lett, 642, L137

Besla, G., Kallivayalil, N., Hernquist, L., et al. 2012, MNRAS, 421, 2109

Bottema, R., Shostak, G. S., & van der Kruit, P. C. 1987, Nature, 328, 401

Brosch, N., Almoznino, E., & Heller, A. B. 2004, MNRAS, 349, 357

Bullock, J. S., & Johnston, K. V. 2005, ApJ, 635, 931

Carlberg, R. G. 2013, ApJ, 775, 90

Carlin, J. L., DeLaunay, J., Newberg, H. J., et al. 2013, ApJ Lett, 777, LL5

Chakrabarti, S., & Blitz, L. 2009, MNRAS, 399, L118

Chapman, S. C., Peñarrubia, J., Ibata, R., et al. 2007, ApJ Lett, 662, L79

Chonis, T. S., Martínez-Delgado, D., Gabany, R. J., et al. 2011, AJ, 142, 166

Chou, M.-Y., Majewski, S. R., Cunha, K., et al. 2007, ApJ, 670, 346

Coleman, M. G., Da Costa, G. S., Bland-Hawthorn, J., & Freeman, K. C. 2005, AJ, 129, 1443

Cooper, A. P., Cole, S., Frenk, C. S., et al. 2010, MNRAS, 406, 744

D'Abrusco, R., Fabbiano, G., & Zezas, A. 2015, ApJ, 805, 26

Deason, A. J., Belokurov, V., Hamren, K. M., et al. 2014, MNRAS, 444, 3975

D'Onghia, E., & Lake, G. 2008, ApJ Lett, 686, L61

D'Onghia, E., Besla, G., Cox, T. J., & Hernquist, L. 2009, Nature, 460, 605

Dorman, C. E., Widrow, L. M., Guhathakurta, P., et al. 2013, ApJ, 779, 103

Dubinski, J., & Chakrabarty, D. 2009, ApJ, 703, 2068

Erkal, D., & Belokurov, V. 2015, MNRAS, 450, 1136

Fabian, A. C., Nulsen, P. E. J., & Stewart, G. C. 1980, Nature, 287, 613

Faure, C., Siebert, A., & Famaey, B. 2014, MNRAS, 440, 2564

Ferguson, A. M. N., Irwin, M. J., Ibata, R. A., Lewis, G. F., & Tanvir, N. R. 2002, AJ, 124, 1452

Font, A. S., Johnston, K. V., Bullock, J. S., & Robertson, B. E. 2006, ApJ, 646, 886

Forbes, D. A., Masters, K. L., Minniti, D., & Barmby, P. 2000, A&A, 358, 471

Foster, C., Lux, H., Romanowsky, A. J., et al. 2014, MNRAS, 442, 3544

Gauthier, J.-R., Dubinski, J., & Widrow, L. M. 2006, ApJ, 653, 1180

Gilbert, K. M., Font, A. S., Johnston, K. V., & Guhathakurta, P. 2009, ApJ, 701, 776

Gilbert, K. M., Guhathakurta, P., Beaton, R. L., et al. 2012, ApJ, 760, 76

Gómez, F. A., Minchev, I., Villalobos, Á., O'Shea, B. W., & Williams, M. E. K. 2012a, MNRAS, 419, 2163

Gómez, F. A., Minchev, I., O'Shea, B. W., et al. 2012b, MNRAS, 423, 3727

Gómez, F. A., Minchev, I., O'Shea, B. W., et al. 2013, MNRAS, 429, 159

Grebel, E. K. 1999, The Stellar Content of Local Group Galaxies, 192, 17

Greggio, L., Rejkuba, M., Gonzalez, O. A., et al. 2014, A&A, **562**, 73

Hartmann, L. W., Geller, M. J., & Huchra, J. P. 1986, AJ, 92, 1278

Hunter, D. A., Wilcots, E. M., van Woerden, H., Gallagher, J. S., & Kohle, S. 1998, ApJ Lett, 495, I 47

Ibata, R., Irwin, M., Lewis, G., Ferguson, A. M. N., & Tanvir, N. 2001, Nature, 412, 49

Ibata, R. A., Lewis, G. F., Irwin, M. J., & Quinn, T. 2002, MNRAS, 332, 915

Johnston, K. V., Sackett, P. D., & Bullock, J. S. 2001, ApJ, 557, 137

Johnston, K. V., Spergel, D. N., & Haydn, C. 2002, ApJ, 570, 656

Johnston, K. V., Bullock, J. S., Sharma, S., et al. 2008, ApJ, **689**, 936

J.L. Carlin et al.

Karachentsev, I. D., Karachentseva, V. E., & Huchtmeier, W. K. 2007, Astronomy Letters, 33, 512
Kazantzidis, S., Bullock, J. S., Zentner, A. R., Kravtsov, A. V., & Moustakas, L. A. 2008, ApJ, 688, 254

Kenney, J. D. P., Geha, M., Jáchym, P., et al. 2014, ApJ, 780, 119

Law, D. R., Johnston, K. V., & Majewski, S. R. 2005, ApJ, 619, 807

Law, D. R., & Majewski, S. R. 2010a, ApJ, 714, 229

Law, D. R., & Majewski, S. R. 2010b, ApJ, 718, 1128

Li, C., Kauffmann, G., Heckman, T. M., Jing, Y. P., & White, S. D. M. 2008, MNRAS, 385, 1903

Malin, D. F. 1981, AAS Photo Bulletin, 27, #....4

Malin, D., & Hadley, B. 1997, PASA, 14, 52

Martin, N. F., McConnachie, A. W., Irwin, M., et al. 2009, ApJ, 705, 758

Martínez-Delgado, D., Peñarrubia, J., Gabany, R. J., et al. 2008, ApJ, 689, 184

Martínez-Delgado, D., Pohlen, M., Gabany, R. J., et al. 2009, ApJ, 692, 955

Martínez-Delgado, D., Gabany, R. J., Crawford, K., et al. 2010, AJ, 140, 962

Martínez-Delgado, D., Romanowsky, A. J., Gabany, R. J., et al. 2012, ApJ Lett, 748, L24

Martínez-Delgado, D., D'Onghia, E., Chonis, T. S., et al. 2014, arXiv:1410.6368

Mateo, M. L. 1998, ARA&A, 36, 435

Mateo, M., Olszewski, E. W., & Morrison, H. L. 1998, ApJ Lett, 508, L55

McConnachie, A. W., Venn, K. A., Irwin, M. J., Young, L. M., & Geehan, J. J. 2007, ApJ Lett, 671, L33

McConnachie, A. W., Irwin, M. J., Ibata, R. A., et al. 2009, Nature, 461, 66

McConnachie, A. W. 2012, AJ, 144, 4

Michel-Dansac, L., Abadi, M. G., Navarro, J. F., & Steinmetz, M. 2011, MNRAS, 414, L1

Miskolczi, A., Bomans, D. J., & Dettmar, R.-J. 2011, A&A, 536, 66

Mouhcine, M., Ibata, R., & Rejkuba, M. 2010, ApJ Lett, 714, L12

Mutch, S. J., Croton, D. J., & Poole, G. B. 2011, ApJ, 736, 84

Ngan, W., Bozek, B., Carlberg, R. G., et al. 2015, ApJ, 803, 75

Nidever, D. L., Majewski, S. R., Munoz, R. R., et al. 2007, Bulletin of the American Astronomical Society, 39, #113.01

Nidever, D. L., Majewski, S. R., Butler Burton, W., & Nigra, L. 2010, ApJ, 723, 1618

Nidever, D. L., Majewski, S. R., Muñoz, R. R., et al. 2011, ApJ Lett, 733, L10

Nidever, D. L., Ashley, T., Slater, C. T., et al. 2013, ApJ Lett, 779, L15

Noeske, K. G., Iglesias-Páramo, J., Vílchez, J. M., Papaderos, P., & Fricke, K. J. 2001, A&A, 371, 806

Paudel, S., Duc, P. A., & Ree, C. H. 2015, AJ, 149, 114

Peñarrubia, J., Martínez-Delgado, D., Rix, H. W., et al. 2005, ApJ, 626, 128

Peñarrubia, J., Benson, A. J., Martínez-Delgado, D., & Rix, H. W. 2006, ApJ, 645, 240

Purcell, C. W., Bullock, J. S., Tollerud, E. J., Rocha, M., & Chakrabarti, S. 2011, Nature, 477, 301 Quinn, P. J. 1984, ApJ, 279, 596

Radburn-Smith, D. J., de Jong, R. S., Seth, A. C., et al. 2011, ApJ Supp, 195, 18

Rich, R. M., Collins, M. L. M., Black, C. M., et al. 2012, Nature, 482, 192

Robotham, A. S. G., Baldry, I. K., Bland-Hawthorn, J., et al. 2012, MNRAS, 424, 1448

Sánchez, S. F., Rosales-Ortega, F. F., Jungwiert, B., et al. 2013, A&A, 554, 58

Sanderson, R. E., & Helmi, A. 2013, MNRAS, 435, 378

Schweizer, F., & Seitzer, P. 1988, ApJ, 328, 88

Searle, L., & Zinn, R. 1978, ApJ, 225, 357

Shang, Z., Zheng, Z., Brinks, E., et al. 1998, ApJ Lett, 504, L23

Siegal-Gaskins, J. M., & Valluri, M. 2008, ApJ, 681, 40

Stierwalt, S., Besla, G., Patton, D., et al. 2015, ApJ, 805, 2

Stinson, G. S., Dalcanton, J. J., Quinn, T., et al. 2009, MNRAS, 395, 1455

Teyssier, M., Johnston, K. V., & Kuhlen, M. 2012, MNRAS, 426, 1808

Tollerud, E. J., Boylan-Kolchin, M., Barton, E. J., Bullock, J. S., & Trinh, C. Q. 2011, ApJ, 738, 102

Tollerud, E. J., Beaton, R. L., Geha, M. C., et al. 2012, ApJ, 752, 45

Toomre, A., & Toomre, J. 1972, ApJ, 178, 623

van Dokkum, P. G., Abraham, R., & Merritt, A. 2014, ApJ Lett, 782, L24

Velazquez, H., & White, S. D. M. 1999, MNRAS, 304, 254

Weinberg, M. D., & Blitz, L. 2006, ApJ Lett, 641, L33

Wetzel, A. R., Deason, A. J., & Garrison-Kimmel, S. 2015, ApJ, 807, 49

Widrow, L. M., Gardner, S., Yanny, B., Dodelson, S., & Chen, H.-Y. 2012, ApJ Lett, 750, L41

Widrow, L. M., Barber, J., Chequers, M. H., & Cheng, E. 2014, MNRAS, 440, 1971

Williams, M. E. K., Steinmetz, M., Binney, J., et al. 2013, MNRAS, 436, 101

Xu, Y., Newberg, H. J., Carlin, J. L., et al. 2015, ApJ, 801, 105

Yanny, B., & Gardner, S. 2013, ApJ, 777, 91

Yoon, J. H., K. V., & Hogg, D. W. 2011, ApJ, 731, 58

Zibetti, S., Charlot, S., & Rix, H.-W. 2009, MNRAS, 400, 1181

Acheron, 91, 100	Clouds, 4, 13, 89, 106, 200, 207, 223, 224, 231,
Action-angle formalism, 115, 146	232
Adiabatic invariants, 116	Cocytos, 91, 100
Age-metallicity relation (AMR), 20, 203, 205,	Complex A, 101
206	Cosmological simulations, 5, 25, 133, 157,
age-metallicity relation (AMR), 38, 40, 44	206, 220, 223, 224, 230
Alpheus, 92, 100	
Andromeda (M31) galaxy, 11, 13, 83, 191–215,	
220–222, 226–228, 238, 241	Dark Energy Spectroscopic Instrument (DESI),
And XXVII, 207	88
Anticenter Stream (ACS), 72, 80, 83, 91, 100	Dark Energy Survey (DES), 108
APOGEE survey, 40, 52, 84, 127, 134	Dark matter halos, 169
APOGEE-2 survey, 43	Dark matter subhalos, 24–26, 99, 229
Aquarius Stream, 125, 126	satellite, 170
Arcturus moving group, 118, 122	Density distribution
Argo, 67, 78, 108	predictions, 152
Arp 2, 33, 43, 44	Dwarf galaxies, 1, 2, 4, 5, 11–14, 22, 24–27,
ATLAS, 108	89, 192, 195, 201, 207, 208, 211,
ATLAS stream, 92, 97	212, 214, 220, 224, 232, 234–239,
	242
	interactions between, 236, 238, 239
Berkeley 29, 44	pre-processing in, 237
Blue horizontal branch (BHB) stars, 6, 8, 9, 15,	satellites of, 235, 236
17, 26, 55, 57, 77, 102	Dynamical friction, 58, 119, 156, 205, 233
Blue straggler stars (BSSs), 5, 8, 9, 15, 17, 102	•
Boötes III, 91, 103	
	Eastern Banded Structure (EBS), 80, 83, 91, 99
	Eastern (E) Cloud, 200, 207, 210
Canis Major, 64, 67, 78, 79, 84, 108	Effective potential, 149
Carbon stars, 9, 33, 38	Elements of Cold HalO Substructure
Catalina Sky Survey, 107	(ECHOS), 21, 100, 109, 131–133
Caustic rings, 70	(201105), 21, 100, 105, 101 105
Cetus Polar Stream, 9, 91, 102, 131	
Chemical abundances, 22, 120, 123, 233	Fornax dwarf spheroidal (dSph), 37, 39, 42,
Chemical tagging/fingerprinting, 22, 43, 120,	44, 117, 235, 237
134, 164	11 , 111, 233, 231

© Springer International Publishing Switzerland 2016 H.J. Newberg, J.L. Carlin (eds.), *Tidal Streams in the Local Group and Beyond*, Astrophysics and Space Science Library 420, DOI 10.1007/978-3-319-19336-6

Gaia, 26, 84, 109, 110, 134–136, 156, 164,	In situ formation, 156
192, 214, 242	Integrals of motion, 116
Gaia/ESO survey, 43, 134, 136	
Galactic disk, 11, 12, 14, 22, 23, 25, 63, 64,	
66–68, 70, 72, 74, 75, 77–79, 83, 84,	Jacobi integral, 149
113, 118, 127, 241	
chemical abundances, 69, 70, 75, 122	
mass, 52	Kapteyn moving group, 119
moving groups in, 5-7, 14, 21, 113, 114,	Kapteyn's Selected Areas, 52, 115
118, 119, 125, 134, 136	KFR08 moving group, 124, 125, 127
oscillation of midplane, 25, 80, 81, 83, 84,	Known debris clouds
106, 241	distances, 93
velocity substructure, 25, 80, 82, 84, 117,	metallicities, 93
126, 241	progenitors, 93
warp and flare, 25, 66, 68, 69, 78, 108	spatial extent, 93
Galactic parallax, 109	table of, 93
Galactic potential, 2, 24, 27, 32, 45–47, 49, 51,	velocities, 93
52, 54, 101, 116, 121, 123	Known streams
shape of, 25, 35, 49–51, 88, 99	distances, 90, 92
	metallicities, 90, 92
GALAH survey, 22, 43, 134	
G1 Clump, 197, 198, 205	progenitors, 90, 92
GD-1, 88, 91, 99	spatial extent, 90, 92
Geneva-Copenhagen survey (GCS), 119, 120,	table of, 90
122	velocities, 90, 92
G1 globular cluster, 198	
Giant Stellar Stream (GSS), 26, 194, 197,	
199–205, 207, 221, 229	Large Magellanic Cloud (LMC), 25, 32, 37,
Globular clusters, 1, 2, 4, 5, 14, 19, 20, 22–24,	42, 44, 51, 56, 58, 180, 235, 236
33, 34, 37, 38, 42, 44, 45, 57, 77, 89,	Large Sky Area Multi-Object Fiber
129, 192, 195, 198, 208–211, 214,	Spectroscopic Telescope
220, 228, 229, 235, 242	(LAMOST), 25, 81, 84, 88, 109, 133
Great circle streams, 224, 225, 227, 228, 231,	Large Synoptic Survey Telescope (LSST), 109,
232	110, 242
Group infall, 56, 80, 105, 106, 235	Lethe, 91, 100
	Liouville's theorem, 155
II 1 A '1 C' 1 11 12 02 106	Luminosity, 105, 107
Hercules-Aquila Cloud, 11–13, 93, 106	luminosity, 37, 53
Hercules moving group, 118, 122, 125	•
Hercules Thick Disk Cloud, 106	
Hermus, 92, 100	M32, 83, 197, 203, 212
Hessian matrix, 148	M33, 100, 198, 206, 212, 213, 215, 236
Hierarchical galaxy formation, 23, 156, 191,	M 54, 33, 38, 39, 43–45
220, 224, 225, 234, 235, 241	M 63, 222, 232, 240
HII regions, 228, 229, 236, 239	Magellanic Stream, 235
Hipparcos mission, 6, 7, 115–117, 119, 124,	Map of known streams
136, 155	northern SDSS footprint, 94
Hubble Space Telescope (HST), 34, 38–40,	southern SDSS footprint, 95
203, 204, 212, 214, 227, 242	Mass of Milky Way, 102
Hyades moving group, 113, 118, 122	• • •
Hydra I, 80, 100	Matched filter, 17–19, 80, 88, 109
Hyllus, 92, 100	Metallicities, 37, 38, 40–43, 67, 69, 72, 74, 75,
-	79, 88, 95, 100–102, 105–107, 109,
IG 10, 220	119, 123–125, 129, 194, 196, 197,
IC 10, 238	199, 200, 204, 205, 207, 208
initial mass function (IMF), 42	Metallicity gradient, 22, 39, 41, 101, 230

M giants, 9, 10, 15, 26, 33–38, 40, 50, 53, 57, 67, 72, 77, 83, 87, 105, 108	map, 104
Missing satellites, 170	
•	Dol 12 42 44
Monoceros Ring, 11, 12, 15, 25, 64–77, 79–81,	Pal 12, 43, 44
83, 84, 89, 90, 102, 105, 108, 131,	Palomar 5, 8, 11, 12, 15–18, 20, 87, 90, 98
240 M. I. I. i. c. I.	Pan-Andromeda Archaeological Survey
Morphologies of debris structures, 153, 224,	(PAndAS), 79, 88, 96, 100, 102,
225, 228, 231–233, 241	106, 195–200, 207–209, 212, 213,
stream-like vs. cloud-like, 94	215
stream-like vs. shell-like, 154	PAndAS Field of Streams, 96
	PAndAS MW Stream, 79, 83, 92, 102
	Panoramic Survey Telescope and Rapid
Naming of streams, 89	Response System (Pan-STARRS),
Navarro, Frenk, & White (NFW) profile, 46,	37, 50, 71, 77, 88, 100, 108
49, 53, 142, 143, 169	Perseus Cloud, 108
N-body simulations, 24, 33, 35, 36, 45–53, 56,	Phase mixing, 115, 117, 118, 121, 124, 131,
58, 77, 101, 102, 106, 115, 117, 118,	133, 135, 143, 232
	full, 154, 155
121, 142, 199, 201, 202, 204, 213,	Photometric parallax, 19
215, 224, 225, 228, 229, 232, 241	Pisces Overdensity, 15, 93, 107
NGC 147, 198, 212, 213	Pisces Stellar Stream, 100
NGC 185, 212, 213	Pisces/Triangulum Stream, 79, 92, 100, 102
NGC 205, 197, 203, 212	Planetary nebulae (PNe), 195, 196, 228, 229
NGC 253, 226, 227	Pleiades moving group, 113, 118, 122
NGC 288, 92, 100	Plummer model, 46
NGC 891, 226, 227	Precession of orbits, 230
NGC 1055, 232	precession of orbits, 35, 36, 49, 50, 54
NGC 1097, 225	Progenitors of streams, 94, 101–103, 105, 107
NGC 2419, 44, 45, 57, 90	201, 203, 204, 221, 224–226, 228,
NGC 4013, 222, 240	
NGC 4449, 236–238	230–233, 239, 240
NGC 4651, 225, 228, 229, 231, 232	dwarf galaxies, 101
NGC 5053, 44	globular clusters, 98
NGC 5387, 239, 240	Proper motions, 26, 47, 51, 52, 78, 80, 100,
NGC 5466, 90, 99, 129	105, 107, 109, 113, 115, 116, 119,
NGC 5634, 44	123–125, 127–130, 133, 134, 192,
NGC 5824, 91, 102	214
NGC 5866, 231	Pyxis, 92
NGC 5907, 6, 224, 225, 228, 231, 232, 240	
NGC 6205, 129	
NGC 6934, 129	QUEST survey, 103
NGC 7089, 129	QCEST Survey, 180
North-East Clump (NE Clump), 198, 199, 205	
North-Eastern (NE) Shelf, 199, 202, 203	
North-West (NW) Stream, 200, 207, 210	Radial velocities, 21, 25, 26, 35, 37, 46, 49,
1101th 1105t (1111) Stream, 200, 201, 210	57, 67, 71–73, 77–79, 84, 88, 89,
	95, 99–109, 116, 119, 123, 125,
Omega Centauri, 22, 119, 120	129–132, 134, 192, 196, 201, 209,
Ophiuchus Stream, 92, 98, 100	210, 221, 228, 229
Orbital distribution, 149	RAdial Velocity Experiment (RAVE), 25, 80,
orbital pole, 34, 47, 50, 54	123–125, 127
Orbit fitting, 24, 80, 99, 101, 102, 104, 200,	Recovering accretion histories, 163
201, 225, 228, 229, 232	Red giant branch (RGB) stars, 6, 11, 13, 15,
Orphan Stream, 11, 91, 101	16, 192, 194, 195, 208, 209, 212,
Overdensities in Virgo, 103, 105	221, 226, 227
	,,

Reduced proper motion diagram (RPMD), 128, 129	Styx, 91, 103 Subdwarfs, 23, 118, 128
RGB tip stars (TRGB), 194–196, 201, 226, 227	Surface brightness, 101, 105, 192–195, 198,
RR Lyrae, 6, 8, 11, 15, 23, 37, 38, 57, 75–78,	199, 212, 220–222, 224, 226–231,
83, 101, 103, 107, 109, 116	233, 234, 236, 239, 241
63, 101, 103, 107, 109, 110	233, 234, 230, 237, 241
Sagittarius (Sgr) dwarf spheroidal (dSph), 3, 5,	Terzan 7, 33, 43, 44
6, 11, 25, 31–34, 36–38, 45, 52, 53,	Terzan 8, 33, 43, 44
55–57, 70, 80, 83, 130, 224	Tidal debris, 2
Sagittarius (Sgr) stream, 9–12, 14, 15, 19, 25,	in cosmological context, 156
26, 31–37, 41–59, 64, 66, 77, 87,	orbital properties, 143, 149
90, 94, 102, 104, 127, 128, 223–226,	physical scales, 151
230, 235	scales of orbital properties, 143
SDSS Field of Streams, 14, 98, 221	Tidal radius, 149
Segue 1, 101	Tidal scale, 149
Segue 2, 106	tidal stirring, 37, 55
SEKBO survey, 37, 103	Treams, 197
Shells, 70, 141, 220, 224–226, 228, 229, 231,	TriAnd1, 11, 12, 15, 79, 81–84, 93, 102, 105
232	TriAnd2, 79, 83, 93, 102, 105
Sirius moving group, 113	Triangulum Stream, 100
Skymapper, 108	Two Micron All Sky Survey (2MASS), 10,
Sloan Digital Sky Survey (SDSS), 7–9, 12, 14,	33–37, 48, 50, 53, 56, 57, 87, 100,
16–20, 25, 34, 35, 37, 48, 50, 52–57,	105, 108, 157
64, 66, 68, 71, 72, 80–82, 87, 94,	
95, 108, 123, 126–129, 131, 134,	
157, 193, 195, 208, 221–223, 226,	Umbrellas, 223, 225, 229, 232
232–236, 239, 240	Ursa Major II (UMaII), 101
Small Magellanic Cloud (SMC), 32, 37, 44,	
51–53, 56, 58, 235, 236	
South-West (SW) Cloud, 200, 207, 210, 211	Velocity dispersion, 22, 25, 27, 65–67, 69, 72,
SPLASH survey, 208, 221	89, 101, 102, 116, 118, 124, 201,
Star formation history (SFH), 203, 205, 206	205, 211, 212
Stäckel potentials, 148	velocity dispersion, 41, 53
star formation history (SFH), 37, 38	Velocity dispersion, 41, 33 Velocity gradient, 101, 201, 210
Statistical photometric parallax, 16, 17, 19–21	Virgo Overdensity (VOD), 11–13, 89, 93, 103,
Stellar density, 102	105
Stellar halos, 3	Virgo Stellar Stream (VSS), 89, 90, 103
models of, 157	Viigo Stellar Stream (VSS), 62, 70, 103
stellar populations in, 159, 194, 196	
Stellar mass, 107	W
Stream A, 200, 207	Western (W) Shelf, 199, 202
Stream B, 200	Whiting 1, 44
Stream C, 200, 210, 211	Wide-Field Infrared Survey Explorer (WISE),
Stream D, 200, 210	57, 87, 100
Stream gaps, 25, 26, 99, 230	
Streams, 89, 141, 192, 195, 196, 200, 207	
photometric searches, 88	Young debris, 154